RHODES UNIVERSITY

Where leaders learn

Dynamics of stimulated luminescence in natural quartz: Thermoluminescence and phototransferred thermoluminescence

A thesis submitted in fulfilment of the

requirements for the degree of

Doctor of Philosophy

in

Physics

by

DAMILOLA ESTHER FOLLEY

March 2020

Abstract

Natural quartz has remained an important mineral that is of topical interest in luminescence and dosimetry-related research. We investigate the dynamics of stimulated luminescence on this material through thermoluminescence (TL) and phototransferred thermoluminescence (PTTL). Measurements were made on unannealed natural quartz as well as quartz annealed at 800 and 1000 °C. The samples were annealed for 10 minutes and for 1 hour. The material, in its un- and annealed state has its main peak between 68 and 72 °C when measured at 1 °Cs^{-1} after a dose of 50 Gy. A study of dosimetric features and kinetic analysis was carried out on two prominent peaks, peak I and III for all the samples. The peaks show a sublinear dose response for irradiation doses between 10 and 300 Gy. Kinetic analysis shows that peak I is a first-order peak and peak III a general-order peak. Interestingly, we observe for peak I for the sample annealed at 800 °C for 1 hour an inverse thermal quenching behaviour. We demonstrate that a peak affected with an inverse thermal quenching-like behaviour can still show effect of thermal quenching when the dose the sample is irradiated to is significantly reduced. We ascribe the apparent dependence of thermal quenching on dose to competition between radiative and non-radiative transitions at the recombination centre. Peaks I, II, and III for all the samples were reproduced under phototransfer when the peaks, initially removed by preheating to a certain temperature are exposed to 470 and 525 nm light. The influence of duration of illumination on the PTTL intensity of these peaks corresponding to various preheating temperatures is modelled using coupled first-order differential equations. The model is based on systems of acceptors and donors whose number and role depends on preheating temperature.

Acknowledgements

My heartfelt gratitude goes to my supervisor Prof Makaiko Chithambo for the opportunity given me to walk this PhD journey under his academic mentorship. I am grateful for all the financial assistance I received from my supervisor through the National Research Foundation of South Africa towards the success of my PhD programme. My appreciation goes to the National Research Foundation of South Africa for the 3 year PhD Bursary awarded to me, and for all the travel support to Conferences and Research visits.

My appreciation goes to Dr Mayank Jain, Prof Andrew Murray, Dr Myung Ho and Mr Raju Kumar of RISO National Laboratory Denmark for hosting me in their research laboratory and for the guidance I received throughout my stay at Roskilde.

I thank in a special way Dr Luyanda Noto and Mr Dumisani Mlotswa of University of South Africa for granting me access to their Luminescence laboratory to carry out my research.

My special thanks goes to my priests friends Fr Elias Otanwa OP, Fr Moses Ani OP, Fr Hubert Obaedo CMF for all their prayers and encouragement.

My sincere gratitude to Joel Lontsi Sob for taking time out to proofread the last result chapter of my thesis when I was too tired to continue.

To my office mates Lexy, Cyndie, Joel, Kate, Robert, and Bokang, I say thank you for the communal life we live. May that cord of love that exists among us never be broken.

I sincerely thank Fatima, Rui, and Sr Ursula of the Christian Life Community, Grahamstown for their prayers for me always. And to everyone I could not mention in my acknowledgments, I am grateful for your kind support in my journey.

My very big THANKS goes to my parents for their love, support and encouragement throughout this journey, for without them I wouldn't have been where and who I am today.

Contents

List of Figures

List of Tables

Chapter 1

Introduction

1.1 Luminescence

The word *luminescence* was first used by a German physicist, Eilhardt Wiedemann, in 1888 (Murthy and Virk, 2014). Luminescence is defined as the process of emission of light from a material following the absorption of ionising radiation e.g. γ rays, β particles, X-rays, etc (Chen and Mckeever, 1997). The most basic process of luminescence is that electrons are excited from the ground (lowest energy) state to an excited state after the absorption of energy through radiation. When an excited electron returns to its ground state, it gives out its excess energy in the form of light termed luminescence.

Luminescence can be classified as fluorescence or phosphorescence depending on the mean-time τ, that is, the delay time between the absorption of excitation energy and the emission of the luminescence. The mean-time is the time that an electron spends in an electron trap. A trap is a point defect in semiconductors or insulators where electrons and holes are captured. The so called trap depth or activation energy of the trap is the energy of this localised level below the conduction band.

When the process of emission of luminescence occurs at a mean-time of $\tau \leq 10^{-8}$ s, the emission is called fluorescence. Thus fluorescence emission takes place effectively with the absorption of radiation and stops immediately the radiation ceases (McKeever, 1985; Chen and Mckeever, 1997). Figure 1.1 shows the schematic description of fluorescence emission. Transition (i) denotes the excitation of an

electron from the ground state, g, to an excited state, e. The return of the excited electron to its ground state (transition (ii)) describes the luminescence transition.

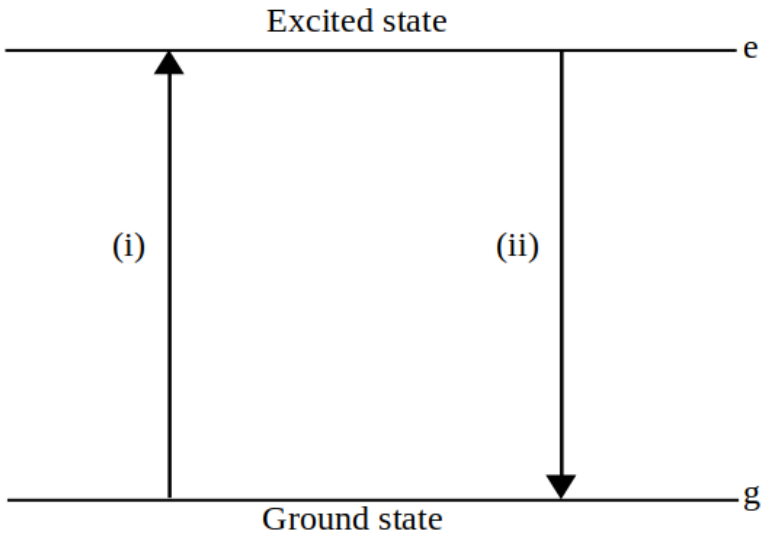

FIGURE 1.1: Energy band diagram showing excitation and emission of fluorescence. Figure reproduced from McKeever (1985).

Phosphorescence, on the other hand, is characterised by $\tau \geq 10^{-8}$ s (McKeever, 1985). Figure 1.2 illustrates the processes involved in phosphorescence. Here, the energy band diagram of Figure 1.1 is modified by the presence of a metastable level m between e and g. An electron excited from g to e (transition (i)) becomes trapped at m (transition (ii)). It remains at m for some time until it is given enough energy E to return to e (transition (iii)). The electron finally returns to g (transition (iv)) accompanied by the emission of light after the delay at m. The energy E of the separation between m and e is the activation energy or trap depth. Phosphorescence, unlike fluorescence, is strongly temperature dependent (McKeever, 1985; Chen and Mckeever, 1997).

If the transition from the metastable state m to the excited state e occurs at a temperature T, such that $E \geq$ several kT, then the electron can reside in m for some time. The probability p per unit time for thermal excitation from the trap is

$$p = s \exp\left(-\frac{E}{kT}\right) \tag{1.1}$$

where k is Boltzmann's constant and s is a constant in units of s^{-1} whose value is in the order of Debye frequency. The lifetime, that is, the time the electron spends in the metastable energy level at temperature T is given by

$$\tau = p^{-1} = s^{-1} \exp\left(\frac{E}{kT}\right) \tag{1.2}$$

Randall and Wilkins (1945) assumed that once an electron is freed from its trap

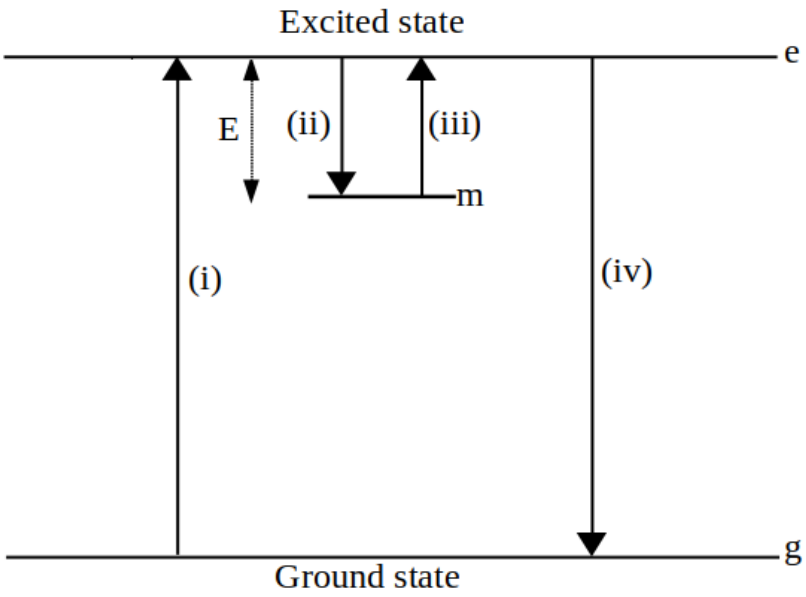

FIGURE 1.2: Energy band describing the process of phosphorescence. Figure reproduced from McKeever (1985) and modified

in the transition from the metastable level to the excited state that is, $m \rightarrow e$, the probability of it returning to m is much less than the probability of it returning to g. If n is the number of trapped electrons at m at a constant temperature T, the rate of thermal excitation from m to e is expressed as

$$\frac{dn}{dt} = -np = -ns \exp\left(-\frac{E}{kT}\right) \tag{1.3}$$

where the negative sign implies a loss of electrons from the electron trap (Chen and Mckeever, 1997).

Equation (1.3) can be rewritten as

$$\frac{dn}{n} = -s \exp\left(-\frac{E}{kT}\right) dt \tag{1.4}$$

Integrating both sides of equation (1.4) gives

$$ln\, n = -st\, \exp\left(\frac{E}{kT}\right) + C \tag{1.5}$$

from which

$$n = n_o\, \exp\left(-st\, \exp(E/kT)\right) \tag{1.6}$$

where n_o is the number of trapped electrons at $t = 0$.

The intensity $I(t)$ of phosphorescence at any time t is proportional to the rate of recombination (i.e. the transition from the excited state e to the ground state g) which is governed by the transitions from the metastable state m to the excited state e (McKeever, 1985). Thus, $I(t)$ is proportional to the rate of release of electrons from the trap and is given by

$$I(t) = -\gamma \frac{dn}{dt} = \gamma np \tag{1.7}$$

where γ is a constant of proportionality.
By integrating equation (1.7), we have

$$I(t) = I_o\, \exp(-pt) \tag{1.8}$$

where I_o is the intensity at $t = 0$, and p is given by equation (1.1).
Equation (1.8) describing phosphorescence decay is thus a simple exponential function of time at a constant temperature (McKeever, 1985; Chen and Mckeever, 1997).

Phosphorescence can further be classified into short period phosphorescence where $\tau < 10^{-4}$ s and long period phosphorescence where $\tau > 10^{-4}$ s. Thermoluminescence, the subject of this thesis is an example of long period phosphorescence. Phosphorescence is therefore a stimulated emission process since external energy is required to detrap electrons from m such that they can produce luminescence.

There are two important categories of stimulated luminescence phenomena namely, thermoluminescence (TL) and optically stimulated luminescence (OSL). In stimulated luminescence, the material under study must be given some external energy in the form of ionizing radiation by which charges are released into the conduction band. Some of these electrons can get trapped at electron traps. The captured

charges are then released thermally by heating, or optically by light, from the traps into the recombination centre from which luminescence occurs.

1.2 Thermoluminescence

Thermoluminescence (TL) is the emission of light from a previously irradiated material during a controlled heating rate. For thermoluminescence to occur, the material must be an insulator or a semiconductor. In addition, the material must have absorbed energy during exposure to ionizing radiation. Lastly, the material must be heated to some maximum temperature at a controlled rate (McKeever, 1985). Thermoluminescence appears as a temperature-resolved set of peaks otherwise known as a glow curve. This is a graph of intensity against temperature. Figure 1.3 shows an example of a glow curve from natural quartz annealed at 1000

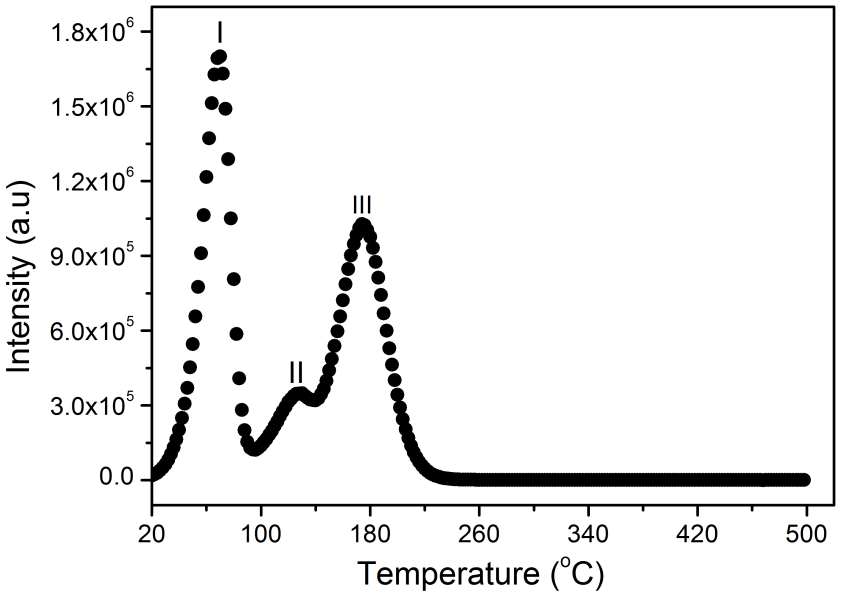

FIGURE 1.3: An example of a TL glow curve from annealed natural quartz measured at 1 °Cs^{-1} following irradiation to 50 Gy.

°C for 1 hour. The glow curve, showing three peaks at 70, 130, and 176 °C, was measured at a heating rate of 1 °Cs^{-1} after the quartz was irradiated to 50 Gy. For each glow peak, the maximum peak intensity, I_m corresponding to a temperature T_m can be extracted from the graph. The individual peaks can be analysed using

various methods.

One aim of measuring and analysing TL is to extract parameters that describe the TL process in the material under study. These parameters include the activation energy or trap depth E, frequency factor s, and order of kinetics, b.

1.2.1 Thermoluminescence models

The simplest model of TL is shown in Figure 1.4. This consists of two localized levels, one acting as a trap (T) and the other as a recombination centre (R). This model is otherwise referred to as the one-trap-one-recombination centre (OTOR) model.

In describing the model, we denote the total concentration of traps in the material as N, the concentration of filled traps in the crystal at a time t as n, the concentration of trapped holes in the recombination centre by n_h, and the initial concentration of filled traps at time $t = 0$ as n_0.

To measure TL, the sample is heated from some initial temperature to a final

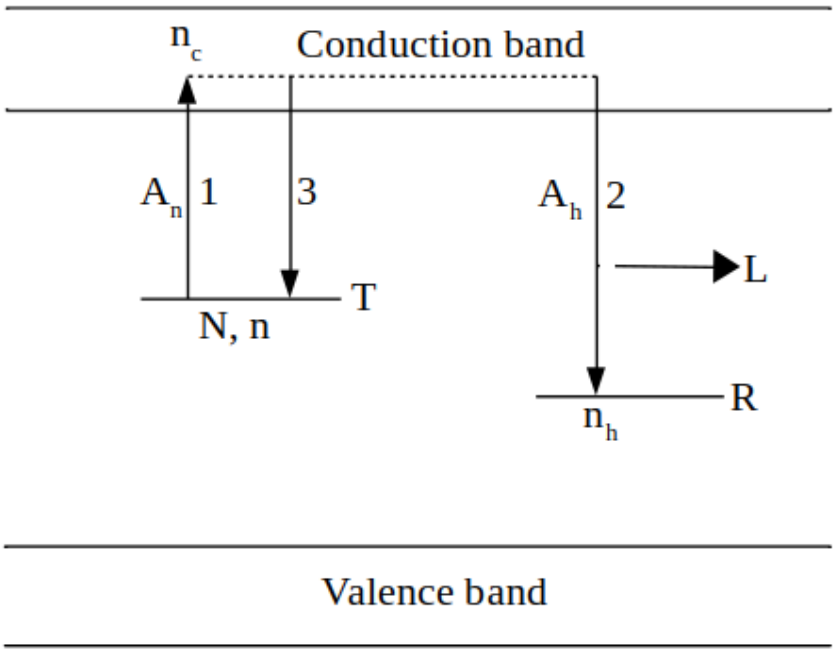

FIGURE 1.4: The simple thermoluminescence model by Garlick and Gibson (1948). Figure reproduced from Sunta (2015) and modified.

temperature at a rate $\beta = dT/dt$. As the temperature of the sample is increased,

electrons are ejected out of the trap and are thermally released into the conduction band (transition 1). These electrons, now in the conduction band, can recombine with holes at the recombination centre (transition 2) to produce luminescence L. Alternatively, the electrons can be retrapped into the electron trap T (transition 3).

The transport of electrons in the OTOR model may be described in terms of three rates as follows

$$\text{Excitation rate, } R_{ex} = np = ns \exp\left(-\frac{E}{kT}\right) \tag{1.9}$$

$$\text{Retrapping rate, } R_{ret} = n_c A_n (N - n) \tag{1.10}$$

$$\text{Recombination rate, } R_{rec} = n_c A_h n_h \tag{1.11}$$

where T is the absolute temperature, n_c is the concentration of electrons in the conduction band, A_n and A_h are the retrapping and recombination coefficients in $\mathrm{m^3 s^{-1}}$ respectively and other parameters are as defined before (McKeever, 1985; Chen and Mckeever, 1997).
The values of the coefficients A_n and A_h in equation (1.9) - (1.11) depend on the electron capture cross sections σ of the traps and recombination centre. These are defined by $A = \sigma_n \upsilon$ and $A = \sigma_h \upsilon$, where υ is the free electron velocity in the conduction band (McKeever, 1985; Chen and Mckeever, 1997).

For the OTOR model, n_h is equal to n. This is called the quasi-equilibrium condition. Considering the rates R_{ret} and R_{rec}, the fraction F of the excited carriers producing luminescence during heating is given as

$$F = \frac{R_{rec}}{R_{rec} + R_{ret}} \tag{1.12}$$

where F changes depending on the parameters in equation (1.9) - (1.11).
Thus the intensity of emitted light is equal to the rate of recombination of electrons and holes in the recombination centre and is given as

$$I(t) = -\frac{dn_h}{dt} \tag{1.13}$$

1.2.1.1 First-order kinetics

Randall and Wilkins (1945) assumed that retrapping during thermal excitation is negligible (i.e $R_{ret} = 0$). Therefore, equation (1.12) reduces to $F = 1$ and the thermoluminescence emission $I(t)$ is proportional to R_{ex} according to equation (1.7)

$$I(t) = \gamma R_{ex} = -\gamma \frac{dn}{dt} = \gamma n s \exp\left(-\frac{E}{kT}\right) \tag{1.14}$$

where γ is a constant.
Equation (1.14) can be rewritten as

$$\frac{dn}{n} = -s \exp\left(-\frac{E}{kT}\right) dt \tag{1.15}$$

Since the sample is heated at a linear rate $T = T_o + \beta t$, $dT/dt = \beta$. Equation (1.15) may then be expressed as

$$\frac{dn}{n} = -\left(\frac{s}{\beta}\right) \exp\left(-\frac{E}{kT}\right) dT \tag{1.16}$$

Integrating both sides of equation (1.16), one obtains the value of n at any temperature T as

$$n = n_o \exp\left[-\int_{T_o}^{T} \left(\frac{s}{\beta}\right) \exp\left(-\frac{E}{kT'}\right) dT'\right] \tag{1.17}$$

where n_o is the number of trapped electrons at $t = 0$ and T', the dummy variable of integration represents the temperature.

Substituting equation (1.17) for n into equation (1.14), we obtain the expression for thermoluminescence intensity as a function of temperature as

$$I(T) = n_o s \exp\left(-\frac{E}{kT}\right) \exp\left[-\frac{s}{\beta} \int_{T_o}^{T} \exp\left(-\frac{E}{kT'}\right) dT'\right] \tag{1.18}$$

Equation (1.18) describes an increase of intensity through a peak with a maximum at some temperature. The peak temperature T_m associated with the maximum peak intensity I_m of a first-order glow peak is obtained by maximising equation (1.18). It is convenient to first eliminate some of the exponentials for easy simplification by taking the logarithm of equation (1.18) prior to taking its derivative.

Here, we have

$$\left[\frac{d}{dT}(lnI)\right]_{T=T_m} = 0 + \frac{E}{kT_m^2} - \frac{s}{\beta}\exp\left(-\frac{E}{kT_m}\right) = 0 \tag{1.19}$$

from which

$$\frac{E}{kT_m^2} = \frac{s}{\beta}\exp\left(-\frac{E}{kT_m}\right) \tag{1.20}$$

Thus, the peak temperature T_m is found to be related to other parameters by

$$\frac{\beta E}{kT_m^2} = s\ \exp\left(-\frac{E}{kT_m}\right) \tag{1.21}$$

Equation (1.21) shows that the peak temperature T_m does not depend on the initial concentration of the trapped electrons, n_o. Therefore, T_m is independent of dose for first order kinetics (Chen and Mckeever, 1997).

1.2.1.2 Second-order kinetics

The second-order kinetics of thermoluminescence was proposed by Garlick and Gibson (1948) using the same OTOR model in Figure 1.4. They assumed that an electron ejected from a trap into the conduction band may either transit to R or be retrapped. The retrapping rate is $A_n(N-n)$. According to equation (1.12), the recombining fraction F for this model is given as

$$F = \frac{A_h n}{A_h n + A_n(N-n)} \tag{1.22}$$

where the parameters A_h, A_n, n, N are as previously defined.

Garlick and Gibson (1948) assumed that $A_h = A_n$ and thus $F = n/N$. The intensity of luminescence given by equation (1.14) is now modified by the factor n/N for γ. Thus,

$$I(t) = -\gamma\frac{dn}{dt} = \left(\frac{n}{N}\right)ns\ \exp\left(-\frac{E}{kT}\right) = \frac{n^2}{N}s\ \exp\left(-\frac{E}{kT}\right) \tag{1.23}$$

In equation (1.23), the intensity $I(t)$ is proportional to n^2 and thus the equation is referred to as the second-order kinetics equation.

By integrating equation (1.23) with respect to time, and noting that $dt = dT/\beta$,

we derive an expression for n at any temperature T as

$$n = n_o \left[1 + \frac{n_o s}{\beta N} \int_{T_o}^{T} \exp\left(-\frac{E}{kT'}\right) dT'\right]^{-2} \tag{1.24}$$

Substituting equation (1.24) for n in equation (1.23), the luminescence intensity as a function of temperature is given by

$$I(T) = \frac{n_o^2}{N} s \exp\left(-\frac{E}{kT}\right) \left[1 + \frac{n_o s}{\beta N} \int_{T_o}^{T} exp\left(-\frac{E}{kT'}\right) dT'\right]^{-2} \tag{1.25}$$

where all parameters have their usual meanings.

For second-order kinetics, the peak temperature T_m corresponding to the maximum peak intensity I_m of a TL glow peak can be obtained by maximising equation (1.25). The relationship between T_m and other parameters in this case is given by

$$\frac{\beta E}{kT_m^2} = \left(1 + \frac{2kT_m}{E}\right) s \exp\left(-\frac{E}{kT_m}\right) \tag{1.26}$$

It is worth noting that the peak temperature T_m depends on the irradiation dose applied to the sample for second-order kinetics.

1.2.1.3 General-order kinetics

May and Partridge (1964) derived an empirical expression for general-order kinetics of thermoluminescence without taking into account the assumptions of the first- and second-order kinetics. They wrote that

$$I(t) = -\frac{dn}{dt} = n^b s' \exp\left(-\frac{E}{kT_m}\right) \tag{1.27}$$

where s' has the dimensions of $m^{3(b-1)}s^{-1}$ and b is the general-order parameter which is not necessarily 1 or 2 (Chen and Mckeever, 1997).
Integrating equation (1.27) for $b \neq 1$ gives

$$I(T) = n_o s'' \exp\left(-\frac{E}{kT}\right) \left[1 + \frac{s''(b-1)}{\beta} \int_{T_o}^{T} \exp\left(-\frac{E}{kT'}\right) dT'\right]^{\frac{-b}{b-1}} \tag{1.28}$$

where $s'' = s' n_o^{(b-1)}$ is the effective frequency factor for general order kinetics.
When b approaches 1 or $b = 2$, equation (1.28) reduces to equation (1.18) or (1.25)

for first- or second-order kinetics respectively.
The condition for the peak maximum by taking $dI/dT = 0$ is given as

$$\frac{\beta E}{kT_m^2} = \left[1 + \frac{2kT_m(b-1)}{E}\right] s \exp\left(-\frac{E}{kT_m}\right) \tag{1.29}$$

where the peak temperature T_m depends on the irradiation dose applied to the sample.

1.3 Aim of thesis/Synopsis of thesis

1.3.1 Aims of thesis

The aim of this thesis is to study and analyse the dynamics of stimulated luminescence from measurements in natural quartz through thermoluminescence and phototransferred thermoluminescence. The specific objectives of this work include:

i. To carry out kinetic analysis of thermoluminescence using a variety of methods including partial and whole curve methods, peak shape methods, and peak position methods in order to evaluate the trap parameters for the peaks investigated thereby contributing to the published works in the literature.

ii. To investigate the influence of annealing on the kinetic parameters of some glow peaks in order to contribute to the understanding of mechanism of luminescence in quartz.

iii. To investigate phototransfer effects using blue and green light emitting diodes and develop models to explain the effect thereby contributing to the understanding of phototransferred thermoluminescence in quartz.

1.3.2 Synopsis of thesis

In this Chapter, we have described luminescence processes as fluorescence and phosphorescence. We also described the stimulated phenomena and thermoluminescence models. Lastly, we present an outline of what is to be expected in other chapters.

Chapter 2 discusses the physical processes, mechanism of luminescence and thermoluminescence. We also describe the ionic pair model for luminescence in natural quartz. The methods of kinetic analysis, peak resolution methods, and thermal quenching are also presented in this chapter.

In Chapter 3, we discuss phototransferred thermoluminescence and the models of PTTL. We describe the simple and phenomenological models of PTTL and competition effects in PTTL. The equipment and sample details used for this study are described in Chapter 4.

Results and discussion of the experiments carried out in this study are presented in Chapters 5 to 8. Dosimetric features and kinetic analysis of TL for unannealed natural quartz is discussed in Chapter 5. We present and discuss the results of kinetic analysis of TL of quartz annealed at 800 °C in Chapter 6. Chapter 7 presents and discusses the influence of annealing on thermoluminescence of natural quartz annealed at 1000 °C. Phototransferred thermoluminescence and competition effects are discussed in Chapter 8. In Chapter 9, we summarise the important results from Chapters 5, 6, 7, and 8 and suggest areas of further research.

Chapter 2

Physical processes of luminescence

2.1 Luminescence of quartz

Quartz is the second most abundant mineral after feldspar used widely in retrospective dosimetry and luminescence dating. It is used as a natural dosimeter in variety of applications (Preusser *et al.*, 2009). Quartz in its natural state crystallises as α-quartz. The crystal structure of quartz is built from SiO_4 tetrahedra that are linked by sharing each of the oxygen corners with other tetrahedra (Preusser *et al.*, 2009; Williams and Spooner, 2018). When quartz is heated, it undergoes phase transitions. At 573 °C, α-quartz changes to β-quartz and at 870 °C, β-quartz changes to β_2 - tridymite (Schilles *et al.*, 2001; Rutley, 2012). Bøtter-Jensen *et al.* (1995) showed that annealing of quartz prior to irradiation can significantly increase its luminescence sensitivity. The sensitivity increase is found to occur between the first two phase transition temperatures. Annealing is also reported to affect the luminescence lifetimes (Galloway, 2002; Chithambo and Ogundare, 2009) and emission bands (Pagonis *et al.*, 2014) of quartz.

There are for quartz, numerous studies on stimulated luminescence reported in the literature e.g thermoluminescence (Ogundare and Chithambo, 2006; Subedi *et al.*, 2011; Zhou *et al.*, 2016), optically stimulated luminescence (Bøtter-Jensen and Duller, 1992; Bøtter-Jensen *et al.*, 2003; Wintle and Murray, 2006), time-resolved optically stimulated luminescence (Chithambo *et al.*, 2016; Chithambo, 2018), radioluminescence (Poolton *et al.*, 2001; Shimizu *et al.*, 2006; Martini *et al.*, 2012),

and electron spin resonance (Toyoda and Ikeya, 1991; Walther and Zilles, 1994; Fujita and Hashimoto, 2007). Of these, thermoluminescence is the most common. Despite the extensive studies on thermoluminescence of quartz, different values of trap parameters are still being reported. The differences are attributed to origin of quartz, nature of quartz, impurities, and the methods used to derive the parameters of quartz (Yazici and Topaksu, 2003; Mebhah *et al.*, 2006). The luminescence properties of quartz and its application as a natural dosimeter is well documented in the review by Preusser *et al.* (2009).

2.2 Mechanism of luminescence

2.2.1 Luminescence processes and point defects

Natural quartz contain a number of point defects which can be intrinsic or extrinsic (Agulló-López *et al.*, 1988). Intrinsic point defects are due to silicon (Si) and oxygen (O) vacancies whereas the extrinsic defects are due to impurities. A vacancy refers to the absence of an atom from its crystalline position. The oxygen vacancy centres present in quartz are the E' and E'' centres (Preusser *et al.*, 2009). For the case of impurity point defects, elements such as Al, Fe, Ge, P, and Ti substitute for Si in quartz. Among the impurity related defects, Al ion is ubiquitous for quartz. Al^{3+} therefore substitutes for Si^{4+}. When the charge is compensated by an alkali ion, a hydrogen ion or a trapped hole, the resulting centres for the point defects are $[AlO_4/M^+]^0$, $[AlO_4/H^+]^0$, and $[AlO_4]^0$; where M is an alkali ion (M^+), H is a hydrogen ion and AlO_4 is a trapped hole respectively (Preusser *et al.*, 2009).

Luminescence can be induced by irradiation which transfers electrons or holes to certain extrinsic or intrinsic defects. These defects are termed electron traps and recombination centres. A simple energy band model as in Figure 1.4 can be used to describe luminescence in terms of point defects in quartz. The defects are labelled T and R termed trapping and recombination centres respectively. During irradiation, electrons are evicted from the valence band and are ionised into the conduction band leaving behind holes. The electrons can move freely in the conduction band and recombine with holes (transition 2) at the recombination centre. When an electron combines with a hole, energy is released as luminescence L. Alternatively, the electrons in the conduction band can be retrapped into the defect

trap T. Due to the natural state of quartz, the number and nature of defects is expected to vary due to the geological origin and history of individual quartz.

2.2.2 Ionic pair model

Itoh *et al.* (2002) proposed an ionic pair model to explain various aspects of luminescence in quartz. The model focusses on the so called 110 and 325 °C TL peaks in quartz. The 110 °C TL peak corresponds to emission at 380 nm whereas the 325 °C peak corresponds to emission at 420 nm. The model is based on the assumption that the energy giving rise to luminescence is stored by defect pairs rather than trapped electrons and holes. The defect pairs relating to the peaks are $[\mathrm{X/M^+}]^+$ and $[\mathrm{AlO_4}]^-$ centres. $[\mathrm{AlO_4}]^-$ is a substitutional centre whereas $[\mathrm{X/M^+}]^+$ is an interstitial ion centre (Itoh *et al.*, 2002). The mechanism is based on the dissociation and recombination of these centres.
According to Itoh *et al.* (2002), the 110 °C TL peak is produced by the reaction

$$[X/M^+]^0 \rightarrow [X/M^+]^+ + e^- \tag{2.1a}$$

$$[AlO_4/h^+]^0 + e^- \rightarrow [AlO_4]^- + \text{photon (380 nm)} \tag{2.1b}$$

and for the 325 °C TL peak, the reaction is

$$[X/M^+]^+ \rightarrow [M^+] + X \tag{2.2a}$$

$$[\mathrm{AlO_4}]^- + M^+ \rightarrow [\mathrm{AlO_4}/M^+]^0 + \text{photon (420 nm)} \tag{2.2b}$$

where $\mathrm{e^-}$ is the electron, $M^+]$ is alkali ion stabilised by defect X. X may be a Ti atom and $M^+]$ a Na atom.
The intensity of the 110 °C peak is proportional to the concentration of $[\mathrm{AlO_4/h^+}]^0$ and $[\mathrm{X/M^+}]^0$ defect pairs. Similarly, the intensity of the 325 °C peak is proportional to the concentration of $[\mathrm{AlO_4}]^-$ and $[\mathrm{X/M^+}]^+$ defect pairs produced by irradiation (Itoh *et al.*, 2002). Williams and Spooner (2018, 2020) observed that the application of the defect pair model by Itoh *et al.* (2002) is not limited to only 110 and 325 °C TL glow peaks. The ionic model can be applied on intermediate glow peaks occurring between 160 and 220 °C and are consistent with the defect pair model for 110 °C.

2.3 Kinetic analysis

Kinetic analysis is the analysis of thermoluminescence glow peaks in order to determine the physical parameters involved in the TL process. These aid in understanding the TL process. There are different methods used to extract the kinetic parameters from glow peaks. These are discussed in the sections that follow.

2.3.1 Initial rise method

The initial rise method, applicable to the rising edge of a well defined glow peak irrespective of its order of kinetics, is used to determine the activation energy. The method is based on the assumption that the amount of trapped electrons in the low temperature region of a glow peak is approximately constant.
Starting from first principles, the first-order kinetics of thermoluminescence is expressed as

$$I(T) = n_o s \exp\left(-\frac{E}{kT}\right) \exp\left[-\frac{s}{\beta}\int_{T_o}^{T} \exp\left(-\frac{E}{kT'}\right) dT'\right] \tag{2.3}$$

As the temperature increases in the initial rise portion of the peak, and as long as $T \cong T_o$, $\int_{T_o}^{T} \exp\left(-\frac{E}{kT'}\right) dT'$ in the second exponential is nearly zero giving

$$\lim_{T \to T_o} \exp\left[-\frac{s}{\beta}\int_{T_o}^{T} \exp\left(-\frac{E}{kT'}\right) dT'\right] \approx 1 \tag{2.4}$$

Equation (2.3) becomes

$$I(T) = n_o s \exp\left(-\frac{E}{kT}\right) \tag{2.5}$$

Similarly for a second and general order kinetics, as $T \cong T_o$, $\int_{T_o}^{T} \exp\left(-\frac{E}{kT'}\right) dT'$ in equations (1.25) and (1.28) is approximately zero. Thus, the temperature-dependent quantities within the square brackets of equations (1.25) and (1.28) are

equal to 1.

$$I(T) = \frac{n_o^2}{N} s \exp\left(-\frac{E}{kT}\right) \tag{2.6}$$

$$I(T) = n_o s'' \exp\left(-\frac{E}{kT}\right) \tag{2.7}$$

It is thus evident from equations (2.5) - (2.7) that $I(T) \propto \exp\left(-\frac{E}{kT}\right)$.

The thermolumoinescence emission in the initial rise region is now described as

$$I(T) = C \exp\left(-\frac{E}{kT}\right) \tag{2.8}$$

where C is the proportionality constant which is equal to sn_o, sn_o^2/N, and $s''n_o$ for first-, second-, and general- order kinetics respectively.

On taking the natural logarithm of both sides of equation (2.8), we have

$$ln\,(I) = C' - E\left(\frac{1}{kT}\right) \tag{2.9}$$

where E is the activation energy in eV, k the Boltzmann's constant in eV/K, and T the absolute temperature.
As a rule of thumb, the region of analysis for the initial rise method is between 5 and 15% of the maximum peak intensity, I_m (McKeever, 1985). Thus, if ln I is plotted as a function of $1/kT$, a straight line is obtained, with slope of magnitude E from which the activation energy E is found. The initial rise technique can only be used when the glow peak is well defined and clearly separated from other peaks.

2.3.2 Whole glow peak method

The whole glow peak method, also called the whole curve method is based on use of the area under the glow peak as shown in Figure 2.1. In the method, the area $n(T)$ under the whole glow peak from a given temperature in the initial rise region up to a final temperature T at the end of the glow peak is given by

$$n(T) = \frac{1}{\beta}\int_{T_o}^{T} I dT' \tag{2.10}$$

For a general order kinetics, equation (2.10) is transformed to

$$\ln\left(\frac{I}{n^b}\right) = \ln\left(\frac{s'}{\beta}\right) - \frac{E}{kT} \tag{2.11}$$

where s' ($\mathrm{cm}^{3(b-1)}$ s^{-1}) is the effective frequency factor for general order kinetics, b represents the order of kinetics, β is the heating rate, and T, the measurement temperature (Pagonis *et al.*, 2006). A plot of $\ln\left(I/n^b\right)$ against $1/kT$ for a specific value of b is expected to be linear, from which E can be evaluated from the slope and s' from the 'y' intercept.

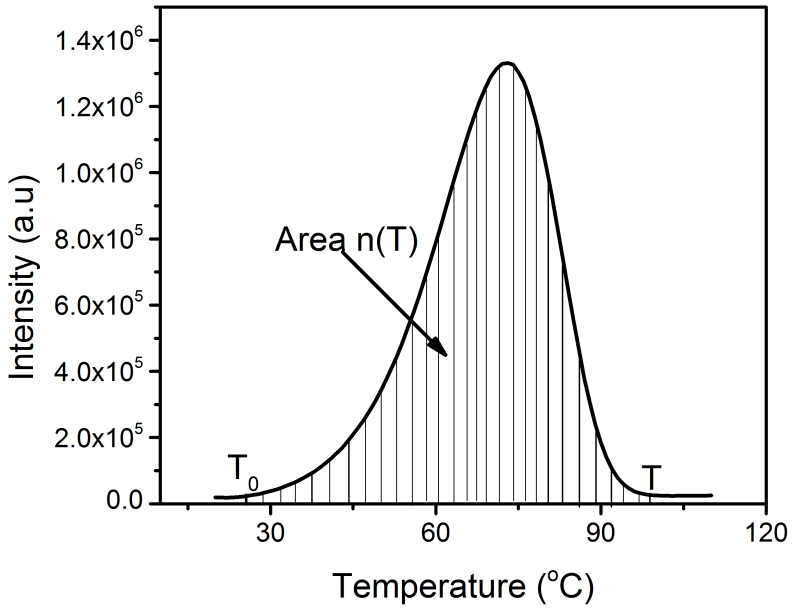

FIGURE 2.1: The area of a TL glow peak used in the calculation of kinetic parameters for the whole glow peak method. Figure produced from experimental data from quartz annealed at 1000 °C.

2.3.3 Variable heating rate method

The variable heating rate method, which depends on the change of peak position T_m with heating rate β is used in determining the activation energy and frequency factor (Chen and Mckeever, 1997). The frequency factor is a measure of how many times a trapped electron attempts to detach from its binding potential (Chithambo *et al.*, 2017b). To show the basis of the method, we consider the first-order kinetics

of thermoluminescence

$$I(T) = n_o s \exp\left(-\frac{E}{kT}\right) \exp\left[-\frac{s}{\beta}\int_{T_o}^{T} exp\left(-\frac{E}{kT}\right) dT\right] \tag{2.12}$$

The natural logarithm of equation (2.12) is

$$In(I) = \ln(n_o s) - \frac{E}{kT} - \frac{s}{\beta}\int_{T_o}^{T} exp\left(-\frac{E}{kT}\right) dT \tag{2.13}$$

At peak maximum, the condition $T = T_m$, $I = I_m$, and $\frac{dI}{dT} = 0$ holds. Thus,

$$\left[\frac{d}{dT}(\ln I)\right]_{T=T_m} = 0 + \frac{E}{kT_m^2} - \frac{s}{\beta}\exp\left(-\frac{E}{kT_m}\right) = 0 \tag{2.14}$$

Therefore,

$$\frac{E}{kT_m^2} = \frac{s}{\beta}\exp\left(-\frac{E}{kT_m}\right) \tag{2.15}$$

which when rearranged gives

$$\frac{T_m^2}{\beta} = \frac{E}{sk}\exp\left(\frac{E}{kT_m}\right) \tag{2.16}$$

Taking the natural logarithm of equation (2.16), one obtains

$$\ln\left(\frac{T_m^2}{\beta}\right) = \left(\frac{E}{K}\right)\frac{1}{T_m} + \ln\left(\frac{E}{sk}\right) \tag{2.17}$$

a linear relationship between T_M and β. Equation (2.17) is the Hoogenstraaten's equation for various heating rates (Hoogenstraaten, 1958). In applying equation (2.17), a graph of $\ln(T_m^2/\beta)$ against $1/kT_m$ should be linear with slope E as the activation energy and intercept $\ln(E/sk)$ from which the frequency factor s can be evaluated.

2.3.4 Peak shape method

In order to further ascertain the kinetic parameters E, s, and b of a glow peak, the peak shape method proposed by Chen (1969) can be used. In the method, the shape or geometrical properties of a peak are considered by utilising three temperature points on the glow peak, namely T_m, T_1, and T_2. A TL glow peak

corresponding to first-order kinetics is characterised by an asymmetrical shape whereas second-order peaks are symmetrical (Chen and Mckeever, 1997).

Figure 2.2 shows an example of a TL glow peak indicating the geometrical properties of a peak. The geometrical parameters are defined as

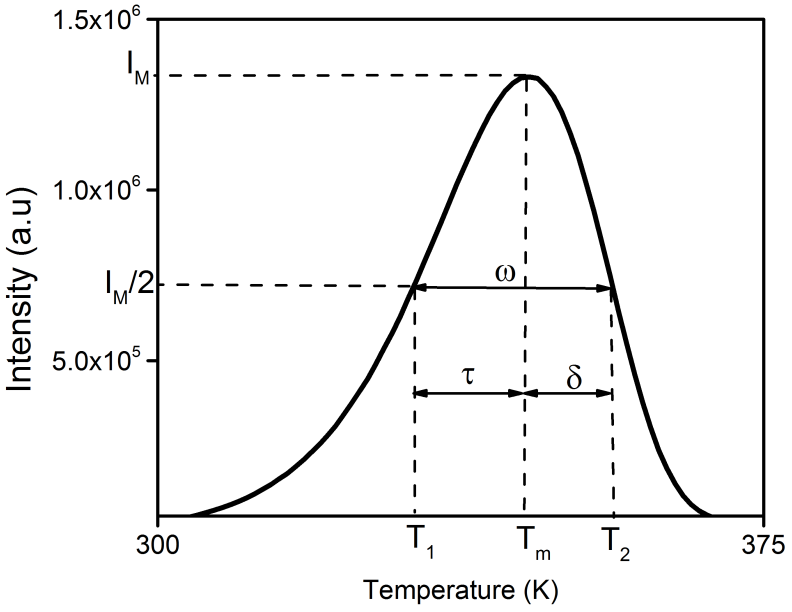

FIGURE 2.2: The geometrical shape of a TL glow peak with its properties. Figure produced from experimental data.

$$\tau = T_m - T_1, \quad \delta = T_2 - T_m, \quad \omega = T_2 - T_1 \tag{2.18}$$

where T_m is the maximum peak temperature, T_1 and T_2 are temperatures on either side of T_m corresponding to half-maximum intensity, τ is the half-width at the low temperature side of the peak, δ is the half-width at the fall off side of the glow peak, and ω the total half-width of the glow peak (Chen and Mckeever, 1997).

The activation energy for the peak is calculated using the general expression

$$E_\alpha = c_\alpha \left(\frac{kT_m^2}{\alpha} \right) - b_\alpha \left(2kT_m \right) \tag{2.19}$$

where α represents any of τ, δ, or ω (Chen, 1969).
The values of c_α and b_α for a general order case are

$$c_\tau = 1.510 + 3.0\,(\mu_g - 0.42)\,; \quad b_\tau = 1.58 + 4.2\,(\mu_g - 0.42) \tag{2.20}$$

$$c_\delta = 0.976 + 7.3\,(\mu_g - 0.42)\,; \quad b_\delta = 0 \tag{2.21}$$

$$c_\omega = 2.52 + 10.2\,(\mu_g - 0.42)\,; \quad b_w = 1 \tag{2.22}$$

The order of kinetics of the glow-peak depends on the geometrical or symmetry factor μ_g which is defined as

$$\mu_g = \frac{\delta}{\omega} \tag{2.23}$$

A first-order peak is characterised by $\mu_g = 0.42$ and a second-order peak by $\mu_g = 0.52$. However, the values of μ_g need not be equal to 0.42 and 0.52 for first- and second-order kinetics respectively. Values close to 0.42 and 0.52 within reasonable margin of error can be used.

2.3.5 Curve fitting method

The curve fitting method aims at evaluating the activation energy E, order of kinetics b, and frequency factor s of a glow curve. The activation energy and order of kinetics can be determined from the fitting whereas the frequency factor is determined mathematically by substituting the values of E, k, T_m and β.

The thermoluminescence data can be analysed using any of the following equations

developed by Kitis *et al.* (1998):

$$I(T) = I_m \exp\left[1 + \frac{E}{kT}\frac{T-T_m}{T_m} - \frac{T^2}{T_m^2}\left(1 - \frac{2kT}{E}\right) \times \exp\left(\frac{E}{kT}\frac{T-T_m}{T_m}\right) - \frac{2kT_m}{E}\right] \tag{2.24}$$

$$I(T) = 4I_m \exp\left(\frac{E}{kT}\frac{T-T_m}{T_m}\right) \times \left[\frac{T^2}{T_m^2}\left(1 - \frac{2kT}{E}\right)\exp\left(\frac{E}{kT}\frac{T-T_m}{T_m}\right) + 1 + \frac{2kT_m}{E}\right]^{-2} \tag{2.25}$$

$$I(T) = I_m b^{\frac{b}{b-1}} \exp\left(\frac{E}{kT}\frac{T-T_m}{T_m}\right) \times \left[1 + (b-1)\frac{2kT_m}{E} + (b-1) \times \left(1 - \frac{2kT}{E}\right)\left(\frac{T^2}{T_m^2}\exp\left(\frac{E}{kT}\frac{T-T_m}{T_m}\right)\right)\right]^{-\frac{b}{b-1}} \tag{2.26}$$

where all parameters have their usual meanings.

The expressions for equations (2.24), (2.25), and (2.26) above represent the first-, second- and general-order kinetics respectively.

These expressions are fitted to experimental data by providing the values of I_m and T_m from experimental data as initial guess parameters. The frequency factors for the first-, second-, and general-order kinetics are determined from equations (1.21), (1.26), and (1.29) respectively as

$$s = \frac{\beta E}{kT_m^2}\, exp\left(\frac{E}{kT_m}\right) \tag{2.27}$$

$$s = \frac{\beta E}{kT_m^2\left(1 + \frac{2KT_m}{E}\right)} \exp\left(\frac{E}{kT_m}\right) \tag{2.28}$$

$$s = \frac{\beta E}{kT_m^2\left(1 + \frac{2KT_m(b-1)}{E}\right)} \exp\left(\frac{E}{kT_m}\right) \tag{2.29}$$

The goodness of fit of the glow curve and reliability of the parameters is tested by the figure of merit (FOM) proposed by Balian and Eddy (1977) as

$$FOM = \frac{\sum \mid y_{exp} - y_{fit} \mid}{\Sigma_i\, y_{fit}} \times 100\% \tag{2.30}$$

where y_{exp} and y_{fit} are the data for the experimental and the fitted glow peaks respectively. A fit is acceptable if $FOM \leq 3.5\%$ (Gartia and Singh, 2011).

2.3.6 Phosphorescence

Phosphorescence involves the measurement of luminescence intensity with respect to time at a constant temperature. The graph of luminescence intensity versus time at constant temperature is called *an isothermal decay curve* or *a phosphorescence decay curve* (Chen and Mckeever, 1997). Phosphorescence decay can be analysed using the first-, second-, or general-order kinetics.

2.3.6.1 First-order decay

The first-order kinetics of phosphorescence decay is an exponential decay given by

$$I(t) = I_o \ \exp(-pt) \tag{2.31}$$

where I_o is the initial intensity, t is time, and p is the probability of thermal simulation given by

$$p(T) = s \ \exp\left(\frac{-E}{kT}\right) \tag{2.32}$$

To verify that the kinetics is of first-order in TL, a plot of $I(t)$ as a function of time on a semilogarithm scale would produce a straight line with slope $-p$ (Chen and Mckeever, 1997). To obtain the activation energy and frequency factor, the isothermal decay is monitored at different temperatures T such that a plot of intensity $I(t)$ against t on a semilogarithm scale produces a slope p for each temperature. Thereafter, one takes the natural logarithm of equation (2.32) to obtain the linear relation

$$\ln \ p(T_i) = -\frac{E}{kT_i} + \ln \ s \tag{2.33}$$

for different values of T.
Finally, a plot of $\ln \ p$ against $1/kT_i$ is required to give the activation energy E determined from the slope. The frequency factor s is found directly from the intercept $\ln \ s$.

2.3.6.2 Second-order decay

The equation governing the second-order decay of phosphorescence is defined as

$$I = -\frac{dn}{dt} = p'n^2 \tag{2.34}$$

where $p' = s' \exp(-E/kT)$.
Integrating both sides of equation (2.34), we have

$$n = \frac{n_o}{1 + p'n_o t} \tag{2.35}$$

By substituting equation (2.35) for n in equation (2.34), we obtain the expression

$$I(t) = \frac{p'n_o^2}{(1 + p'n_o t)^2} \tag{2.36}$$

The solution of equation (2.34) is therefore given as

$$I(t) = \frac{I_o}{(1 + p'n_o t)^2} \tag{2.37}$$

Rearranging, we have

$$\sqrt{I_o/I(t)} = 1 + p'n_o t \tag{2.38}$$

A plot of $\sqrt{I_o/I(t)}$ against t would give a straight line of slope $n_o p' = n_o s' \, exp(-E/kT)$. If a straight line is established, E and s' can be evaluated by taking the natural logarithm of the slope $n_o p'$ and varying the temperature just like in the first-order case.

2.3.6.3 General-order decay

For a general order decay, the governing equation is

$$I(t) = -\frac{dn}{dt} = p'n^b \tag{2.39}$$

where b, a measure of the order of kinetics, is a constant that has values ranging between 0.7 and 2.5 (Chen, 1969; Chen and Mckeever, 1997).

Integrating equation (2.39), we obtain the expression

$$n = [n_o^{1-b} + (b-1)p't]^{1/1-b} \tag{2.40}$$

At a constant temperature T, equation (2.39) gives the solution

$$I(t) = \frac{n_o^b\, p'}{(1+(b-1)p'\, n_o^{b-1}t)^{b/(b-1)}} \tag{2.41}$$

Equation (2.41) is also a decaying function of time, where $b \neq 1$, n_o is the initial concentration of charge undergoing isothermal decay and other variables maintain their previously defined meanings. It is important to note that if $b = 2$, equation (2.41) reduces to equation (2.38), a second-order decay characterised by the linear relationship between $\sqrt{I_o/I(t)}$ and time t.

Equation (2.41) can be simplified as

$$I/I_o = \left[1 + (b-1)p'\, n_o^{b-1}t\right]^{b/(1-b)} \tag{2.42}$$

which leads to

$$[I/I_o]^{(1-b)/b} = 1 + (b-1)p'\, n_o^{b-1}t \tag{2.43}$$

The general-order feature of the phosphorescence decay can be demonstrated by a plot of $[I/I_o]^{(1-b)/b}$ against t which results in a straight line with slope a given by

$$a = n_o^{b-1}(b-1)p' = n_o^{b-1}(b-1)s'\, \exp\left(-\frac{E}{kT}\right) \tag{2.44}$$

The correct value of b inserted into equation (2.42) will produce the best straight line. When the phosphorescence decay is measured at different temperatures, several values of slope a will be obtained. The activation energy is then determined from the slope of a graph of ln a against $1/kT$.

2.3.6.4 Temperature-dependence method based on area under an isothermal decay curve

Chithambo (2014) developed a technique for the analysis of phosphorescence based on the use of the temperature-dependence of the area under an isothermal decay-curve. The technique is not limited to use of areas corresponding to two measurement temperatures as in the method of Furetta (2010). The method, with multiple applications, is derived from a first-order process and is most suitable to calculate the activation energy in the case of first-order kinetics and in limiting cases of general-order kinetics. In addition, the method allows for the analysis of the area under an isothermal decay curve using the curve fitting method by Kitis (2001) to obtain the activation energy and the order of kinetics. Lastly, the method is used in the study of thermal quenching based on the dependence of the area under an isothermal decay curve on the measurement temperature.

Chithambo (2014) described this technique using the area under an isothermal decay curve shown in Figure 2.3 and considered the Randall and Wilkins (1945) equation

$$\frac{dn}{dt} = -np \tag{2.45}$$

where n is the concentration of trapped electrons and p is the probability of thermal stimulation as previously defined in equation (2.32).

Using equation (2.45), the area ϕ under an isothermal decay-curve measured between t and t' at temperature T can be written as

$$\frac{d\phi}{dt} = -\phi p \tag{2.46}$$

where $t' = t - t_a$ and $t_a > t$, ϕ is the area underneath the segment $|(t - t_a)|$ of an isothermal decay curve (Chithambo, 2014). It then follows that,

$$\phi = \phi_m \exp(-pt') \tag{2.47}$$

where ϕ_m is the total area and other parameters are as previously defined.
Noting that $(t - t_a) < 0$ and $e^x \approx 1 + x$, after the approximation $\phi_m (1 - pt') \sim$

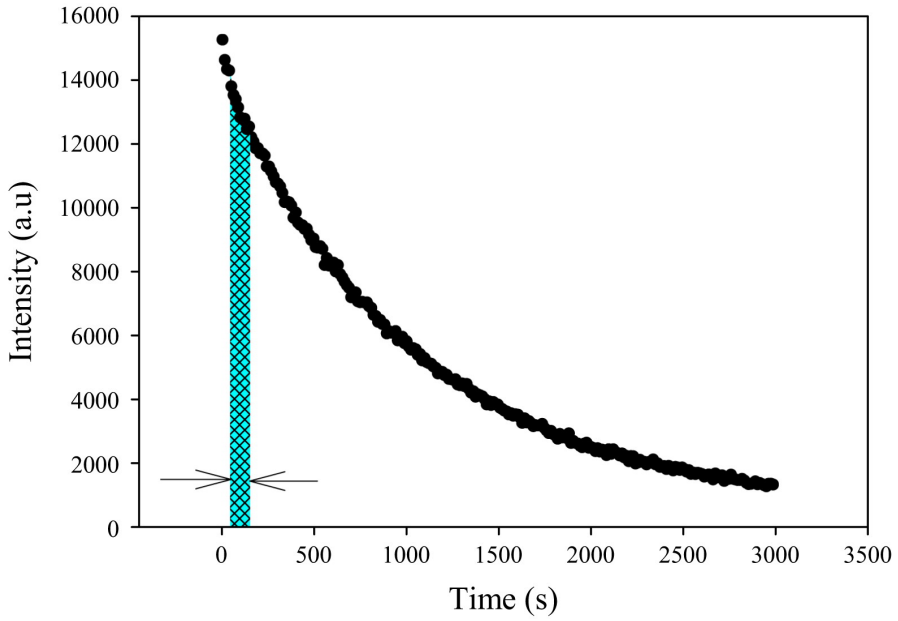

FIGURE 2.3: An isothermal decay curve showing a portion of the area under the decay curve for isothermal analysis. Figure reproduced from Chithambo (2014)

$\phi_m pt'$, equation (2.47) can be simplified to

$$\phi = \phi_m \left(t - t_m\right) s \, \exp\left(-\frac{E}{kT}\right) \tag{2.48}$$

which is expressed simply as

$$\phi = B \, \exp\left(-\frac{E}{kT}\right) \tag{2.49}$$

where B is a constant equal to $\phi_m \left(t - t_m\right) s$.Plotting ϕ against $1/kT$ on a semilogarithm scale will yield a straight line with a slope E equal to the activation energy.

2.3.6.4.1 Analysis of the temperature-dependent areas by curve fitting

When ϕ is plotted against temperature, it produces a TL-like glow peak. This curve can then be analysed using equation (2.26) of the Kitis *et al.* (1998) glow-curve deconvolution method expressed simply as

$$\phi(T) = \phi_m b^{\frac{b}{b-1}} \exp\left(\frac{E}{kT}\frac{T-T_m}{T_m}\right) \times \left[1 + (b-1)\frac{2kT_m}{E} + (b-1) \times \left(1 - \frac{2kT}{E}\right)\left(\frac{T^2}{T_m^2}\exp\left(\frac{E}{kT}\frac{T-T_m}{T_m}\right)\right)\right]^{-\frac{b}{b-1}} \tag{2.50}$$

where T_m is only a dummy variable representing the maximum of the peak, ϕ_m is the area corresponding to the peak maximum, b is the order of kinetics, and other parameters have their usual meanings.

2.4 Peak resolution methods

Some of the methods described above e.g. initial rise, whole glow peak, peak shape methods can only be applied to a glow peak that is well defined and clearly separated from other peaks. However, in the case where overlapping peaks are present thereby, rendering some of the peaks unisolated and ill defined, it becomes necessary to employ the peak separation techniques suggested by McKeever (1985) before applying any of the methods of kinetic analysis.

2.4.0.1 Thermal cleaning

Thermal cleaning is a peak separation technique used to obtain a clear rising edge of a glow peak. It also helps in determining the number of peaks in a glow curve. As the peaks are being separated through thermal cleaning, any concealed peaks become visible.

In the technique as described by McKeever (1985), a sample irradiated to a specific dose is heated to a temperature above the temperature of the first peak that needs to be cleaned. In this way, the traps responsible for the peak are emptied. The sample is thereafter cooled rapidly to room temperature and reheated to a final temperature in order to record the whole glow curve. The procedure is repeated

by irradiating the sample to the same dose and then heating the sample to a temperature just beyond the maximum of the next peak, and so on throughout the whole glow curve. At the end of each cycle, a clean rising edge of the next glow peak is likely to be seen in the whole glow curve recorded.

2.4.0.2 T_m - T_{stop} method

The $T_m - T_{stop}$ technique is used to monitor the position of the TL peak as the temperature T_{stop} is increased. The technique consists of heating a previously irradiated sample at a linear heating rate to a temperature T_{stop} corresponding to a position on the low temperature tail of the first glow peak. The sample is then cooled to room temperature and reheated at the same heating rate to measure the whole glow curve. The procedure is repeated on a freshly irradiated sample with a T_{stop} increased at every 2 or 3 °C (McKeever, 1985).

A graph of T_m against T_{stop} is used to determine the order of kinetics of a peak. For a first-order peak, T_m is expected to be independent of T_{stop} indicating that T_m is independent of the initial concentration of trapped charges. For a second-order peak, T_m increases with T_{stop} (McKeever, 1985).

2.5 Thermal quenching

A decrease of luminescence intensity with heating rate is a general phenomenon for the presence of thermal quenching in luminescent materials (Chen and Pagonis, 2011). Thermal quenching occurs as a decrease in the luminescence efficiency with increasing temperature (Wintle, 1975). This effect can be observed in several luminescence experiments e.g. radioluminescence (Wintle, 1975; Pagonis *et al.*, 2014), optically stimulated luminescence (McKeever *et al.*, 1997; Chithambo and Costin, 2017), thermoluminescence (Nanjundaswamy *et al.*, 2002) in which luminescence is monitored as a function of measurement temperature. In TL studies, thermal quenching effect is manifest when a set of glow curves is measured at various heating rates. As the heating rate increases, the glow peaks are observed to shift to higher temperatures. If thermal quenching is present, the peak height and the peak area decreases with heating rate (Gorbics *et al.*, 1969). In the absence of thermal quenching, the peak height remains constant with increasing heating

rate. However, if the peak height and peak area increases with heating rate, an inverse thermal quenching behaviour is eminent.

Two models namely the Mott-Seitz and Schön-Klasens mechanisms have been developed to describe the phenomenon of thermal quenching(Chen and Pagonis, 2011). The Mott-Seitz mechanism is described using a configuration coordinate diagram shown in Figure 2.4.
In the mechanism, electrons captured into the excited state of the recombination centre undergo either a radiative recombination route for the emission of light or a non-radiative recombination route for the emission of phonons only. The non-radiative route is thermally assisted into the ground state of the recombination centre giving up a phonon energy W otherwise referred to as the activation energy for thermal quenching. With the assumption of the radiative and non radiative processes competing within the confines of the recombination centre (Chen and Pagonis, 2011), the temperature dependence of the excited state lifetime τ is given by

$$\frac{1}{\tau} = \frac{1}{\tau_{rad}} + \nu \exp\left(-\frac{W}{kT}\right) \tag{2.51}$$

where τ_{rad} is the lifetime for radiative transitions and ν is a frequency factor (Bøtter-Jensen *et al.*, 2003). The luminescence decay time is thus given by

$$\tau = \frac{\tau_{rad}}{1 + \nu\tau_{rad} \exp(-W/kT)} \tag{2.52}$$

The ratio of the probability of the radiative transition to the total transition is thus defined as the luminescence efficiency η and mathematically expressed as

$$\eta = \frac{\tau}{\tau_{rad}} = \frac{1}{1 + C \exp(-W/kT)} \tag{2.53}$$

where $C = \nu\tau_{rad}$ (Bøtter-Jensen *et al.*, 2003).

As Gorbics *et al.* (1969) pointed out, if the luminescence intensity measured as peak height as well as peak integral reduces with heating rate, thermal quenching effect is evident in the material studied. Following this fact, the radiative luminescence intensity I can be expressed as

$$I_q = \frac{I_{uq}}{1 + C \exp(-W/kT)} \tag{2.54}$$

where I_q and I_{uq} represent the most quenched and lesser quenched intensities measured at the highest and other heating rates respectively.

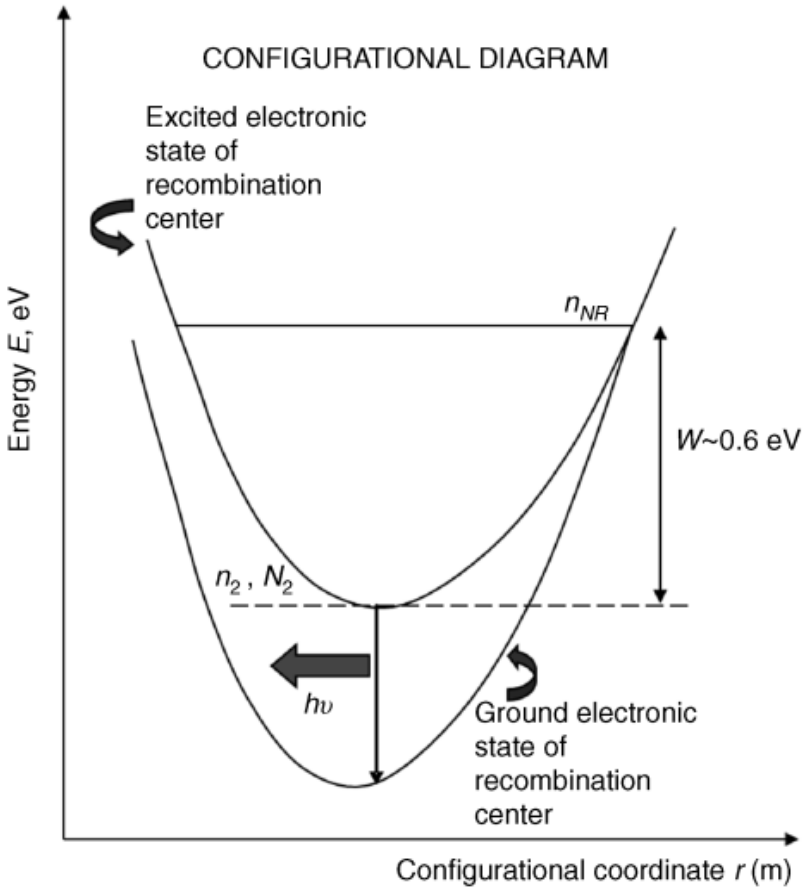

FIGURE 2.4: The configurational coordinate diagram describing the Mott-Seitz mechanism of thermal quenching. Figure reprinted from Chen and Pagonis (2011)

2.5.1 Analysis of thermal quenching using the area under an isothermal decay-curve

In analysing the area under an isothermal decay curve for thermal quenching, Chithambo (2014) stated that, if a TL peak is affected by thermal quenching, then the area ϕ_q under the isothermal decay-curve at a corresponding temperature T

will be related to the unquenched ones ϕ_{uq} by definition as

$$\phi_q = \frac{\phi_{uq}}{1 + C\ \exp(-\Delta E/kT)} \tag{2.55}$$

where ϕ_q is defined as the area corresponding to the highest measurement temperature T_q and ϕ_{uq} as areas corresponding to all other measurement temperatures T_{uq} in the rising edge of the graph of ϕ against measurement temperature.
The value of the activation energy for thermal quenching ΔE can be determined from the slope of the graph of $\ln(\phi_q/\phi_{uq})$ against $1/kT$.

Chapter 3

Phototransferred thermoluminescence

Phototransferred thermoluminescence (PTTL) is the thermoluminescence produced from shallow electron traps as a result of transfer, by light, of charge from deeper electron traps (Alexander *et al.*, 1997; Chen and Mckeever, 1997). PTTL has been studied in a wide variety of materials including quartz e.g. (Milanovich-Reichhalter and Vana, 1990, 1991; Wintle and Murray, 1997; Santos *et al.*, 2001; Bertucci *et al.*, 2011; Chithambo *et al.*, 2018) and is a useful tool in radiation dosimetry and dating of ceramic materials (Bailiff *et al.*, 1977; Alexander *et al.*, 1997).

The procedure for producing PTTL consists of four steps namely irradiation, preheating, illumination, and heating. The sample to be studied is first irradiated at room temperature to fill electron traps. The irradiation creates electron-hole pairs. Electrons are trapped at the various traps whereas holes are trapped at the recombination centre. The trapped electrons at a specific electron trap are then removed by heating the sample to a temperature high enough to empty that trap. This is otherwise called preheating. After the trap has been emptied by preheating, the sample is cooled to room temperature and then exposed to light of a specific wavelength for a time t. This illumination transfers charge from the deep (or source) traps to the empty shallower ones. Some of the charges recombine at the recombination centre producing optically stimulated luminescence (if radiative). The last step is heating the sample to a final temperature in order to monitor the presence of any PTTL from the shallower electron traps.

3.1 Models of phototransferred thermoluminescence

In order to observe phototransferred thermoluminescence in any material, there must be at least two electron traps - one deep trap which serves as the source trap for the electrons during illumination, and one shallow acceptor trap. A hole trap which acts as a radiative recombination centre is also required.

3.1.1 The simple model: Two traps and one centre model

The simplest model used to describe phototransferred thermoluminescence is shown in Figure 3.1. The diagram consists of one shallow trap (level 1) into which the charge is transferred, one deep trap (level 2) from which the charge is excited, and one recombination centre (level 3) (Alexander *et al.*, 1997; Alexander and McKeever, 1998). The concentrations of electrons in the shallow and deep traps are denoted by n_1 and n_2 respectively, and the concentration of holes in the recombination centre as m.

Alexander and McKeever (1998) described the transport of electrons from the deep traps to the shallower traps at the irradiation, preheating, illumination and heating stages. They described the process in terms of coupled non-linear differential equations. These equations have no analytical solution. The equations set up require numerical approximations which were then used to generate plots of illumination time dependent plots of the PTTL intensity taking into account various assumptions such as negligible retrapping. In summary, the method of Alexander and McKeever (1998) is based on computational simulation.

The analysis of the PTTL here has two initial conditions. The first is that the initial concentration of electrons in the shallow trap is zero i.e. $n_{10} = 0$. The second condition states that the initial concentration of electrons in the deep trap is equal to the initial concentration of holes in the recombination centre i.e. $n_{20} = m_0$. These occur at some point after sample irradiation and immediately at the start of the illumination. The condition for charge neutrality is

$$n_c + n_1 + n_2 = m \tag{3.1}$$

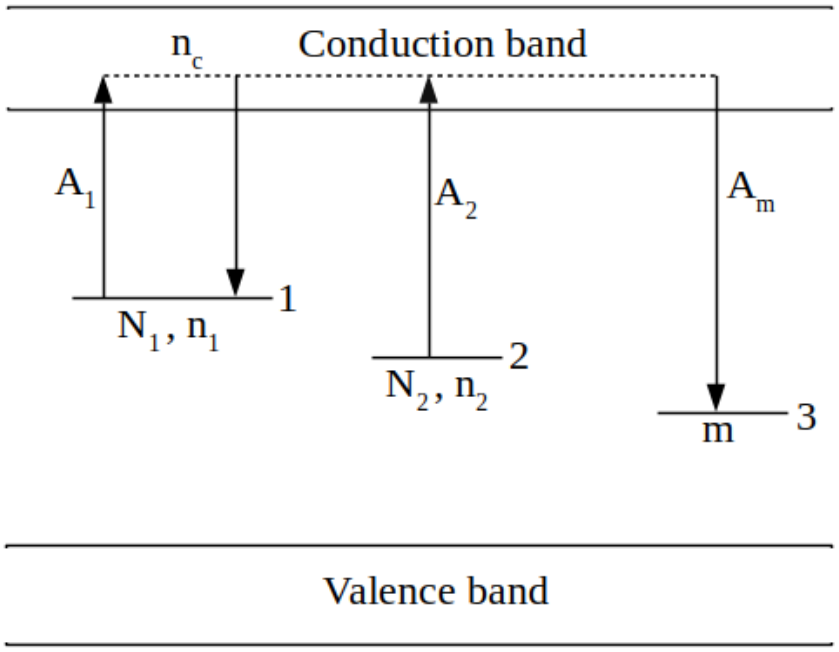

FIGURE 3.1: A simple model of PTTL composed of one shallow trap (level 1), one deep trap (level 2), and one recombination centre (level 3). Figure reproduced from Chen and Mckeever (1997).

During illumination, electrons are excited from the deep traps at a rate $f = \sigma\Phi$ (where σ is the photoionisation cross-section and Φ the photon flux). The transport of charge between electron traps and to the recombination centre is described by the following sets of equations

$$\frac{dn_2}{dt} = -n_2 f_2 + n_c(N_2 - n_2)A_2 \tag{3.2}$$

$$\frac{dn_1}{dt} = n_c(N_1 - n_1)A_1 \tag{3.3}$$

$$\frac{dm}{dt} = -n_c m A_m = \frac{m}{\tau} \tag{3.4}$$

where $\tau = (n_c A_m)^{-1}$ is the lifetime, A_m the recombination probability, A_1 and A_2 are the trapping probalitites for the shallow and deep traps respectively and n_c is the concentration of free electrons.

With the assumptions of quasi-equilibrium (i.e. $dn_c/dt \ll dn_i/dt, dm/dt; i = 1, 2$) and no retrapping into the source or deep trap such that $n_2 f_2 \gg n_c(N_2 - n_2)A_2$

and $n_c(N_1 - n_1)A_1 \propto n_2 f$, the solution to equations (3.2) - (3.4) are given by

$$n_2(t) = n_{20} \exp(-ft) \tag{3.5}$$

$$n_1(t) = N_1[1 - \exp(-Bt)] \tag{3.6}$$

$$m(t) = m_0 \exp\left(-\frac{t}{\tau}\right) \tag{3.7}$$

where $B = n_c A_1$ and τ are approximately constant only if the quasiequilibrium approximation $dn_c/dt \approx 0$ holds (Chen and Mckeever, 1997). At the end of the illumination period, where $t = t^*$, it is expected to have a certain concentration of charges in each of the traps and recombination centre as defined by equations (3.5) - (3.7).

Now considering heating of sample after illumination to yield a PTTL signal, one takes into account the competition for the released charges to either retrap in empty deep traps (i.e. $N_2 - n_2(t^*)$) or recombine with trapped holes (i.e. $m(t^*)$). Assuming also a state of quasiequilibrium such that $n_1(t^*) \ll N_2 - n_2(t^*)$, the area under the PTTL peak is given by

$$S(t^*) = \frac{C^* m(t^*) n_1(t^*)}{N_2 - n_2(t^*)} \tag{3.8}$$

where C^* is a constant.

Substituting equations (3.5), (3.6), and (3.7) into equation (3.8), the variation in the PTTL peak as a function of illumination time is described by

$$S(t^*) = \frac{C \exp(-t^*/\tau) N_1[1 - \exp(-Bt^*)]}{N_2/n_{20} - \exp(-t^* f)} \tag{3.9}$$

Equation (3.9) describes a monotonically increasing function of the PTTL signal.

3.1.2 Two traps and two centres model

An alternative model to describing PTTL is shown in Figure 3.2 (Alexander *et al.*, 1997; Alexander and McKeever, 1998). The model consists of one shallow trap (level 1), two deep traps with one optically active (level 2) and the other optically inactive (level 3), one radiative recombination centre (level 4) and a non-radiative recombination centre (level 5). The non-radiative recombination centre provides

a competing recombination pathway. With the addition of the new traps to the existing simple model, the conditions of charge neutrality become

$$n_c + n_1 + n_2 + n_3 = m_4 + m_5 \tag{3.10}$$

where n_1, n_2, and n_3 are the concentrations of electrons in the electron traps, and m_1 and m_2 are the concentration of holes in the radiative and non-radiative recombination centres respectively. During illumination, holes are removed from the

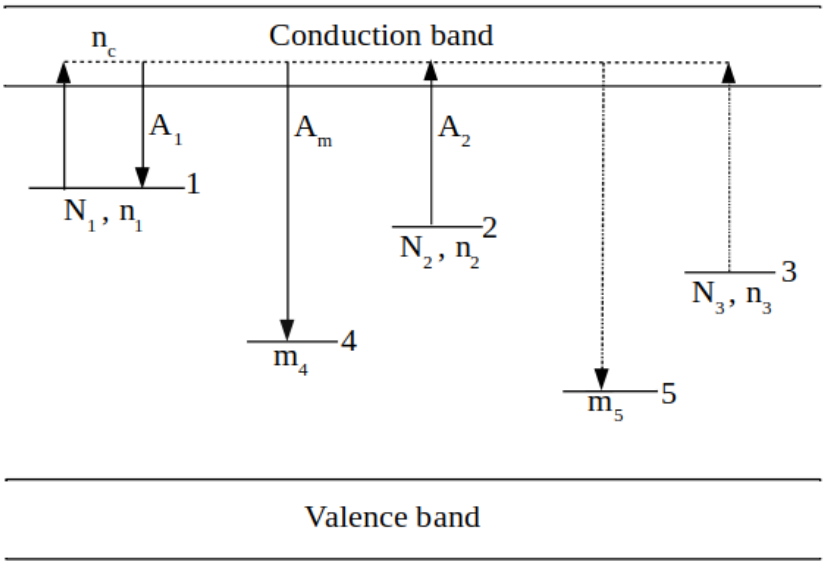

FIGURE 3.2: A complex model to describe PTTL, cotaining a shallow trap (level 1), an optically active deep trap (level 2), a deep optically inactive trap (level 3), a radiative recombination centre (level 4), and a nonradiative recombination centre (level 5). Figure reproduced from Chen and Mckeever (1997)

radiative recombination centre. As the illumination time increases, there exists a reduction in the PTTL signal due to the holes removal. A similar occurrence is seen in the simple model, although $n_1 \leqslant m$ due to the neutrality condition (3.1). It follows that although n_1 increases during illumination, there will always be enough holes available such that the PTTL signal follows n_1.

In the model, n_1 may be less or greater than m_4 according to the neutrality condition (3.10). This implies that even though n_1 may be increasing, there may be, at a particular illumination time, insufficient holes in the radiative recombination centre to allow for an increase. Although the total number of available holes $(m_4 + m_5)$ will always be greater or equal to the number of electrons in the shallow traps, the PTTL signal will only be dominated by m_4 (Alexander *et al.*, 1997;

Chen and Mckeever, 1997). Thus, at the start of the illumination, the number of electrons in the shallow traps n_1 will be less than the number of holes in the radiative recombination centre m_4. It is thus expected that the PTTL intensity will grow as n_1 increases. At longer illumination times, n_1 may become greater than m_4. If this occurs, the PTTL intensity will be proportional to m_4 and decreases as m_4 decreases. The PTTL intensity is now described by

$$S = min(n_1, m_4) \tag{3.11}$$

Alexander *et al.* (1997) stated clearly that equation (3.11) becomes invalid when there is competition and multiple recombination pathways for the electrons. The resultant PTTL area is only accounted for by solving numerically the given set of conditions and parameter values.

3.1.3 Wintle and Murray (1997) Model

Wintle and Murray (1997) used the model shown in Figure 3.3 to describe the dependence of PTTL intensity on duration of illumination. The concentration of eletrons in the deep and shallow traps are denoted by N_1 and N_2 respectively. Electrons are optically stimulated out of the deep trap (level 1) to the conduction band at a stimulation rate λ_1. The electrons are then transferred to the shallow trap (level 2) at a rate λ_2. PTTL is produced when electrons from the shallow trap recombine with holes at the recombination centre (level 3). The transport of electrons from the deep and shallow traps are described using a set of rate equations

$$\frac{dN_1}{dt} = -\lambda_1 N_1 \tag{3.12}$$

$$\frac{dN_2}{dt} = -\lambda_2 N_2 - a\frac{dN_1}{dt} = -\lambda_2 N_2 + a\lambda_1 N_1 \tag{3.13}$$

where equation (3.12) refers to the rate of optical stimulation of electrons from the deep trap, and equation (3.13) is the rate of loss of electrons from the acceptor trap. The constant a represents that a fraction of the electrons stimulated from the deep trap is retrap at the acceptor trap (Wintle and Murray, 1997).

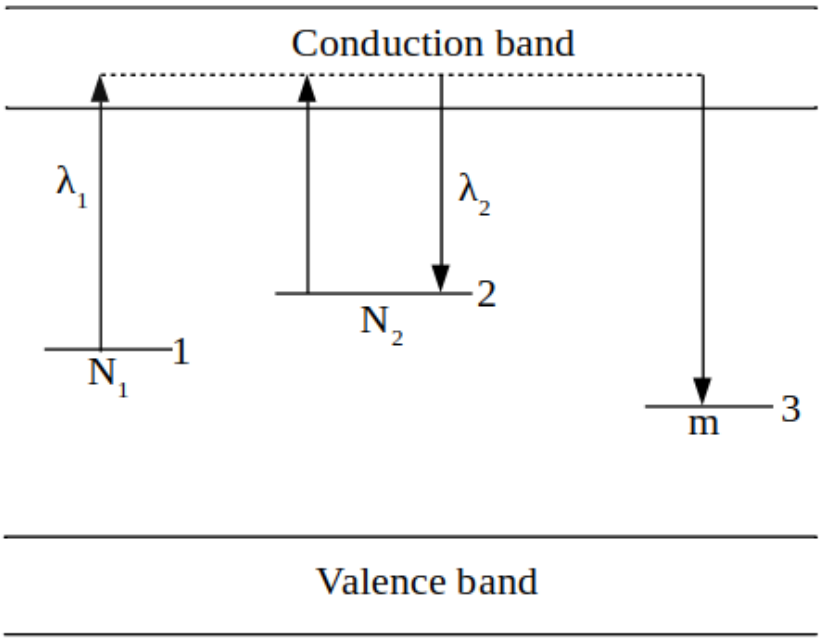

FIGURE 3.3: A simple one trap one recombination centre model for PTTL.

If the acceptor is initially empty, the solution to equations (3.12) and (3.13) is

$$N_2 = \frac{a\lambda_1 N_o}{\lambda_2 - \lambda_1}[e^{-\lambda_1 t} - e^{-\lambda_2 t}] \tag{3.14}$$

where N_o is the number of electrons initially stored in the deep trap. It is thus assumed that the PTTL signal recorded after illumination is proportional to N_2.

3.1.4 Phenomenological model of Chithambo et. al (2017)

A phenomenological model to describe PTTL was reported by Chithambo *et al.* (2017a). This is shown in Figure 3.4 as applied to α-Al_2O_3 :C. The model consists of one shallow trap (level 1), one main trap (level 2), an intermediate electron trap (level 3), one deep trap (level 4), one hole trap, and one recombination centre. These levels are decided by experiments.

In contrast with the models of Alexander *et al.* (1997); Alexander and McKeever (1998) or Wintle and Murray (1997), the phenomenological model of Chithambo *et al.* (2017a) describes a system of multiple acceptors and multiple donors. The transport of electrons from the donor to the acceptor is described at the illumination stage only. Experimentally, the number of electron traps acting as acceptors

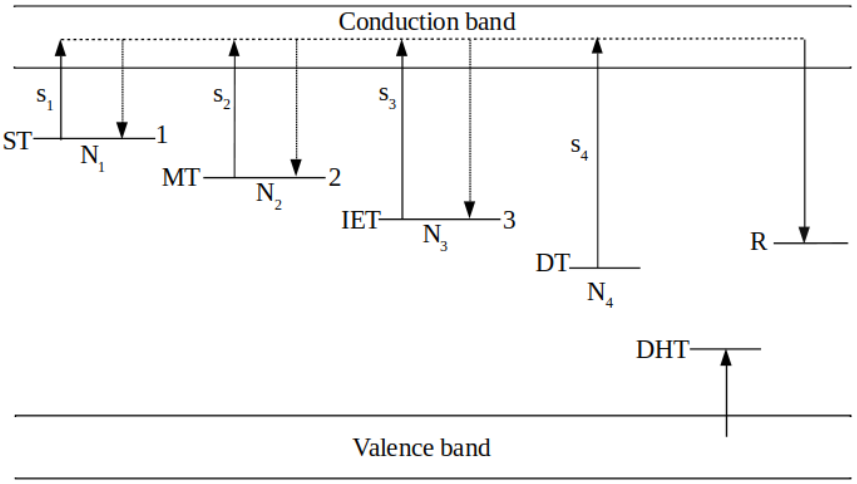

FIGURE 3.4: A phenomenological model used to describe PTTL. The symbols ST, MT, IET, and DT represent the shallow-, main-, intermediate-energy, and deep electron traps whereas DHT stand for deep hole trap. Figure reproduced from Chithambo *et al.* (2017a) but slightly modified.

or donors changes with preheating temperature. If only one peak is removed by preheating an irradiated sample to T_i, all electron traps corresponding to peaks after the removed peak can act as donors. If two or more peaks are removed by preheating, the removed peaks can act as acceptors. The number of donors decreases depending on preheating. The rate equations are set up invoking two assumptions, namely that retrapping is negligible and secondly, that only a portion of electrons is transferred to the acceptor trap during illumination.

In the case of α-Al_2O_3 :C studied by Chithambo *et al.* (2017a) for this model, three peaks were seen after measuring the thermoluminescence glow curve. When the first peak was removed by preheating, it was reproduced under phototransfer following illumination. The electron traps corresponding to the reproduced peak act as an acceptor, whereas those corresponding to peaks beyond the first peak as well as the deep trap act as donors.

The transport of charge from the donor traps to the shallow trap is described by

the following coupled linear differential equations

$$\frac{dN_2}{dt} = -s_2 N_2 \tag{3.15}$$

$$\frac{dN_3}{dt} = -s_3 N_3 \tag{3.16}$$

$$\frac{dN_4}{dt} = -s_4 N_4 \tag{3.17}$$

$$\frac{dN_1}{dt} = -s_1 N_1 + a_1 s_2 N_2 + a_2 s_3 N_3 + a_3 s_4 N_4 \tag{3.18}$$

where s_1 represents the stimulation of electrons from the acceptor trap, and s_2, s_3, s_4 denote the electron stimulation from the donor traps at the designated levels (Chithambo *et al.*, 2017a). The stimulation probability $s = \Phi\sigma$ where Φ is the photon flux and σ is the photoionisation cross-section (Bøtter-Jensen *et al.*, 2003). Equation (3.18) states that a portion of electrons released from each donor is captured at the acceptor.

The solution of the coupled linear differential equations (3.15) - (3.18) is

$$N_1 = A_1(e^{-s_2 t} - e^{-s_1 t}) + A_2(e^{-s_3 t} - e^{-s_1 t}) + A_3(e^{-s_4 t} - e^{-s_1 t}) \tag{3.19}$$

where $A_1 = a_1 s_2 N_{2i}/s_1 - s_2$, $A_2 = a_2 s_3 N_{3i}/s_1 - s_3$, $A_3 = a_3 s_4 N_{4i}/s_1 - s_4$. N_{2i}, N_{3i}, and N_{4i} are each the initial concentration of electrons at the donor and deep traps. a_1, a_2, and a_3 are constants of proportionality. Equation (3.19) describes a system of one acceptor and three donors. It is assumed just as in Wintle and Murray (1997) model that the PTTL intensity $I(T)$ is proportional to the concentration of electrons at the acceptor trap i.e. $I(T) \propto N_1$.

A system of one acceptor and one donor results if one peak is reproduced after the removal of all other peaks in the TL glow curve. The model for this system is described by the coupled equations

$$\frac{dN_i}{dt} = -s_i N_i \tag{3.20}$$

$$\frac{dN_1}{dt} = -s_1 N_1 + a s_i N_i \tag{3.21}$$

The time-dependence of the occupancy of the acceptor trap is

$$N_1 = A(e^{-s_i t} - e^{-s_1 t}) \tag{3.22}$$

where i represents any of level 2, 3, or 4 of the donor electron traps, $A = as_iN_{i0}/s_1 - s_i$, a is a constant of proportionality, N_{i0} is the initial concentration of electrons at the donor electron traps after illumination, and other parameters have the same meanings. The model can be adapted for any number of acceptors and donors describing PTTL in any material.

3.2 Competition effects in PTTL

The conventional discussion of PTTL assumes that as electrons are released from donor or source traps during illumination, they can either transit to recombination centres, get re-trapped or move to the acceptor traps. This assumption helps to facilitates mathematical description in PTTL for a number of acceptors and donors. It is worth noting that phototransfer is subject to competition effects. By this we mean processes that enhance or depress the capture of charge at electron traps during illumination, and how this affects the output from acceptors or contribution of donors. These effects are based on experimental results.
Competition effects have been described for PTTL in α-Al_2O_3 :C (Chithambo *et al.*, 2017a) and natural quartz (Chithambo *et al.*, 2019).

Chapter 4

Experimental Details

This chapter describes the sample and the equipment details used for the experiments in this study. The equipment used in this study is a Risø TL/OSL-DA-20 Luminescence Reader.

4.1 Instrumentation

The instrument used for irradiation, stimulation, and the detection of luminescence in this study is the Risø TL/OSL-DA-20 Luminescence Reader. The instrument enables measurement of both thermoluminescence (TL) and optically stimulated luminescence (OSL).

The Risø system consists of two units, the Reader and the Controller. Figure 4.1 shows the essential components of the Reader. The components include the light detection system, the luminescence stimulation system and the irradiation source. These components will be described in detail in the sections that follows.

The Controller is responsible for proper timing of commands to be executed and controls the performance of the hardware components of the Reader (Nutech, 2015). The Controller shows the current status of the system and displays the command currently being executed e.g. sample positioning, error checking, irradiation, OSL, etc. It also reveals failure messages and invalid commands. Figure 4.2 shows a picture of the controller for the Risø Reader.

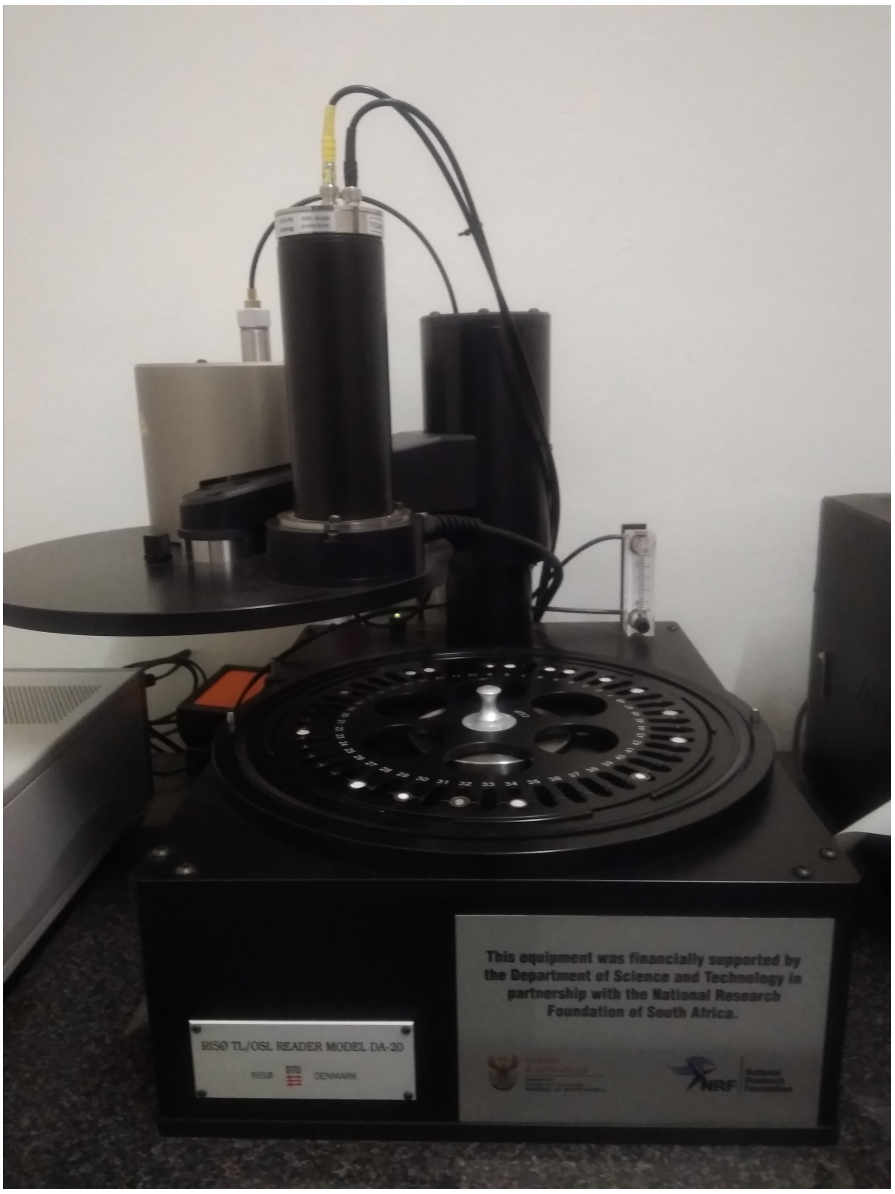

FIGURE 4.1: A picture of the Risø TL/OSL-DA-20 Luminescence Reader.

FIGURE 4.2: A picture of the Controller.

4.1.1 Light detection system

The light detection system comprises of the photomultiplier tube (PMT) and the detection filters. The emitted luminescence is detected by a photomultiplier tube whereas the detection filters shield the PMT from scattered stimulation light.

4.1.1.1 Photomultiplier tube

The photomultiplier tube (PMT) in the Risø TL/OSL reader used for this study is a blue/UV sensitive bialkali EMI 9235QB photomultiplier tube, operated in photon counting mode. It has maximum detection efficiency between 200 and 400 nm, making it suitable for detection of luminescence from both quartz and feldspar (Nutech, 2015). Figure 4.3 illustrates the efficiency of the PMT as a function of wavelength.

4.1.1.2 Detection filters

Detection filters are primarily used to define the spectral range of the measured luminescence. The filters also help to prevent scattered stimulation light from

reaching the PMT when measuring the emitted luminescence. For quartz samples, luminescence is measured through a 7.5 mm thick Hoya U-340 filter (transmission band 280 - 390 nm). Quartz has a strong emission centred on 365 nm (near UV) (Nutech, 2015).

4.1.2 Luminescence stimulation system

Our Risø TL/OSL reader has two luminescence stimulation systems namely, a heating system that can be used for TL measurements, and a light stimulation system that can be used for OSL measurements. The two stimulation sources can be used in combination e.g. OSL at elevated temperature is possible.

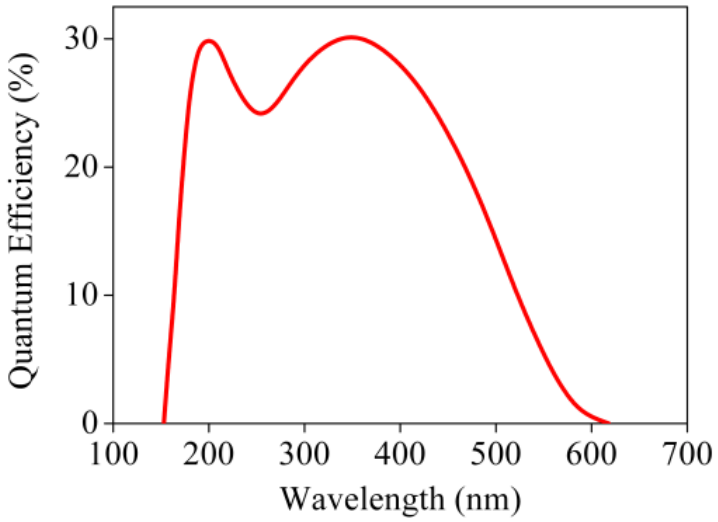

FIGURE 4.3: Quantum efficiency of the PMT as a function of wavelength. Reprinted from Nutech (2015).

4.1.2.1 Heating system

The heating system, comprising of the heating element and lift mechanism, is located directly underneath the position of the photomultiplier tube. The heating element plays two roles. One is to heat the sample and the other is to lift the sample into the measurement position (Nutech, 2018). The heating system is shown in Figure 4.4. The heater strip is made of a high resistance alloy, shaped with a depression to provide good heat transmission to the sample and to lift it securely and reproducibly into the measurement position. Heating is accomplished

by feeding a controlled current through the heating element (Nutech, 2018). The heating system is capable of heating up samples from room temperature up to 700 °C at constant heating rates ranging from 0.1 to 10 Ks^{-1}. The heating strip for the Risø system is cooled by a nitrogen flow, which also protects the heating system from oxidation at high temperatures (Nutech, 2015).

FIGURE 4.4: A picture of the heater at position 15 with the sample carousel in place.

4.1.2.2 Light stimulation system

The light stimulation system also called the optical stimulation system uses light emitting diodes (LEDs) as the light stimulation sources. LEDs are so chosen for optical stimulation mainly because of their long lifetime and stability (Nutech, 2018). The LEDs offer the possibility of stimulation at different intensities and varying the stimulation intensity as a function of stimulation time (Nutech, 2015). The LEDs for our Risø TL/OSL Reader are the blue-, green-, and infrared (IR) LEDs. The LEDs are arranged in clusters. Each cluster contains seven LEDs. The blue LEDs have a peak emission at 470 nm (FWHM = 20 nm) and an optical power density of 80 $mWcm^{-2}$ at sample position. The green LEDs emit at 525 nm (FWHM = 30 nm) with a maximum power density of 40 $mWcm^{-2}$ at sample position. For the IR LEDs, the wavelength and power density are 850 nm (FWHM

= 33 nm) and 300 mWcm^{-2} respectively. The LED modules can be operated in continuous wave and linear modulation modes.

4.1.3 Irradiation source

Irradiation of samples in this study is done using an inbuilt ^{90}Sr/^{90}Y beta source in the Risø system. The beta source emits beta particles with a maximum energy of 2.27 MeV and a half life of 28 years. The activity of the source is about 1.48 GBq which corresponds to a dose rate of 0.10 Gys^{-1}. The irradiation is software controlled. Before the start of the irradiation, the carousel is rotated to position the sample disc directly below the irradiation source.

4.2 Samples

Natural quartz of grain size 90 - 250 μm commercially available from BDH Ltd (UK) was used. The same quartz have been used previously for thermoluminescence and luminescence lifetimes investigations (Chithambo and Galloway, 2000; Galloway, 2002; Chithambo, 2014, 2015; Chithambo *et al.*, 2016; Thomas and Chithambo, 2018). The samples used for this study were unannealed quartz as well as quartz annealed at 800 and 1000 °C for 10 minutes and for 1 hour in each case. The quartz samples were all annealed at the various temperatures before use in order to remove any residual luminescence and to improve their sensitivity to thermal stimulation.

For each measurement, a few milligrams of the quartz sample was placed on a stainless steel sample disc of 1 mm thickness and 10 mm diameter with the aid of silicon spray. The sample was then placed at a given position on the carousel. The carousel can accommodate up to 48 samples which are individually heated and irradiated. Once the sample is placed on the carousel, the irradiation, stimulation and detection of the luminescence signal are software controlled through the program *Sequence Editor*.

Chapter 5

Thermoluminescence of unannealed natural quartz

This chapter reports and discusses the results obtained from thermoluminescence (TL) measurements conducted on unannealed natural quartz. The kinetic analysis of the main and secondary peaks is reported. The dosimetric features of the main peak is also presented. Unless otherwise stated, all quartz samples were irradiated to 50 Gy.

5.1 General features of the TL glow curve

The unannealed sample was first heated to 500 °C at a heating rate of 1 °Cs^{-1}. Figure 5.1 shows the natural glow curve consisting of two peaks at 238 and 286 °C. The occurrence of natural TL prior to laboratory irradiation is an evidence of sensitivity of the material to natural irradiation (Chithambo *et al.*, 2017b). The background signal (open symbol) recorded on a second TL readout is shown in Figure 5.1.

The same aliquot from which the natural TL was measured was then irradiated to 50 Gy and heated to 500 °C also at 1 °Cs^{-1}. The glow curve produced after this measurement is shown in Figure 5.2. The glow curve shows a prominent peak at 72 °C. Plotting the TL data on a semilogarithmic scale reveals five other peaks as shown in the inset. Thus, the thermoluminescence peaks obtained in the glow curve measured after a dose of 50 Gy are at 72, 122, 174, 254, 280, and 418

°C labelled I, II, III, IV, V, and VI respectively. The positions of these peaks were verified using the thermal cleaning technique which was described in section 2.4.0.1.

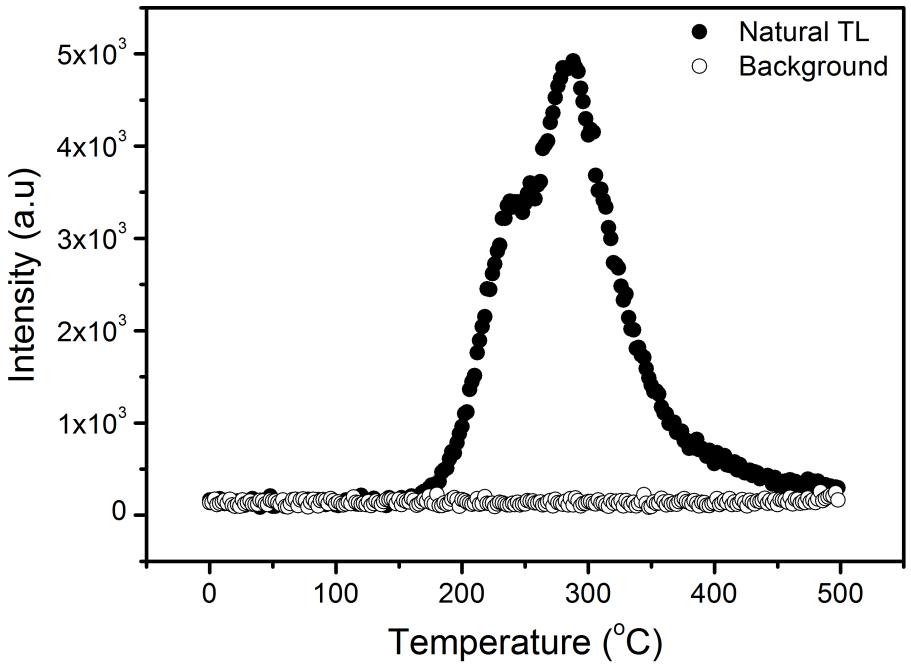

FIGURE 5.1: A thermoluminescence glow curve for natural TL obtained at first readout without irradiation. A background signal obtained at second readout of TL measurements is shown as open symbol.

5.2 Thermal cleaning

The thermal cleaning method (McKeever, 1985) was used to determine the number of isolated peaks in the glow curve in Figure 5.2. In the procedure, a quartz sample irradiated to 50 Gy was first heated to 500 °C. Peak I at 72 °C appears. Thereafter, the sample freshly irradiated, was partially heated to 100 °C to remove peak I, cooled, and reheated to 500 °C. This revealed peak II at 122 °C. The procedure was repeated by preheating the sample to 150 °C to remove peaks I and II. The glow curve measured after removal of these two peaks showed peak III at 174 °C. To determine the position of peak IV, the sample irradiated to the same dose of 50 Gy was preheated to 210 °C to erase peaks I - III. Peak IV was found at 254

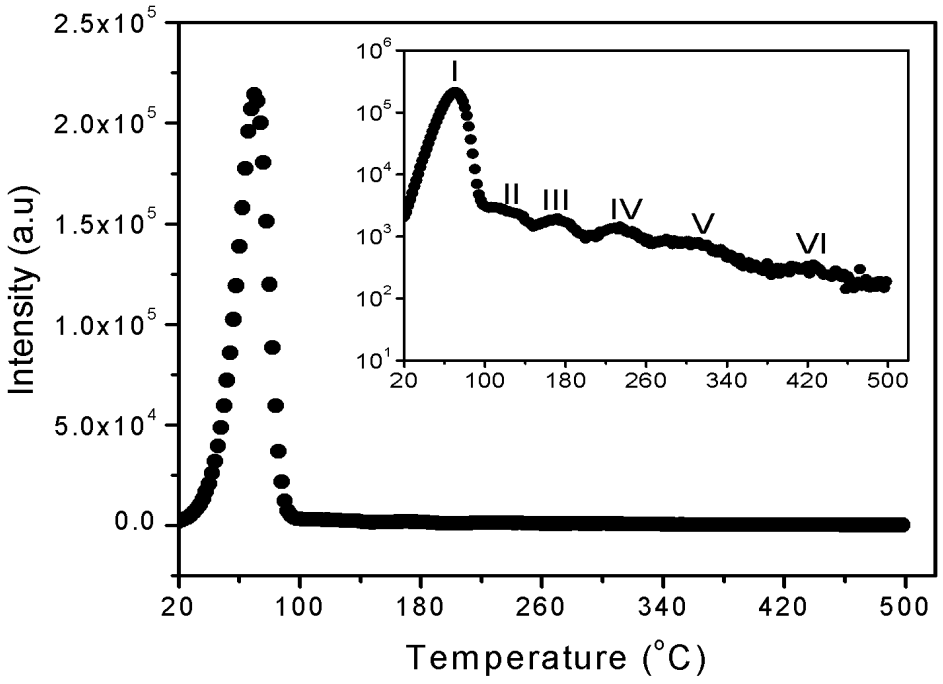

FIGURE 5.2: A thermoluminescence glow curve of the unannealed quartz measured at 1 °Cs^{-1} after a dose of 50 Gy. The inset shows the presence of other peaks on a semilogarithmic scale.

°C. Peak V and an ill-defined peak VI were found at 280 and 416 °C respectively after preheating the irradiated sample to 270 and 370°C to remove peaks I - IV and peaks I - V respectively. Figure 5.3 shows the results of thermal cleaning.

5.3 Dosimetric features

For a material to be considered a good dosimeter, its luminescence signal should be properly reproducible, ideally not fade or if so only slowly and it must have a linear dose response. These dosimetric features were studied on the main peak (peak I) of the unannealed quartz.

5.3.1 Reproducibility

The ability of a TL material to replicate its response under identical experimental conditions is termed reproducibility. Peak I was investigated for reproducibility by

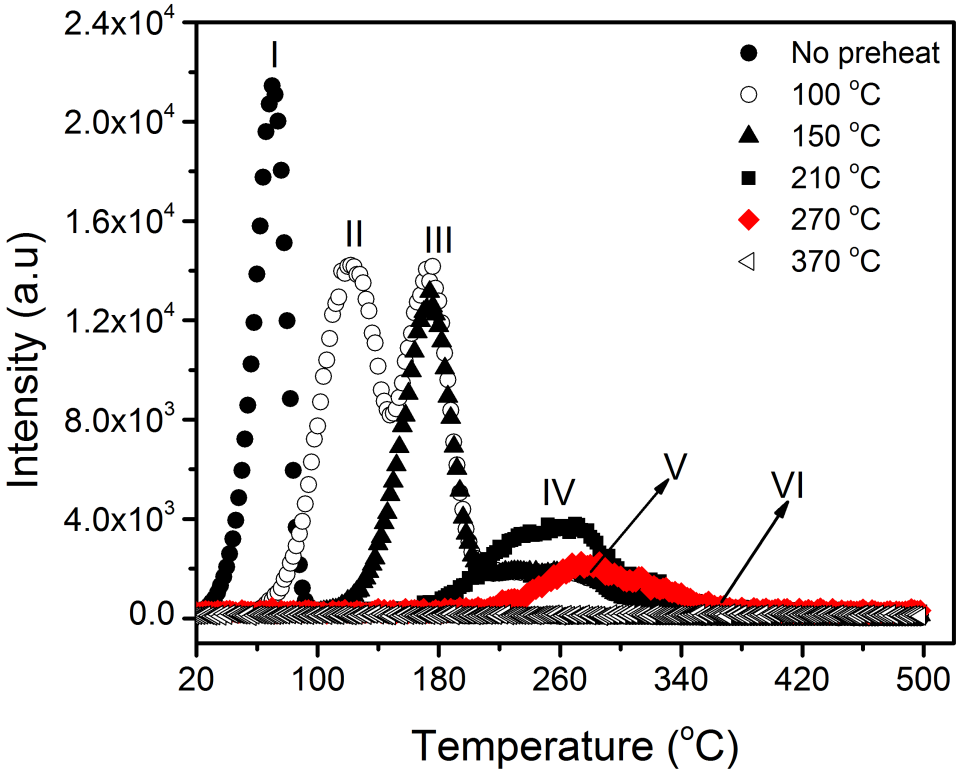

FIGURE 5.3: A plot of TL intensity against temperature for the thermal cleaning technique used to verify the positions of peaks I, II, III, IV, V, and VI with no preheating and after preheating to 100, 150, 210, 270, and 370 °C respectively. The data corresponding to no preheating was reduced by 10. Data corresponding to preheating to 210 and 270 °C have been scaled up by ×2 to aid visual clarity.

making series of TL measurements on a single aliquot of the unannealed sample. The same aliquot of unannealed quartz used previously was irradiated to 50 Gy and heated to 500 °C at 1 °Cs^{-1} to measure the TL signal. This procedure was repeated ten times and the intensity, as well as the peak position T_m was noted for peak I. Figure 5.4 shows the influence of repetitive measurements on the peak positions of the main TL peak. The position of peak I was stable at 72.0 ± 0.1 °C. Thus, peak I is unaffected by re-use of the sample. Similarly, the variation of the intensity of peak I with measurement number is shown in Figure 5.5. The intensity of peak I (noted as peak height) increases with repeated measurements. This increase can be attributed to the changes in the sensitivity of the sample due to repeated irradiation and heating otherwise called pre-dose effect (McKeever *et al.*, 1985; Yang and McKeever, 1990). In order to further ascertain the reproducibility

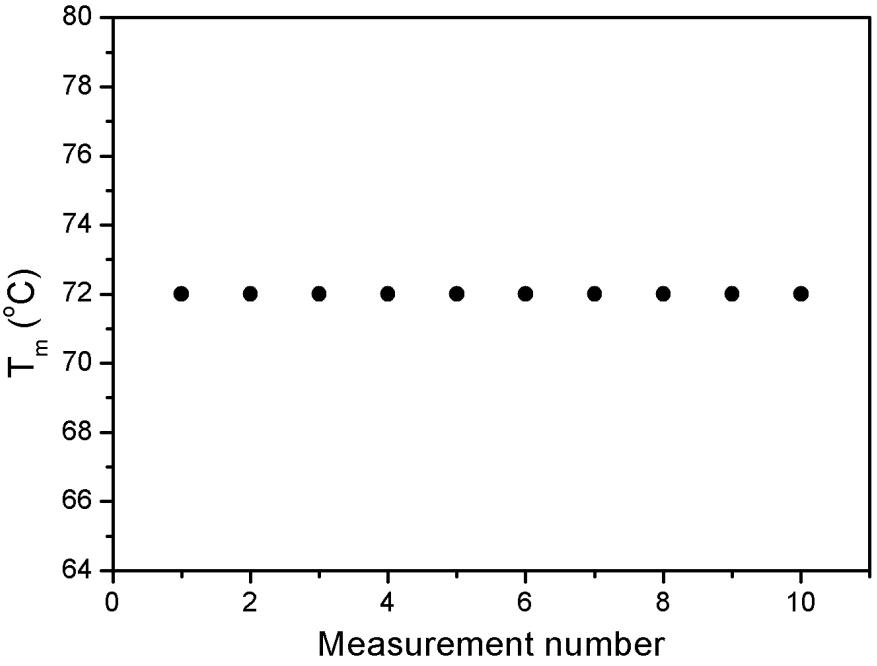

FIGURE 5.4: A graph of T_m against repeated measurements for peak I.

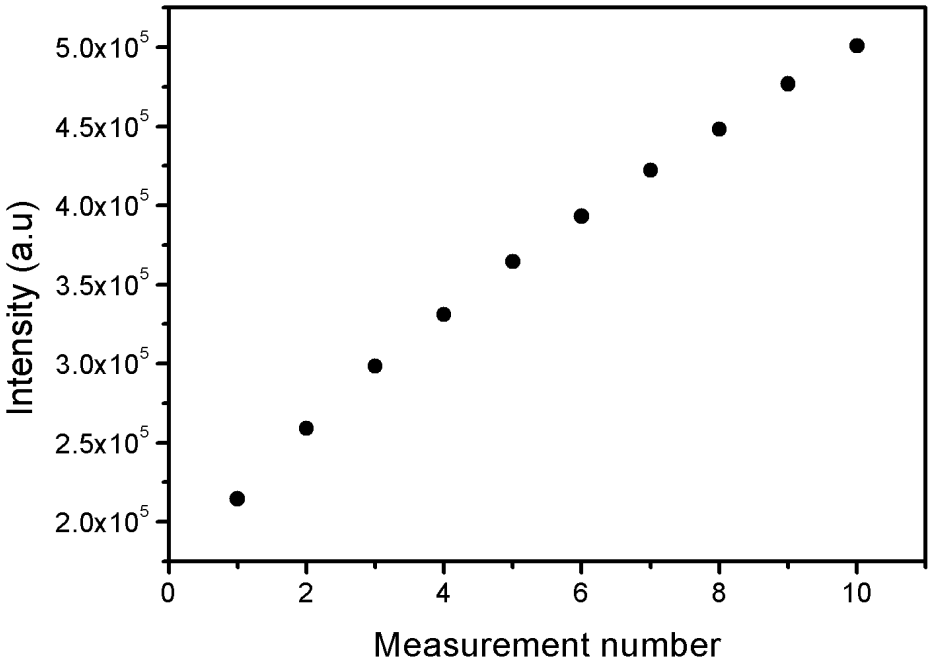

FIGURE 5.5: The maximum intensity of peak I against repeated measurements.

of the TL signal for peak I, the coefficient of variation (CV) for the peak intensity was determined. CV was calculated as $6.04 \pm 0.80\%$. For dosimetry purposes, a TL system is said to be reproducible if CV $\leq 5\%$ (Furetta, 2010). Based on this criterion, peak I is not reproducible as evident from the plot in Figure 5.5.

5.3.2 Fading

Fading of a TL signal occurs as a result of escape of electrons from an electron trap between irradiation and measurement. This causes the TL intensity to decrease or fade between irradiation and measurement. For this study, the intensity of peak I was monitored for different durations between irradiation and measurement up to 5 hours. Figure 5.6 shows the change of TL intensity with delay for peak I measured after a dose of 50 Gy. The intensity fades with delay. The data is fitted with the function

$$I = I_0\, exp(-t/\tau) \tag{5.1}$$

where t is the delay time, τ is the mean lifetime, and I_0 is the initial intensity. The intensity of peak I decreases exponentially with time with a mean lifetime of 3443 s as evaluated from the fit.

5.3.3 Dose response

The dose response, that is, the dependence of TL intensity on irradiation dose is of great importance in dating applications and radiation dosimetry (Pagonis *et al.*, 2006). In order to investigate the dose response of peak I, the quartz was exposed to different doses of irradiation ranging between 10 and 300 Gy. Figure 5.7 shows the dependence of peak intensity on dose for peak I. The intensity increases monotonically with dose up to 100 Gy and then decreases towards saturation.
The dose response of Figure 5.6 for the main peak was qualitatively modelled as

$$y(D) = A(1 - e^{-BD}) - CDe^{-BD} \tag{5.2}$$

where D is the dose in Gy, A (in arbitrary units) is the TL response at saturation, B and C (in Gys^{-1}) are constants.

The quantitative analysis of the dose response was done by using the superlinear-

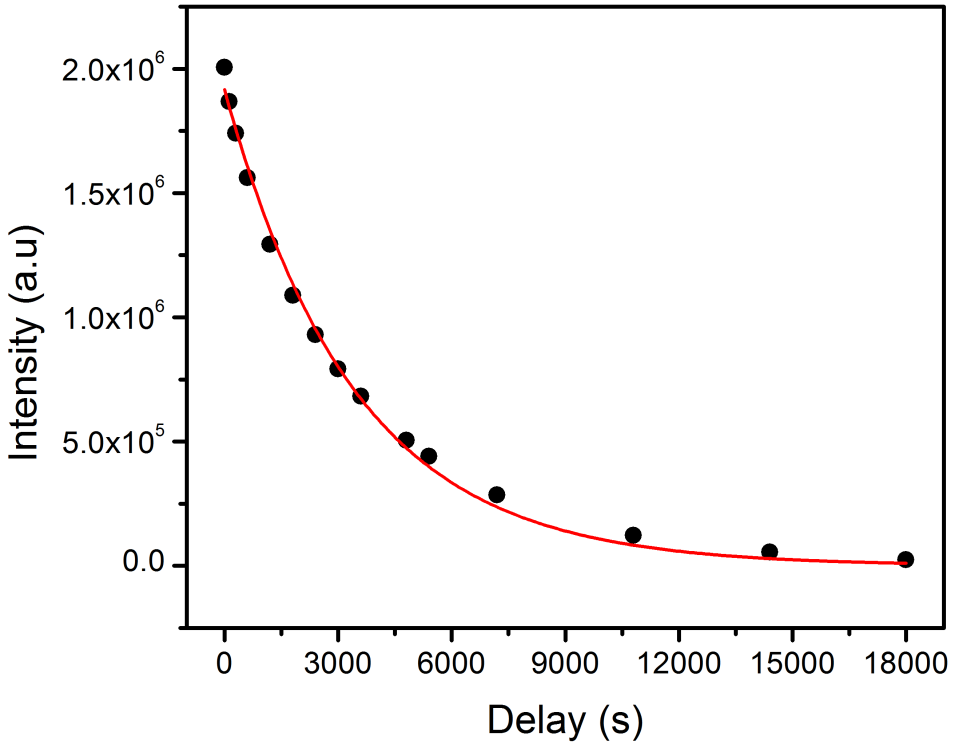

FIGURE 5.6: The variation of the TL intensity with delay time between irradiation and measurements. The solid line between data points is the best fit of Eq. 5.1.

ity and supralinearity indices. The superlinearity index gives an indication of the change in the slope of the dose response whereas the supralinearity index expresses the amount of deviation from linearity. The superlinearity index $g(D)$ is defined as

$$g(D) = \frac{Dy''(D)}{y'(D)} + 1 \tag{5.3}$$

whereas the supralinearity index $f(D)$ is defined as

$$f(D) = \frac{y(D)/D}{y(D_1)/D_1} \tag{5.4}$$

where D represents the dose in Gy, $y(D)$ is the intensity as a function of dose, D_1 is the normalization dose in the initial linear range of $y(D)$ curve, $y'(D)$ and $y''(D)$ are respectively, the first and second derivatives of the function $y(D)$. A value of $g(D) = 1$ signifies a linear dose response whereas $f(D) \sim 0$ indicates a

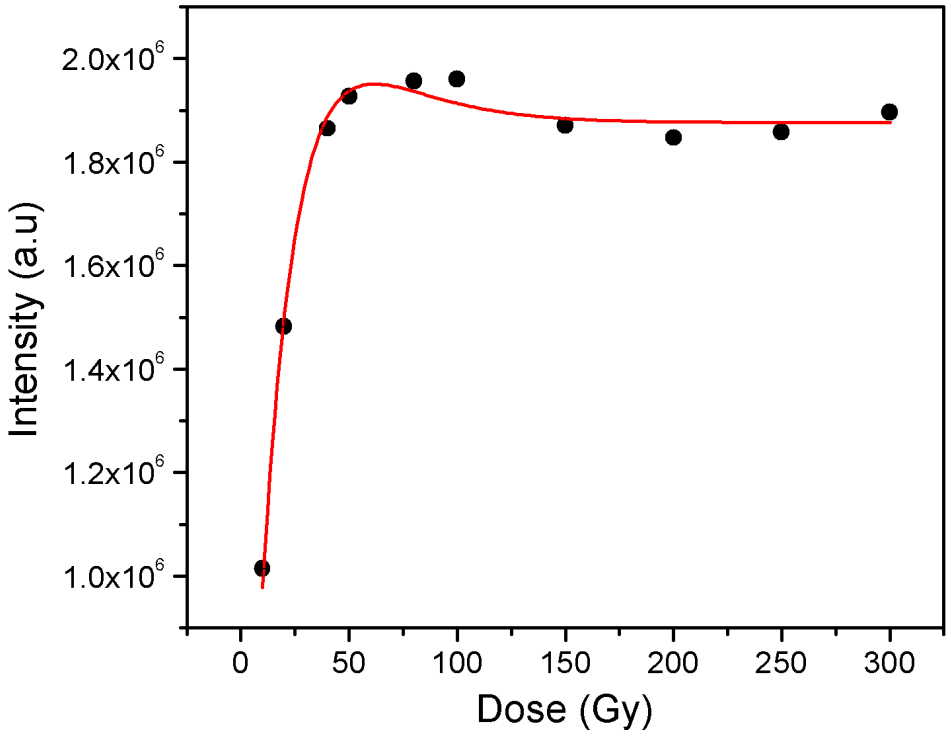

FIGURE 5.7: The influence of dose on the maximum intensity of peak I. The line passing through the data points is the best fit of Eq. (7.1).

saturation region. For sublinearity, both $g(D)$ and $f(D) < 1$, whereas $g(D) > 1$ and $f(D) > 1$ denote superlinearity (Pagonis *et al.*, 2006). Figure 5.8 shows the plots of super- and supra- linearity index against dose response for peak I. The figure shows that the dose response is sublinear for both g(D) and f(D) between 10 and 300 Gy.

5.4 Assessing the order of kinetics

In order to assess the order of kinetics of the main peak, the method based on the influence of dose on peak position and the $T_m - T_{stop}$ method were used.

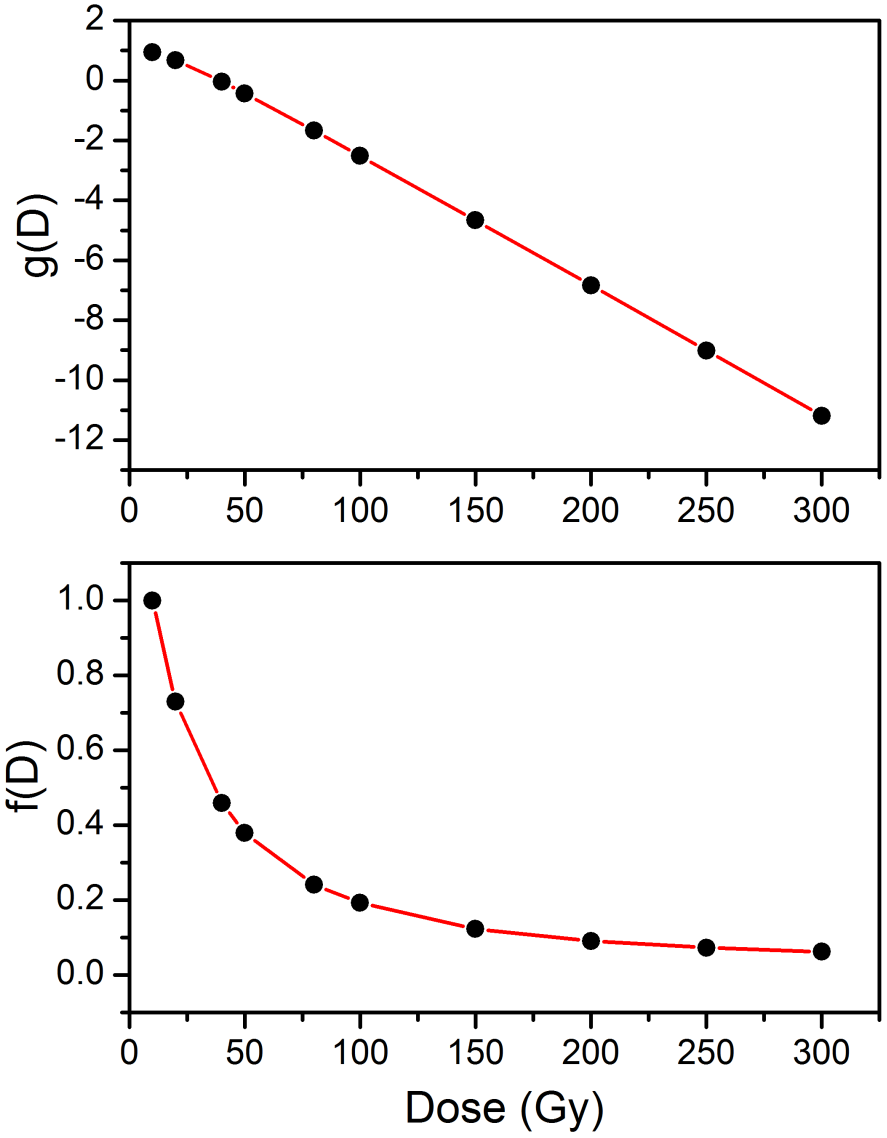

FIGURE 5.8: Plots of superlinearity and supralinearity indices against dose for peak I.The solid lines passing through the data points are the best fits of Eq. (5.3) and (5.4).

5.4.1 Influence of dose on peak position

The order of kinetics of the main peak was assessed using the dependence of peak position T_m on dose. For a first order peak, T_m is independent of dose whereas T_m decreases with dose for a second order peak (Chen and Mckeever, 1997). In order to evaluate the dependence of peak position T_m on dose, a plot of T_m against dose was made for peak I. Figure 5.9 shows a plot of T_m against dose for doses between 10 and 300 Gy. T_m is independent of dose at 72.0 ± 0.1 °C confirming that peak I is of first order kinetics.

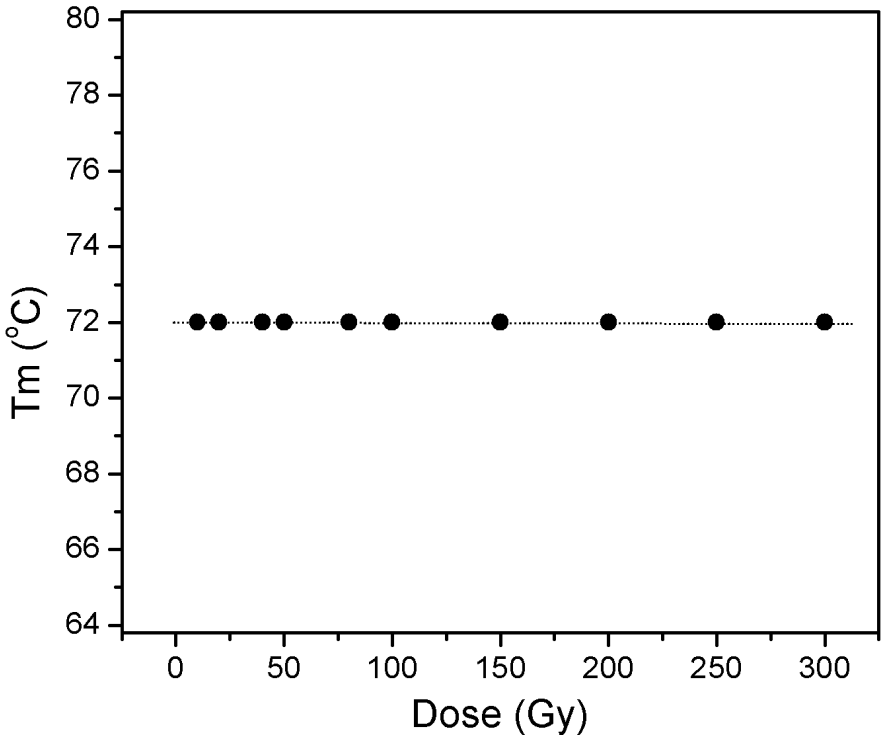

FIGURE 5.9: The influence of dose on the peak position of peak I. Each data point is an average of three measurements and the margin of error in T_m is the standard deviation of each set of three measurements. The dotted line through the data points is only a visual guide.

5.4.2 T_m - T_{stop} method

The $T_m - T_{stop}$ method was used in determining the number of peaks present in the glow curve and to investigate the order of kinetics of the peaks. In this method, a sample irradiated to 50 Gy was preheated to a temperature T_{stop} of 20 °C at a heating rate of 1 °Cs^{-1}, cooled to room temperature, and then reheated to measure the remaining glow curve. The procedure was repeated for different values of T_{stop} in steps of 2 °C up to 58 °C. The peak position T_m corresponding to each value of T_{stop} was noted. The whole measurement of $T_m - T_{stop}$ was carried out three times and the average taken. Figure 5.10 shows a graph of T_m against T_{stop} for temperatures between 20 and 60 °C, where it is evident that T_m is independent of T_{stop}. This is a feature of first order kinetics. The result also shows that peak I is single. The position T_m of peak I was determined to be independent of T_{stop}

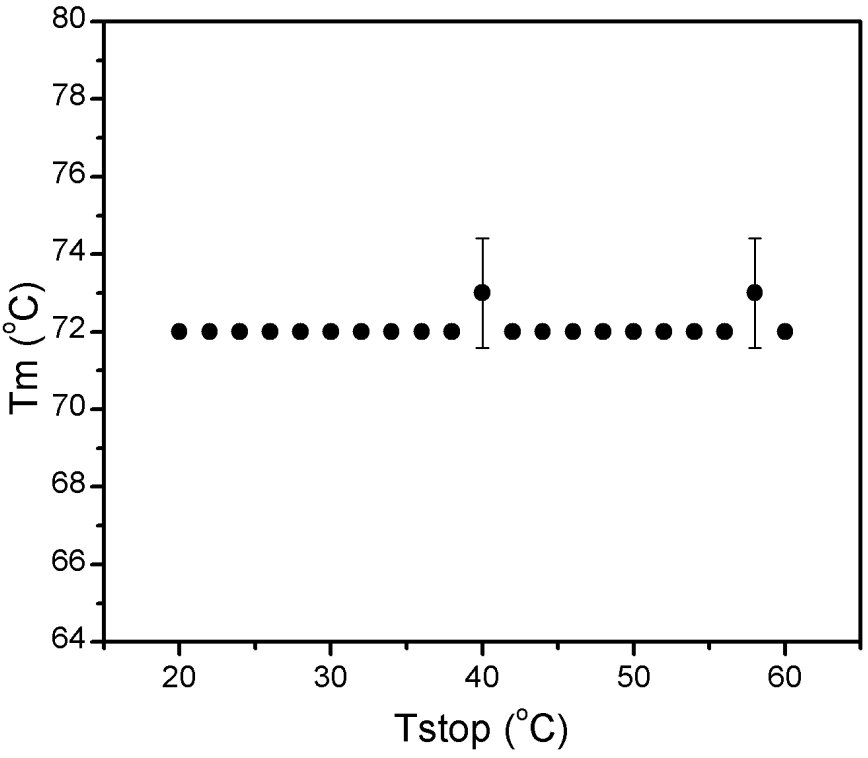

FIGURE 5.10: A graph of T_m against T_{stop} for peak I. Each data point is an average of three measurements. The error bars between data points are obtained from the standard deviation of each of the three measurements.

at $72.5 \pm 0.4\,^{\circ}$C. The results from the $T_m - T_{stop}$ method agrees with the dose dependence of peak position method.

5.5 Kinetic analysis

Kinetic analysis was carried out on the main and secondary peaks using the initial rise, whole glow peak, peak shape, and curve fitting methods. Other methods consisting of the variable heating rate and phosphorescence based methods were also used. These methods have been described extensively in Chapter 2. Several methods were used in evaluating the kinetic parameters in order to ascertain consistency in results by comparing values obtained from the different methods. For completeness, we also compare our values with ones from the literature.

5.5.1 Initial rise method

The initial rise method (section 2.3.1) was applied on the clear rising edge of peak I in order to determine the trap depth responsible for the peak. With the assumption of useable data being within 5 - 15% of the maximum peak intensity I_m, the data range for this method was extracted for a glow peak measured at 1 $^{\circ}$Cs^{-1} after an irradiation of 50 Gy. To apply the method on peak III, data was extracted for a glow peak measured after preheating the sample to 150 $^{\circ}$C following irradiation to remove peaks I and II. Figure 5.11 shows the graphs of $ln\, I$ against $1/kT$ made for peak I and peak III using the initial rise method. The activation energy E for peak I was determined from the slope as 0.93 ± 0.03 eV. This value is in satisfactory agreement with 0.92 eV reported by Mebhah *et al.* (2009) for unannealed fired quartz irradiated to 10 Gy. The activation energy recorded in this method agrees also with 0.90 ± 0.01 eV (Yazici and Topaksu, 2003) for an unannealed synthetic quartz irradiated to 50 Gy. Similarly for peak III, the activation energy was found as 0.98 ± 0.04 eV. This value compares well with 1.11 ± 0.07 eV reported by Thomas and Chithambo (2018) for peak III for the same quartz irradiated to 10 Gy.

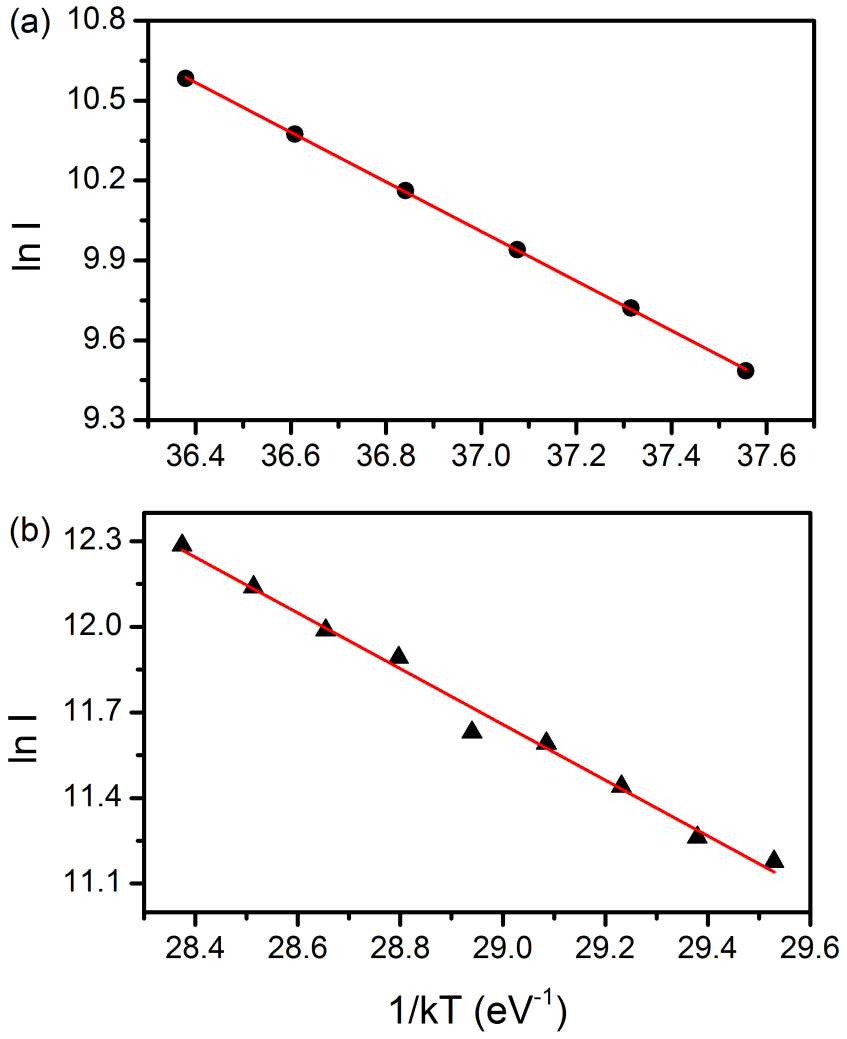

FIGURE 5.11: Plots of $ln\, I$ against $1/kT$ for (a) Peak I (b) peak III.

5.5.2 Whole glow peak method

Using the whole glow peak method discussed in section 2.3.2, the activation energy and effective frequency factor of peaks I and III were determined. From equation (2.11), a plot of $ln(I/n^b)$ against $1/kT$ was made for different values of b. Figure 5.12 shows the plot made for peak I for different values of b ranging between 1.0 and 1.2. The plot was found to be linear for $b = 1.1$ (where $R^2 = 0.998$). Similarly for peak III, $b = 1.1$ (where $R^2 = 0.998$). This suggests that the peaks follow first order kinetics. The activation energy E evaluated from the slope was 0.98 ± 0.01 and 1.06 ± 0.01 eV respectively. The value of E obtained for peak III is in good

agreement with 1.09 ± 0.02 eV reported by Thomas and Chithambo (2018) for the same quartz irradiated to 10 Gy. The effective frequency factors obtained from the intercept are 2.0×10^{13} and $2.1 \times 10^{11} s^{-1}$ for peaks I and III respectively.

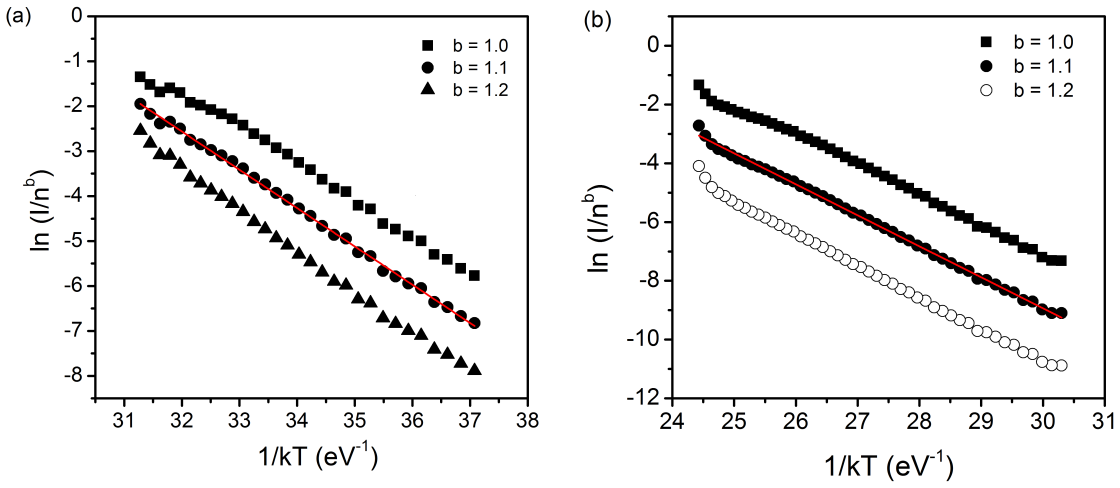

FIGURE 5.12: A plot of $ln(TL/n^b)$ against $1/kT$ for different values of b.

5.5.3 Peak shape method

The peak shape method was used to further determine the activation energy and order of kinetics of peaks I and III. From the glow curve of Figure 5.2, the temperatures T_m, T_1, and T_2 are selected and used to calculate the half-widths (τ and δ) and the total half-widths (ω) of the glow peaks. Thereafter, the order of kinetics of the peaks was obtained through the geometrical factor μ_g using equation (2.23). In this method, μ_g was calculated as 0.43 ± 0.06 and 0.43 ± 0.04 for peaks I and III suggesting that both peaks follow first-order kinetics.

The values of the activation energy for the individual half-widths were calculated as $E_\tau = 1.00 \pm 0.11$ eV, $E_\delta = 0.91 \pm 0.10$ eV, and $E_\omega = 1.07 \pm 0.11$ eV. These values differ due to the shape and value of the half-widths. However, E_ω is more reliable because it considers the total half-width of the glow peak. A major limitation of the peak shape method is that the temperatures T_m, T_1, and T_2 selected from a glow peak are most times not accurately determined due to approximations of the half maximum intensity. For peak III which was obtained after preheating to 150 °C, the values of the activation energy were calculated as $E_\tau = 1.14 \pm 0.08$ eV, $E_\delta = 1.13 \pm 0.08$ eV, and $E_\omega = 1.14 \pm 0.08$ eV. Although these values are necessarily dependent on τ, δ, ω, they are consistent for peak III.

5.5.4 Curve fitting method

The kinetic parameters E, s, and b were also determined by curve fitting using equation (2.26) due to Kitis *et al.* (1998). The experimental glow curve (Figure 5.2) was fitted by providing the values of T_m and I_m as initial parameters and by also initiating guess parameters for E and b. The best fit obtained for peak I is shown in Figure 5.13 giving $E = 1.01 \pm 0.01$ eV and $b = 1.07 \pm 0.02$ with $R^2 = 0.999$. The goodness of fit of the glow curve was tested by using equation

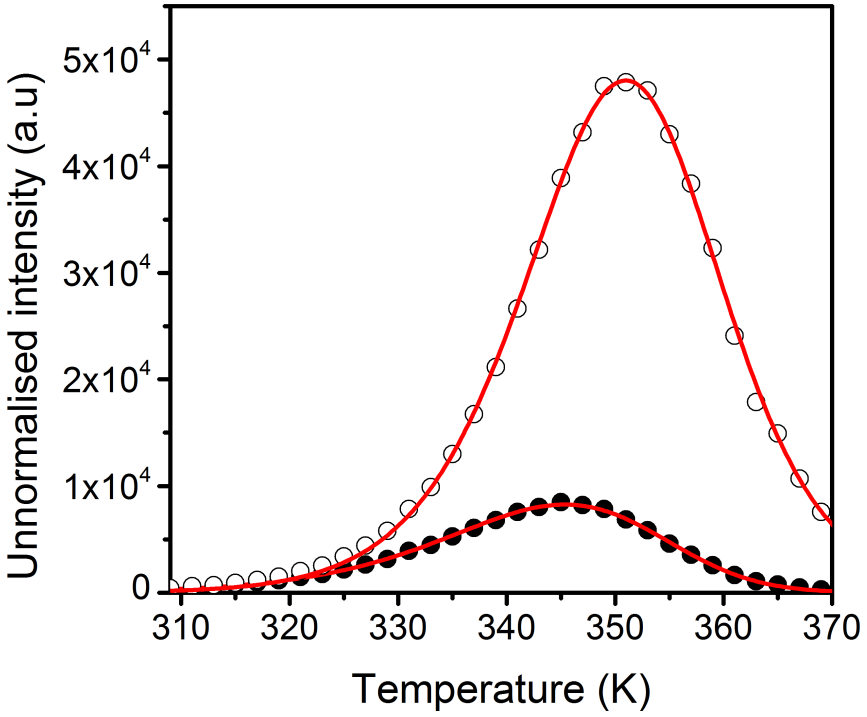

FIGURE 5.13: Result of curve fitting for peak I. The solid lines through data are the best fits of Eq. (2.26). The open symbols represent experimental data corrected for thermal quenching.

(2.30) and calculated as $FOM = 0.43\%$. For a good fit, $FOM \leq 3.5\%$ (Gartia and Singh, 2011). That $b = 1.07$ implies that peak I is of first-order kinetics. In order to determine the frequency factor, the values of E, T_m and β were substituted into equation (2.27) to give $s = 6.1 \times 10^{14}$ s^{-1}. The activation energy for peak I found using this method is consistent with 0.98 ± 0.01 eV from the whole glow peak method.

The kinetic parameters obtained for peak III are $E = 1.21 \pm 0.02$ eV, $b = 1.43 \pm 0.04$, and $s = 3.3 \times 10^{12}$s^{-1}. The goodness of fit was confirmed to be reliable

and calculated as 0.40%. The value of b suggests that peak III is of general order kinetics. The value of the activation energy obtained for peak III is consistent with 1.21 ± 0.04 eV reported by Thomas and Chithambo (2018) for the same quartz for 10 Gy.

5.5.5 Variable heating rate method

In the variable heating rate method, the activation energy E and frequency factor s were determined by using equation (2.17). The sample, irradiated to 50 Gy, was heated to nine different heating rates comprising 0.2, 0.4, 0.6, 0.8, 1, 2, 3, 4, and 5 °Cs^{-1}. Three different measurements were made for the listed heating rates and the average taken. The analysis was done for peak I using equation (2.17). Figure 5.14 shows a graph of $ln\,(T_m^2/\beta)$ against $1/kT_m$ for the various heating rate method. The activation energy obtained from the slope is 0.76 ± 0.01 eV. For the frequency factor evaluated from the intercept of the graph, $s = 7.7 \times 10^9$ s^{-1}. The

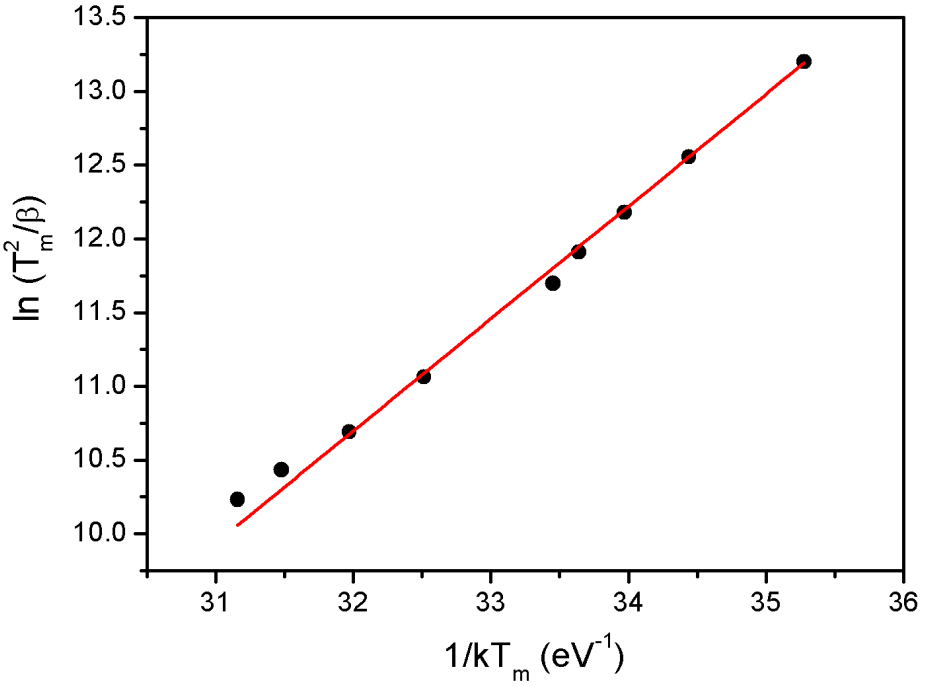

FIGURE 5.14: A graph of $ln\left(T_m^2/\beta\right)$ against $1/kT_m$ for the various heating rate method.

VHR method seems to underestimate the value of the activation energy compared

to other methods. Pagonis *et al.* (2013) have also shown that the VHR method can sometimes systematically underestimate the value of the activation energy.

5.5.5.1 Influence of heating rates on peak intensity

Figure 5.15 shows the dependence of TL intensity (denoted as peak area) on heating rate for the quartz sample irradiated to 50 Gy. The TL intensity in counts decreases with heating rate. For first order kinetics, this indicates that the peak is affected by thermal quenching. A decrease of luminescence intensity with heating rate is a general phenomenon for the presence of thermal quenching in luminescent materials (Chen and Pagonis, 2011). In the absence of thermal quenching, it is

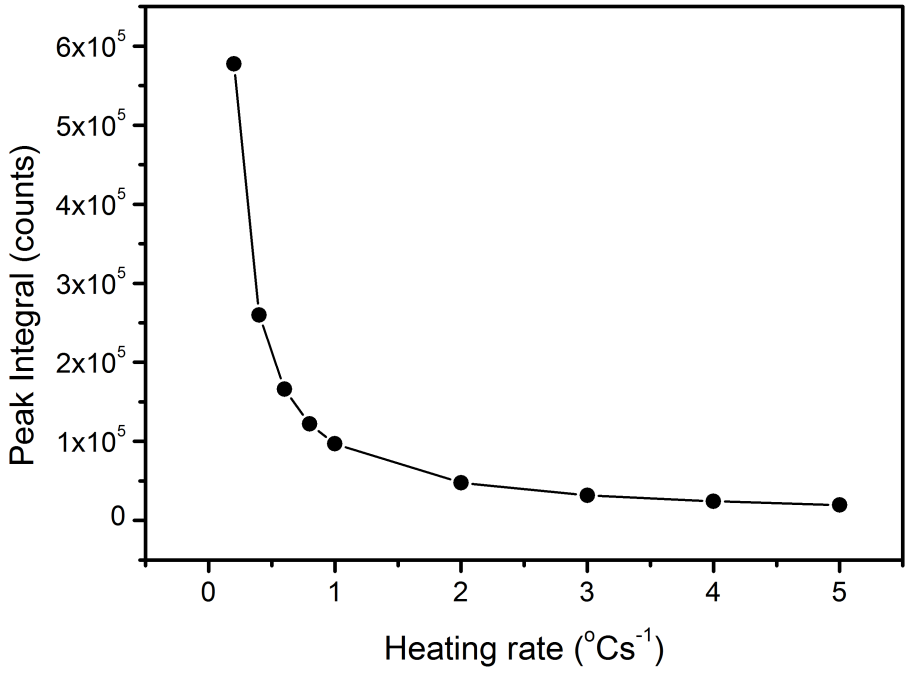

FIGURE 5.15: The influence of heating rates on the area of peak I.

expected that the TL intensity remains approximately constant with increasing heating rate (Gorbics *et al.*, 1969). The activation energy for thermal quenching was evaluated using equation (2.54). The peak area was utilised to calculate for the activation energy. The TL measured at 0.2 $^{\circ}\mathrm{Cs}^{-1}$ was assumed to experience the least amount of quenching. Figure 5.16 shows the graph of $ln[(A_{uq}/A_q) - 1]$ against $1/kT_m$. The activation energy for thermal quenching for peak I was evaluated as $\Delta E = 0.89 \pm 0.06$ and $C = 3.6 \times 10^{13}$. The ΔE value is in good agreement

with published values in the literature for quartz e.g. 0.85 ± 0.01 eV (Chithambo and Ogundare, 2009).

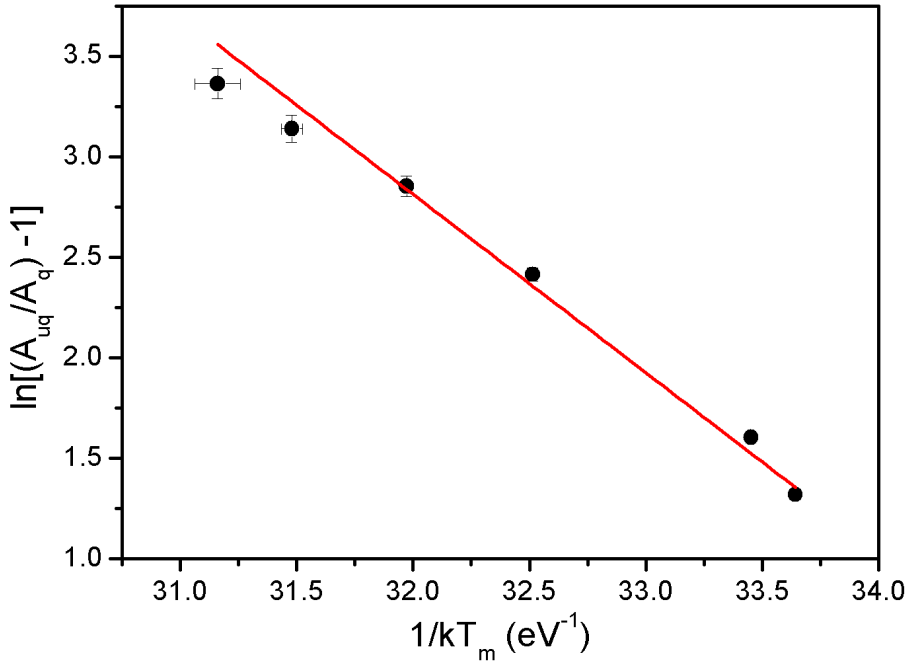

FIGURE 5.16: A graph of $ln[(A_{uq}/A_q) - 1]$ against $1/kT_m$ used to evaluate thermal quenching.

5.5.6 Phosphorescence

Phosphorescence or isothermal decay methods were also used to evaluate the kinetic parameters of the main peak for completeness. In this method, the sample irradiated to 50 Gy was heated to a specific temperature at which the phosphorescence decay was observed. Isothermal analysis was studied using two methods; one based on change of intensity with time (McKeever, 1985) and the second one based on change of the area under an isothermal decay curve with measurement temperature (Chithambo, 2014).

5.5.6.1 Isothermal analysis based on first and general order kinetics

The isothermal decay for first order kinetics has been defined in section 2.3.6.1 by $I(t) = I_o\ exp(-pt)$. Phosphorescence measurements were made for 500 s at different temperatures between 40 and 62 °C at intervals of 4 °C. For each temperature, the luminescence intensity decreased exponentially with time. A plot of $I(t)$ as a function of time on a semilogarithmic scale produced a straight line with slope $-p$ for each temperature. This is a true test of first order kinetics of phosphorescence (Chen and Mckeever, 1997). Equation (2.33) was then used in obtaining the activation energy and frequency factor. A plot of $ln\,p$ against $1/kT_i$ for measurements made at various T_i (where $i = 40, \ldots, 62$) is shown in Figure 5.17. The activation energy and frequency factor were found to be $E = 1.04 \pm 0.03$ eV and $s = 1.8 \times 10^{14}$ s^{-1} respectively.

The general order kinetics of phosphorescence was further used to examine the

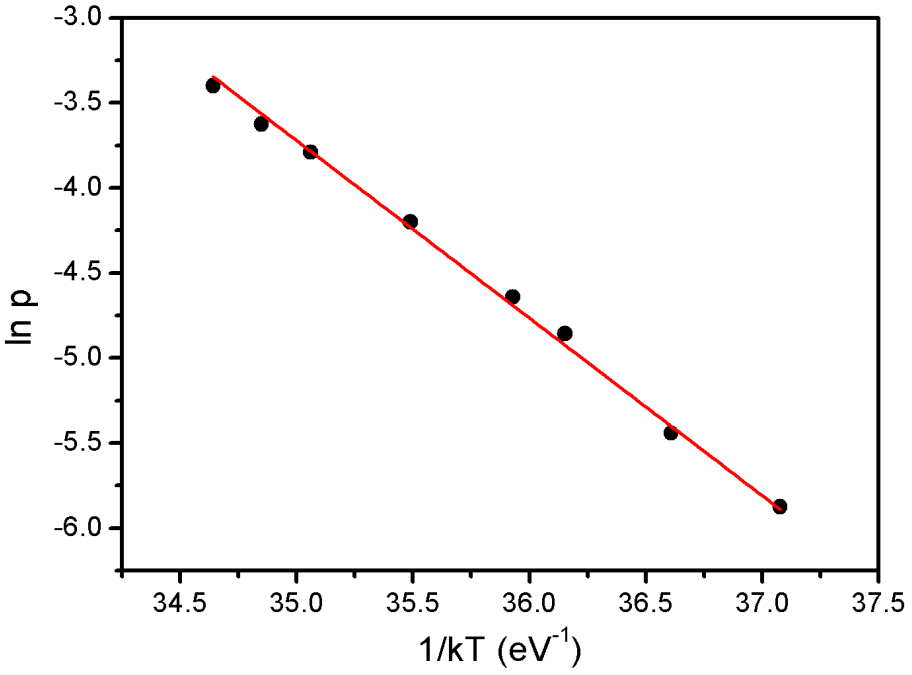

FIGURE 5.17: A graph of $ln\,p$ against $1/kT$ to evaluate the activation energy for phosphorescence based on first order kinetics.

order of kinetics and activation energy of the main peak by making a plot of $I^{(1-b)/b}$ against t. Figure 5.18 shows a plot of $ln[(b-1)n_0^{(b-1)}s']$ against $1/kT_i$ for the general order kinetics of phosphorescence from which the best value of $b = 1.1$.

The activation energy and frequency factor were determined as 0.99 ± 0.02 eV and 1.3×10^{12} s^{-1} respectively. The values of E from this method compare well with 0.98 ± 0.01 eV from the whole glow peak method.

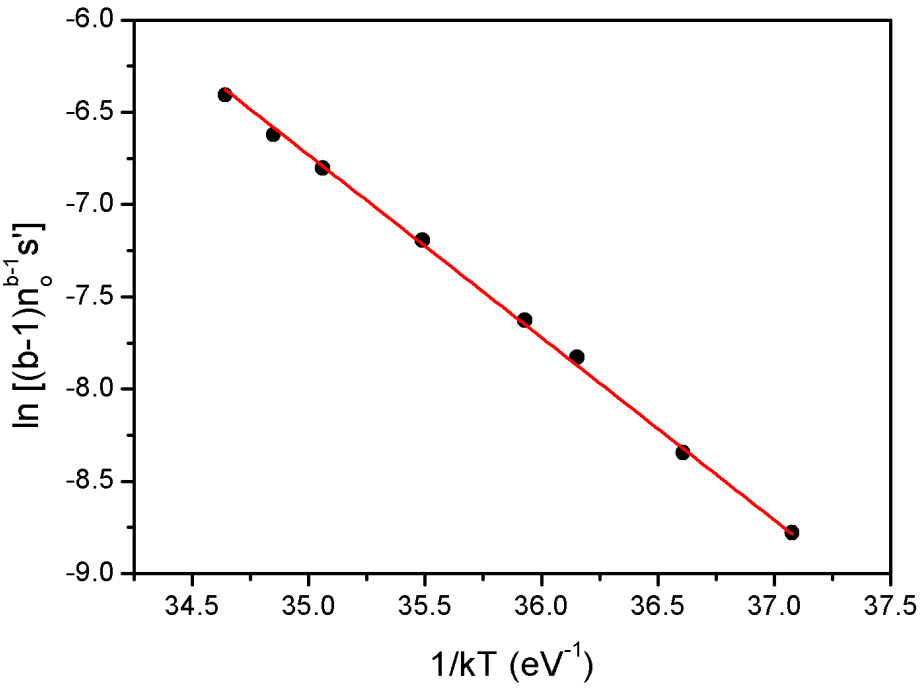

FIGURE 5.18: A graph of $ln[(b-1)n_0^{(b-1)}s']$ against $1/kT_i$ for general order kinetics of phosphorescence

5.5.6.2 Analysis of phosphorescence based on the area under an isothermal decay curve

The area-based phosphorescence method developed by Chithambo (2014) was applied on isothermal decay curves. Phosphorescence was measured for 5 s at temperatures between 30 and 58 °C after irradiation to 50 Gy. The area ϕ was determined at each temperature. Figure 5.19 shows a plot of $ln\,\phi$ against $1/kT$ for peak I. The activation energy obtained from this plot is 0.88 ± 0.03 eV.

5.5.6.3 Analysis of the temperature-dependent areas by curve fitting

When ϕ determined from section 5.5.6.2 is plotted against temperature, it produces a TL-like glow peak. This curve can be analysed using equation (2.26) by Kitis

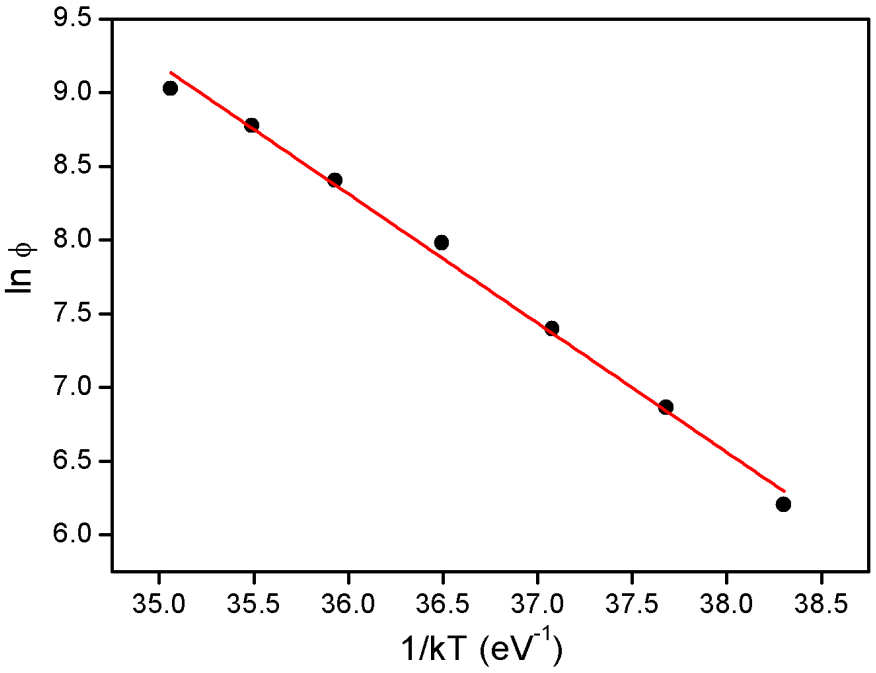

FIGURE 5.19: A plot of $ln\,\phi$ against $1/kT$ for the area ϕ under an isothermal decay curve.

et al. (1998). Figure 5.20 shows the curve fitting for temperatures between 30 and 100 °C from which E, b, s, and FOM were evaluated as 0.98 ± 0.02 eV, 1.10 ± 0.03, 3.3×10^{13} s^{-1}, and 0.17% respectively. The value of E is consistent with 1.01 ± 0.01 eV recorded earlier from the curve fitting method.

5.5.6.4 Analysis of thermal quenching using the area under an isothermal decay-curve

Thermal quenching was analysed using the the method based on the area under an isothermal decay-curve developed by Chithambo (2014). Equation (2.55) was used in evaluating the activation energy for thermal quenching. Here the quenched and the unquenched areas correspond to the highest (i.e. 58 °C in this case) and other measurement temperatures in the rising edge of the graph of ϕ against measurement temperature. Figure 5.21 shows a graph of $ln(\phi_q/\phi_u)$ against $1/kT$ for measurements made for 5 s. The value of the activation energy for thermal quenching determined from the slope of the graph is 0.91 ± 0.02 eV. This value is consistent with 0.89 ± 0.06 eV evaluated in Figure 5.16.

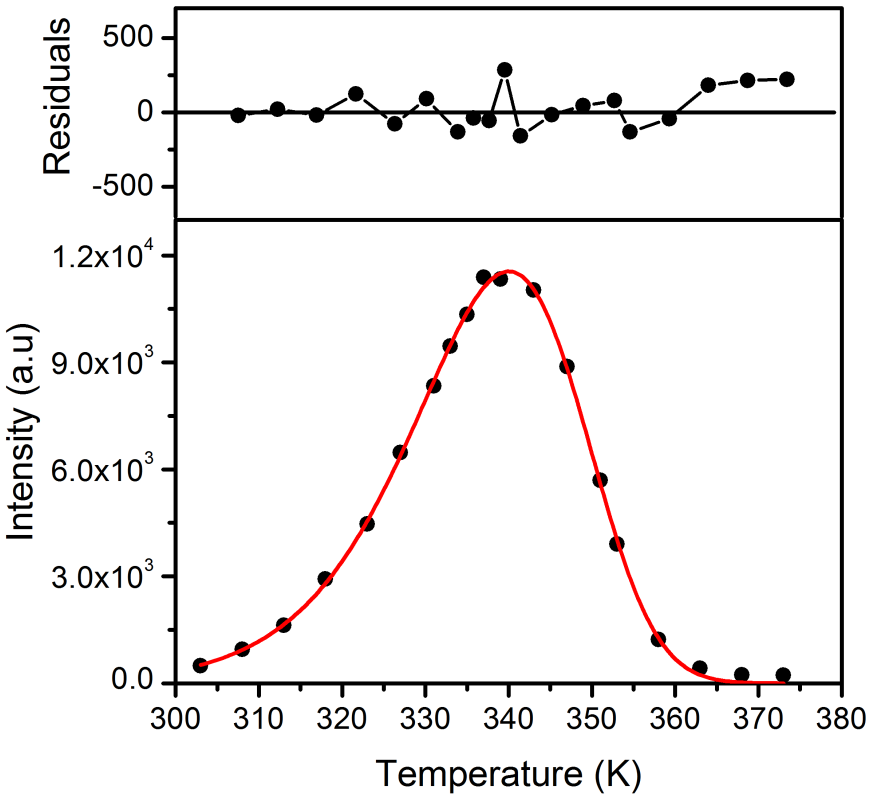

FIGURE 5.20: The temperature dependence of areas under isothermal decay curves each measured for 5 s. The solid line is the best fit of Eq. (2.26). The residuals, fluctuating about zero are evidence of a good fit.

5.6 Summary

A study of dosimetric features and kinetic analysis of the TL from unannealed natural quartz have been carried out on the main peak (peak I) and a secondary peak (peak III). The position of the main peak was noted to be independent of repetitive measurement. The intensity of peak I was also noted to be sublinear with dose and fades with a mean lifetime of ~ 3400 s. Irrespective of the method of kinetic analysis used, the results show that the main peak is of first order kinetics. The activation energy obtained using the various methods is ~ 1 eV for both peaks and agrees with published values in the literature. The frequency factors for peaks I and III are between $10^9 - 10^{14}$ and $10^{12} - 10^{13}$ s^{-1}. Table 5.1 gives a summary of the kinetic parameters E, b, and s for the methods applied.

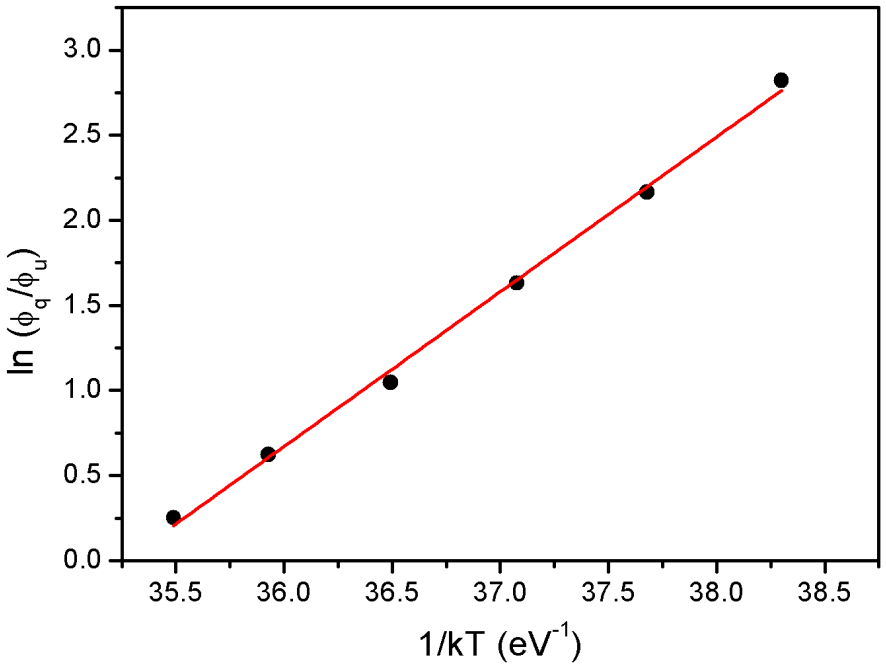

FIGURE 5.21: A graph of $ln(\phi_q/\phi_u)$ against $1/kT'$ in a study of thermal quenching using the area under an isothermal decay-curve

TABLE 5.1: Kinetic parameters of the main and secondary TL peaks of unnannealed natural quartz. The acronyms IR, WGP, PS, CF, VHR, and IDC refers to the initial rise, whole glow peak, peak shape, curve fitting, variable heating rate and isothermal decay methods.

Peak	Method	E (eV)	b	s (s^{-1})	ΔE (eV)	Reference
I	T_m-Dose		1			
	T_m-T_{stop}					
1						
	IR	0.93 ± 0.03				Fig. 5.11(a)
		0.92				Mebhah *et al.* (2009)
	WGP	0.98 ± 0.01	1.1	2.0×10^{13}		Fig. 5.12
	PS	$1.00 \pm 0.11^{\tau}$				
		$0.91 \pm 0.10^{\delta}$	1			Sect. 5.5.3
		$1.07 \pm 0.11^{\omega}$				
	CF	1.01 ± 0.01	1.07 ± 0.02	6.1×10^{14}		Fig. 5.13
	VHR	0.76 ± 0.01		7.7×10^{9}	0.89 ± 0.06	Fig. 5.14
	IDC, 1st order	1.04 ± 0.03	1	1.8×10^{14}		Fig. 5.17
	IDC, Gen. order	0.99 ± 0.02		1.3×10^{12}		Fig. 5.18
	IDC, Area	0.88 ± 0.03			0.91 ± 0.02	Fig. 5.19
	IDC, GCD	0.98 ± 0.02	1.10 ± 0.03	3.3×10^{13}		Fig. 5.20
III	IR	0.98 ± 0.04				Fig. 5.11(b)
		1.11 ± 0.07				Thomas and Chithambo (2018)
	WGP	1.06 ± 0.01	1.1	2.1×10^{11}		
	PS	1.14 ± 0.08^{a}				
		1.13 ± 0.08^{b}	1			
		1.14 ± 0.08^{c}				
	CF	1.21 ± 0.02	1.43 ± 0.04	3.3×10^{12}		Sect. 5.5.4
		1.20 ± 0.02				Thomas and Chithambo (2018)

Chapter 6

Thermoluminescence of natural quartz annealed at 800 °C

This chapter presents results of kinetic analysis and dosimetric features of quartz annealed at 800 °C for 10 minutes and for 1 hour. The quartz was annealed to increase its luminescence sensitivity. The same methods of analysis used for the unannealed samples are also employed here. Results from the sample annealed at 800 °C for 10 minutes are reported first in section 6.1. This is followed by a report of the kinetic analysis on quartz annealed for 1 hour in section 6.2. We report in section 6.3 analysis of thermal quenching and inverse thermal quenching. We demonstrate that inverse thermal quenching is a dose dependent feature. A comparative analysis of results of quartz annealed for 10 minutes and 1 hour is also presented.

6.1 Thermoluminescence of quartz annealed at 800 °C for 10 minutes

6.1.1 Characteristics of the thermoluminescence glow curve

Figure 6.1 shows a glow curve measured at 1 °Cs^{-1} from a sample of annealed natural quartz after irradiation to 50 Gy. The inset shows the same glow curve on a semi-logarithmic scale to better show the presence of other peaks. The glow curve consists of five peaks. The most intense peak (labelled I) referred to as the

main peak is at 73 °C. The secondary peaks are at 120, 176, 276, and 334 °C and labelled II, III, IV, and V respectively as shown.

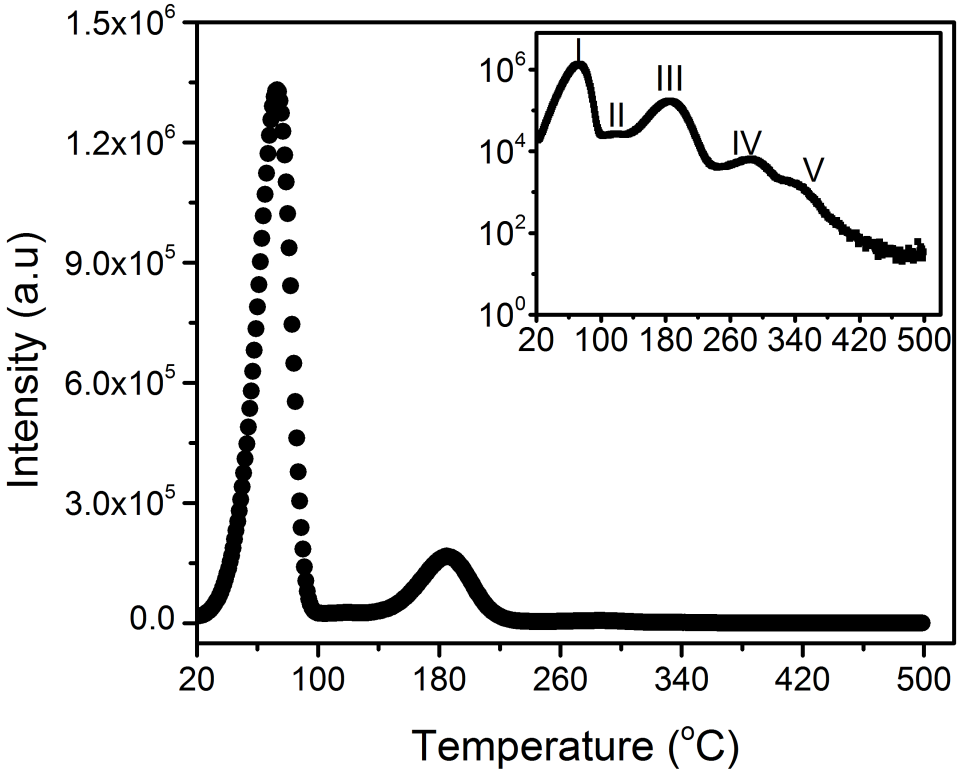

FIGURE 6.1: A thermoluminescence glow curve measured at 1 °Cs^{-1} from quartz annealed at 800 °C for 10 min following a dose of 50 Gy.

6.1.2 Thermal cleaning

The thermal cleaning technique was used to determine the position and number of peaks present in the glow curve of Figure 6.1. In the measurement, the sample irradiated to 50 Gy and heated to 500 °C showed peak I at 73 °C. After cooling, the sample was again irradiated and preheated to 100 °C to remove peak I. Subsequent heating of the sample to measure the whole glow curve revealed peak II at 120 °C. To confirm the positions of other peaks, the sample irradiated each time for every TL measurement was preheated to 140, 240, and 300 °C in each turn to remove peaks II, III, and IV respectively. Further heating of the sample to measure the whole glow curve revealed peaks III, IV, and V at 176, 276, and 334 °C respectively. The results of the thermal cleaning conducted are shown in Figure 6.2.

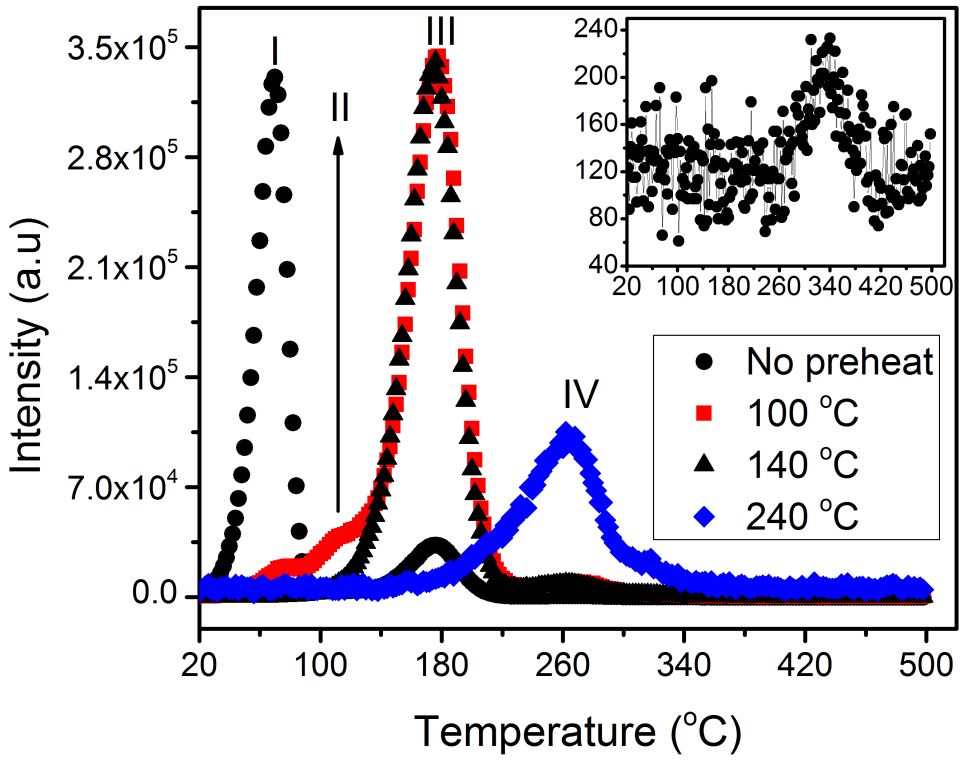

FIGURE 6.2: Thermally cleaned TL glow curves of quartz annealed at 800 °C for 10 min following a dose of 50 Gy. The peaks labelled I - V are recorded without preheat (I) and after preheating to 100 (II), 140 (III), and 240 (IV) °C. The inset shows data for peak V after preheating to 300 °C. The data corresponding to no preheat was reduced by 2 whereas the data corresponding to 100, 140 and 240 °C have been scaled up for visual clarity by ×5, ×4, and ×50 respectively.

6.1.3 Dosimetric features of TL

To study the dosimetric features of the quartz annealed at 800 °C for 10 minutes, the reproducibility, dose response and fading of the TL signal for peak I were investigated .

6.1.3.1 Reproducibility

After the verification of the peak positions using the thermal cleaning technique, it is essential to determine the reproducibility of the peaks and their intensity. The reproducibility of the TL signal was investigated for peak I by taking repeated

TL measurements of the quartz sample freshly irradiated to 50 Gy and heated at 1 °Cs^{-1} each time. The measurements were made ten times. The position and intensity of peak I was noted each time the measurement was taken. Figure 6.3 shows the variation of peak position and peak intensity with repeated measurements. The position of peak I was constant at 73 °C. This implies that peak I is unaffected by sample re-use. The intensity of peak I increases slightly with repeated measurements. This increase may be due to a change in the sensitivity of the sample due to repeated heating.

6.1.3.2 Influence of dose on TL intensity

The influence of irradiation dose on peak intensity for peak I was studied for doses between 10 and 300 Gy. Figure 6.4 shows the growth curve for peak I. The intensity of peak I increases monotonically with dose up to 100 Gy and then decreases towards saturation.

6.1.3.3 Fading

Fading of the TL signal between irradiation and measurement was studied for peak I. Figure 6.5 shows a graph of intensity against delay between irradiation of 50 Gy and measurements for delay up to 5 hrs (18000 s). Figure 6.5 was fitted using equation (5.1). The mean lifetime determined from the fit is 4581 s.

6.1.4 Assessing the order of kinetics using T_m-dose method

The dependence of peak position T_m on irradiation was used to determine the order of kinetics for peak I. The quartz sample was irradiated to doses ranging from 10 to 300 Gy. The peak position was noted for every TL readout. Figure 6.6 shows the influence of dose on peak position T_m for peak I. The error bars between data is the standard deviation of each set of three measurements. The position of peak I was stable at 72.1 ± 0.7 °C where it is evident that T_m is independent of dose. This feature suggests that the peak is of first order kinetics. .

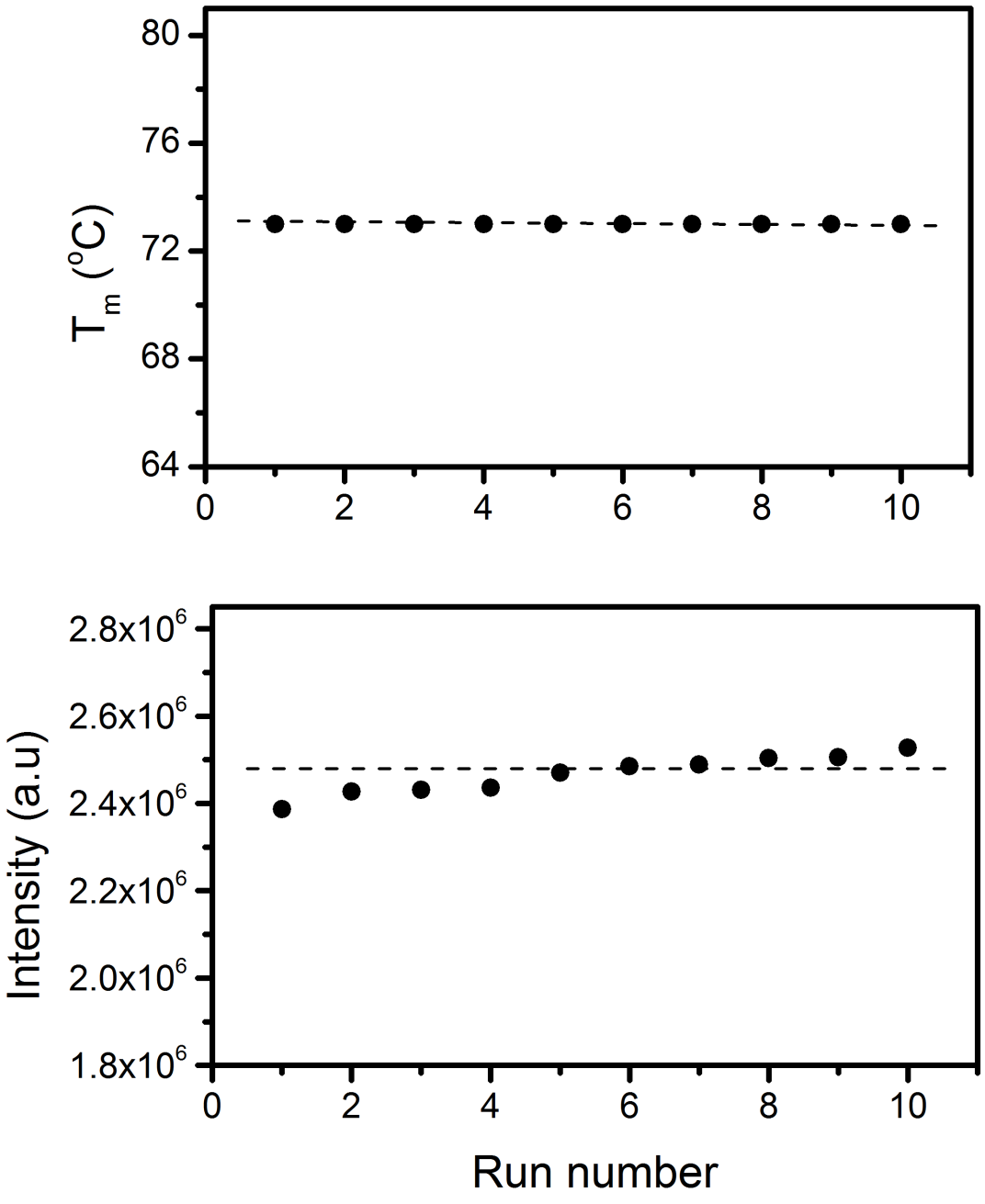

FIGURE 6.3: Plots of peak position and intensity against repeated measurement for peak I. The dotted lines between data are only visual guides.

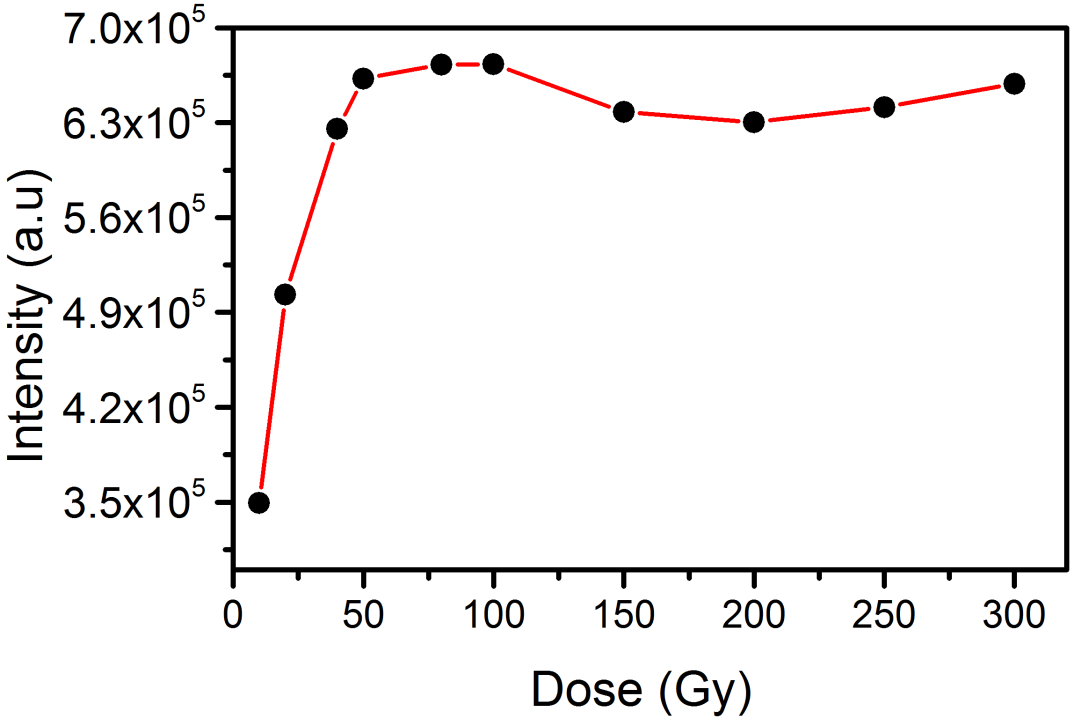

FIGURE 6.4: Plots of peak intensity against dose for peak I.

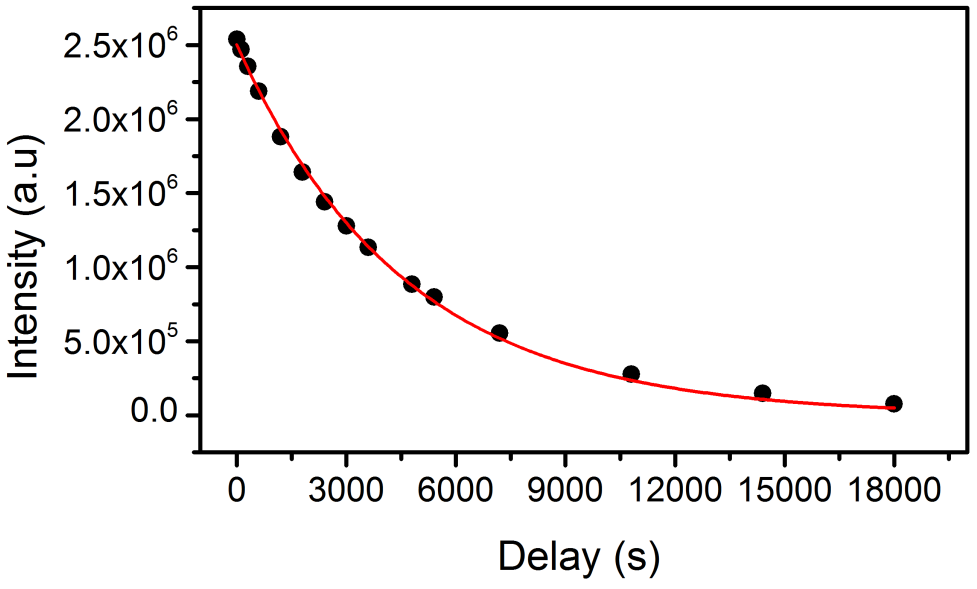

FIGURE 6.5: Plot of peak intensity against delay for peak I for fading study.

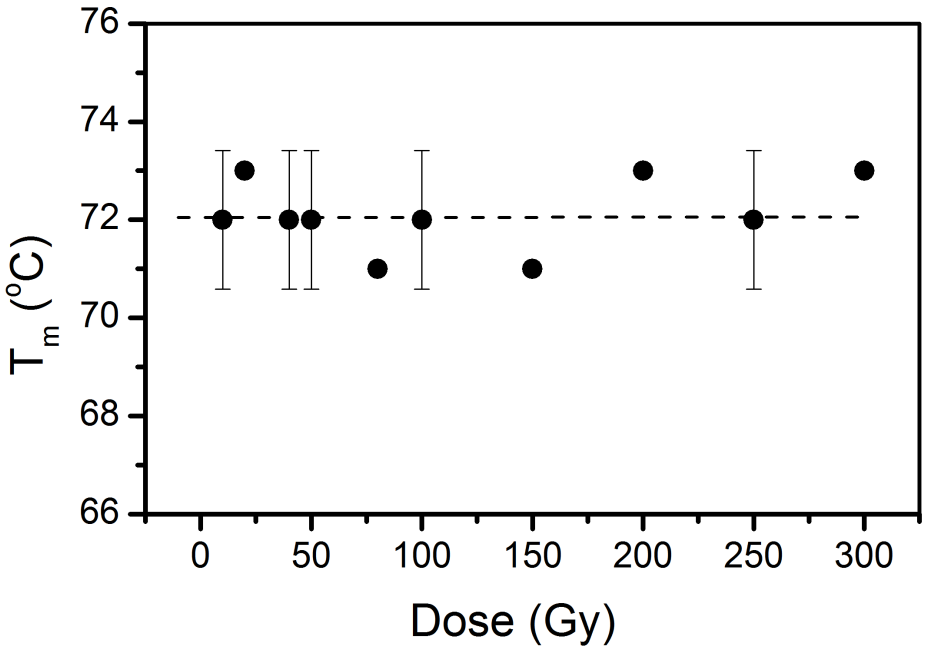

FIGURE 6.6: Dependence of peak position T_m on irradiation for doses.

6.1.5 Kinetic analysis

Kinetic analysis was carried out on peaks I and III using the initial rise-, whole glow peak-, peak shape-, variable heating rate and curve fitting methods. Phosphorescence analysis, based on first order kinetics (McKeever, 1985) and the method using the temperature dependence of area under an isothermal decay curve (Chithambo, 2014) was also used to evaluate the kinetic parameters.

6.1.5.1 Initial rise method

The initial rise method was applied on the rising edges of peaks I and III in order to evaluate the activation energy responsible for the traps. Data corresponding to $5-15\%$ of the maximum peak intensity was used for the analysis. Plots of $ln\, I$ against $1/kT$ for the initial rise portions of the peaks are shown in Figure 6.7. The activation energy was evaluated as 0.93 ± 0.01 eV for peak I and 1.01 ± 0.01 eV for peak III. The activation energy for peak I is in satisfactory agreement with 0.94 ± 0.01 eV reported by (Chithambo, 2014) for the same quartz irradiated to 10 Gy.

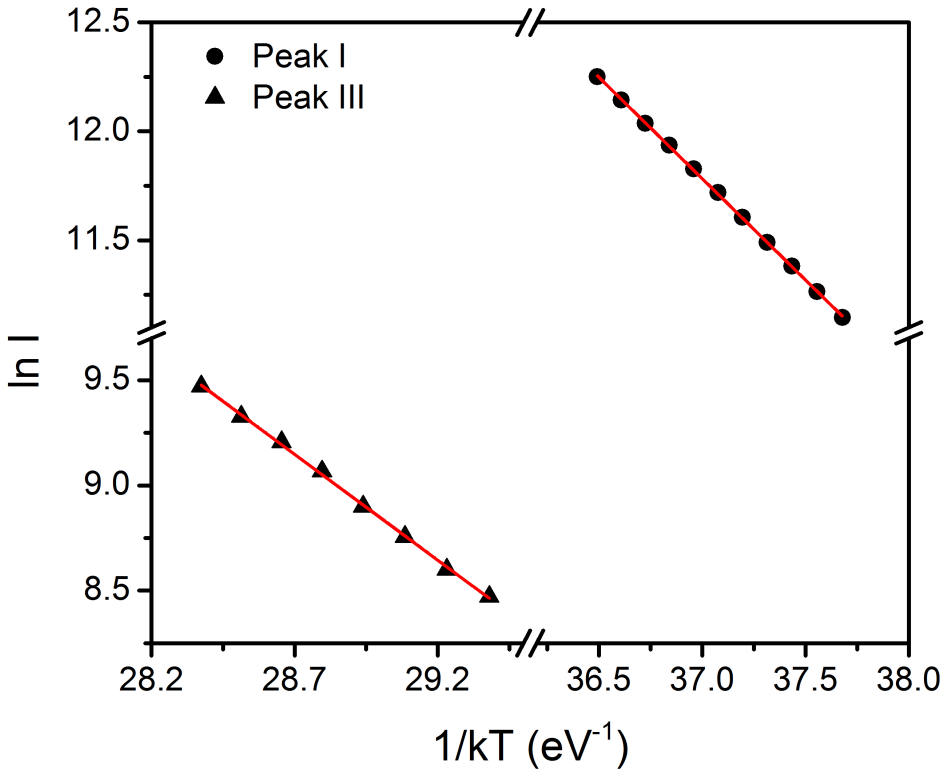

FIGURE 6.7: A plot of $ln\, I$ against $1/kT$ for peak I and peak III.

6.1.5.2 Whole glow peak method

The kinetic parameters for peaks I and III were further analysed using the whole glow peak method. This method, unlike the initial rise method does not require a clear rising edge. The method needs an isolated peak whose area can be determined from selected temperatures at either end of the glow peak. Temperatures selected for peak I were from 37 to 95 °C and from 110 - 220°C for peak III. Equation (2.11) was used to evaluate the order of kinetics and activation energy of both peaks. Plots of $ln\left(I/n^b\right)$ against $1/kT$ for different values of b ranging between 1.0 and 1.2 are shown in Figure 6.8. For peak I, the best fit was determined at $b = 1.0$ whereas $b = 1.2$ for peak III. These values of b suggest that the peaks are of first order kinetics. The activation energy was evaluated as $E = 0.90 \pm 0.01$ eV and $E = 1.06 \pm 0.01$ eV for peaks I and III respectively. The effective frequency factors obtained from the intercept were 1.1×10^{12} s^{-1} for peak I and 4.8×10^{10} s^{-1} for peak III. The values of the activation energy for peaks I and III using this method compare favourably with those from the initial rise method.

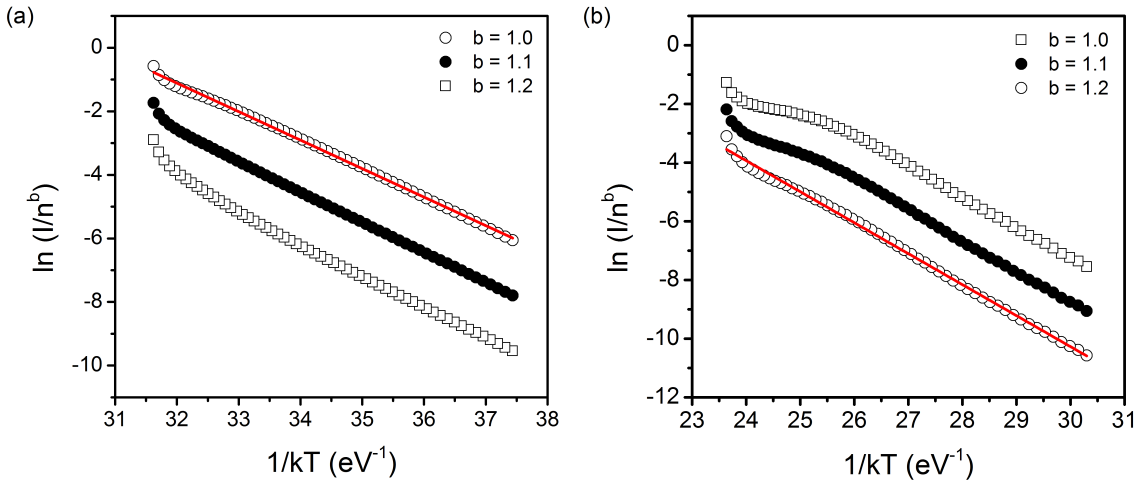

FIGURE 6.8: A graph of $ln(I/n^b)$ against $1/kT$ for different values of b for (a) peak I (b) peak III.

6.1.5.3 Peak shape method

The peak shape method was also used to evaluate the activation energy of peaks I and III. The method relies on careful selection of temperatures T_m, T_1, and T_2 (defined in section 2.3.4) from the glow peaks. These temperatures were used to calculate the half- and total half-widths of the glow peaks. The total half-width ω of peak I was calculated as 26 whereas it was 38 for peak III.

The order of kinetics of peaks I and III was determined through the symmetry factor μ_g using equation (2.23) as 0.42 ± 0.03 and 0.42 ± 0.04 respectively. This implies that the peaks are of first-order kinetics. The values of the activation energy, based on the geometrical properties of the peaks were calculated for peak I as $E_\tau = 0.94 \pm 0.05$ eV, $E_\delta = 0.92 \pm 0.04$ eV, and $E_\omega = 0.94 \pm 0.05$ eV. Similarly for peak III, $E_\tau = 1.07 \pm 0.07$ eV, $E_\delta = 1.06 \pm 0.07$ eV, and $E_\omega = 1.07 \pm 0.07$ eV. The values of the activation energy are consistent for each peak. The values are also in good agreement with the initial rise and whole glow peak methods.

6.1.5.4 Variable heating rate method

Peaks I and III were also analysed for kinetic parameters using the variable heating rate method. The sample irradiated to 50 Gy was heated to nine different heating rates between 0.2 and 5 $°Cs^{-1}$. Measurements were made thrice for both peaks and the average taken. Figure 6.9 shows the plots of $ln\,(T_m^2/\beta)$ against $1/kT_m$ for the various heating rate method. The activation energy was found as 0.93 ± 0.02 eV

for peak I and the frequency factor was evaluated as $s = 5.2 \times 10^{12}$ s^{-1}. The value of E is consistent with the values obtained using the initial rise, whole glow peak, and peak shape methods. This value is also in good agreement with 0.96 ± 0.03 eV reported by Chithambo (2014) for the same quartz irradiated to 10 Gy. For peak III, the activation energy and frequency factor were found as $E = 1.50 \pm 0.01$ eV and $s = 5.8 \times 10^{15}$ s^{-1} respectively. These values are higher than other methods discussed thus far.

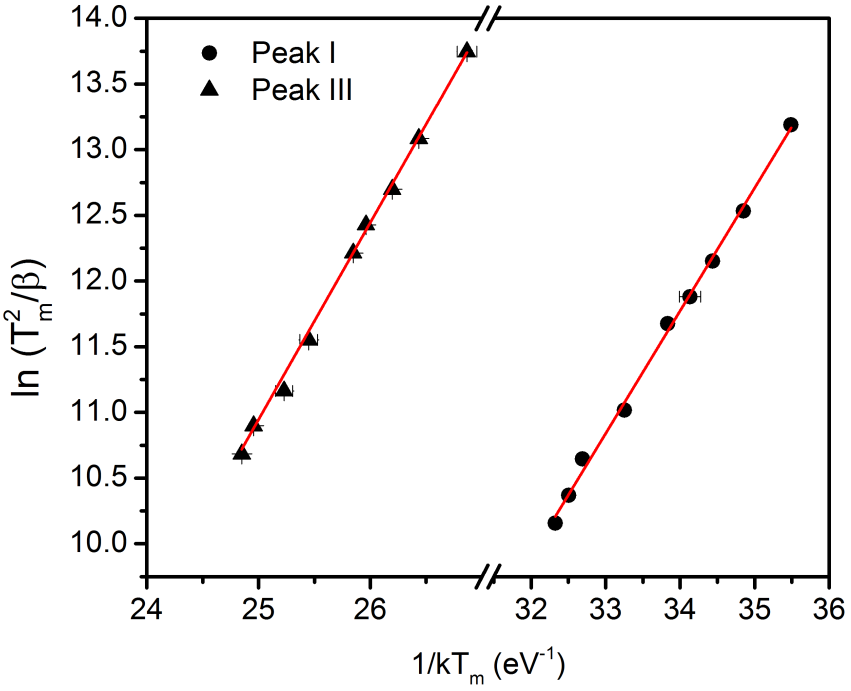

FIGURE 6.9: A graph of $ln\left(T_m^2/\beta\right)$ against $1/kT_m$ for peak I and peak III for the various heating rate method.

6.1.5.5 Curve fitting method

Further analysis by curve fitting was also used to evaluate the kinetic parameters E, s, and b for peaks I and III. These peaks were fitted using equation (2.26) developed by Kitis *et al.* (1998). Figure 6.10(a) shows the best fit for peak I giving $E = 0.95 \pm 0.01$ eV, $s = 6.3 \times 10^{12}$ s^{-1}, and $b = 1.05 \pm 0.01$ with $R^2 = 0.999$. The value of b suggests that peak I follows first-order kinetics in agreement with other methods. The value of the activation energy is consistent with the values

obtained from other methods already discussed.

Similarly in Figure 6.10(b), the kinetic parameters for peak III were found as $E = 1.19 \pm 0.01$ eV, $s = 1.7 \times 10^{12}$ s^{-1}, and $b = 1.31 \pm 0.04$.

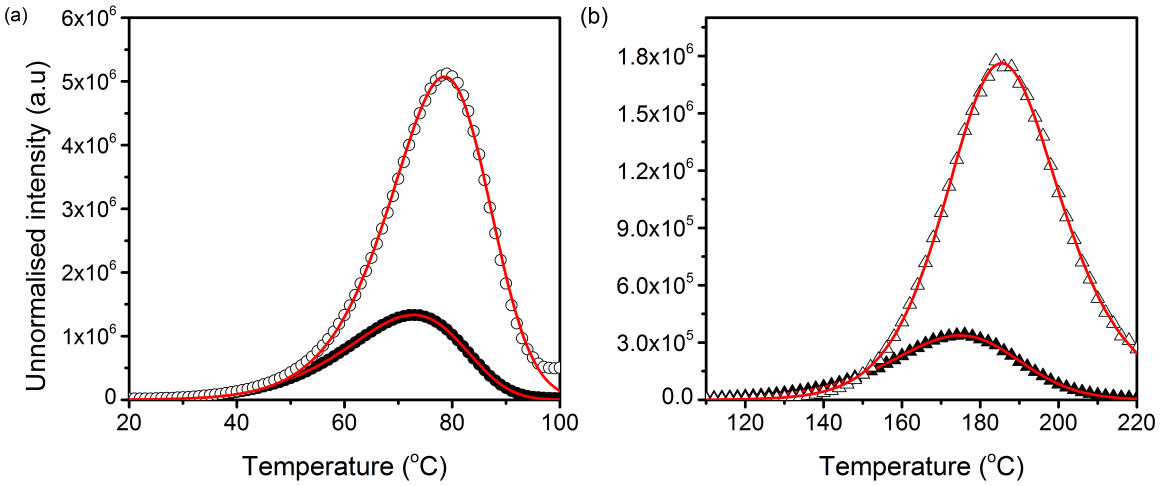

FIGURE 6.10: Results of curve fitting for (a) peak I (b) peak III. The open symbols represent curve fit data corrected for thermal quenching.

6.1.6 Phosphorescence analysis

Phosphorescence analysis was carried out on peak I in order to evaluate the activation energy and frequency factor. The sample irradiated to 50 Gy was heated to a specific temperature which was kept constant while measuring the phosphorescence decay at a given time interval. To analyse for kinetic parameters, the method based on change of intensity with time (McKeever, 1985) and method based on area under an isothermal decay curve with measurement temperature (Chithambo, 2014) were used.

6.1.6.1 Analysis of phosphorescence based on first-order kinetics

Phosphorescence measurements were made at different temperatures between 40 and 62 °C for peak I. Equation (2.33) was used to determine the activation energy and frequency factor. Plot of $ln\, p$ against $1/kT_i$ made for peak I is shown in Figure 6.11. The activation energy and frequency factor were found to be $E = 1.008 \pm 0.004$ eV and $s = 6.5 \times 10^{13}$ s^{-1}.

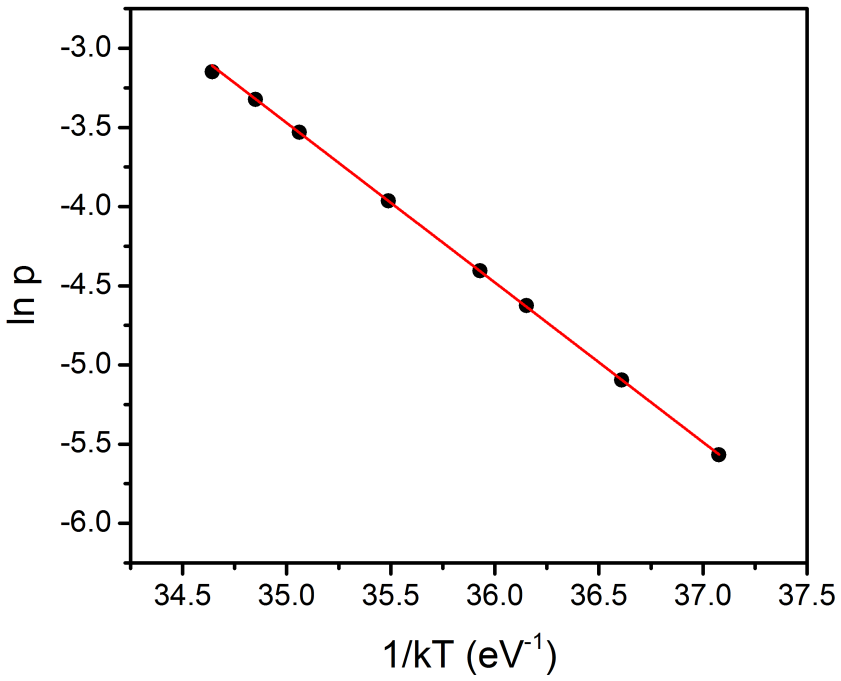

FIGURE 6.11: A graph of $ln\,p$ against $1/kT$ to evaluate the activation energy for phosphorescence based on first order kinetics.

6.1.6.2 Analysis based on area under an isothermal decay curve

The area-based method of isothermal analysis by Chithambo (2014) was applied on isothermal decay curves measured for 5 s. The decay curves were measured at temperatures between 30 and 58 °C following irradiation to 50 Gy. The area ϕ of an isothermal curve was calculated at each temperature. Figure 6.12 shows the semilogarithmic plots of ϕ against $1/kT$ for peak I. The activation energy was obtained as 0.87 ± 0.03 eV. This value of E is in satisfactory agreement with 0.85 ± 0.02 reported by Chithambo (2014).

6.1.6.3 Analysis of the temperature-dependent areas by curve fitting

The area ϕ plotted against temperature produces a TL-like glow peak shown in Figure 6.13. This curve was fitted using equation (2.26) by Kitis *et al.* (1998). The kinetic parameters E, b, and s were evaluated from the fit as 1.02 ± 0.02 eV, 1.06 ± 0.02, and 2.1×10^{14} s^{-1} respectively. The value of the activation energy agrees satisfactorily with the value obtained from the first order phosphorescence

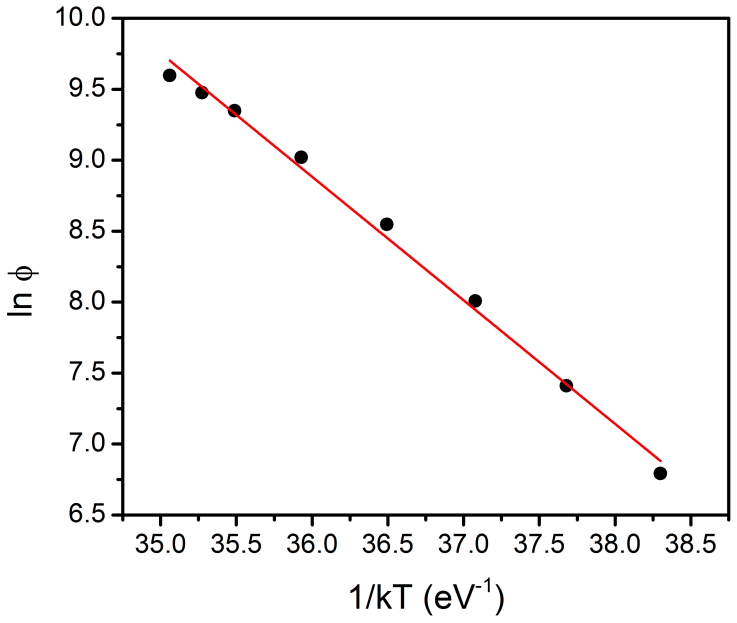

FIGURE 6.12: A plot of $ln\,\phi$ against $1/kT$ used to calculate the activation energy for the area under an isothermal decay curve.

method. The value of b confirms that peak I is of first order kinetics in comparison with other methods.

6.1.6.4 Analysis of thermal quenching using the area under an isothermal decay-curve

The area under an isothermal decay curve was also used to analyse for thermal quenching. Using equation (2.55), the activation energy for thermal quenching was evaluated. Figure 6.14 shows a graph of $ln(\phi_q/\phi_u)$ against $1/kT'$ for measurements made for 5 s. The value of the activation energy for thermal quenching determined from the slope of the graph is 0.89±0.02 eV. This value is consistent with published values for quartz in the literature e.g. 0.85 ± 0.01 eV (Chithambo and Ogundare, 2009).

6.1.7 Summary

A TL study of quartz annealed at 800 °C for 10 minutes has been presented. Peak I (main) and peak III (secondary) of the sample were studied using various

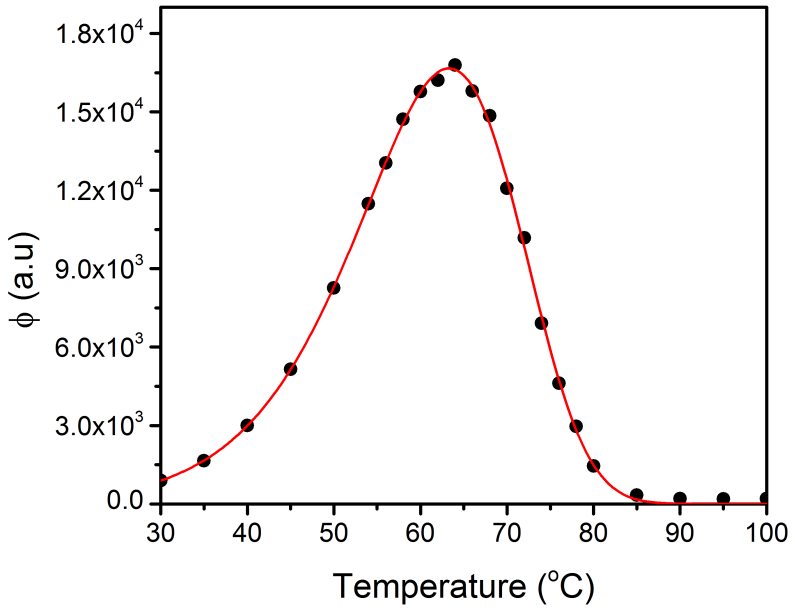

FIGURE 6.13: The temperature dependence of areas under isothermal decay curves measured for 5 s. The solid lines passing through data points are the best fits of Eq. (2.26).

methods of kinetic analysis. The Peaks were noted to follow first order kinetics using the whole glow peak, peak shape and curve fitting methods. The values of the trap depth for peak I using the initial rise, whole glow peak, peak shape, variable heating rate, and curve fitting methods are consistent and agree with published values in the literature. The frequency factors are of the order of 10^{12} - 10^{14} s^{-1} for peak I. Table 6.1 presents a summary of the kinetic parameters obtained from the various methods for peak I and peak III. The acronyms on the table are as defined previously.

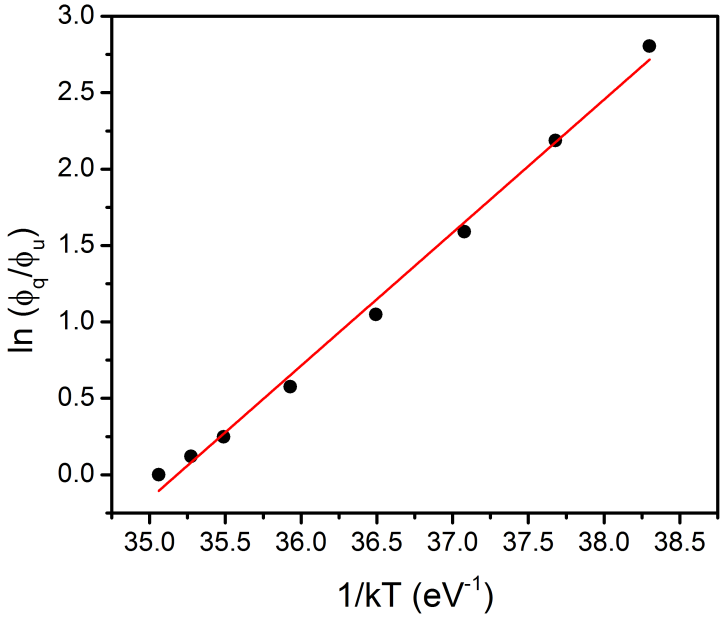

FIGURE 6.14: A graph of $ln(\phi_q/\phi_u)$ against $1/kT$ used to evaluate activation energy of thermal quenching.

6.2 Thermoluminescence of quartz annealed at 800 °C for 1 hour

Kinetic analysis of the main TL peak is reported in this section for the sample annealed at 800 °C for 1 hour. Measurements were carried out using a RISO TL/OSL Luminescence Reader with a Hoya U-340 detection filter (transmission band 250 - 390 nm). The same methods of analysis used previously are also adopted here.

6.2.1 Glow curve characteristics

The standard procedure of first heating a sample to 500 °C to confirm the presence of natural TL was carried out. Only a background signal was recorded. Figure 6.15 shows a glow curve measured after sample irradiation to 50 Gy. The glow curve shows two peaks at 72 and 180 °C. To ascertain the presence of other peaks, the thermoluminescence data was replotted on a semilogarithmic scale as shown

TABLE 6.1: Kinetic parameters for the main and secondary peaks of natural quartz annealed at 800 °C for 10 minutes

Peak	Method	E (eV)	b	s (s^{-1})	Reference
I	IR	0.93 ± 0.01			Fig. 6.7
	WGP	0.90 ± 0.01	1.0	1.1×10^{12}	Fig. 6.8(a)
	PS	$0.94 \pm 0.05^{\tau}$ $0.92 \pm 0.04^{\delta}$ $0.94 \pm 0.05^{\omega}$	1		Sect. 6.1.5.3
	VHR	0.93 ± 0.03		5.2×10^{12}	Fig. 6.9
	CF	0.95 ± 0.01	1.05 ± 0.01	6.3×10^{12}	Fig. 6.10(a)
	IDC, 1st order	1.008 ± 0.004		6.5×10^{13}	Fig. 6.11
	IDC, Area	0.87 ± 0.03			Fig. 6.12
	IDC, CF	1.02 ± 0.02	1.06 ± 0.02	2.1×10^{14}	Fig. 6.13
III	IR	1.01 ± 0.01			Fig. 6.7
	WGP	1.06 ± 0.01	1.2	4.8×10^{10}	Fig. 6.8(b)
	PS	$1.07 \pm 0.07^{\tau}$ $1.06 \pm 0.07^{\delta}$ $1.07 \pm 0.07^{\omega}$	1		Sect. 6.1.5.3
	VHR	1.50 ± 0.01		5.8×10^{15}	Fig. 6.9
	CF	1.19 ± 0.01	1.31 ± 0.04	1.7×10^{12}	Fig. 6.10(b)

in the inset of Figure 6.15 giving other peaks at 120, 282, 334, and 364 °C. The entire peaks in the glow curve are labelled I, II, III, IV, V, and VI as shown.

6.2.2 Reproducibility

The reproducibility of the TL signal was studied by taking repeated measurements of TL for the sample irradiated to 50 Gy. The TL measurement was done ten times for this study. The position and intensity of peak I was noted for each measurement. Figure 6.16 shows the influence of repeated measurements on the peak position and intensity of peak I. The position of peak I was independent of repeated measurements giving an average value of 71.6 ± 0.8 °C. This implies that peak I is unaffected by sample re-use. The intensity of peak I was noted to increase with repeated measurements implying that long use of the sample will improve the sensitivity of the material.

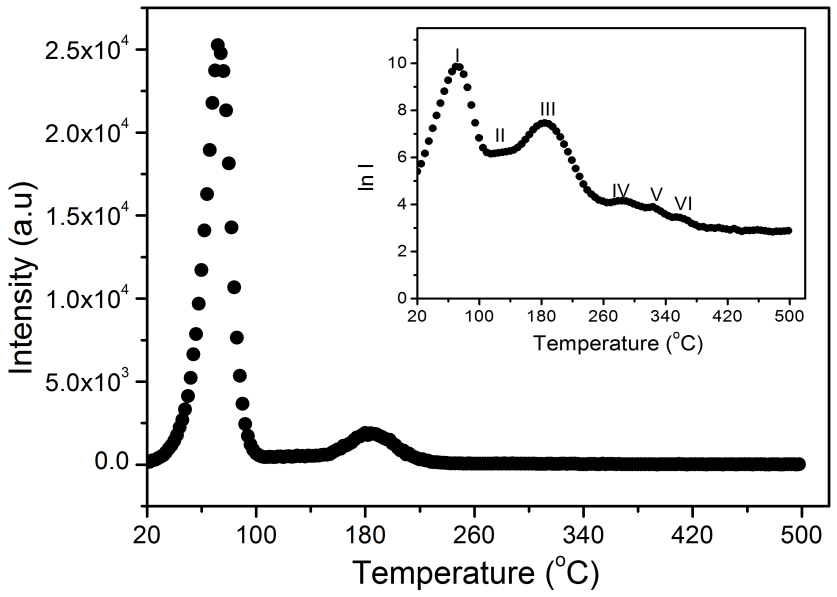

FIGURE 6.15: A thermoluminescence glow curve of the annealed quartz measured at 1 °Cs^{-1} after a dose of 50 Gy. The inset shows the presence of other peaks on a semilogarithmic scale.

6.2.3 Establishing the order of kinetics

The order of kinetics of the main peak was established using the dependence of peak position T_m on dose and the $T_m - T_{stop}$ method.

6.2.3.1 Dose dependence of peak position

The order of kinetics of the main peak was assessed using the dependence of peak position T_m on dose. The quartz sample was irradiated to different doses ranging between 10 and 300 Gy. The TL signal was recorded after each irradiation and the peak position T_m noted. Figure 6.17 shows the plot of T_m against dose. The peak position is stable at 70.6 ± 0.2 °C and independent of doses confirming that peak I is of first order kinetics.

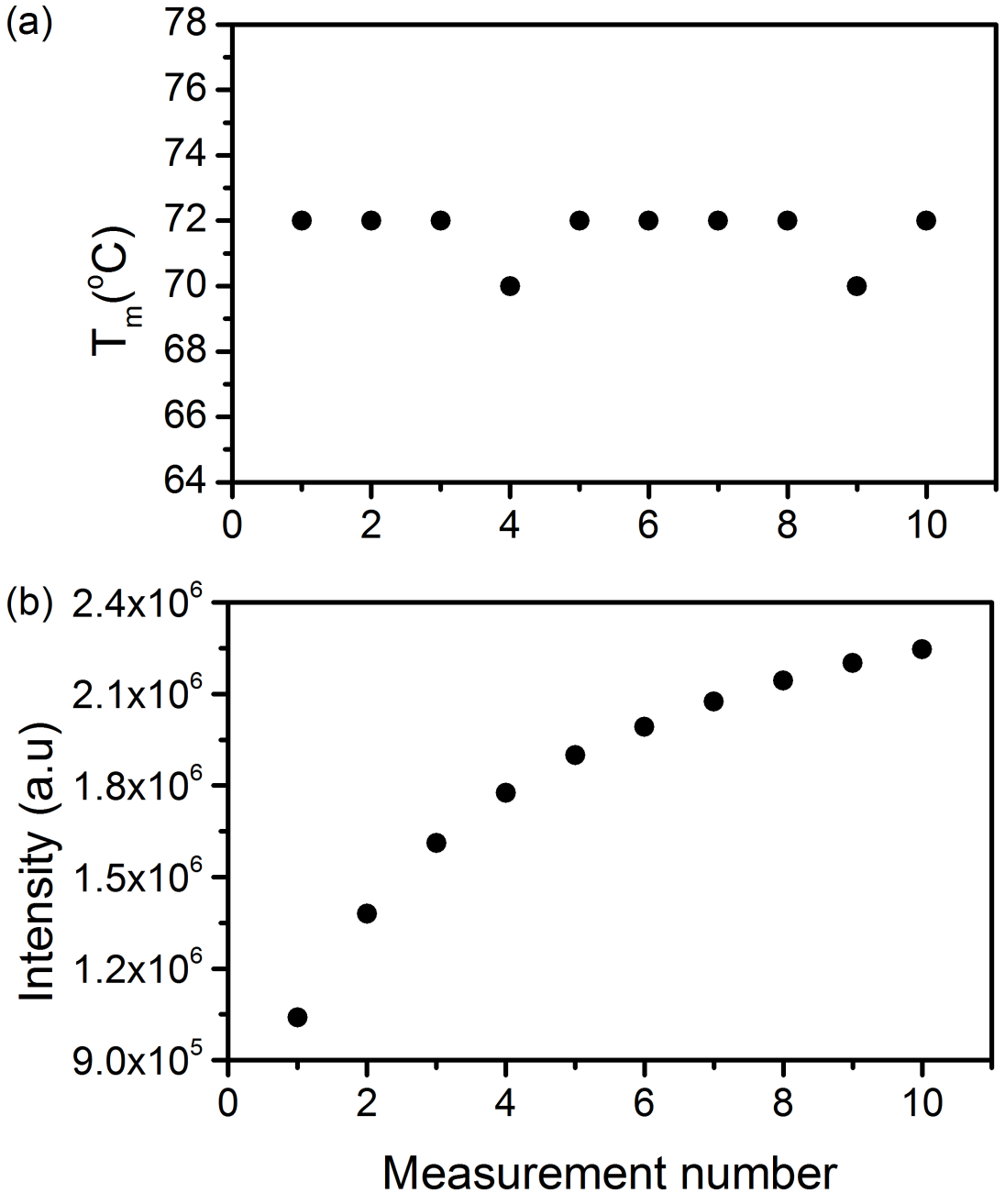

FIGURE 6.16: The influence of repeated measurements on (a) position and (b) intensity of peak I.

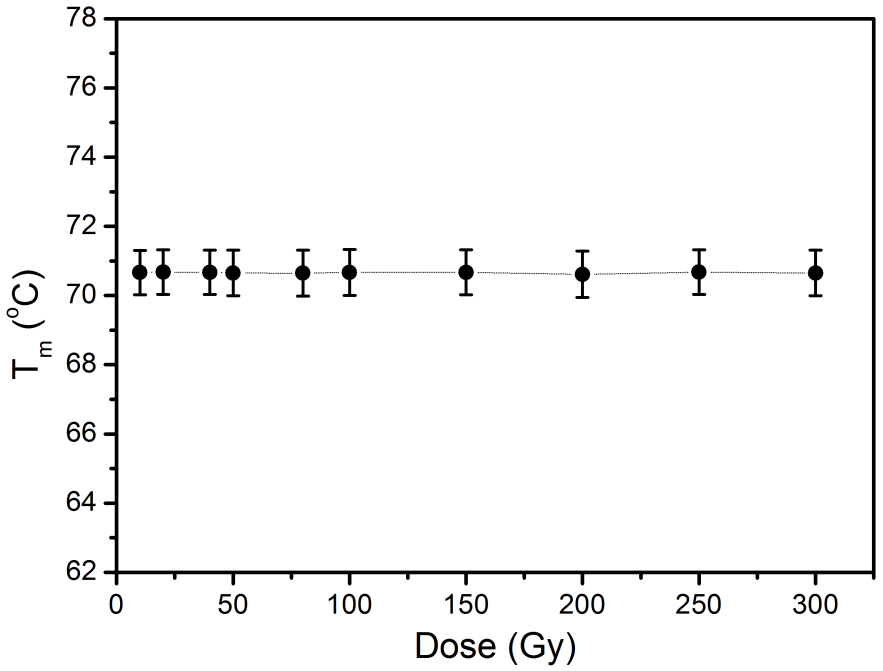

FIGURE 6.17: A graph of T_m against irradiation doses for peak I. Each data point is an average of three measurements and the margin of error in T_m is the standard deviation of the set.

6.2.3.2 T_m-T_{stop} method

Using the $T_m - T_{stop}$ method, the order of kinetics of peak I was determined. For this method, the quartz sample was irradiated to 50 Gy, preheated to temperatures corresponding to different T_{stop} between 20 and 58 °C, and heated to 500 °C to measure the whole glow curve. For each T_{stop} sequence, the peak position T_m was noted. Figure 6.18 shows the plot of T_m against T_{stop} for peak I from an average of three sets of measurements. T_m is independent of T_{stop} at 72.0 ± 0.1 °C.

6.2.4 Kinetic analysis

6.2.4.1 Initial rise method

In order to determine the trap depth responsible for peak I, the initial rise method was applied on the clear rising edge of this peak. By following the rule of thumb of 5 - 15% of the maximum peak intensity I_m, the analysis for this method was

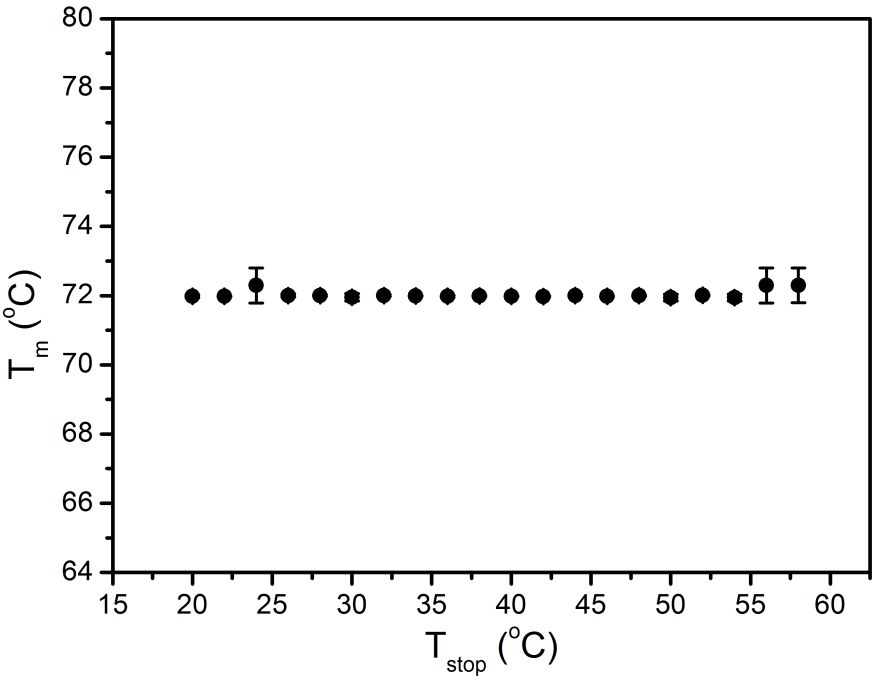

FIGURE 6.18: A graph of T_m against T_{stop} for peak I.

done for the specified data range. For this method, data was extracted for a glow peak measured at 1 °Cs^{-1} after an irradiation of 50 Gy. Figure 6.19 shows a plot of $ln\, I$ against $1/kT$ made for peak I using the initial rise method. The activation energy E was determined from the slope as 0.91 ± 0.01 eV. The activation energy for peak I is in satisfactory agreement with 0.93 ± 0.01 eV recorded for the same quartz annealed at 800 °C for 10 minutes and with 0.94 ± 0.02 eV reported by Chithambo (2014).

6.2.4.2 Whole glow peak method

The kinetic parameters of the main peak was also analysed using the whole glow peak method. This method is suitable for an isolated glow peak. The activation energy and effective frequency factor of peak I were evaluated using equation (2.11) for different values of b. Figure 6.20 shows the semilogarithmic plot of $ln\,(I/n^b)$ against $1/kT$ for different values of b between 1.0 and 1.2. The best fit is for $b = 1.2$ (where $R^2 = 0.999$). The value of b suggests that peak I follows first order kinetics. The activation energy E evaluated from the slope was 1.10 ± 0.01 eV. The effective frequency factor obtained from the intercept is 8.5×10^{13} s^{-1}.

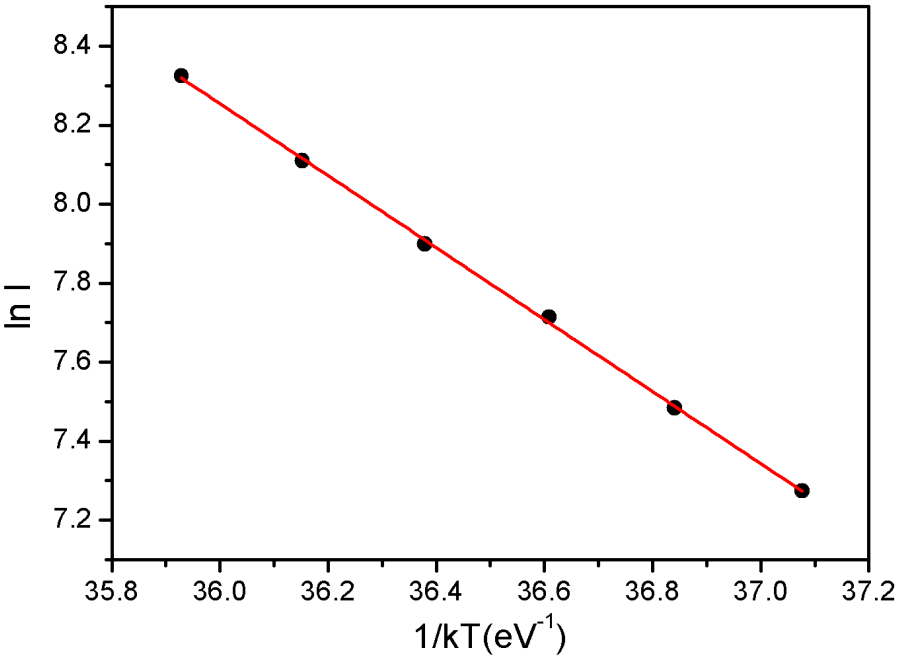

FIGURE 6.19: A plot of $ln(I)$ against $1/kT$ for the initial rise method.

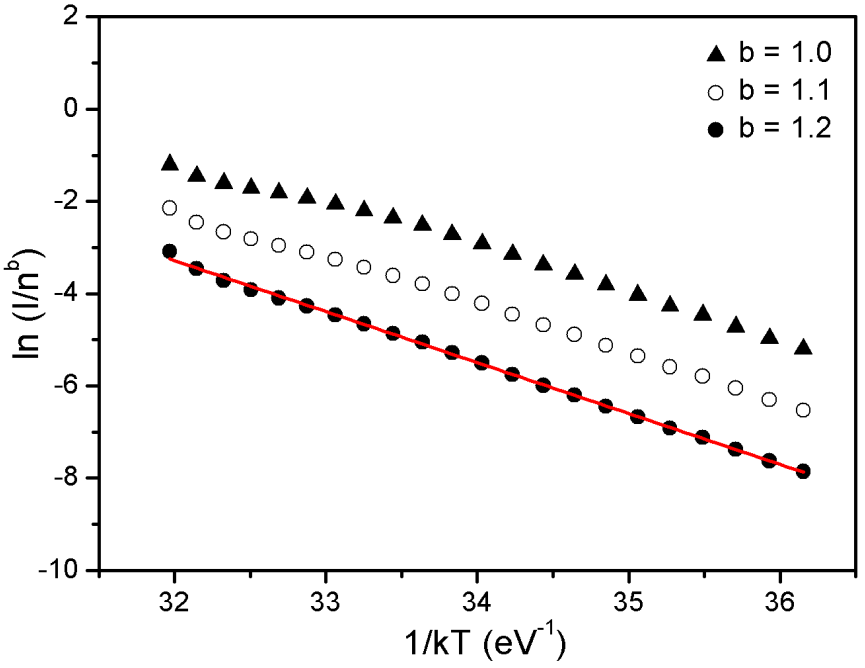

FIGURE 6.20: A plot of $ln(I/n^b)$ against $1/kT$ for different values of b.

6.2.4.3 Peak shape method

To further ascertain the kinetic parameters of the main peak, the peak shape method was used. The order of kinetics of the glow peak was calculated through the geometrical factor (equation (2.23)) as $\mu = 0.42$. This suggests that peak I follows first order kinetics (Chen, 1969) and agrees with the findings from the whole glow peak method. The values of the activation energy for the individual half-widths were calculated as $E_\tau = 1.14 \pm 0.13$ eV, $E_\delta = 1.09 \pm 0.12$ eV, and $E_\omega = 1.13 \pm 0.12$ eV. These values, though higher than those obtained from other methods, are necessarily dependent on τ, δ, ω and are consistent.

6.2.4.4 Curve fitting method

The kinetic parameters E, s, and b of the main peak were also analysed by curve fitting using equation (2.26) by Kitis *et al.* (1998). Figure 6.21 shows the results of the curve fit giving $E = 1.17 \pm 0.02$ eV and $b = 1.20 \pm 0.03$ with $R^2 = 0.999$. The goodness of fit of the glow curve was tested by using equation (2.30) and calculated as $FOM = 0.42\%$. The value of b suggests that peak I follows first order kinetics. In order to determine the frequency factor, the values of E, T_m and β were substituted into equation (2.27) to give $s = 1.5 \times 10^{16}$ s^{-1}. The value of E using this method is in partial agreement (within the margins of error) with 1.10 ± 0.06 eV reported by Yüksel *et al.* (2016) for natural quartz annealed at 800 ∘C for 30 minutes irradiated to 34 Gy.

6.2.5 Phosphorescence analysis

6.2.5.1 Phosphorescence analysis based on first order kinetics

Phosphorescence measurements were made at different temperatures between 40 and 62 °C. Equation (2.33) was used in obtaining the activation energy and frequency factor. A plot of $ln\, p$ against $1/kT_i$ for measurements made at various T_i where $i = 40, \ldots, 62$ is shown in Figure 6.22. The activation energy and frequency factor were found to be $E = 1.03 \pm 0.01$ eV and $s = 1.1 \times 10^{14}$ s^{-1}.

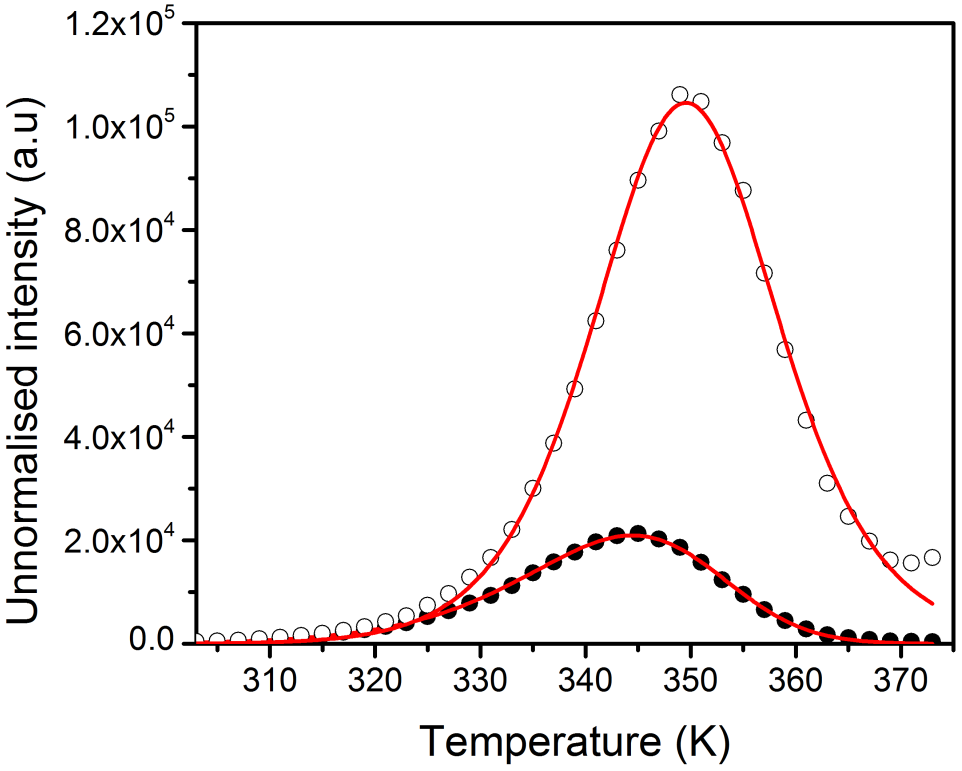

FIGURE 6.21: Results of curve fitting for the main peak. The open symbols represent same data corrected for thermal quenching. The solid line is the best fit of Eq. (2.26).

6.2.5.2 Phosphorescence analysis based on general order kinetics

The general order kinetics of phosphorescence was further used to examine the order of kinetics and activation energy of the main peak by making a plot of $I^{(1-b)/b}$ against t which was linear for $b = 1.1$. Figure 6.22 shows a plot of $ln[(b-1)n_0^{(b-1)}s']$ (denoted as $ln\,p$) against $1/kT_i$ for the general order kinetics of phosphorescence. The activation energy and frequency factor were determined as 0.91 ± 0.03 eV and 6.7×10^{10} s^{-1} respectively. The value of the activation energy is consistent with that obtained using the initial rise method.

6.2.5.3 Analysis based on the area under an isothermal decay curve

The area-based method of phosphorescence analysis by Chithambo (2014) was applied on isothermal decay curves measured for 5 s. The decay curves were

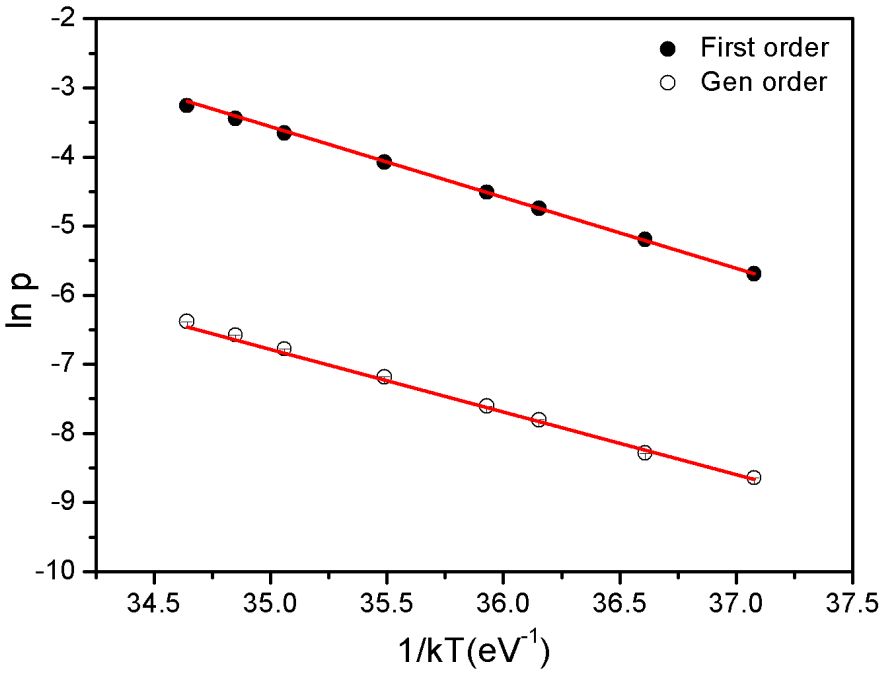

FIGURE 6.22: A graph of $ln\,p$ against $1/kT$ to evaluate the activation energy for phosphorescence based on first and general order kinetics.

measured at temperatures between 30 and 58 °C after irradiation to 50 Gy. For each temperature, the area ϕ of an isothermal curve was calculated. Figure 6.23 shows a plot of $ln\,\phi$ against $1/kT$ for peak I. The activation energy obtained from this plot is 0.91 ± 0.02 eV. This value is consistent with the values obtained from the initial rise and general-order phosphorescence methods.

6.2.5.4 Analysis of the temperature-dependent areas by curve fitting

The area ϕ plotted against temperature produces a TL-like glow peak shown in Figure 6.24. This curve was fitted using the GCD equation by Kitis *et al.* (1998). The kinetic parameters E, b,and s were evaluated from the fit as 1.19 ± 0.03 eV, 1.30 ± 0.05, 6.4×10^{16} s^{-1} respectively. The value of the activation energy agrees with 1.17 ± 0.02 eV recorded earlier from the curve fitting method.

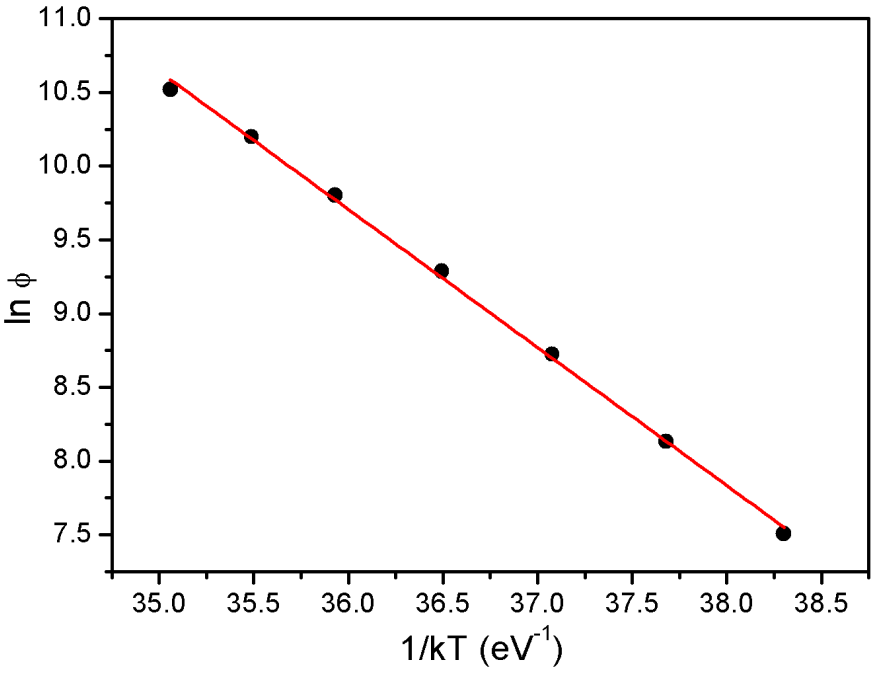

FIGURE 6.23: A plot of $ln\,\phi$ against $1/kT$ for area under an isothermal decay curve.

6.2.6 Variable heating rate method

The variable heating rate method was further applied on the main peak in order to evaluate the activation energy and frequency factor. The method was applied on three sets of measurements on the quartz sample irradiated to 50 Gy and heated to nine different heating rates between 0.2 and 5 °Cs^{-1}. The analysis was done for peak I using equation (2.17). Figure 6.25 shows a plot of $ln\,(T_m^2/\beta)$ against $1/kT_m$ for the various heating rate method. The activation energy obtained from the slope is 0.81 ± 0.01 eV. For the frequency factor evaluated from the intercept of the graph, $s = 6.3 \times 10^{10}$ s^{-1}. The results from the VHR method is less than the results obtained from other methods. Pagonis *et al.* (2013) have shown using the semi-localised model (Mandowski, 2004) that the variable heating rate method can systematically underestimate the value of the activation energy. However, the value of the activation energy obtained in this method is consistent with 0.80 eV reported by Ogundare and Chithambo (2006) for the same sample annealed at 900 °C for 10 minutes.

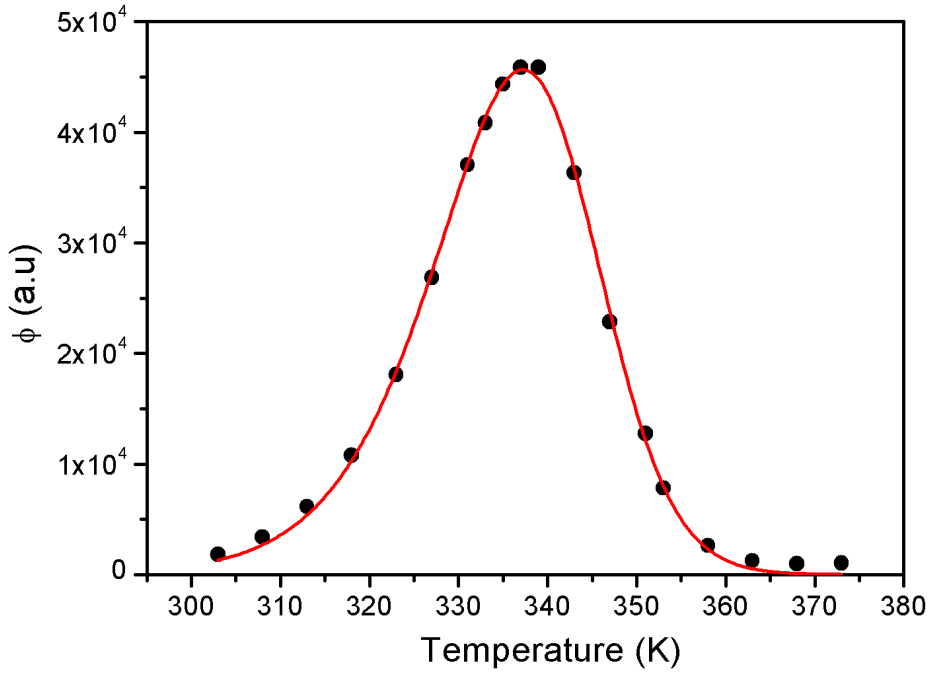

FIGURE 6.24: The temperature dependence of the area under the isothermal decay curve for 5 s. The solid line is the best fit of Eq. (2.26).

6.3 Thermal quenching and inverse thermal quenching

Figure 6.26 shows the dependence of TL intensity (in counts/°C) on heating rate for the quartz sample irradiated to 50 Gy. The TL intensity increases monotonically with heating rate. This would indicate that the sample is not affected by thermal quenching. Repeated measurements on fresh aliquots gave similar results.

6.3.1 Analysis of thermal quenching based on change of TL intensity with heating rate

In order to examine thermal quenching effects on this sample, the principle that luminescence emission is subject to competing radiative and non-radiative routes as applied on a secondary peak in α-Al_2O_3 :C was considered (Chithambo and

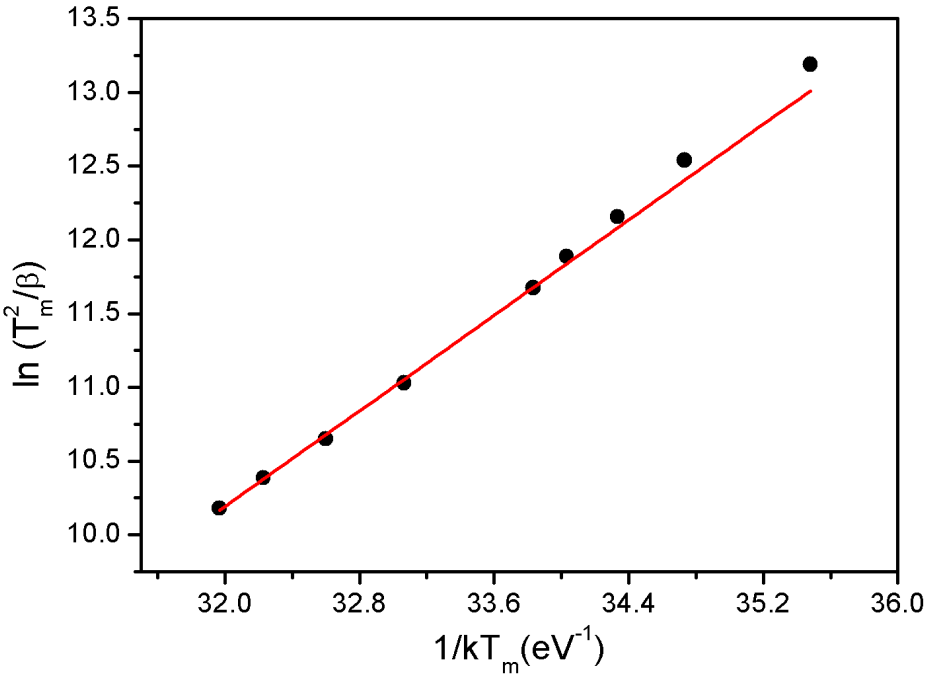

FIGURE 6.25: A plot of $ln\left(T_m^2/\beta\right)$ against $1/kT_m$ for the various heating rate method.

Costin, 2017). As Chithambo and Costin (2017) pointed out, if the number of electrons undergoing transitions at the recombination centre is very low, the radiative transitions cannot be high enough to ameliorate against the non-radiative route. This fact can be used as an independent test for presence of any thermal quenching. This test was applied on the quartz sample by significantly reducing the dose used from 50 to 3 Gy.

Figure 6.27 shows the new effect of heating rate on TL intensity from the sample irradiated to 3 Gy. The TL intensity (in counts/°C) as well as the peak integral (in counts) now decreases significantly with heating rate in a behaviour consistent with thermal quenching. Thus, the increase of TL intensity with heating rate cannot on its own be proof that a sample is not affected by thermal quenching. The activation energy for thermal quenching was evaluated using the temperature dependent luminescence function in equation (2.54). We now describe the temperature luminescence function in terms of peak area as

$$A_q = \frac{A_{uq}}{1 + C\,exp(-\Delta E/kT_m)} \tag{6.1}$$

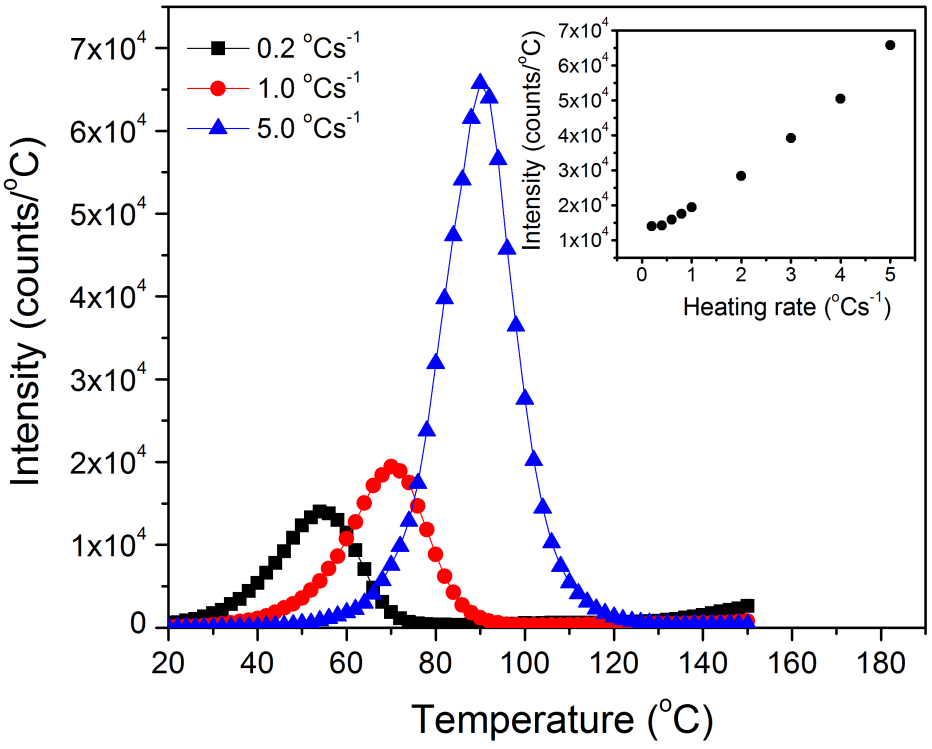

FIGURE 6.26: Examples of TL glow-curves measured at different heating rates. The inset shows the dependence of intensity on heating rate.

where A_q and A_{uq} represent the most quenched and lesser quenched areas of the glow peaks measured at the highest and other heating rates respectively. Figure 6.28 shows the graph of $ln[(A_{uq}/A_q)-1]$ against $1/kT_m$. The activation energy for thermal quenching was evaluated as $\Delta E = 0.99 \pm 0.02$ and $C = 9.3 \times 10^{14}$. The ΔE value is in agreement with published values in the literature e.g. 0.92 ± 0.01 eV (Chithambo, 2015).

6.3.2 Analysis of thermal quenching using the area under an isothermal decay-curve

Thermal quenching was analysed using the area under an isothermal decay-curve for a sample irradiated to 50 Gy. Equation (2.55) was used to evaluate the activation energy for thermal quenching; where the quenched and the unquenched areas correspond to the highest (i.e. 58 °C in this case) and other measurement temperatures in the rising edge of the graph of ϕ against measurement temperature. Figure

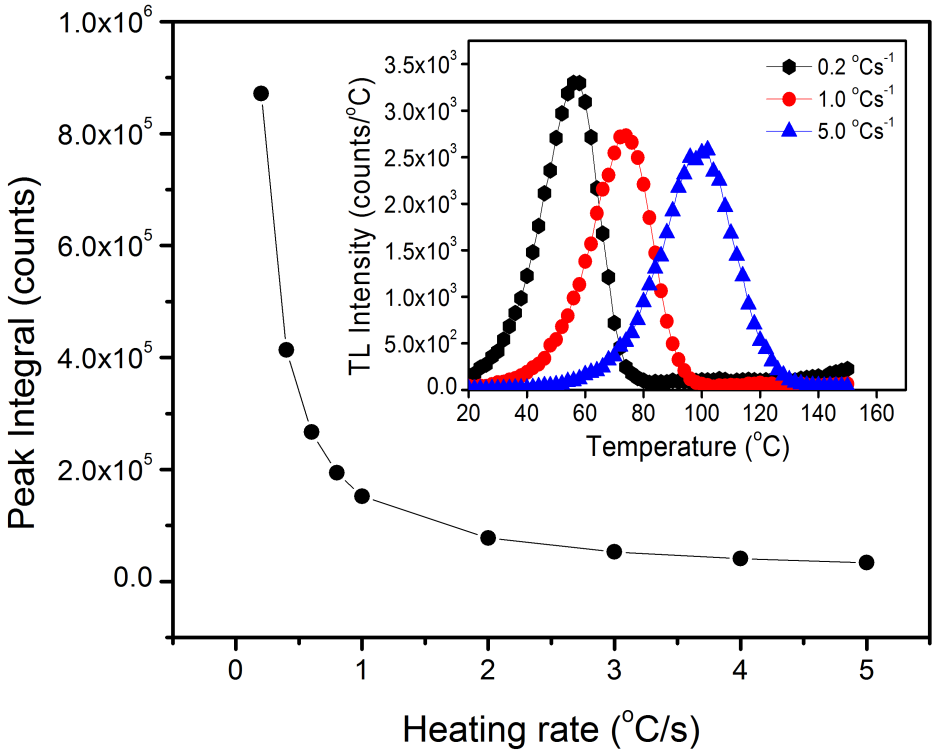

FIGURE 6.27: A plot of peak integral against heating rate for the sample irradiated to 3 Gy. The inset shows an example of TL glow-curves measured at different heating rates.

6.29 shows a graph of $ln(\phi_q/\phi_u)$ against $1/kT$ for measurements made for 5 s. The value of the activation energy for thermal quenching determined from the slope of the graph is 0.96 ± 0.02 eV. This value is consistent with 0.99 ± 0.02 eV determined in Figure 6.28 for the sample irradiated to 3 Gy. An important conclusion from this study is that increase of TL intensity with heating rate, sometimes referred to as inverse thermal quenching e.g. (Pagonis *et al.*, 2013) does not necessarily imply the absence of thermal quenching. We have also shown that with respect to thermal quenching, the method based on the area under an isothermal decay curve (Chithambo, 2014) is not influenced by the dose the sample is irradiated to unlike the conventional method based on change of TL intensity with heating rate (Pagonis *et al.*, 2006).

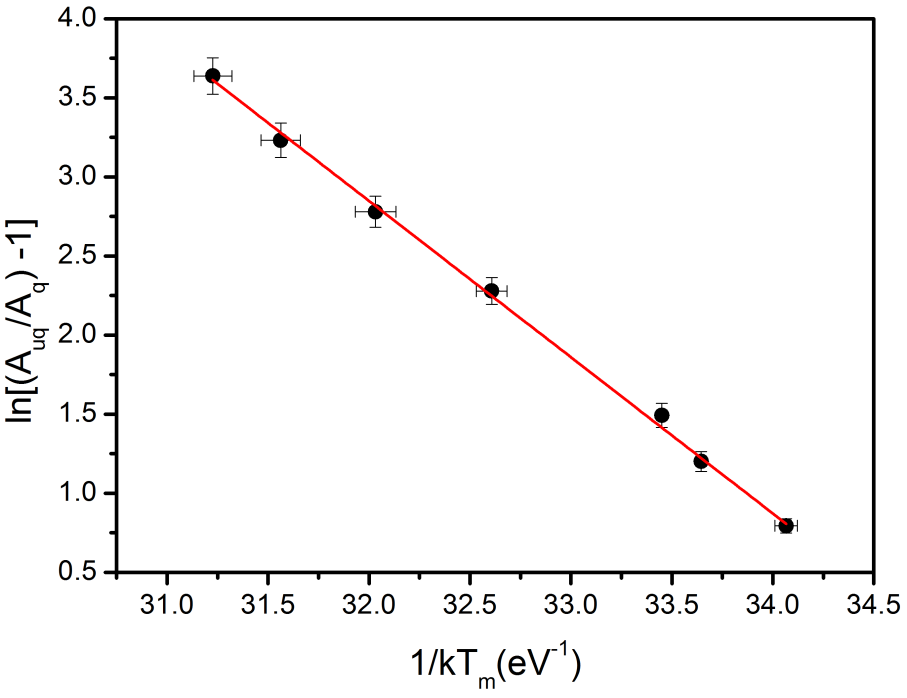

FIGURE 6.28: A graph of $ln[(A_{uq}/A_q) - 1]$ against $1/kT_m$ used to evaluate thermal quenching.

6.3.3 Summary

Kinetic analysis conducted on the main peak has been carried out using various methods. The main peak observed at 72 °C is a first order peak as discovered from the methods used. The values of the activation energy evaluated using the methods were consistent (except for the VHR method). The TL intensity of the main peak increased with heating rate implying that the sample is not affected by thermal quenching. However, when the same sample was irradiated to a low dose of 3 Gy, the TL intensity decreases with heating rate showing presence of thermal quenching. The summary of kinetic parameters for the different methods is presented in Table 6.2.

6.4 Conclusion

This chapter has reported the thermoluminescence properties of natural quartz annealed at 800 °C for 10 minutes and 1 hour. Dosimetric and kinetic analyses were

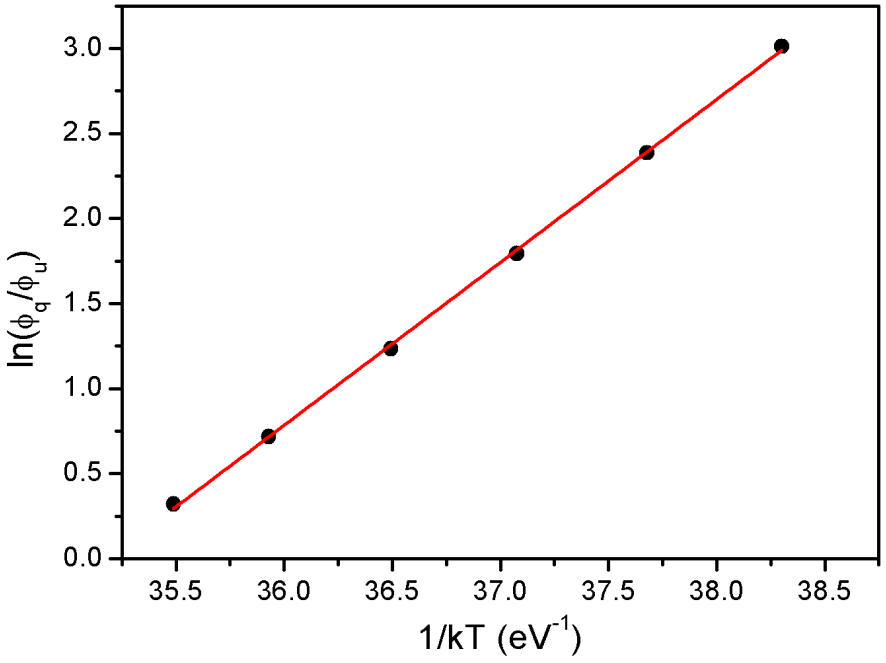

FIGURE 6.29: A graph of $ln(\phi_q/\phi_u)$ against $1/kT'$ in a study of thermal quenching using area under isothermal decay-curve

TABLE 6.2: Kinetic parameters of the main TL peak of natural quartz annealed at 800 °C for 1 hour.

Method	E (eV)	b	s (s^{-1})	ΔE (eV)	Reference
T_m-Dose		1			
T_m-T_{stop}		1			
IR	0.91 ± 0.03				Fig. 6.19
WGP	1.10 ± 0.01	1.2	8.5×10^{12}		Fig. 6.20
PS	$1.14 \pm 0.13^{\tau}$ $1.09 \pm 0.12^{\delta}$ $1.13 \pm 0.12^{\omega}$	1			Sect. 6.2.4.3
CF	1.17 ± 0.02	1.20 ± 0.03	1.5×10^{16}		Fig. 6.21
VHR	0.81 ± 0.01		6.3×10^{10}	0.89 ± 0.06	Fig. 6.25
IDC, 1st order	1.03 ± 0.01	1	1.1×10^{14}		Fig. 6.22
IDC, Gen. order	0.91 ± 0.03				
IDC, Area	0.91 ± 0.02			0.96 ± 0.01	Fig. 6.23
IDC, CF	1.19 ± 0.03	1.30 ± 0.05	6.4×10^{16}		Fig. 6.24

carried out on the two most prominent peaks, peaks I and III. The studies show that the peaks follow first order kinetics using various methods. A comparative analysis of kinetic parameters of the main peak is presented in Table 6.3. The kinetic parameters obtained for the quartz annealed for 1 hour for each method are higher than for those annealed for 10 minutes (except for the initial rise and variable heating rate methods). The results show that the duration of annealing has an effect on the kinetic parameters. The quartz annealed at 800 °C for 1 hour showed an inverse thermal quenching at 50 Gy. This was demonstrated to be a dose-dependent feature. When the sample was irradiated to 3 Gy, thermal quenching became apparent. We have demonstrated that as regards analysis for thermal quenching, the method based on the area under an isothermal decay curve (Chithambo, 2014) is not influenced by the dose the sample is irradiated to unlike the conventional one based on change of TL intensity with heating rate.

TABLE 6.3: A comparative analysis of kinetic parameters for peak I from samples of quartz annealed at 800 °C

Method	800 ° C, 10 minutes		800 ° C, 1 hour	
	E (eV)	s (s^{-1})	E (eV)	s (s^{-1})
IR	0.93 ± 0.01		0.91 ± 0.03	
WGP	0.90 ± 0.01	9.5×10^{11}	1.10 ± 0.01	8.5×10^{12}
PS	$0.94 \pm 0.05^{\tau}$ $0.92 \pm 0.04^{\delta}$ $0.94 \pm 0.05^{\omega}$		$1.14 \pm 0.13^{\tau}$ $1.09 \pm 0.12^{\delta}$ $1.13 \pm 0.12^{\omega}$	
VHR	0.93 ± 0.03	5.2×10^{12}	0.81 ± 0.01	6.3×10^{10}
CF	0.95 ± 0.01	6.3×10^{12}	1.17 ± 0.02	1.5×10^{16}
IDC, 1st order	1.008 ± 0.004	6.5×10^{13}	1.03 ± 0.01	1.1×10^{14}
IDC, Area	0.87 ± 0.03		0.91 ± 0.03	6.7×10^{10}
IDC, CF	1.02 ± 0.02	2.1×10^{14}	0.91 ± 0.02	1.1×10^{14}

Chapter 7

Influence of annealing on thermoluminescence of natural quartz annealed at 1000 °C

This chapter discusses the influence of annealing on the kinetic parameters of quartz annealed at 1000 °C for 10 minutes and for 1 hour. The samples were annealed to enhance their luminescence sensitivity. Dosimetric and kinetic analysis were carried out on the main and secondary peaks of both samples using various methods. Results from the quartz annealed at 1000 °C for 10 minutes are reported first in section 7.1. These are compared with those obtained from the unannealed quartz reported in Chapter 5. This is done to investigate the influence of annealing on the trap parameters of the peaks. Results from the quartz annealed at 1000 °C for 1 hour are reported and discussed in section 7.2.

7.1 Thermoluminescence of quartz annealed at 1000 °C for 10 minutes

Results of dosimetric features and kinetic analysis of the TL from quartz annealed at 1000 °C for 10 minutes are reported in this section. The results of the analysis are compared with those from the unannealed quartz in order to study the influence of annealing on the kinetic parameters.

7.1.1 Glow curve characteristics

Figure 7.1 shows a glow curve measured at 1 °Cs^{-1} from a sample irradiated to 50 Gy. The glow curve shows three peaks at 68, 130, and 176 °C labelled I, II, and III. The inset shows the same data on a semilogarithmic scale. This revealed an additional peak at 276 °C labelled IV. The positions of these peaks were further verified through thermal cleaning.

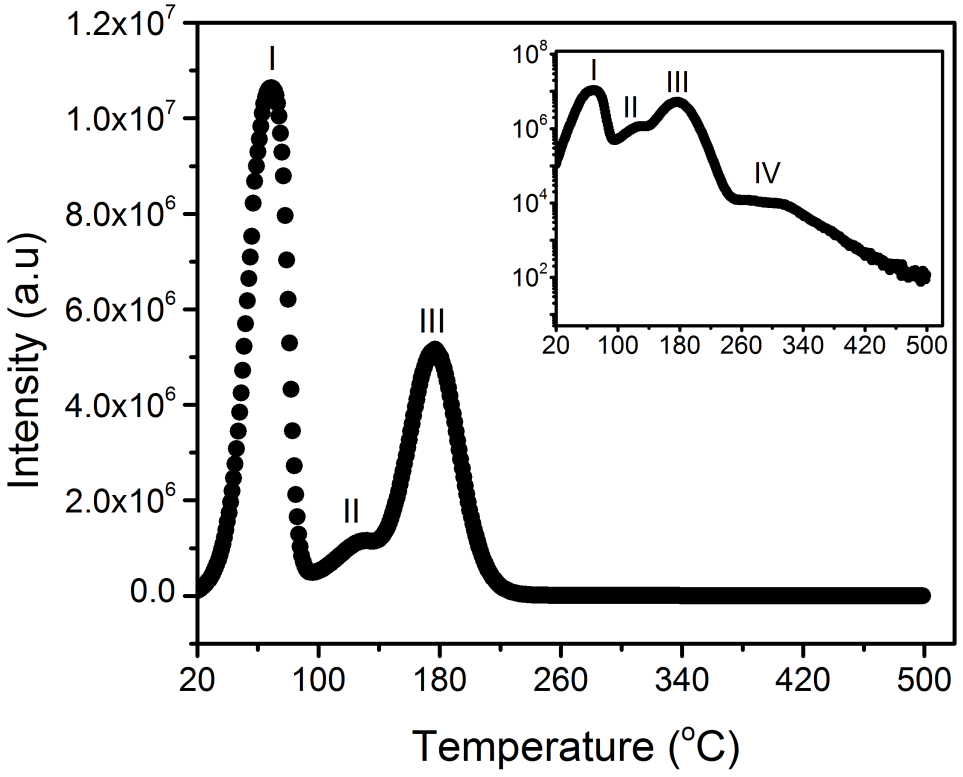

FIGURE 7.1: A TL glow curve of the quartz sample measured at 1 °Cs^{-1} following irradiation to 50 Gy. The inset shows the same glow curve on a semilogarithmic scale in order to reveal hidden peaks.

7.1.2 Thermal cleaning

Thermal cleaning was used to confirm the number and positions of peaks in Figure 7.1. Figure 7.2 shows the results of thermal cleaning. The preheating temperatures were 100, 140, 250, 350, and 400 °C. The procedure revealed peaks II, III, IV, V, VI, and VII at 130, 176, 276, 300, 360 and 416 °C respectively.

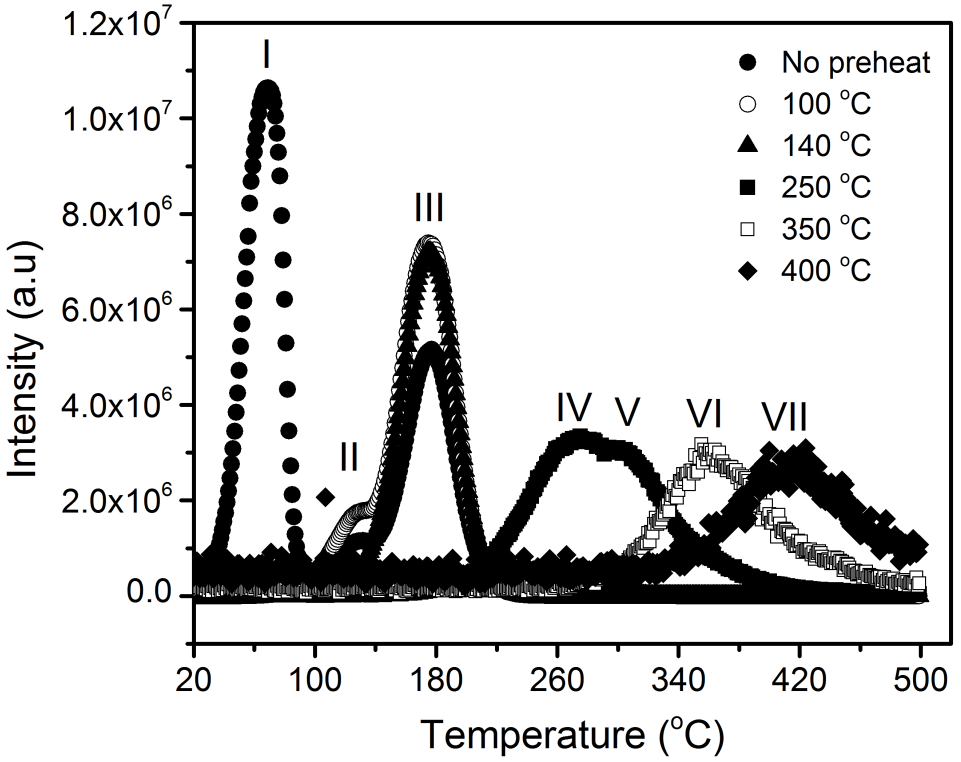

FIGURE 7.2: Thermally cleaned glow peaks recorded after irradiation, preheating and heating. Peaks I - VII were recorded with no preheating and after preheating to 100, 140, 250, 350, and 400 °C. The data corresponding to preheating to 250, 350 and 400 have been scaled up by ×300, ×2000, and ×7000 respectively to aid visual clarity.

7.1.3 Dosimetric features

Dosimetric studies consisting of reproducibility, dose response and fading were carried out on peaks I and III, the two most prominent peaks. These peaks are well defined compared to other peaks in the glow curve.

7.1.3.1 Reproducibility

The reproducibility of the TL signal was investigated for peaks I and III by measuring the TL seven times. The sample was irradiated to 50 Gy each time. Figure 7.3 shows the influence of repeated measurement on the peak position T_m and intensity of peaks I and III.

T_m was stable at 68 and 176 °C for peaks I and III respectively. The positions of the peak are thus unaffected by sample reuse. The intensity of peak I was noted to increase with repeated measurements whereas that of peak III was independent of the number of runs. The increase in intensity of peak I with repeated measurements may be due to change in sensitivity of the sample due to repeated irradiation and heating. The intensity of peak III being constant shows that the TL signal of peak III is reproducible.

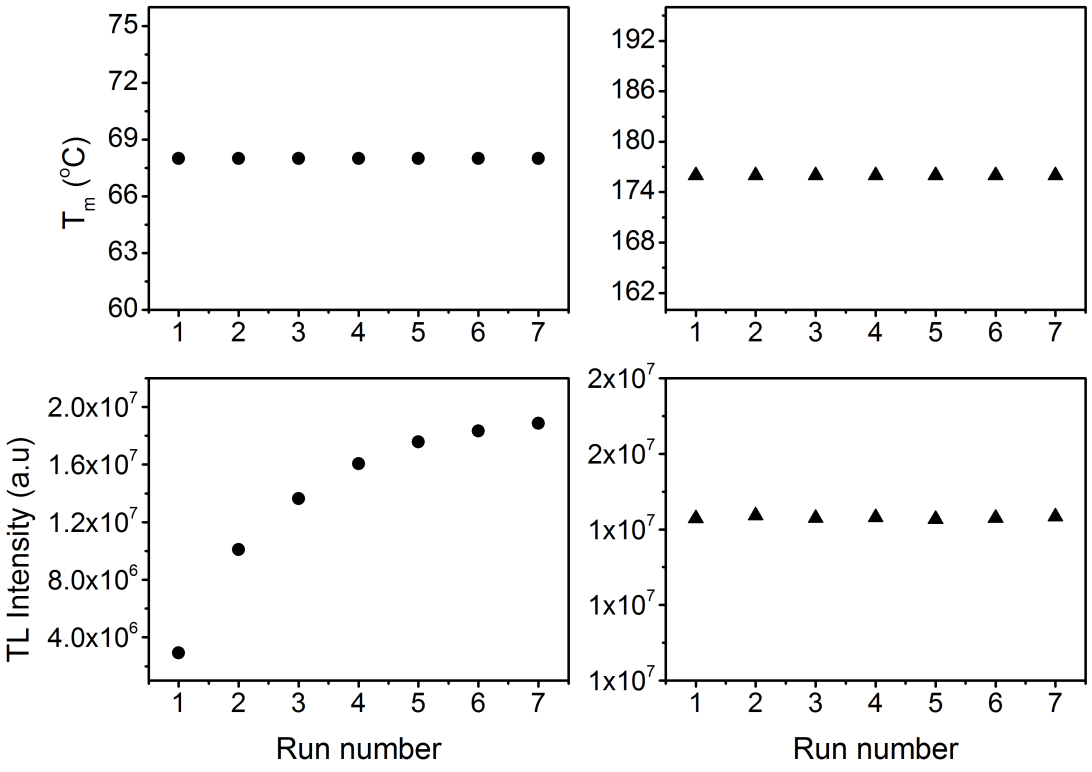

FIGURE 7.3: The influence of repeated measurements on peak position and peak intensities for peaks I and III. The circle and triangle symbols represent data corresponding to peaks I and III respectively.

7.1.3.2 Dose response

The influence of irradiation dose on the intensity of peaks I and III was investigated for doses between 10 and 300 Gy. Figure 7.4 shows the dependence of intensity on dose for peaks I and III. The intensity of peak I increases at a constant value

towards saturation whereas the intensity of peak III increases monotonically towards saturation. Repeated measurements using a neutral density filter of optical density OD3 and 0.1% transmittance to reduce the TL signal gave similar results. The dose response of these peaks were qualitatively modelled as

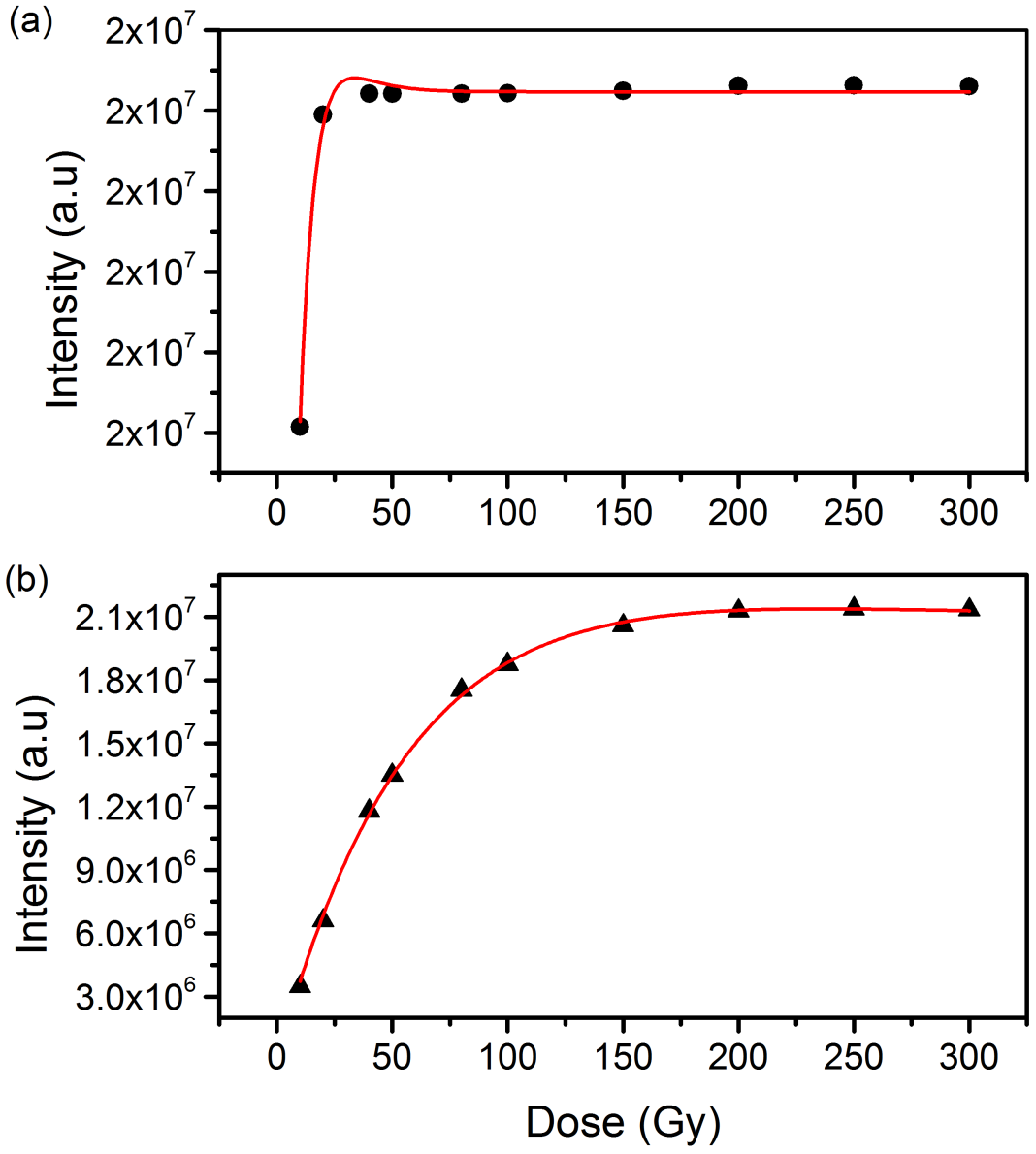

FIGURE 7.4: The influence of dose on the maximum intensity of (a) peak I and (b) peak III. The solid lines through data is in each case a fit of Eq. (7.1).

$$y(D) = A(1 - e^{-BD}) - CDe^{-BD} \tag{7.1}$$

where D is the dose in Gy, A in arbitrary unit is the TL response at saturation, B and C in Gys^{-1} are constants.
The lines passing through the data points in Figure 7.4 are the best fits of equation (7.1).
Qualitatively, the dose response is sublinear for peaks I and III. This response is consistent with other annealed quartz studied in this work.

7.1.3.3 Fading

Fading of the TL signal was studied for peak I for a delay up to 5 hours. Figure 7.5 shows a graph of intensity against delay between irradiation to 50 Gy and measurement. The TL intensity decreases with delay. The inset shows that the position of peak I did not change by more than 2 °C as the intensity decreases. The TL signal was fitted by a function $I = I_0\, exp(-t/\tau)$ from which the mean lifetime τ was evaluated as 7784 s.

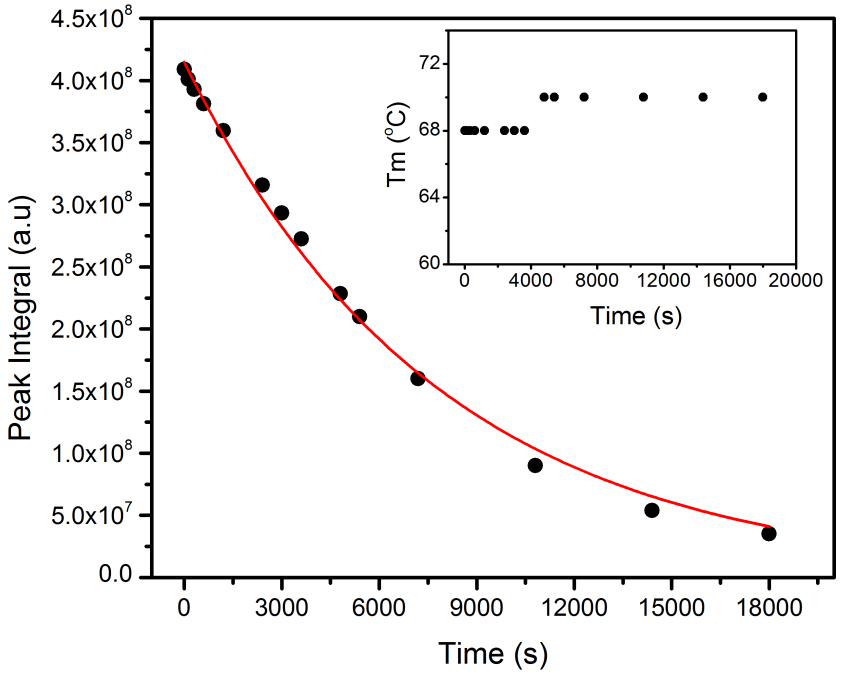

FIGURE 7.5: The fading of the TL signal against delay between irradiation and measurement. The line passing through the data points is the best fit of Eq. (5.1). The inset shows that the position of the peak remains stable as the peak fades.

7.1.4 Kinetic analysis

Kinetic analysis was carried out on peaks I and III using the initial rise-, whole glow peak-, peak shape-, variable heating rate, curve fitting, and phosphorescence methods.

7.1.4.1 Initial rise method

Plots of $ln\, I$ against $1/kT$ for the initial rise portions of the peaks are shown in Figure 7.6. The activation energy was evaluated as 0.934 ± 0.004 eV for peak I and as 1.18 ± 0.01 eV for peak III. The activation energy obtained for peak I is consistent with 0.93 ± 0.03 eV for the same peak of an unannealed quartz using the same method. This shows that annealing has little effect on the activation energy.

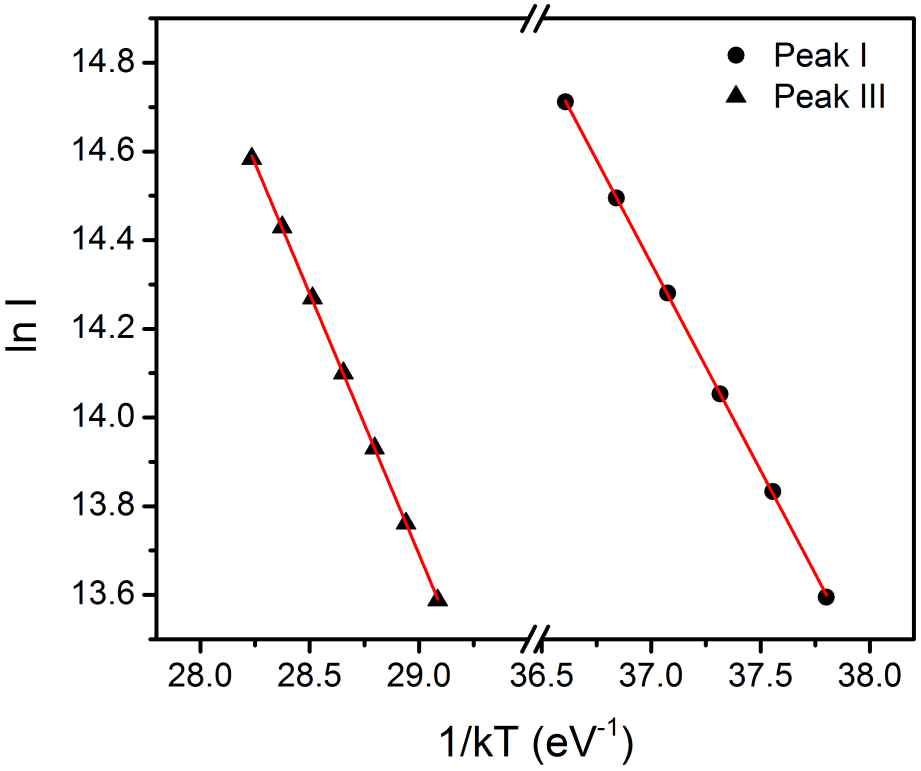

FIGURE 7.6: A plot of $ln\, I$ against $1/kT$ for peak I and peak III using the initial rise method.

7.1.4.2 Whole glow peak method

The whole glow peak method was used to determine the activation energy, order of kinetics and frequency factor of peaks I and III. Figure 7.7 shows a graph of $ln\left(I/n^b\right)$ against $1/kT$ for different values of b between 1.0 and 1.2. The best fit

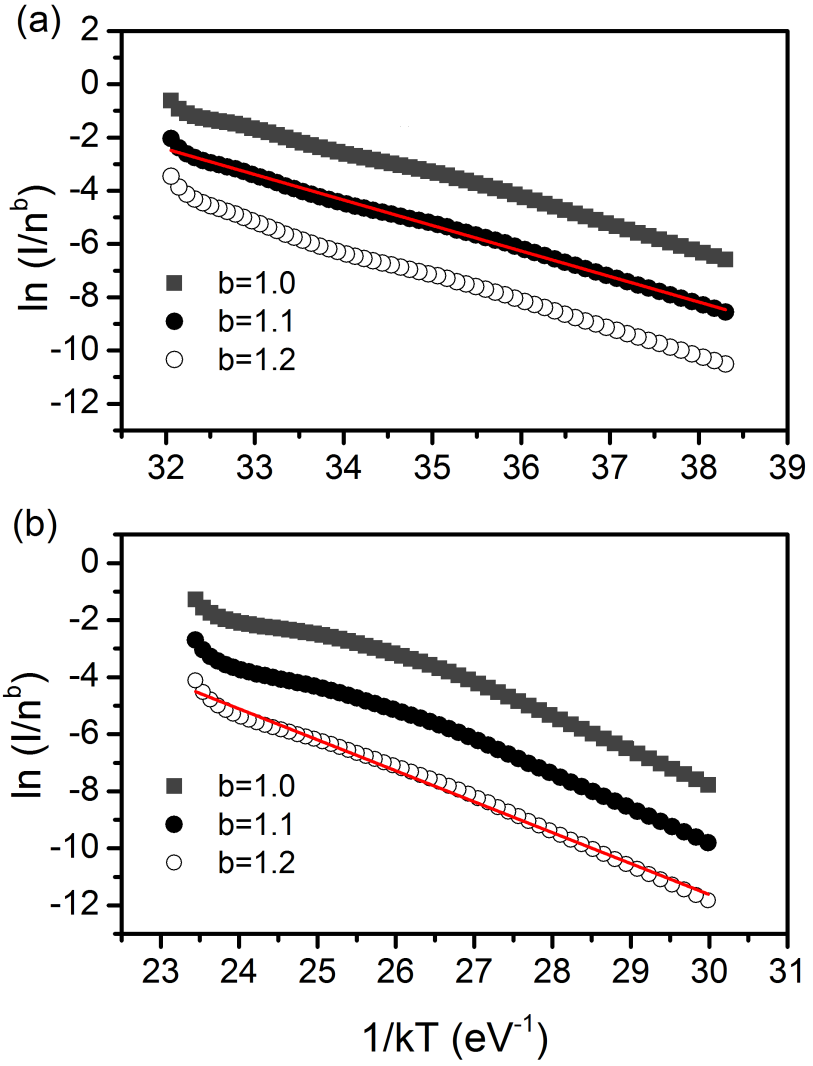

FIGURE 7.7: Plots of $ln(I/n^b)$ against $1/kT$ for different values of b for (a) peak I (b) peak III.

was determined as $b = 1.1\,(R^2 = 0.997)$ for peak I and as $b = 1.2$ for peak III. These values of b suggest that the peaks are of first order kinetics. The activation energy was found as $E = 0.96 \pm 0.01$ eV for peak I and as $E = 1.09 \pm 0.01$ eV for peak III. These values are in good agreement with 0.98 ± 0.01 and 1.06 ± 0.01 eV obtained for peaks I and III respectively for the unannealed quartz suggesting

that annealing has little effect on the activation energy. The effective frequency factors obtained from the intercept of the fits are 1.5×10^{13} and 1.1×10^{11} s^{-1} respectively for peaks I and III.

7.1.4.3 Peak shape method

The order of kinetics of peaks I and III was determined as 0.46±0.06 and 0.46±0.04 respectively using the peak shape method. The values suggest that peaks I and III are of general order kinetics. This does not agree with the whole glow peak method. However, it can be said that the peaks follow first order kinetics within the margins of error of the symmetry factor.
The values of the activation energy, based on the geometrical properties of the peaks were calculated for peak I as $E_\tau = 1.06 \pm 0.09$ eV, $E_\delta = 1.06 \pm 0.09$ eV, and $E_\omega = 1.07 \pm 0.10$ eV.
Similarly for peak III, $E_\tau = 1.15 \pm 0.07$ eV, $E_\delta = 1.16 \pm 0.07$ eV, and $E_\omega = 1.16 \pm 0.07$ eV. In comparison, the values of E for peaks I and III are in satisfactory agreement with the values obtained for the unannealed quartz using same method.

7.1.4.4 Curve fitting method

The glow curves for peaks I and III extracted from thermal cleaning were fitted using equation (2.26). Figure 7.8 shows the best fit obtained for peaks I and III. The kinetic parameters determined are $E = 1.01 \pm 0.01$ eV and $b = 1.14 \pm 0.02$ with $FOM = 0.21\%$ for peak I and $E = 1.23 \pm 0.01$ eV and $b = 1.46 \pm 0.01$ with $FOM = 0.36\%$ for peak III. The E values obtained for peaks I and III are consistent with $E = 1.01 \pm 0.01$ eV and $E = 1.21 \pm 0.02$ eV obtained for peaks I and III for the unannealed quartz. The values of b suggest that peaks I and III follow first- and general-order kinetics respectively. The frequency factor for peak I and III was calculated a $s = 7.7 \times 10^{13}$ and $s = 4.5 \times 10^{12}$ s^{-1} respectively.

7.1.4.5 Variable heating rate method

Peaks I and III were also analysed for kinetic parameters using the variable heating rate method. The activation energy E and frequency factor s were determined using equation (2.17). Figure 7.9 shows the plots of $ln\,(T_m^2/\beta)$ against $1/kT_m$.

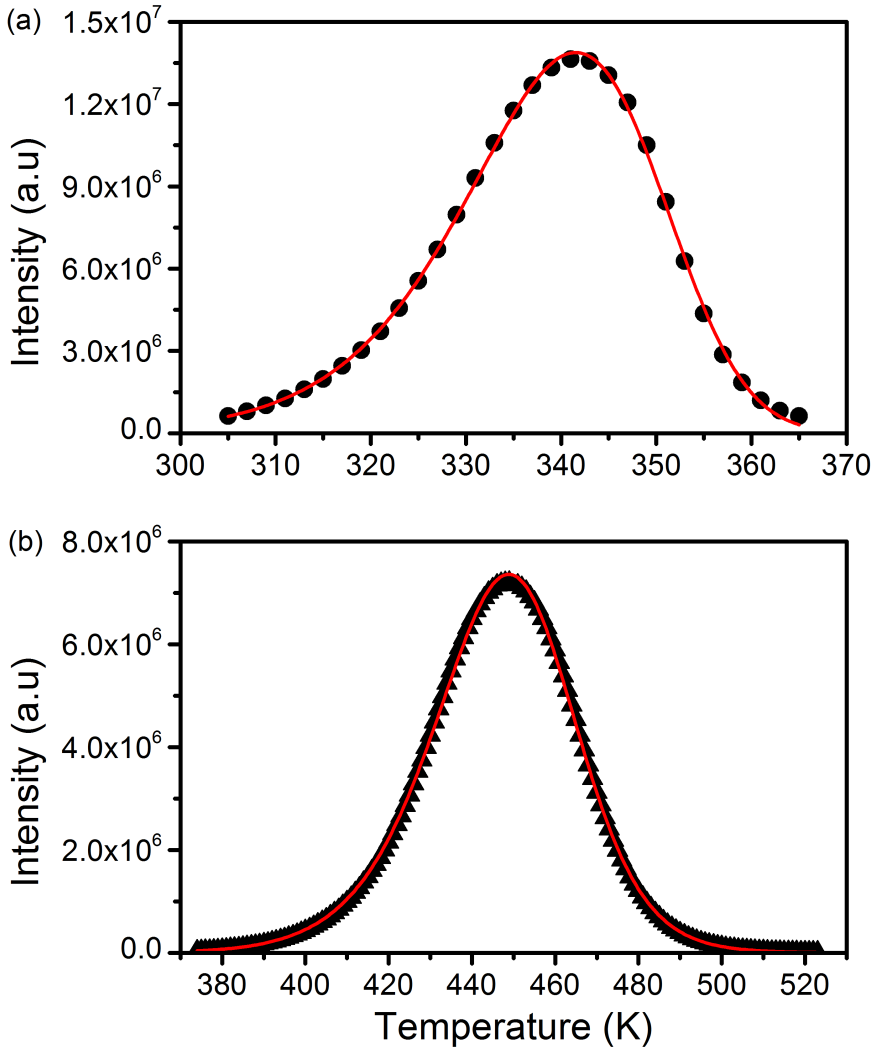

FIGURE 7.8: Results of curve fitting for (a) peak I (b) peak III. The solid lines passing through data points are the best fits of Eq. (2.26)

The activation energy obtained from the slope of the plot is 0.94 ± 0.03 eV for peak I and 1.56 ± 0.02 eV for peak III. The frequency factors were evaluated as 5.3×10^{12} and 3.2×10^{16} s^{-1} for peaks I and III respectively.

7.1.5 Phosphorescence methods

The kinetic parameters for peaks I and III were further determined by phosphorescence analysis. The sample was irradiated to 50 Gy each time.

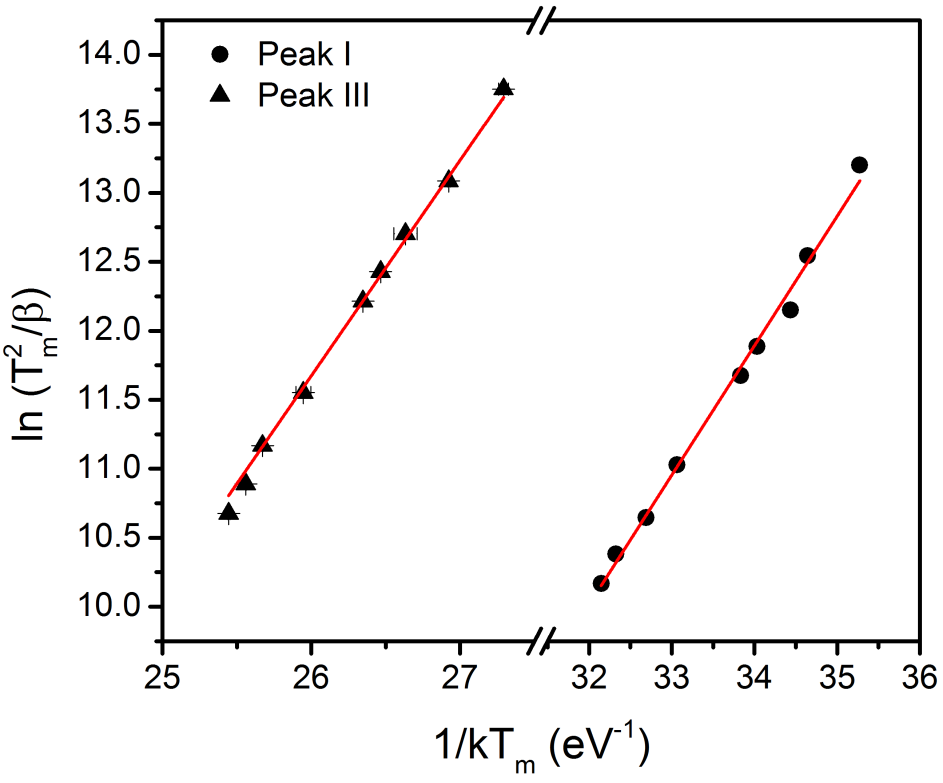

FIGURE 7.9: A graph of $ln\left(T_m^2/\beta\right)$ against $1/kT_m$ for the various heating rate method for peaks I and III

7.1.5.1 Isothermal analysis based on first order kinetics

Figure 7.10 shows a semilogarithmic plot of p against $1/kT$ made for peaks I and III. The activation energy and frequency factor were found to be $E = 0.92 \pm 0.01$ eV and $s = 2.0 \times 10^{13}$ s^{-1} for peak I and $E = 0.98 \pm 0.01$ eV and $s = 3.4 \times 10^{9}$ s^{-1} for peak III. The value of E for peak I agrees satisfactorily with the value obtained from the whole glow peak method.

7.1.5.2 Phosphorescence analysis based on area under an isothermal decay curve

The area-based method of isothermal analysis by Chithambo (2014) was applied on isothermal decay curves measured for 5 s for peak I only. The decay curves were measured at temperatures between 30 and 56 °C following irradiation to 50 Gy. Figure 7.11 shows a semilogarithmic plot of ϕ against $1/kT$ from the activation

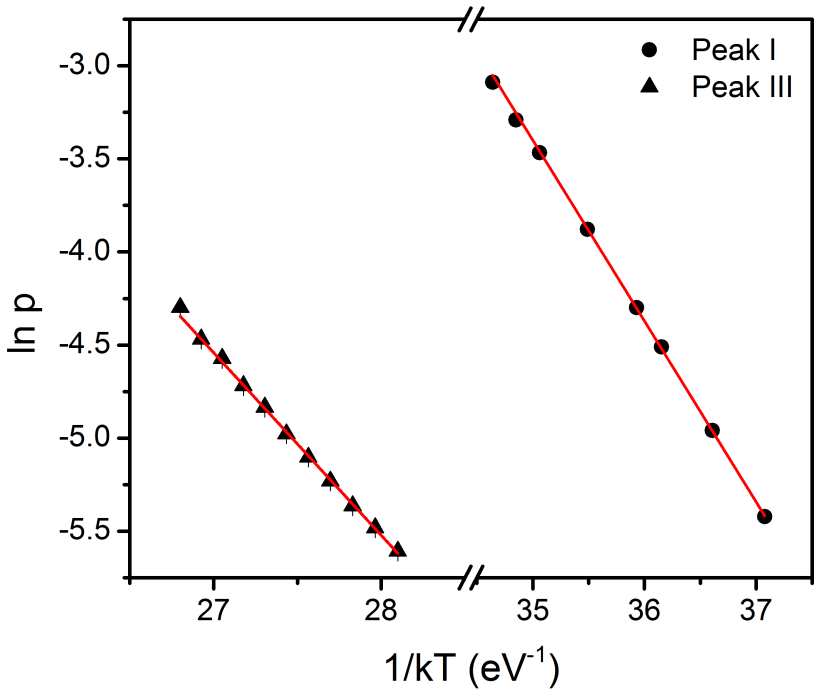

FIGURE 7.10: A plot of $ln\, p$ against $1/kT_i$ for peak I and peak III for first order kinetics of phosphorescence.

energy was evaluated as 0.89 ± 0.03 eV. This value is consistent with 0.88 ± 0.03 eV for the unannealed quartz using the same method.

7.1.5.3 Analysis of the temperature dependent areas by curve fitting

The area ϕ plotted against temperature produces a TL-like glow peak shown in Figure 7.12. This curve was fitted using equation (2.26) by Kitis (2001). The kinetic parameters obtained from this fit are $E = 0.98 \pm 0.03$ eV, $b = 1.11 \pm 0.04$, and $s = 5.6 \times 10^{13}$ s^{-1}. The values of E and b are in good agreement with the values obtained from the whole glow peak, variable heating rate, and curve fitting methods.

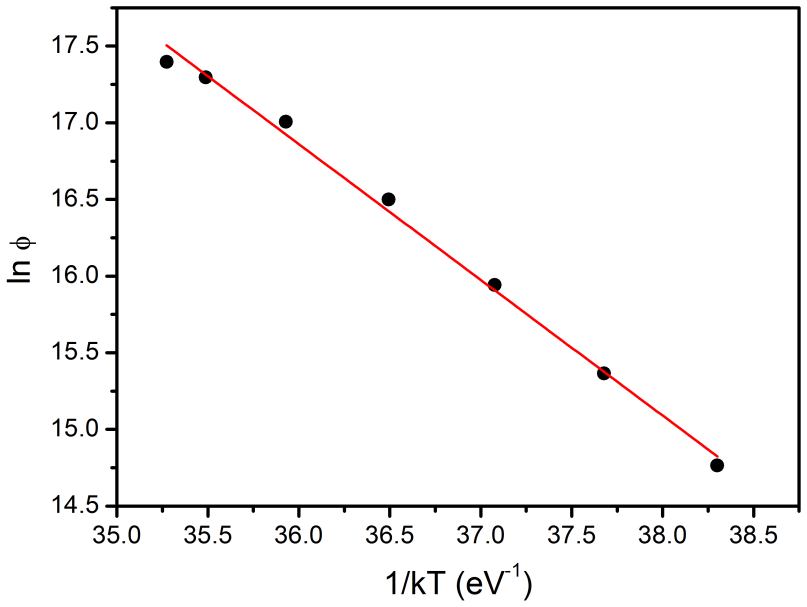

FIGURE 7.11: A plot of $ln\,\phi$ against $1/kT$ for the area under an isothermal decay curve method.

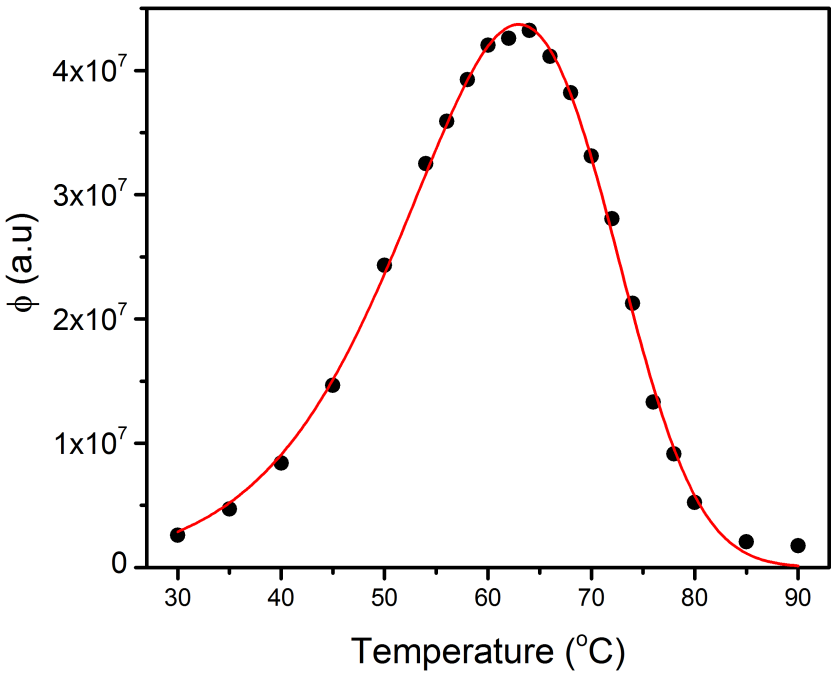

FIGURE 7.12: The temperature dependence of the area under the isothermal decay curve for 5 s. The solid line is the best fit of Eq. (2.26).

7.1.5.4 Thermal quenching analysis by area under an isothermal decay method

The area under an isothermal decay curve was also used to analyse for thermal quenching. Using equation (2.55), the activation energy for thermal quenching was evaluated. Figure 7.13 shows a graph of $ln(\phi_q/\phi_u)$ against $1/kT'$ for measurements made for 5 s. The activation energy for thermal quenching was determined as 0.89 ± 0.03 eV. This value is consistent with published value for quartz in the literature e.g. 0.85 ± 0.01 eV (Chithambo and Ogundare, 2009).

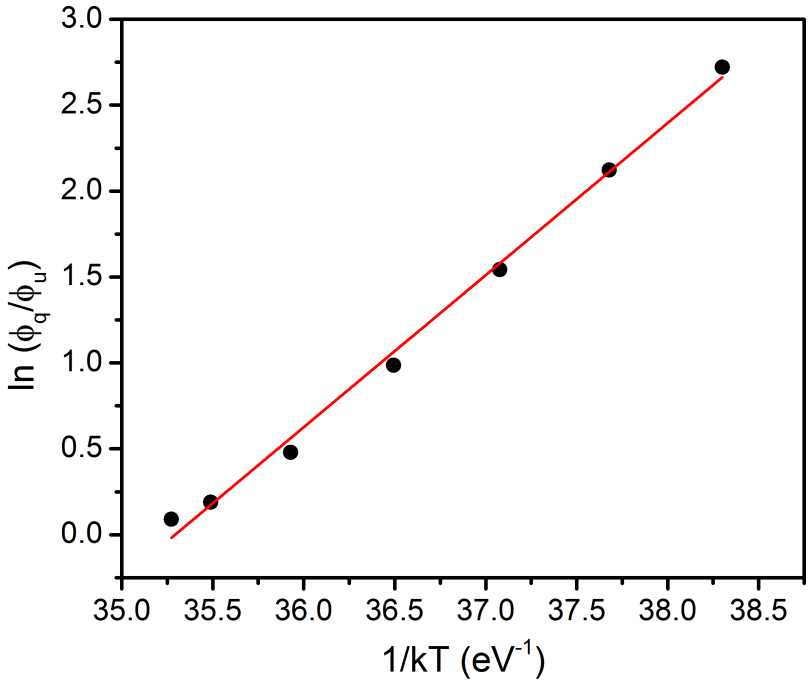

FIGURE 7.13: A graph of $ln(\phi_q/\phi_u)$ against $1/kT$ in a study of thermal quenching using area under isothermal decay-curve

7.1.6 Summary

Kinetic analysis have been carried out on the main and secondary peaks of the quartz annealed at 1000 °C for 10 minutes using various methods. Except for the peak shape method, the main peak was observed to follow first order kinetics. The value of the activation energy obtained for peak I using the various methods of

analysis compare favourably and are consistent with the values obtained for an unannealed natural quartz. The results show that annealing has little influence on the trap parameters of the main glow peak. Table 7.1 gives a summary of results for the kinetic analysis conducted on the main and secondary peaks of the quartz annealed at 1000 °C for 10 minutes.

TABLE 7.1: Kinetic parameters for quartz annealed at 1000 °C for 10 minutes. The acronyms IR, WGP, PS, CF, VHR, and IDC refers to the initial rise, whole glow peak, peak shape, curve fitting, variable heating rate and isothermal decay methods.

	Peak I			Peak III			
Method	E (eV)	b	s (s^{-1})	E (eV)	b	s (s^{-1})	Reference
IR	0.934 ± 0.004 0.93 ± 0.01			1.18 ± 0.01			Fig. 7.6 Sect. 5.5.1
WGP	0.96 ± 0.01 0.98 ± 0.01	1.1	1.5×10^{13}	1.09 ± 0.01 1.06 ± 0.01		1.1×10^{11}	Fig. 7.7 Sect. 5.5.2
PS	$1.06 \pm 0.09^{\tau}$ $1.06 \pm 0.09^{\delta}$ $1.07 \pm 0.10^{\omega}$	Gen order		$1.15 \pm 0.07^{\tau}$ $1.16 \pm 0.07^{\delta}$ $1.16 \pm 0.07^{\omega}$	Gen order		Sect. 7.1.4.3
CF	1.01 ± 0.01	1.14 ± 0.02	7.7×10^{13}	1.23 ± 0.01	1.46 ± 0.01	4.5×10^{12}	Fig. 7.8
VHR	0.94 ± 0.03		5.3×10^{12}	1.56 ± 0.02		3.2×10^{16}	Fig. 7.9
IDC, 1st ord	0.97 ± 0.01		2.0×10^{13}	0.98 ± 0.01		3.4×10^{9}	Fig. 7.10
IDC, Area	0.89 ± 0.03 0.88 ± 0.03						Fig. 7.11 Sect. 5.5.6.2
IDC, CF	0.98 ± 0.03 0.98 ± 0.02	1.11 ± 0.04	5.6×10^{13}				Fig. 7.12 Sect. 5.5.6.3

7.2 Thermoluminescence of quartz annealed at 1000 °C for 1 hour

Kinetic and dosimetric features of natural quartz annealed at 1000 °C for 1 hour is reported in this section. The results of the analysis are compared with the sample annealed for 1 hour in order to investigate the influence of duration of annealing on the kinetic parameters.

7.2.1 Characteristics of the TL glow curve

The TL glow curve measured after sample irradiation to 50 Gy is shown in Figure 7.14. The glow curve shows three peaks at 70, 128, and 176 °C labelled I, II, and III respectively. In order to better show the presence of other peaks, the data was re-plotted on a semilogarithmic scale and is shown in the inset. Peak IV which was not visible in the linear plot was observed through this means. Further verification of the peak positions was initiated by applying the thermal cleaning technique.

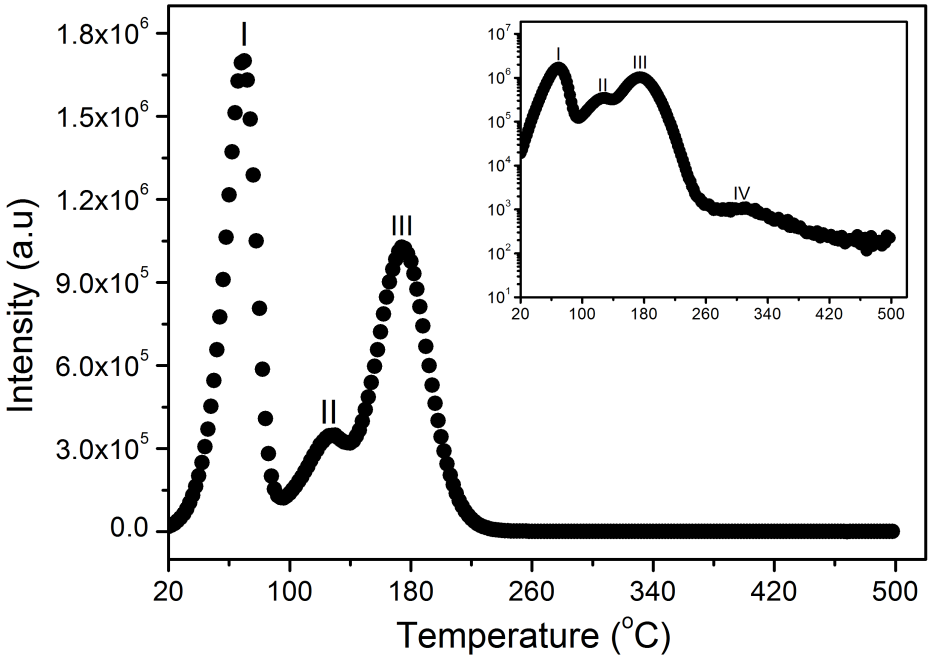

FIGURE 7.14: A TL glow curve measured at 1 °Cs^{-1} following irradiation to 50 Gy. The inset shows the same plot on a semilogarithmic scale.

7.2.2 Thermal cleaning

The thermal cleaning technique was adopted to verify the positions of the peaks in Figure 7.14. The sample, irradiated to 50 Gy, and heated to 500 °C showed peak I at 70 °C. Thereafter, the sample was heated in turn to 95, 140, and 240 °C following irradiation to 50 Gy each time. Subsequently, the whole glow curve was measured. The procedure revealed the positions of peaks II, III, IV, and V at 128, 176, 234, and 308 °C respectively. Figure 7.15 shows the individual peaks recorded from the thermal cleaning procedure.

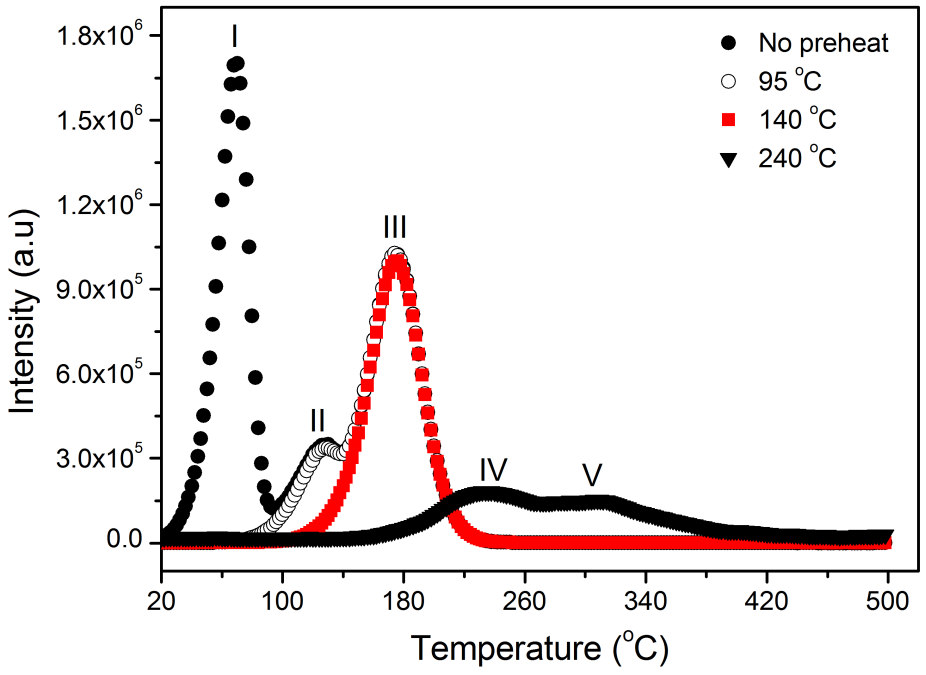

FIGURE 7.15: A plot of intensity against temperature for the thermal cleaning techniques used to verify the positions of peaks I - V after preheating to 0, 95, 140, and 240 °C. The data for preheating to 240 has been scaled up by ×150 to aid visual clarity.

7.2.3 Dosimetric features

To study the dosimetric features of quartz annealed at 1000 °C for 1 hour, the influence of repeated measurements on the TL signal, dose response and fading of

the TL signal for peaks I - III were studied. To record the TL signal for peaks II and III, the irradiated sample was first preheated to 95 and 140 °C respectively to remove peaks I and II before measuring the whole glow curve.

7.2.3.1 Repeatability of TL measurements

The reproducibility of the TL signal of peaks I - III was investigated by measuring the TL ten times. Figure 7.16 shows the repeatability measurements made for peaks I - III. The positions of peaks I, II, and III are approximately constant at

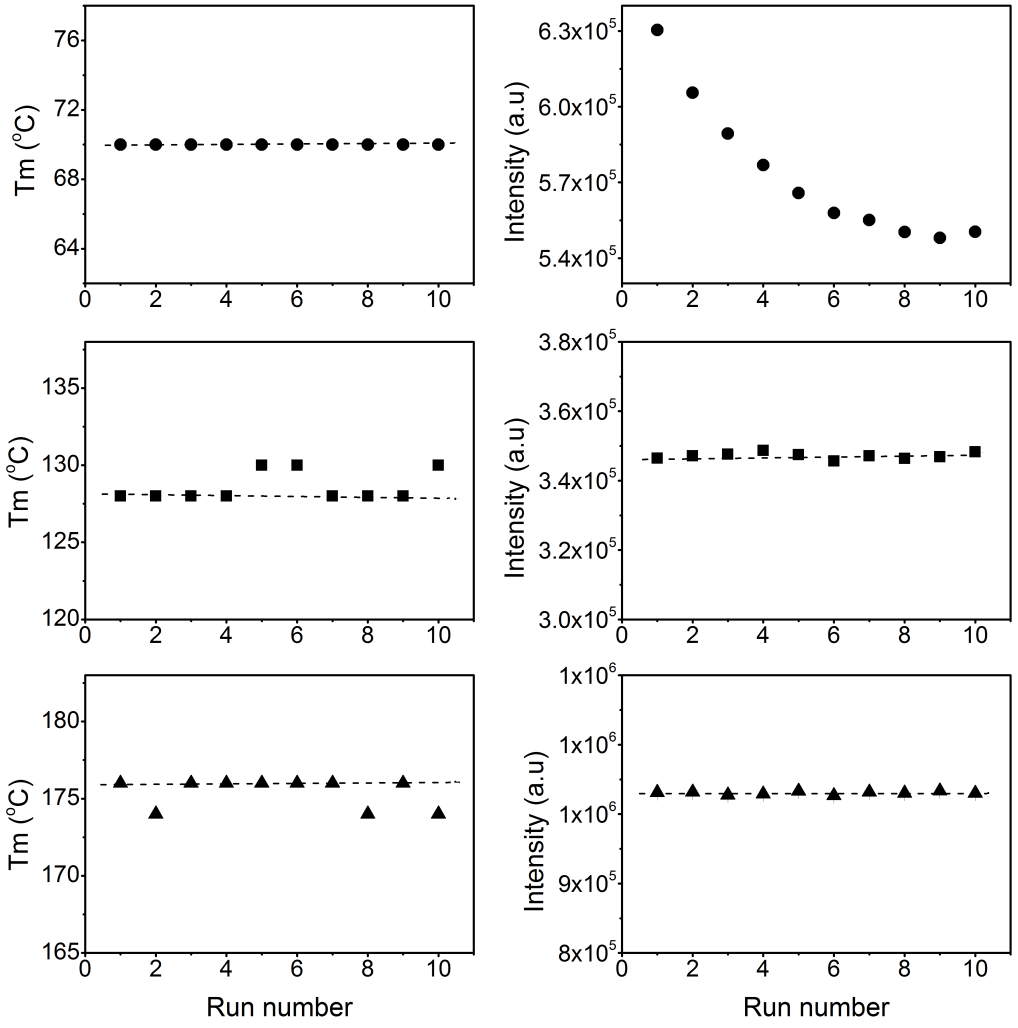

FIGURE 7.16: Plots of peak positions and intensities against measurement runs for peak I (circles), peak II (squares), and peak III (triangles). The error bars in the intensity plots are based on the square root rule for counting experiments. The dotted lines between data points are only visual guides.

70.0, 128.6 ± 0.9, and 175.4 ± 0.9 °C respectively, implying that the peaks are unaffected by sample reuse. In the same way, the intensity of peak I (circles) decreases with repeated irradiation and heating whereas it is constant for peaks II (squares) and III (triangles). The decrease of intensity of peak I with sample reuse may be due to change in sensitivity of the sample due to repeated measurements.

7.2.3.2 Fading

Fading of the TL signal between irradiation of 50 Gy and measurement was studied for peak I for a delay up to 5 hours. Figure 7.17 shows a graph of intensity against delay between measurements for peak I. The TL intensity decreases exponentially

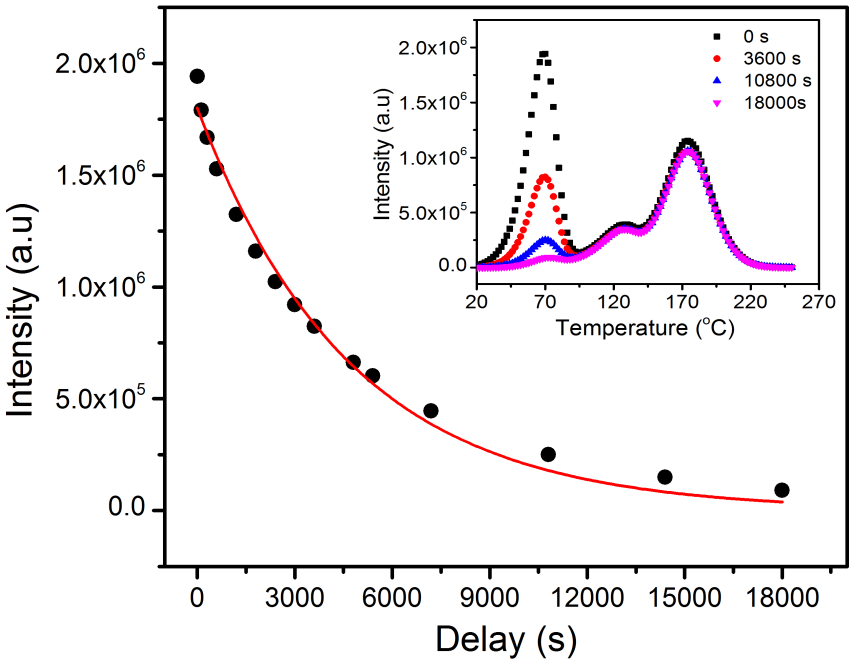

FIGURE 7.17: The variation of TL intensity with delay between irradiation and measurements for peak I. The inset shows examples of glow curves truncated at 250 °C, measured after the delay between 0 and 18000 s.

with delay with a mean lifetime of 4686 s. This is lower than 7784 s recorded for the same quartz annealed for 10 mins. The result shows that peak I fades faster at a long duration annealing. The inset, as a way to illustrate the fading of the TL signal shows examples of glow curves recorded at different delay between 0 and 18000 s.

7.2.3.3 Dose response

The dose response of peaks I - III was studied for irradiation doses between 10 and 300 Gy. Figure 7.18 shows the dose response of peaks I - III. The intensity of

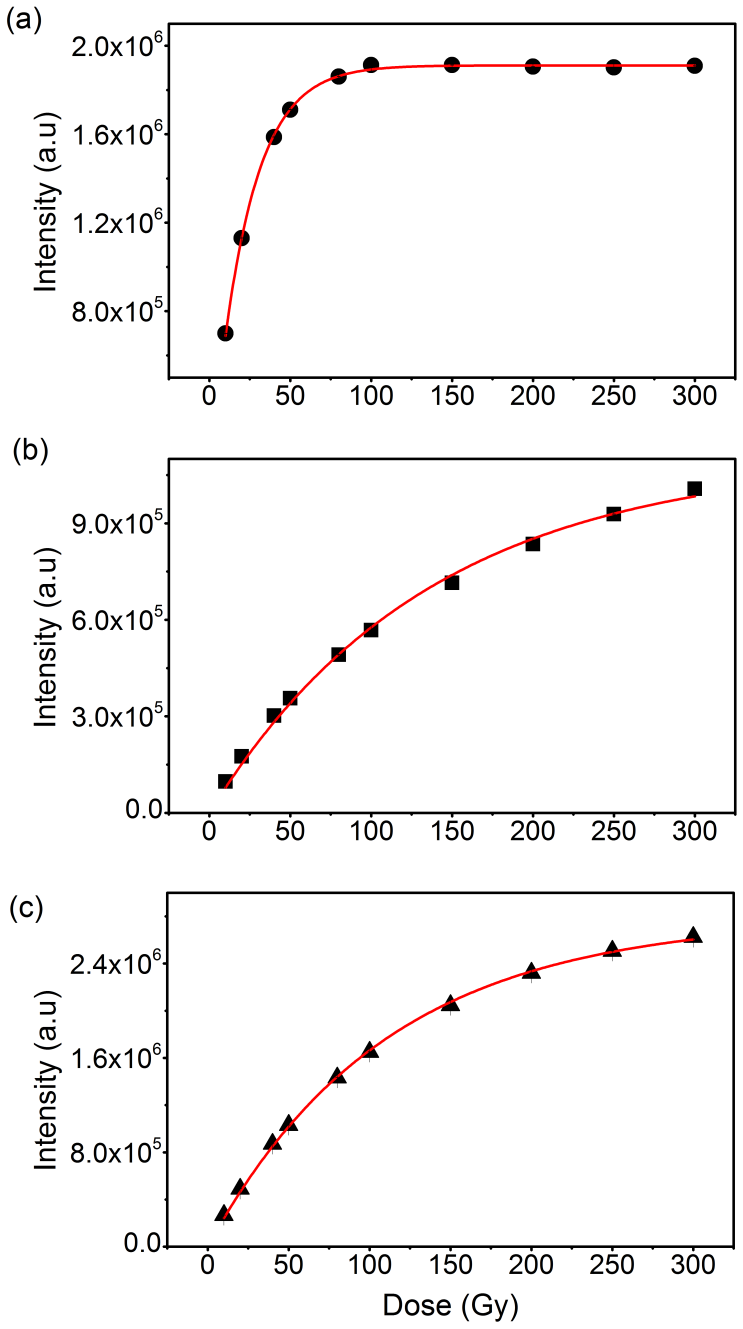

FIGURE 7.18: The influence of dose on the maximum intensity of peaks I (a), II (b), and III (c). The line passing through the data points for each peak is the best fit of Eq. (7.1).

peak I increases monotonically towards saturation whereas those for peaks II and III increases monotonically without saturating.

Qualitatively, the dose response of peaks I - III was analysed for superlinearity and supralinearity. Figure 7.19 shows the plots of super- and supra- linearity index against dose for peaks I - III. Dose response is sublinear for both g(D) and f(D).

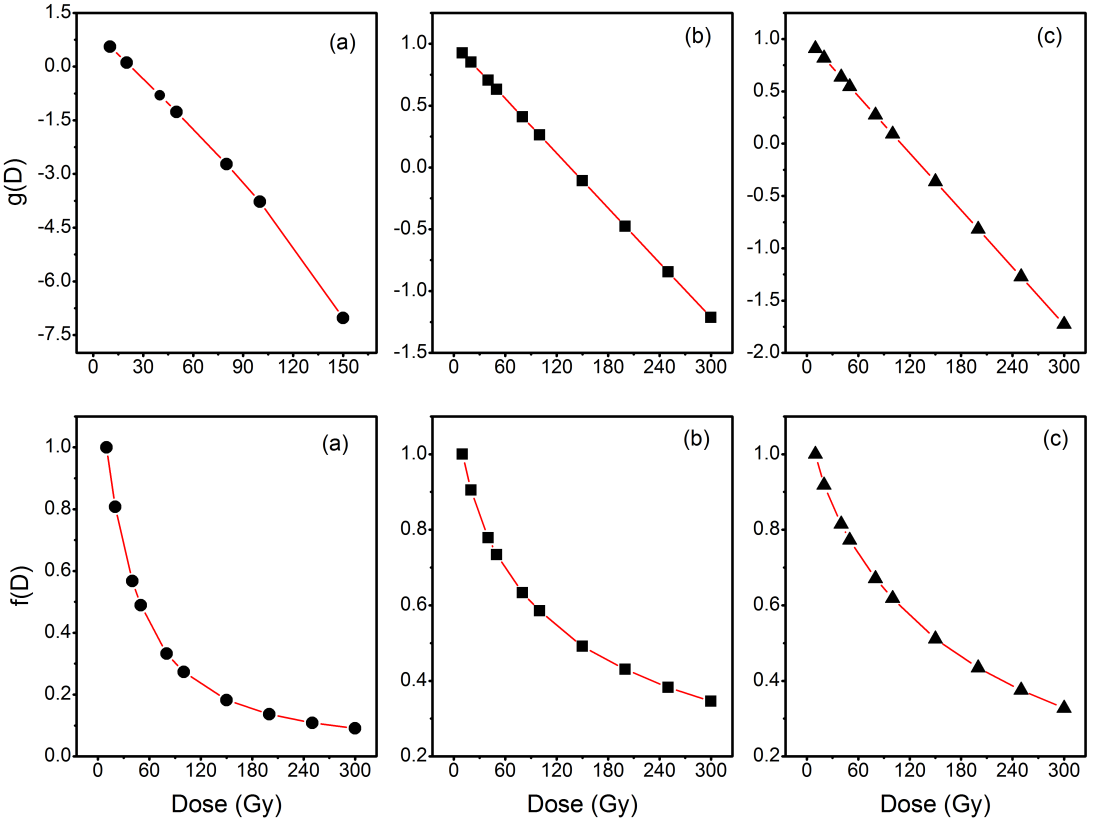

FIGURE 7.19: Plots of superlinearity and supralinearity indices against dose for peaks I (a), II (b), and III (c). The solid lines passing through the data points are the best fits of equation (5.3) and (5.4).

7.2.4 Assessing the order of kinetics

The order of kinetics of the glow peaks were assessed using two methods; the $T_m - T_{stop}$ method and the $T_m - dose$

7.2.4.1 T_m-T_{stop} method

To determine the order of kinetics of peaks I - III, the $T_m - T_{stop}$ method was used. Figure 7.20(a) - (c) shows the peak position T_m against T_{stop} made for peaks I - III. T_m was independent of T_{stop} for peaks I, II, and III at 69.7 ± 0.6, 130 ± 1.3 and 176 °C respectively implying that the peaks are of first order kinetics.

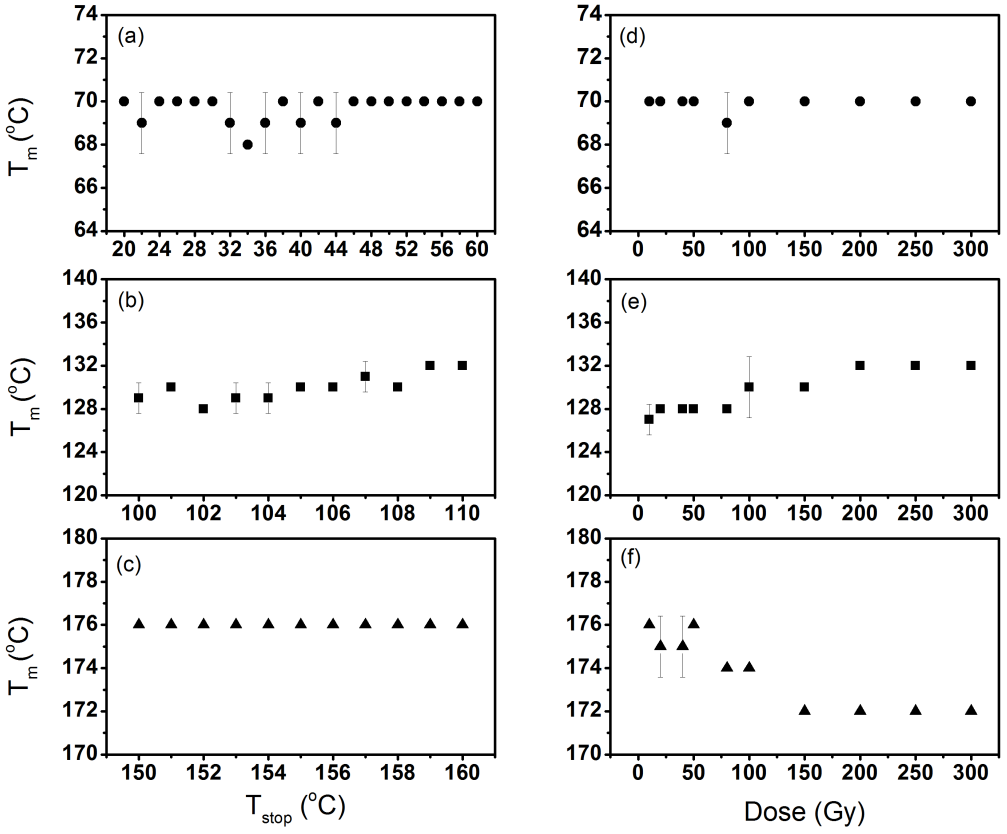

FIGURE 7.20: Establishing the order of kinetics for peaks I - III by the T_m - T_{stop} and T_m - Dose methods. The circle, square, and triangle symbols represent data for peaks I, II, and III respectively.

7.2.4.2 T_m - Dose method

The dose dependence of peak position was further used to ascertain the order of kinetics of peaks I - III. The quartz sample was irradiated to different doses of irradiation between 10 and 300 Gy. Figure 7.20(d) - (f) shows the plots of T_m against dose for peaks I - III. The position of peak I is independent of dose confirming that peak I is of first order kinetics. The position of Peak II increases with dose but in three different levels where it is independent of dose. For peak III, T_m decreases with dose in a staircase manner, from which T_m is independent of dose at different levels of the decrease. The decrease of peak position with dose is a feature of second order kinetics (Chen and Mckeever, 1997). That the positions of peaks II and III are independent of dose in different levels could imply that these peaks are general order peaks.

7.2.5 Kinetic analysis

In order to evaluate the kinetic parameters of the peaks in this sample, kinetic analysis was carried out. The initial rise method was applied on peaks I - III. Additional methods consisting of the whole glow peak-, peak shape-, curve fitting-, variable heating rate-, and phosphorescence-based methods were applied on peaks I and III only.

7.2.5.1 Initial rise method

The initial rise method was applied on the clear rising edge of peaks I, II, and III in order to determine the trap depth responsible for the individual peaks. Figure 7.21 shows the plots of $ln\, I$ against $1/kT$ made for peaks I - III using the initial rise method. The activation energies evaluated from the slope are $E = 0.904 \pm 0.004$ eV, $E = 0.99 \pm 0.01$ eV, and $E = 1.10 \pm 0.01$ eV for peaks I, II, and III respectively. In comparison, the values of E for peaks I and III are slightly less than those obtained for the same quartz annealed for 10 minutes. One would have expected that an increase in the duration of annealing would yield an increase in the activation energy, but this is not the case here.

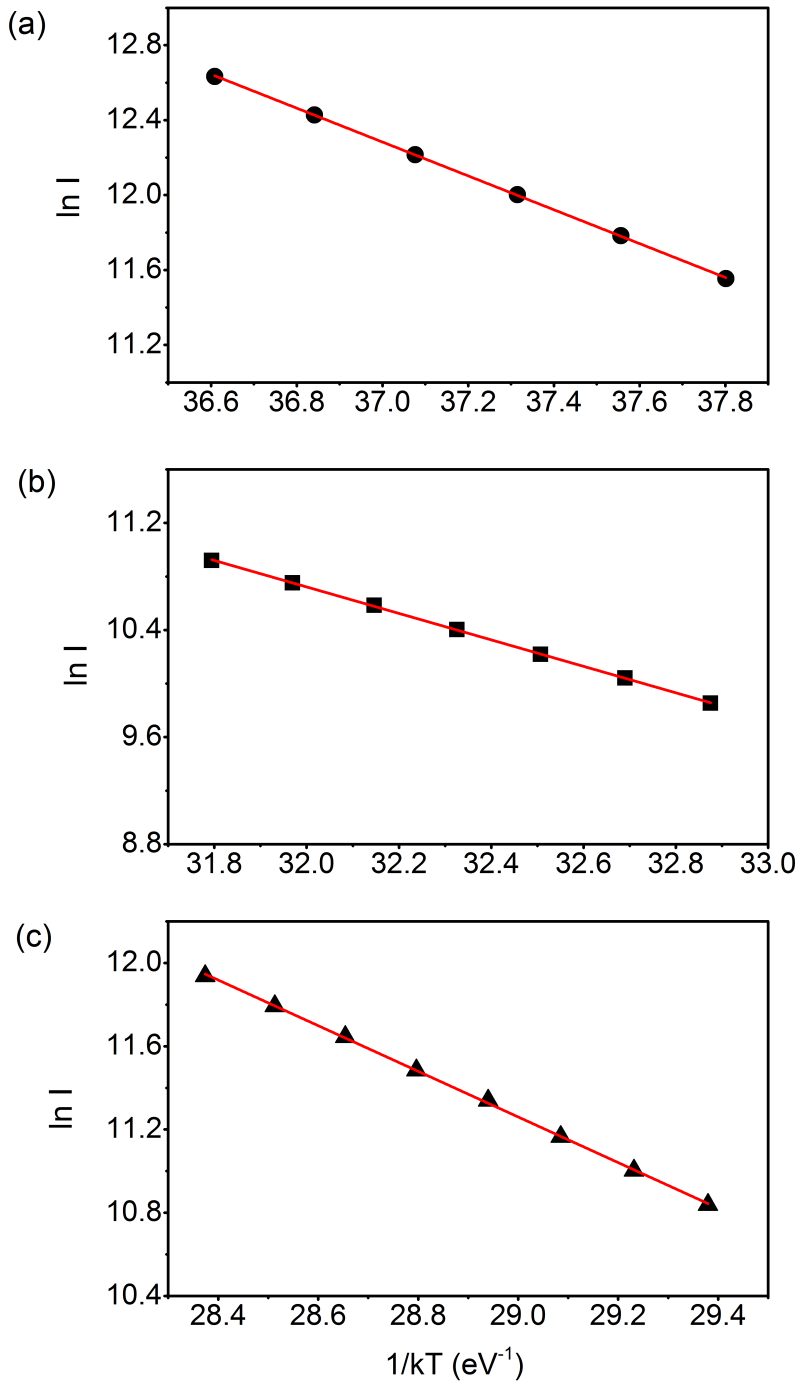

FIGURE 7.21: A plot of $ln\, I$ against $1/kT$ for the initial rise method for (a) peak I (b) peak II (c) peak III.

7.2.5.2 Whole glow peak method

Peaks I and III were analysed using the whole glow peak method, in order to evaluate the activation energy E, effective frequency factor s', and the order of

kinetics b. The same glow peaks analysed using the initial rise methods were also used for this method. Figure 7.22 shows the plots of $ln\left(I/n^b\right)$ against $1/kT$ for

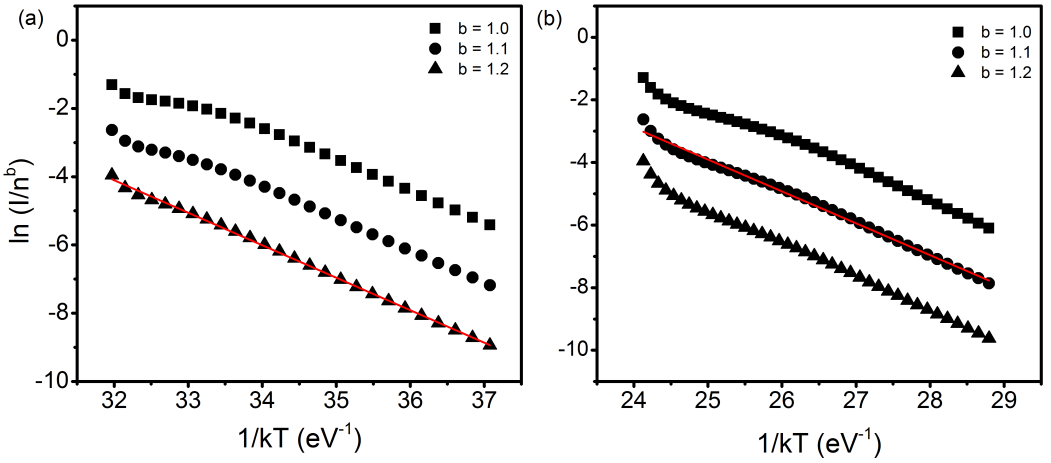

FIGURE 7.22: A plot of $ln(I/n^b)$ against $1/kT$ for different values of b for (a)peak I and (b)peak III.

peaks I and III. The plot was found to be linear for $b = 1.2\,(R^2 = 0.999)$ for peak I and $b = 1.1$ for peak III. The results show that the peaks follow first-order kinetics. The activation energy E was evaluated as 0.95 ± 0.01 eV for peak I. The frequency factor obtained from the intercept was 8.5×10^{12} s^{-1}. For peak III, the activation energy and effective frequency factor were evaluated as 1.02 ± 0.01 eV and 6.5×10^{10} s^{-1}. The value of E for peak I obtained using this method is consistent with 0.96 ± 0.01 eV obtained for peak I for the same quartz annealed at 1000 °C for 10 minutes and with the unannealed quartz. Thus, annealing has little effect on the activation energy of peak I.

7.2.5.3 Peak shape method

Peaks I and III were further analysed using the peak shape method. The order of kinetics of peaks I and III were obtained through the geometrical factor μ_g (2.23) as 0.42 ± 0.06 and 0.46 ± 0.04 for peaks I and III respectively. The geometrical factors suggest that peak I follows first-order kinetics and that peak III is of general order kinetics. The values of the activation energy for the individual half-widths for peak I were calculated as $E_\tau = 1.00 \pm 0.11$ eV, $E_\delta = 0.99 \pm 0.10$ eV, and $E_\omega = 1.01 \pm 0.11$ eV. These values, though lower are in good agreement with the

values obtained for the sample annealed for 10 mins using the same method. For peak III, the E values were calculated as $E_\tau = 1.15 \pm 0.07$ eV, $E_\delta = 1.16 \pm 0.07$ eV, and $E_\omega = 1.16 \pm 0.07$ eV. Although these E values are necessarily dependent on τ, δ, ω, they are consistent with the values of obtained for the sample at 10 minutes. This suggests that the shape of peak III is not altered by annealing.

7.2.5.4 Curve fitting method

To further ascertain the consistency in kinetic parameters E, s, and b, peaks I and III were analysed by the curve fitting method using equation (2.26). Figure 7.23 shows the best fits obtained for peaks I and III. The kinetic parameters determined from these fits are $E = 1.04 \pm 0.02$ eV and $b = 1.22 \pm 0.04$ with $FOM = 0.48\%$ for peak I, and $E = 1.204 \pm 0.004$ eV and $b = 1.50 \pm 0.01$ with $FOM = 0.33\%$ for peak III. The values of b suggest that peak I follows first-order kinetics whereas peak III follows general order kinetics. This agrees with the findings from the peak shape method. The frequency factors calculated using equation (2.27) were 2.0×10^{14} and 2.0×10^{12} s^{-1} for peaks I and III respectively. The values of E for both peaks are in good agreement with the values obtained from the peak shape method and with the values obtained for the quartz annealed for 10 minutes.

7.2.5.5 Variable heating rate method

Peaks I and III were also analysed for kinetic parameters using the variable heating rate method. The activation energy E and frequency factor s of the peaks were determined by applying equation (2.17) to experimental data. Figure 7.24 shows a plot of $ln\,(T_m^2/\beta)$ against $1/kT_m$ for the various heating rate method. The activation energy obtained from the slope for peak I is 0.90 ± 0.01 eV. For the frequency factor evaluated from the intercept of the graph, $s = 1.7 \times 10^{12}$ s^{-1}. For peak III, the activation energy and frequency factor were found as 1.42 ± 0.01 eV and 6.3×10^{14} s^{-1} respectively. These values are lower than the values obtained for the 10 minutes annealing. The influence of annealing on the trap parameters of these samples is thus noticeable. Nonetheless, the value of the activation energy for peak I is consistent with that obtained using the initial rise method, and compares favourably with the value from the curve fitting method. In addition, the value obtained for peak III is overestimated in comparison with other methods.

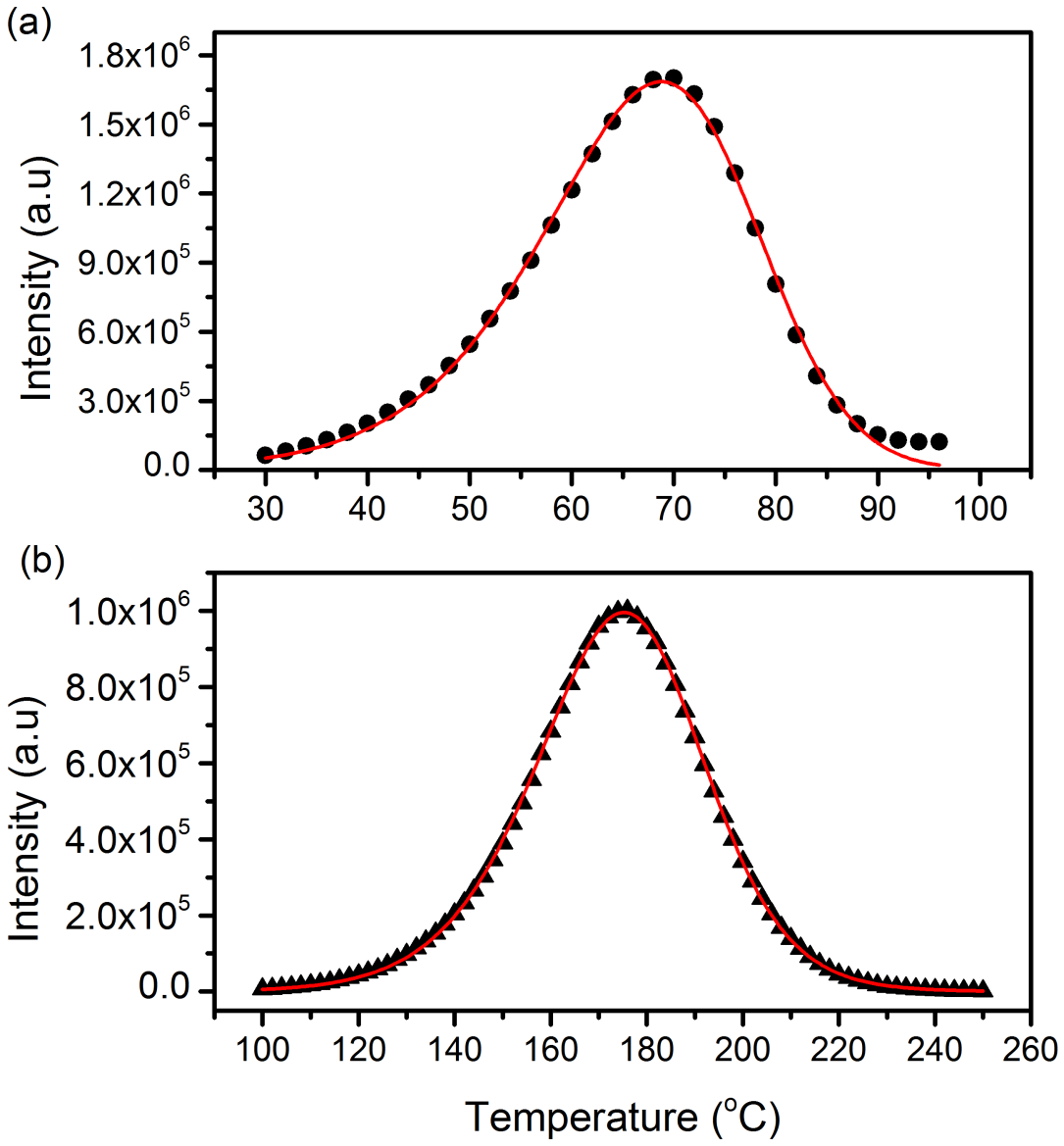

FIGURE 7.23: Results of curve fitting for (a) peak I (b) peak III. The solid lines are the best fits of equation (2.26)

7.2.5.5.1 Thermal quenching

Figure 7.25 shows the dependence of TL intensity (denoted as peak height and peak area) on heating rate for the quartz sample irradiated to 50 Gy. The TL intensity, measured in counts/°C and counts for peak height and peak area respectively, decreases with heating rate for peak I. This would indicate that the sample is affected by thermal quenching. In the absence of thermal quenching, it is expected

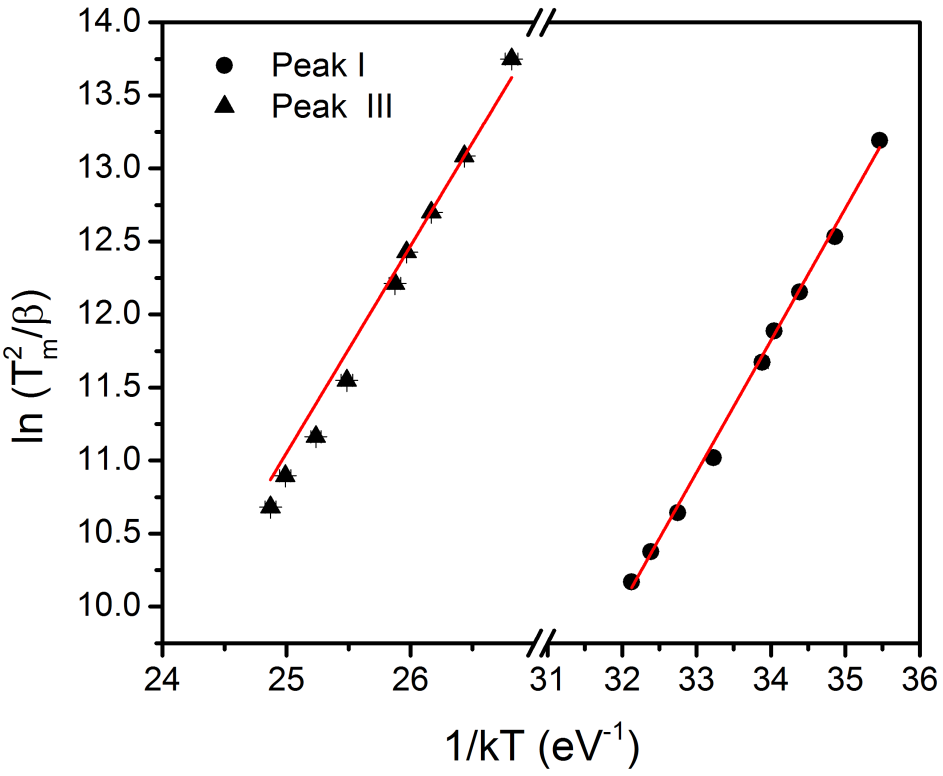

FIGURE 7.24: A graph of $ln\left(T_m^2/\beta\right)$ against $1/kT_m$ for the various heating rate method for peak I and peak III.

that the TL intensity remains approximately constant with increasing heating rates (Gorbics *et al.*, 1969). The activation energy for thermal quenching was evaluated using the temperature dependent luminescence function in equation (2.54). The peak area was used to calculate for the activation energy. The TL measured at 0.2 and 5 °Cs^{-1} were assumed to experience the least and greatest amount of quenching respectively. Figure 7.26 shows the graph of $ln[(A_{uq}/A_q) - 1]$ against $1/kT_m$. The activation energy for thermal quenching was evaluated as $\Delta E = 1.08 \pm 0.04$ and $C = 2.8 \times 10^{16}$. The ΔE value is in agreement with published values in the literature e.g. 0.92 ± 0.01 eV (Chithambo, 2015). The frequency factor for the non-radiative process ν was calculated from $C = \nu\tau_{rad}$, where τ_{rad} is the luminescence lifetime corresponding to radiative recombination (Chithambo, 2007). For natural quartz annealed at 1000 °C, luminescence lifetime is 34 μs (Chithambo, 2015). Hence, the frequency factor for non-radiative recombination due to the luminescence lifetime is 2.8×10^{-20} s^{-1}.

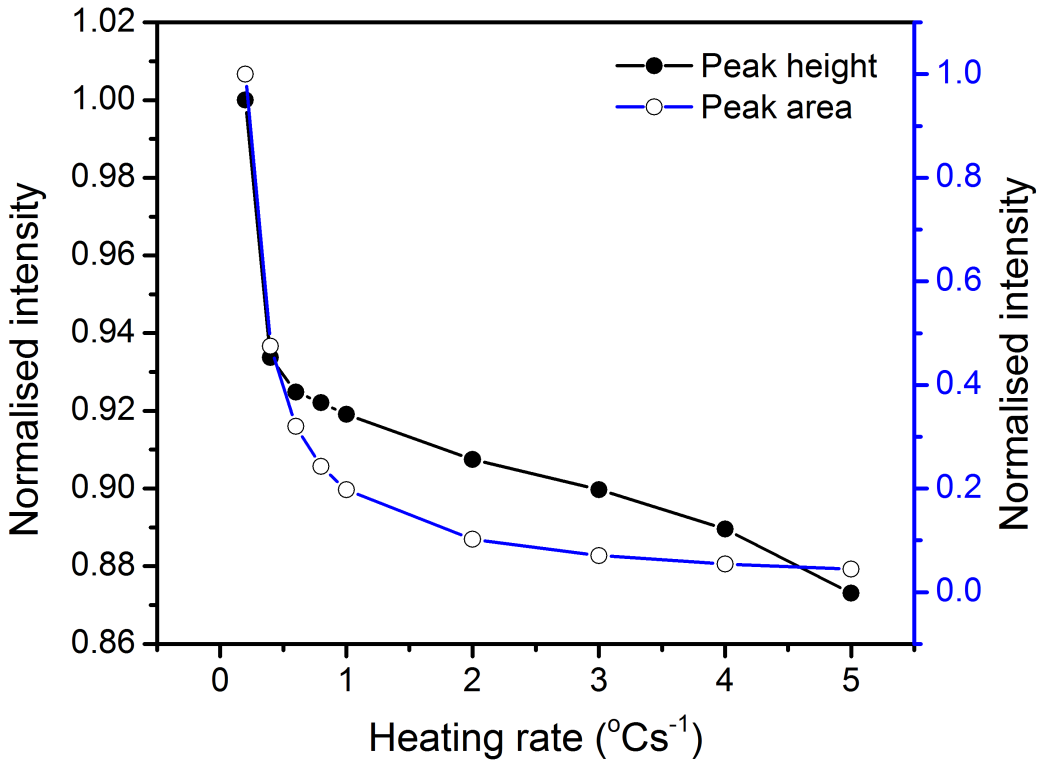

FIGURE 7.25: Dependence of peak intensity on heating rates.

7.2.6 Phosphorescence analysis

Phosphorescence analysis was carried out on peaks I and III in order to evaluate the activation energy and frequency factor. In this method, the sample irradiated to 50 Gy is heated to a specific temperature which is kept constant while measuring the phosphorescence decay at a given time interval.

7.2.6.1 Isothermal analysis based on first order kinetics

Phosphorescence decay measurements were made for 500 s at different temperatures between 40 and 62 °C for peak I, and between 140 and 160 °C for peak III. Equation (2.33) was used to evaluate the activation energy and frequency factor of these peaks. Plots of $ln\, p$ against $1/kT_i$ made for peaks I and III are shown in Figure 7.27. The activation energy and frequency factor for peak I were found to be $E = 0.822 \pm 0.04$ eV and $s = 9.1 \times 10^{10}$ s^{-1} whereas $E = 1.00 \pm 0.02$ eV and $s = 6.8 \times 10^{9}$ s^{-1} for peak III. The value of E for peak III compare favourably

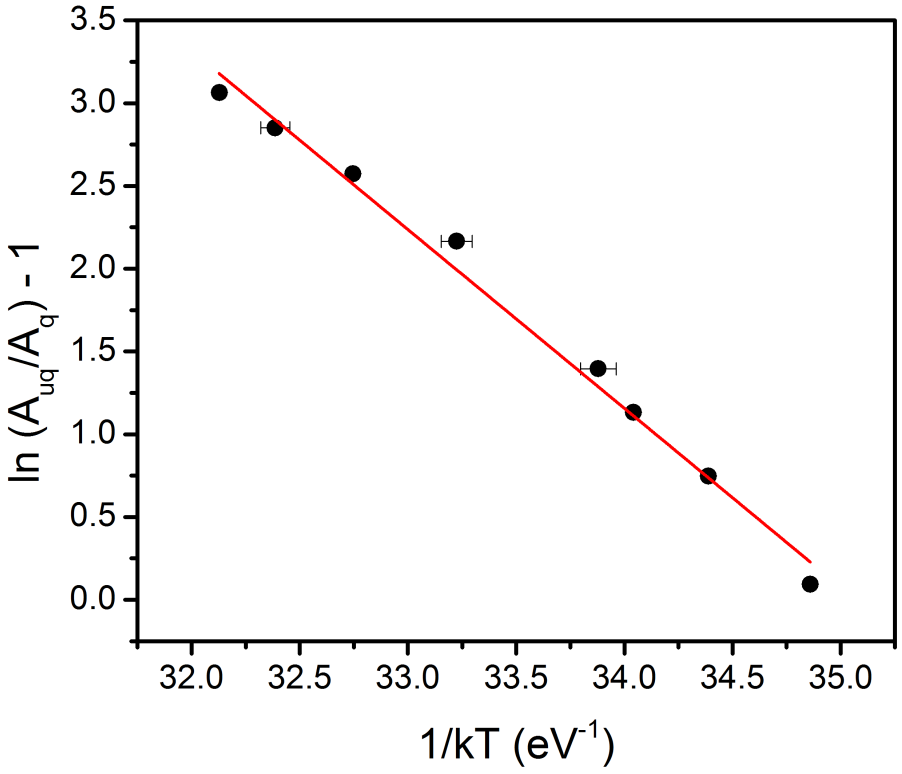

FIGURE 7.26: A graph of $ln[(A_{uq}/A_q) - 1]$ against $1/kT_m$ used to evaluate thermal quenching.

with the value obtained using the whole glow peak method for the same peak and with 0.98 ± 0.01 eV for the quartz annealed for 10 mins.

7.2.6.2 Analysis based on area under an isothermal decay curve

The area-based method of isothermal analysis by Chithambo (2014) was applied on isothermal decay curves measured for 5 s for peak I only. The decay curves were measured at temperatures between 30 and 58 °C after irradiation to 50 Gy. The area ϕ of an isothermal curve was calculated at each temperature. Figure 7.28 shows a plot of $ln\,\phi$ against $1/kT$ for peak I. The activation energy obtained from this plot is 0.81 ± 0.02 eV. The value of E is in satisfactory agreement with 0.822 ± 0.04 eV obtained through the first order kinetics of phosphorescence. This value of E is less than 0.89 ± 0.03 eV obtained for the 10 mins annealing. It is thus evident that annealing has little influence on the trap parameters of the glow peak.

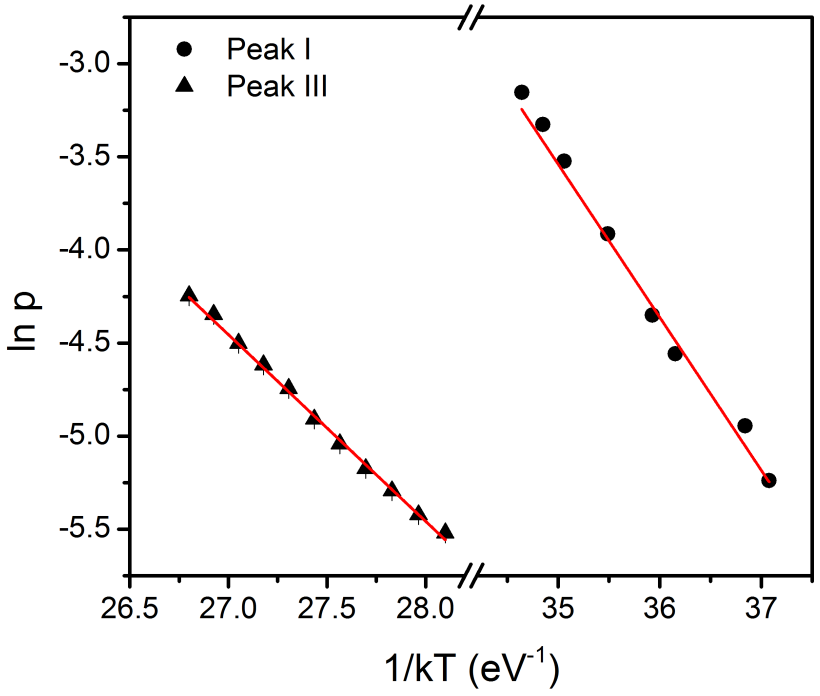

FIGURE 7.27: A graph of $ln\,p$ against $1/kT$ for peaks I and peak III to evaluate the activation energy for phosphorescence based on first order kinetics.

7.2.6.3 Analysis of the temperature-dependent areas by curve fitting

The area ϕ plotted against temperature produces a TL-like glow peak shown in Figure 7.29. This curve was fitted using equation (2.26) by Kitis *et al.* (1998). The solid line through the data points is the curve fit of equation (2.26). The kinetic parameters E, b,and s were evaluated from the fit as 1.02 ± 0.03 eV, 1.17 ± 0.05, 2.1×10^{14} s^{-1} respectively. The value of the activation energy is consistent with the value obtained from the peak shape method.

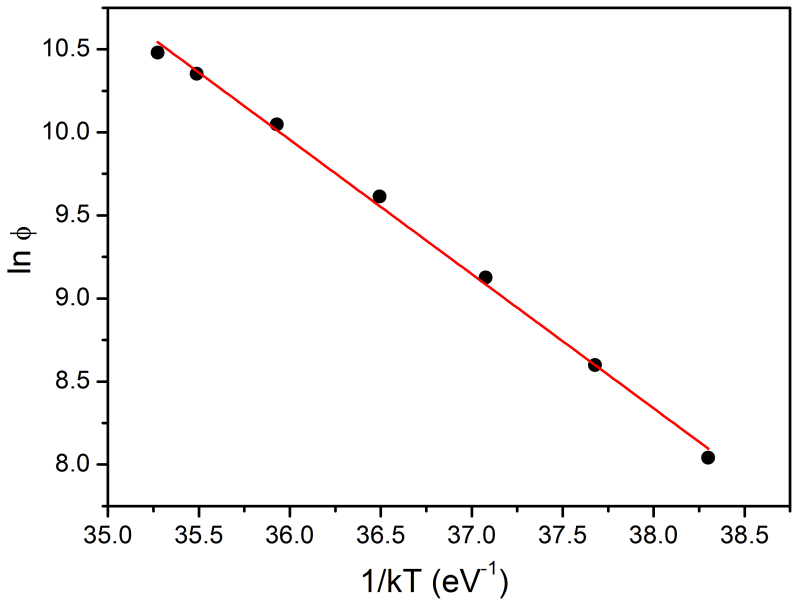

FIGURE 7.28: A plot of $ln\,\phi$ against $1/kT$ for area under an isothermal decay curve.

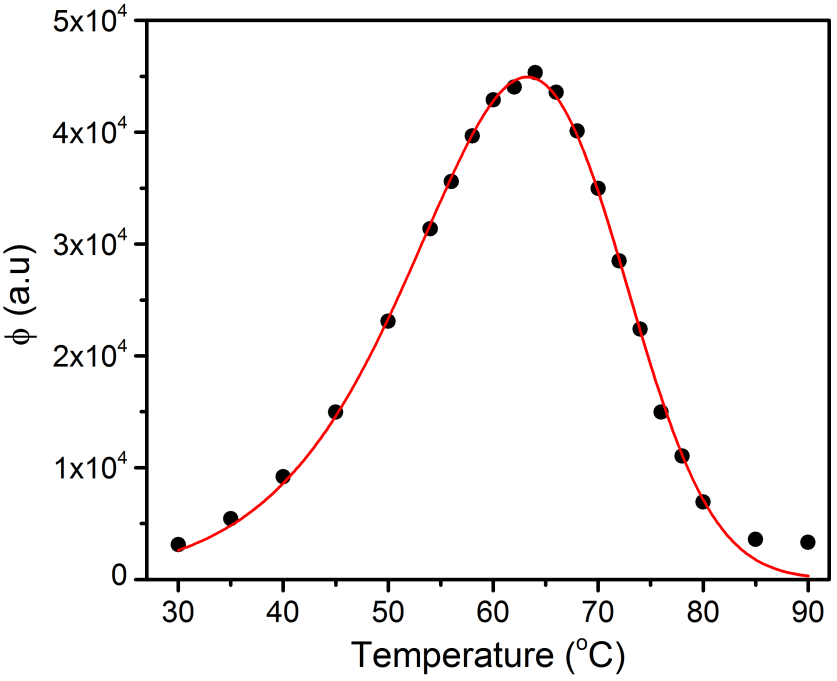

FIGURE 7.29: The temperature dependence of the area under the isothermal decay curve for 5 s. The solid line is the best fit of Eq. (2.26).

7.2.6.4 Analysis of thermal quenching using the area under an isothermal decay-curve

Thermal quenching was analysed using the area under an isothermal decay-curve, a method proposed by Chithambo (2014). Figure 7.30 shows a graph of $ln(\phi_q/\phi_u)$ against $1/kT'$ for measurements made for 5 s. The value of the activation energy for thermal quenching determined from the slope of the graph is 0.81 ± 0.02 eV. This value is consistent with published values for quartz e.g. 0.85 ± 0.01 eV (Chithambo and Ogundare, 2009).

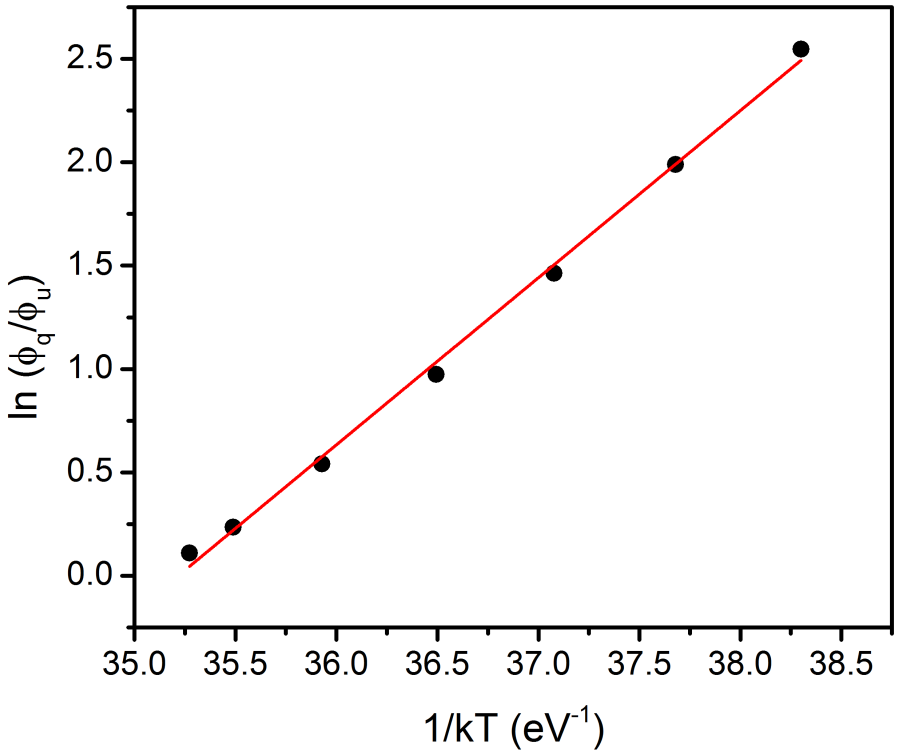

FIGURE 7.30: A graph of $ln(\phi_q/\phi_u)$ against $1/kT'$ in a study of thermal quenching using area under isothermal decay-curve

Table 7.2 gives a summary of the kinetic parameters for the methods applied.

TABLE 7.2: Kinetic parameters of the main and secondary TL peaks of natural quartz annealed at 1000 °C for 1 hour.

	Peak I (70 °C)			Peak III (176 °C)			
Method	E (eV)	b	s (s^{-1})	E (eV)	b	s (s^{-1})	Reference
IR	0.904 ± 0.004			1.10 ± 0.01			Fig. 7.21
WGP	0.95 ± 0.01	1.2	8.5×10^{12}	1.02 ± 0.01	1.1	6.5×10^{10}	Fig. 7.22
	$1.00 \pm 0.11^{\tau}$			$1.15 \pm 0.07^{\tau}$			
PS	$0.99 \pm 0.10^{\delta}$			$1.16 \pm 0.07^{\delta}$	$\mu_g = 0.46 \pm 0.04$		Sect. 7.2.5.3
	$1.01 \pm 0.11^{\omega}$			$1.16 \pm 0.07^{\omega}$			
CF	1.04 ± 0.02	1.22 ± 0.04	2.0×10^{14}	1.204 ± 0.004	1.50 ± 0.01	2.0×10^{12}	Fig. 7.23
VHR	0.90 ± 0.01		1.7×10^{12}	1.42 ± 0.01		6.3×10^{14}	Fig. 7.24
IDC							
1st order	0.82 ± 0.04	1	9.1×10^{10}	1.00 ± 0.02		6.8×10^{9}	Fig. 7.27
IDC,							
Area	0.81 ± 0.02						Fig. 7.28
IDC,							
CF	1.02 ± 0.03	1.17 ± 0.05	2.1×10^{14}				Fig. 7.29

7.3 Influence of annealing on thermoluminescence of natural quartz

The influence of annealing on thermoluminescence beyond the second phase inversion temperature on natural quartz in early studies show a sensitivity enhancement effect (Bøtter-Jensen *et al.*, 1995). The sensitivity enhancement effects are attributed to the alterations in the recombination centres which are created during annealing (Rendell *et al.*, 1994; Hashimoto *et al.*, 1994). Annealing of quartz can induce the recombination of electrons and holes at the $[AlO_4]^o$ centres (Bøtter-Jensen *et al.*, 1995). An increase in luminescence lifetimes with annealing temperature and annealing duration is observed between 800 and 1000 °C (Galloway, 2002; Chithambo, 2015). High temperature annealing beyond the second phase inversion was also reported to alter the population of the $E^{'}$ centres and creation of $[TiO_4/Li^+]^o$ and $[TiO_4/H^+]^o$ donors (Poolton *et al.*, 2000) when a high frequency electron paramagnetic resonance is used.

In this study, the influence of annealing on TL was investigated through various methods of kinetic analysis. The influence was also monitored based on the duration of annealing of the material. It is found that the thermoluminescence intensities of peaks I and III for the sample annealed for 10 minutes are greater than those annealed for 1 hour. However, this study revealed that annealing has little effect on the trap depth of the samples. The values of the trap depth recorded for the sample annealed for 10 minutes are higher compared with the sample annealed for 1 hour. In addition, annealing was noted to affect the thermal quenching of the peaks for each sample. The activation energy of thermal quenching for the sample annealed for 10 minutes are higher than for those recorded for 1 hour. This implies that the duration of annealing at 1000 °C has an effect on the trap parameters of a natural quartz sample.

Chapter 8

Phototransferred thermoluminescence

Phototransferred thermoluminescence (PTTL) related to multiple acceptors and donors is reported in this chapter. The study is carried out on samples of quartz annealed at 800 °C and 1000 °C for 10 minutes and for 1 hour for each annealing temperature. Results from quartz annealed at 1000 °C are reported first in section 8.1. This is followed by a comparative analysis of PTTL for quartz annealed at 800 °C for 10 minutes studied under green and blue light stimulation in section **??**. In addition, results of PTTL studies on quartz annealed at 800 °C for 10 minutes using a BG-39 filter under green light stimulation is included. Kinetic analysis of the phototransferred peaks I and III using a BG-39 filter is also presented. In section 8.3, we present and discuss the results of PTTL measurements for quartz annealed at 800 °C for 1 hour using a Hoya U-340 filter.
We adopt the model of Chithambo *et al.* (2017a) on our experimental data and describe the PTTL-time response curves on the basis of acceptors and donors whose number changes depending on preheating.

8.1 PTTL of quartz annealed at 1000 °C for 10 minutes and for 1 hour

The results from PTTL measurements on quartz annealed at 1000 °C for 10 minutes and for 1 hour are reported in this section. Experiment was performed using

a RISO TL/OSL Luminescence Reader with a Hoya U-340 detection filter (transmission band 250 - 390 nm) in place under blue light emitting diodes (LEDs). To measure phototransferred thermoluminescence, an irradiated sample was preheated to a specific temperature T_i to remove a given glow peak. In order to induce transfer of charge from deeper to shallower electron traps, the sample was thereafter exposed to 470 nm blue light providing an optical power density of 72 $mWcm^{-2}$ at sample position. A complete glow curve was then measured after illumination to monitor the presence of any PTTL peak.

8.1.1 Glow curve characteristics

Figure 8.1 shows the glow curves measured at 1 °C s^{-1} from samples of natural quartz annealed at 1000 °C for 10 minutes (solid symbol) and for 1 hour (open symbol). The samples are irradiated to 300 Gy. The high dose was used to significantly increase the concentration of electrons in the donor traps and so, induce a good PTTL signal. The glow curves show four peaks for each sample. An intense peak at 70 °C (labelled I) is recorded for each of the sample annealed for 10 minutes and for 1 hour. The secondary peaks labelled II, III, and V are recorded at 124, 170 and 298 °C respectively. The peaks II, III, and IV are at 130, 170, and 298 °C respectively for the sample annealed for 1 hour. The position of each of these peaks was verified by applying the thermal cleaning technique described in chapter 2.

PTTL was measured after preheating to the same temperatures as for the thermal cleaning method and illumination for a specific time. Figure 8.2 shows an example of a glow curve from the quartz sample annealed for 10 minutes, measured at 1 °Cs^{-1}, following irradiation to 300 Gy, preheating to 140 °C and illumination for 60 s. This shows a PTTL peak here labelled as P1. For ease of reference, PTTL peaks reproduced after removal of peaks I, II and III are referred to as P1, P2, and P3 respectively.

8.1.2 Identification of electron traps as donors and acceptors by pulse annealing

To identify which electron traps act as acceptors and which act as donors or source traps, the pulse annealing experiment (Bøtter-Jensen *et al.*, 2003) was carried out.

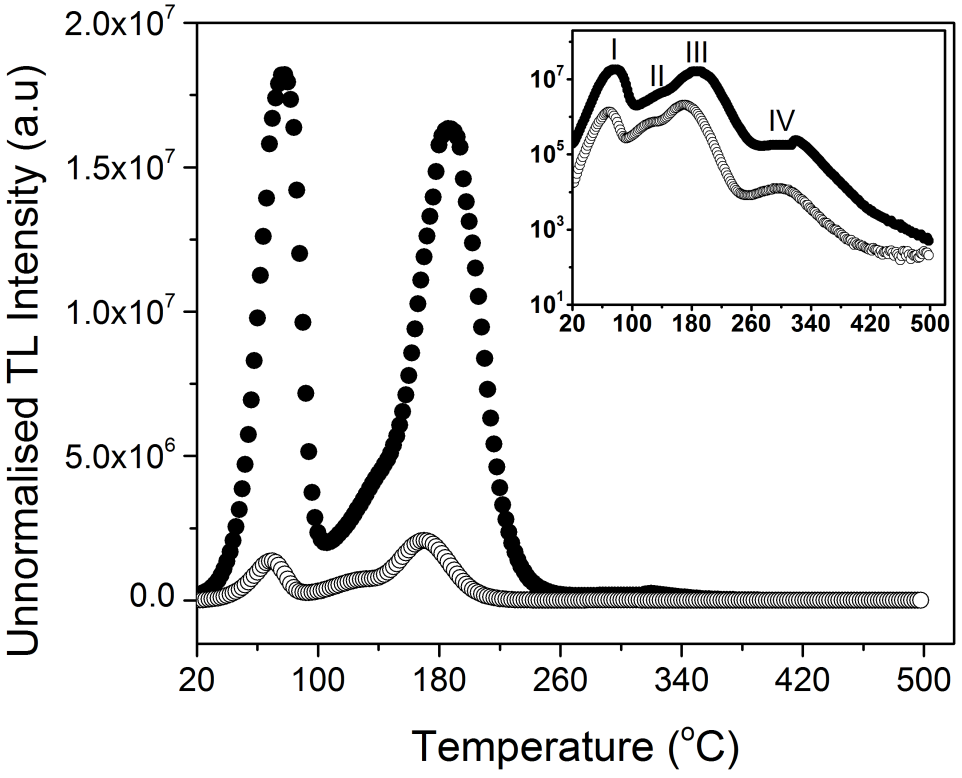

FIGURE 8.1: TL glow curves measured at 1 °C s^{-1} following irradiation to 300 Gy. The inset shows the same plots on a logarithmic scale to better show the presence of peak IV. The solid and open symbols represent data for the sample annealed for 10 minutes and 1 hour respectively.

The method exploits the dependence of PTTL intensity on preheating temperature. Measurements were made on a sample irradiated to 300 Gy, preheated in turn between 80 and 380 °C in steps of 10 °C, and illuminated for 60 s each time. Figure 8.3(a) shows the peak intensity against preheating temperatures for peaks I, III and IV for the samples annealed for 10 minutes. The peak intensity against preheating temperatures for peaks I - IV for the sample annealed for 1 hour is shown in Figure 8.3(b). The intensity of peak I, at 70 °C, for both samples decreased consistently with preheating between 80 and 370 °C. This decrease in intensity of peak I, an acceptor, reflects a depletion with preheating temperature in the concentration of charge at the donors. Thus in this case all electron traps corresponding to peaks II – IV act as donors. The intensity of peak II for the sample annealed for 10 minutes could not be reliably monitored since this peak is embedded between the falling edge of peak I and rising edge of peak III. However, the intensity of peak II was able to be monitored for the sample annealed for 1

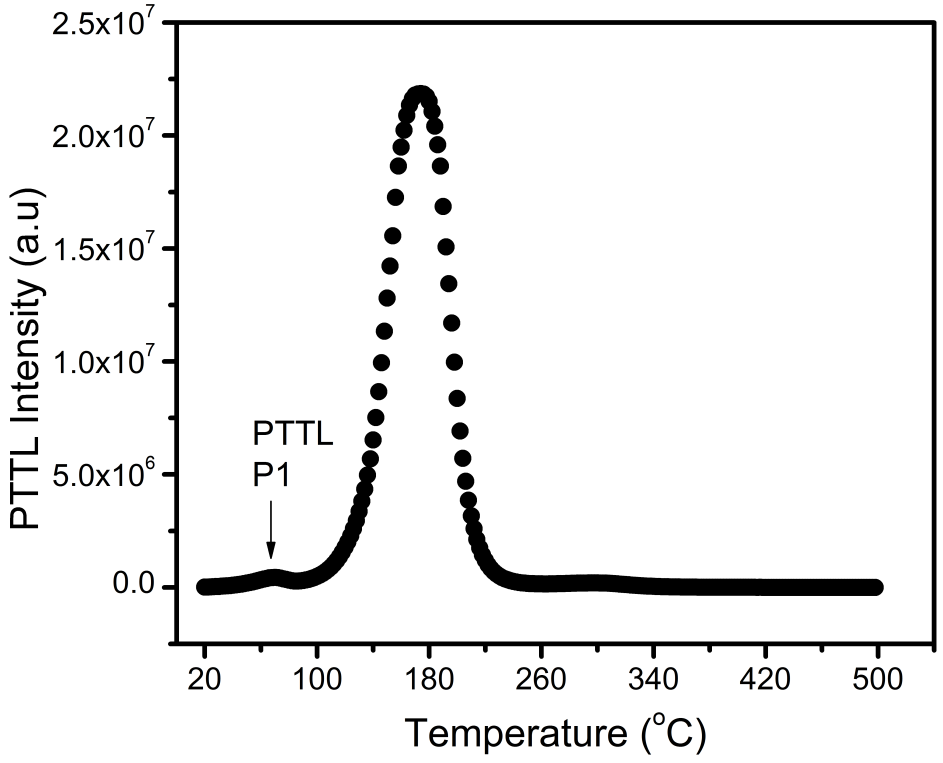

FIGURE 8.2: A TL glow curve measured at 1 °C s^{-1} following a dose of 300 Gy, preheating to 140 °C and illumination for 60 s showing phototransfer at peak P1. This is for the quartz sample annealed at 1000 ∘C for 10 minutes.

hour. The intensity of this peak was observed to be independent of preheating between 80 and 100 °C after which it decreased when the temperature was increased from 110 to 210 °C. Between 220 and 270 °C, the intensity of peak II was again independent of preheating. That the intensity of peak II was independent of preheating between 80 and 100 °C and between 220 and 270 °C implies that the concentration of charge at the donor electron traps is minimally affected by preheating. Additionally, peak II acts as a donor to peak I at these temperatures. The intensity further decreases monotonically from 280 to 370 °C. The decrease and constant intensity of peak II at different temperature intervals suggests that peak II can act as a competitor.

The intensity of peak III, at 170 °C for both samples, was constant for preheating between 80 and 140 °C but decreased significantly with further preheating up to 220 °C. That the intensity of peak III remains constant for preheating between 80 and 140 °C indicates that the concentration of charge at its donors is little affected by the preheating. The decrease of intensity from 140 to 220 °C implies a

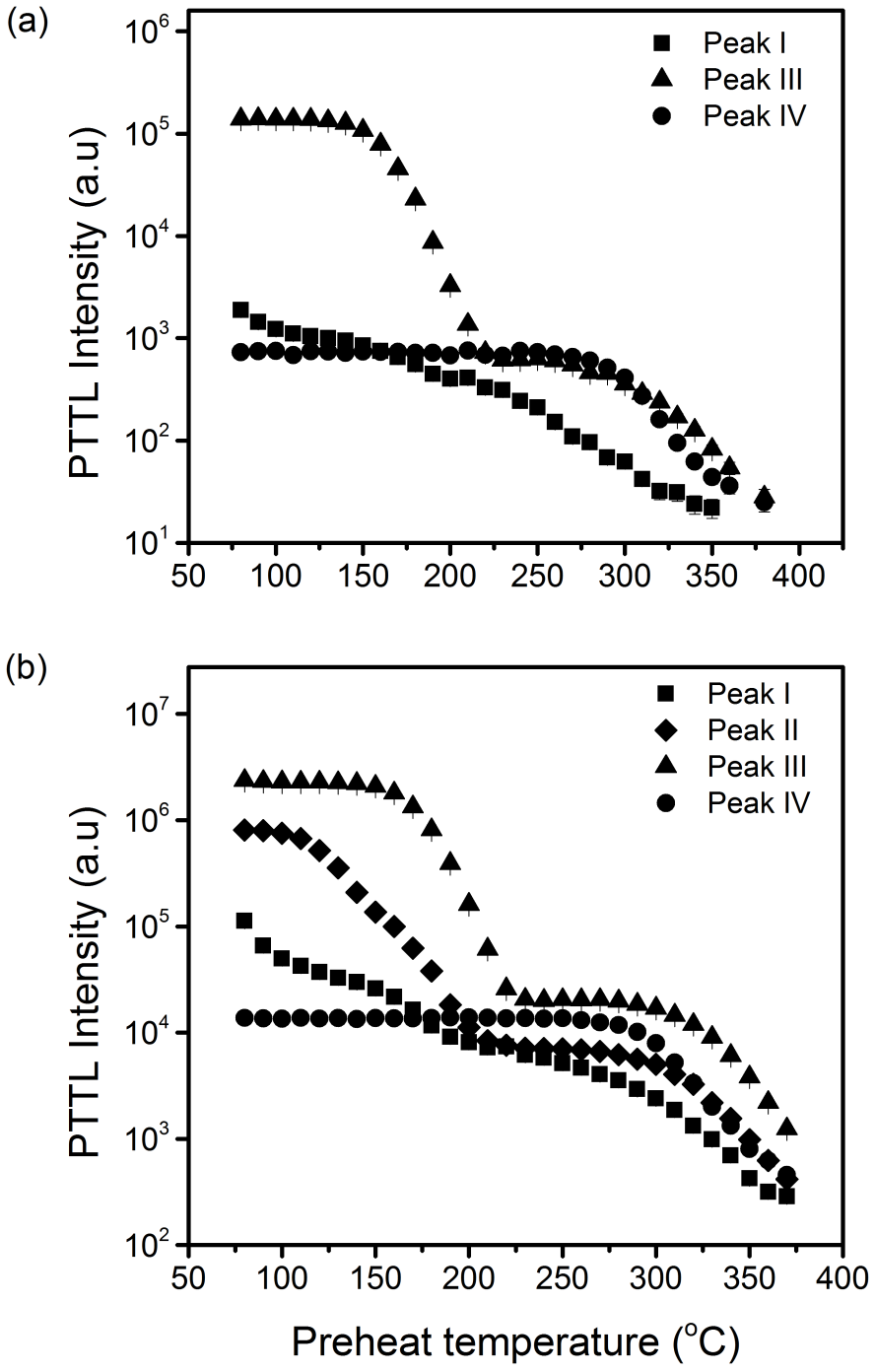

FIGURE 8.3: The influence of preheating temperature on peak intensity in a pulse annealing experiment (a) for the sample annealed for 10 minutes (b) for the sample annealed for 1 hour. The error bars in each data point are determined using square root rule for counting experiments.

decrease in the concentration of charge at its donor. Between 220 and 250 °C for the sample annealed for 10 minutes and between 220 and 270 °C for the sample

annealed for 1 hour, the intensity was again constant before decreasing monotonically with preheating up to 380 °C. Peak III observed between 220 and 270 °C is a phototransferred peak. The constant intensity of this peak between 220 and 250 or 270 °C implies that peak III acts again as a donor to peaks I and II. Additionally, the preheating did not affect any of its donor electron traps.

Peak III is thus seen to play a dual role of an acceptor and a donor between 80 and 380 °C. For peak IV, the intensity was constant from 80 to about 250 °C for the sample annealed for 10 minutes and between 80 and 270 °C for the sample annealed for 1 hour. Afterwards, the intensity decreased progressively to background level at 380 °C. The behaviour of the intensity of peak IV implies that its electron trap acts as a donor to electron traps whose peaks occur at lower temperatures.

8.1.3 Dependence of PTTL intensity on the duration of illumination

The intensity of the PTTL peaks was studied as a function of illumination time starting from 2 s. In the measurements, the quartz was irradiated to 300 Gy and PTTL monitored corresponding to preheating to 100, 140, 250, and 500 °C. These are the same temperatures used for thermal cleaning except 500 °C used to sense deep traps.

8.1.3.1 PTTL following preheating to 100 °C

A PTTL peak (peak P1) is reproduced under phototransfer when an irradiated sample is preheated to 100 °C and illuminated for 60 s. The dependence of its PTTL intensity on the duration of illumination between 2 and 1000 s is shown in Figure 8.4. The variation of the intensity of P1 with illumination time corresponding to the sample annealed for 10 minutes is shown in Figure 8.4(a) whereas the plot for the sample annealed for 1 hour is shown in Figure 8.4(b). The intensity increases up to a maximum and decreases thereafter for both samples, although the increase in intensity was observed for an extended time of 150 s in Figure 8.4(b). The PTTL-time response curve recorded for these samples is a common feature for PTTL signals from quartz e.g. (Milanovich-Reichhalter and Vana, 1991; Chithambo *et al.*, 2018), α-Al_2O_3:C e.g. (Bulur and Göksu, 1999; Chithambo *et al.*, 2017a), α-Al_2O_3:C, Mg (Kalita and Chithambo, 2017).

The increase of intensity at short illumination times as qualitatively explained by Chithambo *et al.* (2017a) implies that the trapping of electrons in the shallow trap exceeds any removal by optical stimulation. The decrease of the PTTL intensity at long illumination times means that removal of electrons from the shallow trap by optical stimulation is more than any trapping.

We show later the intensity - time plots of peaks II - IV which are not PTTL peaks, but whose contribution to phototransfer is important for mathematical models of PTTL.

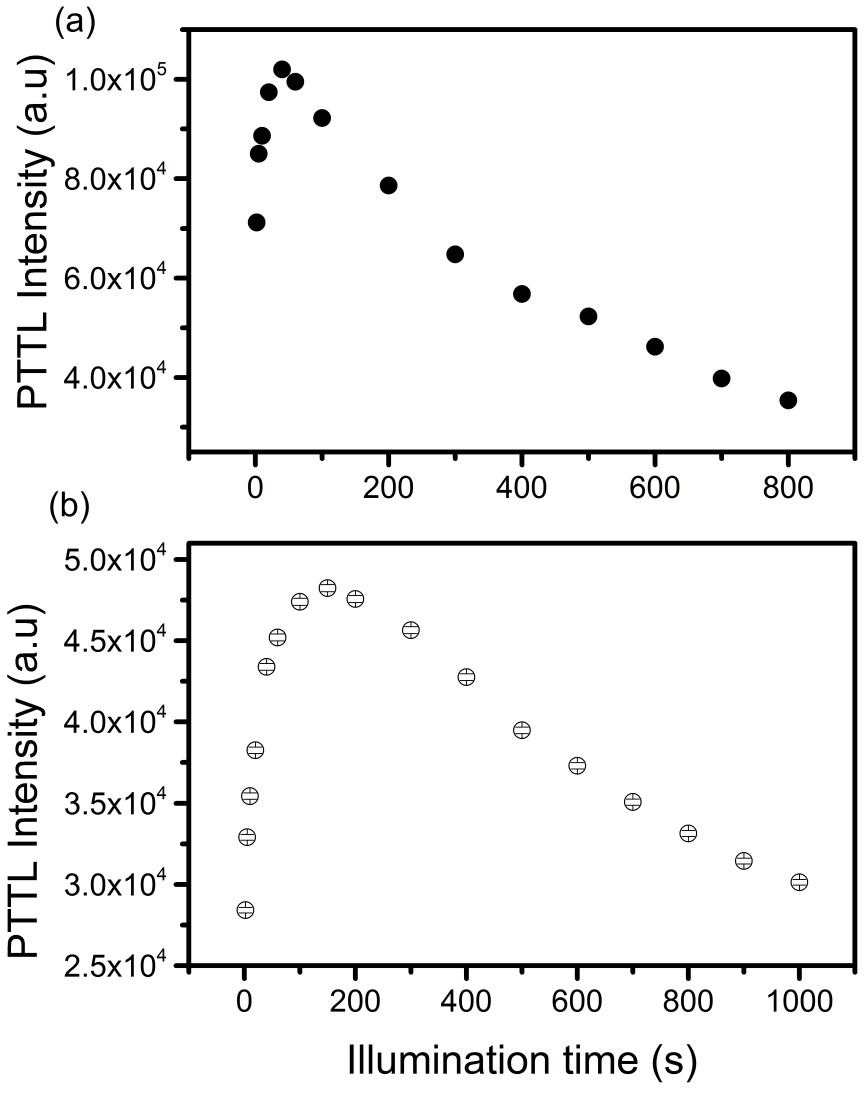

FIGURE 8.4: Dependence of PTTL intensity on duration of illumination for peak P1 (a) for the sample annealed for 10 minutes (b) for the sample annealed for 1 hour after preheating to 100 °C.

8.1.3.2 PTTL following preheating to 140 °C

When the sample was preheated to 140 °C after irradiation to remove peaks I and II, and its glow curve measured after illumination, the removed peaks were reproduced under phototransfer for the sample annealed for 1 hour. However, for the sample annealed for 10 minutes, only peak I is reproduced under phototransfer.

Figure 8.5 shows the time-dependence of PTTL from P1 and P2 after preheating to 140 °C. The PTTL intensity also goes through a peak with illumination time. As a matter of interest, we show in Figure 8.6(a) the time-dependence of intensity for peak III from the sample annealed for 10 minutes which is not a PTTL peak but a donor for P1 at this stage. The intensity of this peak does not decrease consistently with illumination as might be expected of a donor (as observed in Figure 8.6(b) in the case of the sample annealed for 1 hour) but increases for the first 10 s before decreasing. The electron trap for peak III thus acts as a competitor for photo-stimulated charge from deeper electron traps. The competition effects of this peak will be discussed later.

8.1.3.3 PTTL following preheating to 250 °C

Figure 8.7 shows a glow curve measured after preheating to 250 °C and illuminating for 60 s. This glow curve is from the sample annealed for 10 minutes. Peaks I, II and III are reproduced under phototransfer at 70, 130, and 180 °C respectively and are shown as P1, P2, and P3. Of these, P3 is the most intense. This is also true for the sample annealed for 1 hour shown in the inset to Figure 8.7.

Figure 8.8 shows the dependence of the PTTL intensity on duration of illumination for PTTL peaks P1, P2 and P3 from the sample annealed for 10 minutes. Figure 8.8(a) shows the behaviour for peak P1 where the intensity decreases with illumination consistently. The initial increase characteristic of PTTL as observed in Figures 8.4(a) and 8.5(a) is absent. This is an effect of competitive retrapping at electron traps for peaks II and III. For the sample annealed for 1 hour (Figure 8.8(b)), the intensity of P1 increases up to a maximum and decreases slowly with time. This decrease is different from other decrease recorded for the same peak at preheating to 100 and 140 °C.

The time-dependence of the PTTL intensity from peak P2 is shown in Figure 8.8(c)-(d) and for peak P3 in Figure 8.8(e)-(f). The results differ from all else

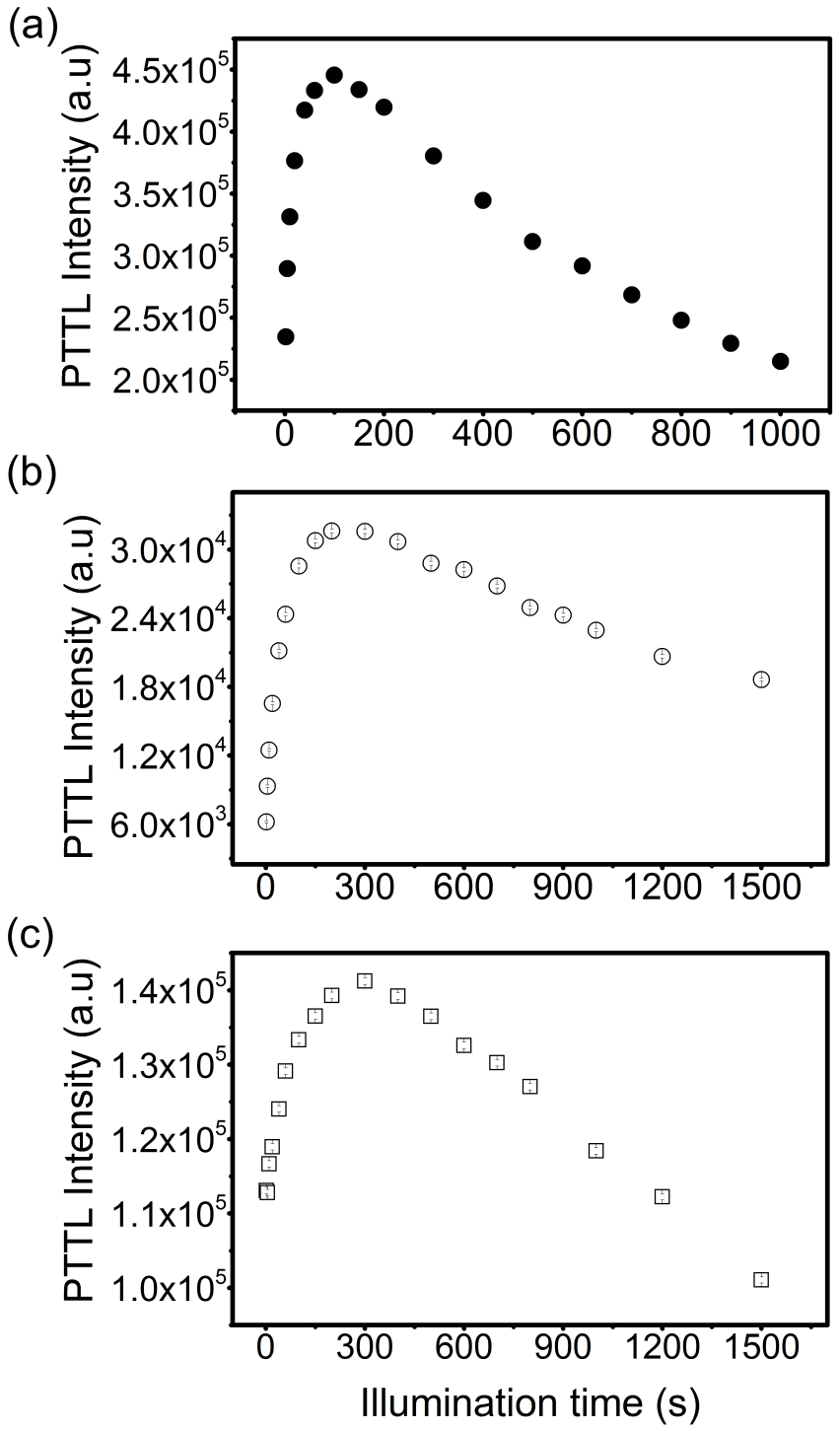

FIGURE 8.5: Dependence of PTTL intensity on duration of illumination for (a) P1 for the sample annealed for 10 minutes (b) P1 for the sample annealed for 1 hour (c) P2 for the sample annealed for 1 hour after preheating to 140 ° C.

discussed thus far. The PTTL intensities for peaks P2 and P3 for the sample annealed for 10 minutes increase slowly for an extensive period of about 1500 s

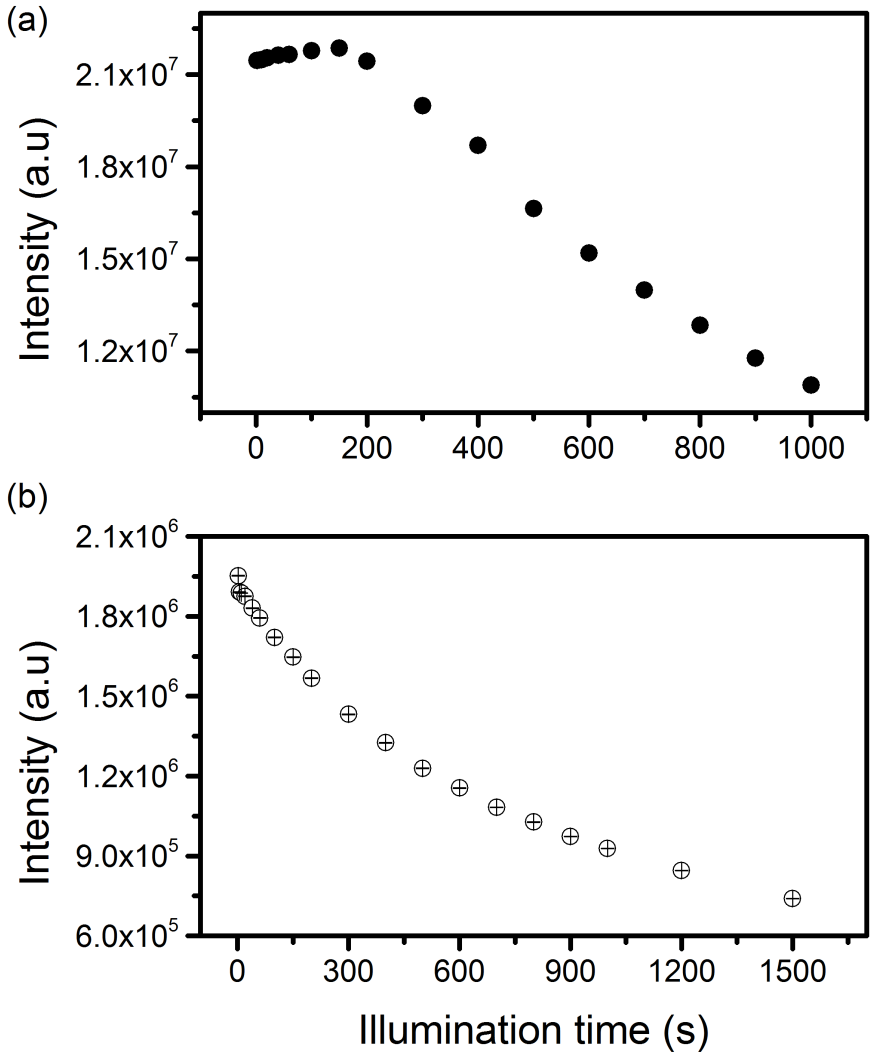

FIGURE 8.6: Dependence of PTTL intensity on duration of illumination after preheating to 140 °C (a) for the sample annealed for 10 minutes (b) for the sample annealed for 1 hour.

before the onset of a decrease. The change for peak P3 is perhaps to be expected given that its supposed electron trap shows evidence of being an effective charge competitor. The same may apply for peak P2. For the sample annealed for 1 hour, the intensities of peaks P2 and P3 increase also for an extensive period but towards saturation.

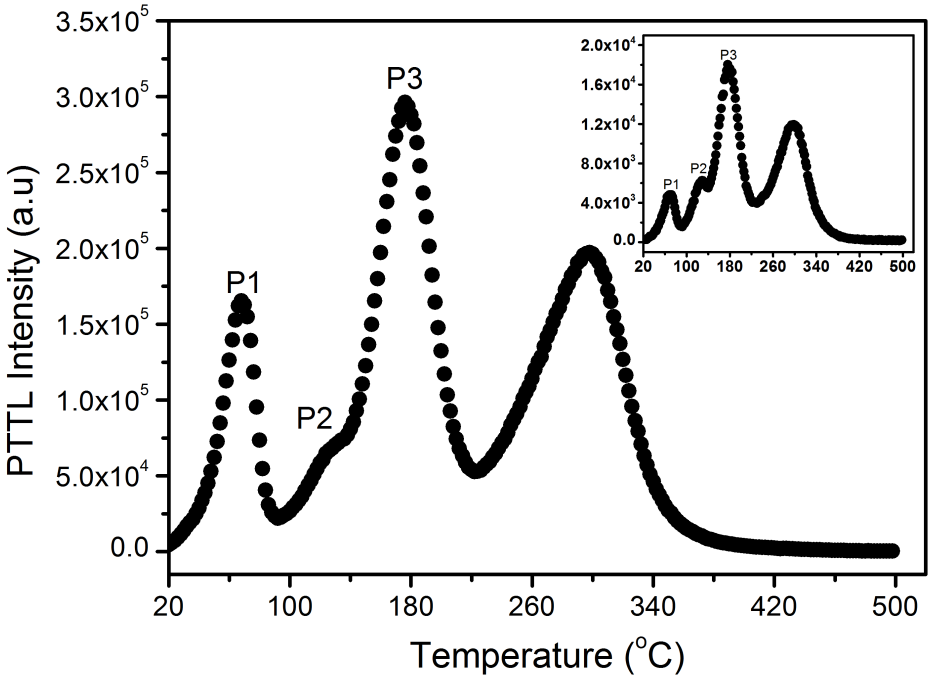

FIGURE 8.7: A glow curve measured at 1 °Cs^{-1} after a dose of 300 Gy, preheating to 250 °C and illumination for 60 s.

8.1.3.4 PTTL following preheating to 500 °C

Preheating the quartz sample to 500 °C and illuminating for 60 seconds reproduces only peaks I and III for the sample annealed for 10 minutes. However, no peak was reproduced for the sample annealed for 1 hour. Figure 8.9(a) shows the time-dependence of the PTTL intensity for peak P1 and in Figure 8.9(b) for peak P3. Both cases show a typical increase followed by a decrease although for peak P3, the decrease is slower and appears linear.
The time-dependence of the PTTL intensity in all the examples shown will be described using some mathematical models.

8.1.4 Dose dependence of PTTL intensity

The influence of irradiation on the PTTL intensity from peak P1 was studied by measuring its dose dependence corresponding to different preheating temperatures. The PTTL intensity was measured for doses between 20 and 400 Gy for preheating to 100, 140, and 250 °C. Figure 8.10(a) shows the growth curves of the PTTL

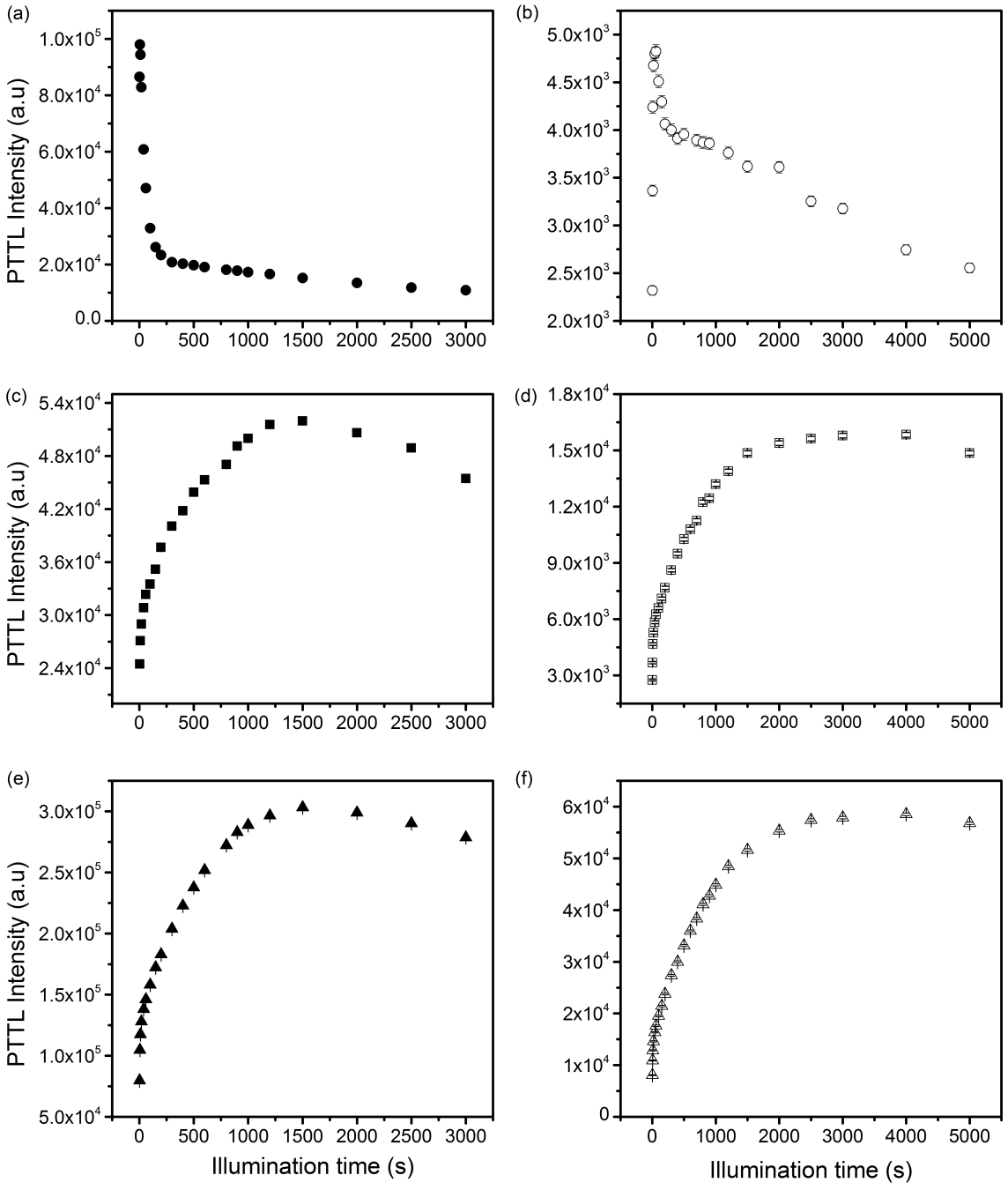

FIGURE 8.8: Change of PTTL intensity with illumination time for peak (a) P1 for the sample annealed for 10 minutes (b) P1 for the sample annealed for 1 hour (c) P2 for the sample annealed for 10 minutes (d) P2 for the sample annealed for 1 hour (e) P3 for the sample annealed for 10 minutes and (f) P3 for the sample annealed for 1 hour after preheating to 250 °C.

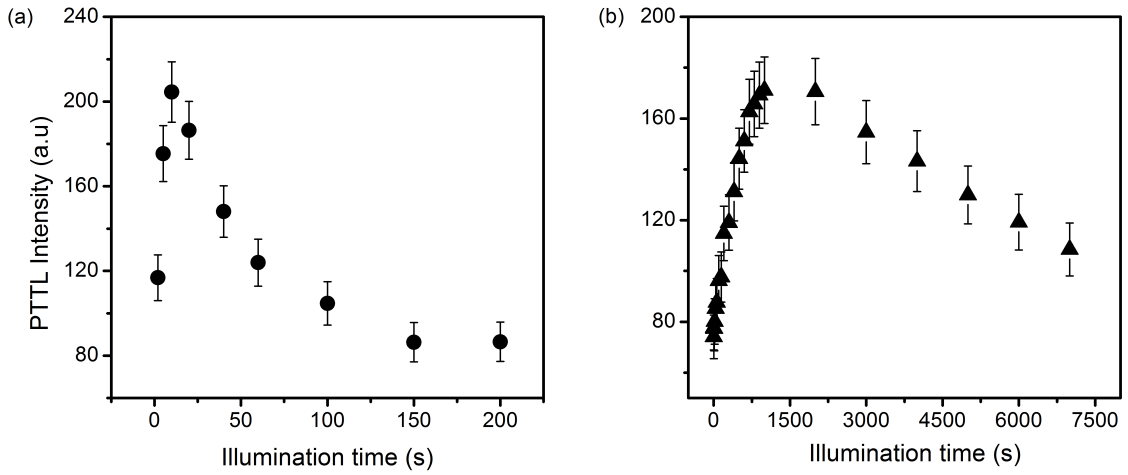

FIGURE 8.9: PTTL intensity versus illumination time for (a) peak P1 (b) peak P3 after preheating to 500 °C.

measured for peak P1 after preheating to 100, 140 and 250 °C respectively for the sample annealed for 10 minutes. Figure 8.10(b) shows the growth curve for peak P1 for the sample annealed for 1 hour.The growth curves demonstrate that all higher peaks seem to be donor for PTTL Peak I. The dose response of peak P1 is sublinear and consistent for each sample.

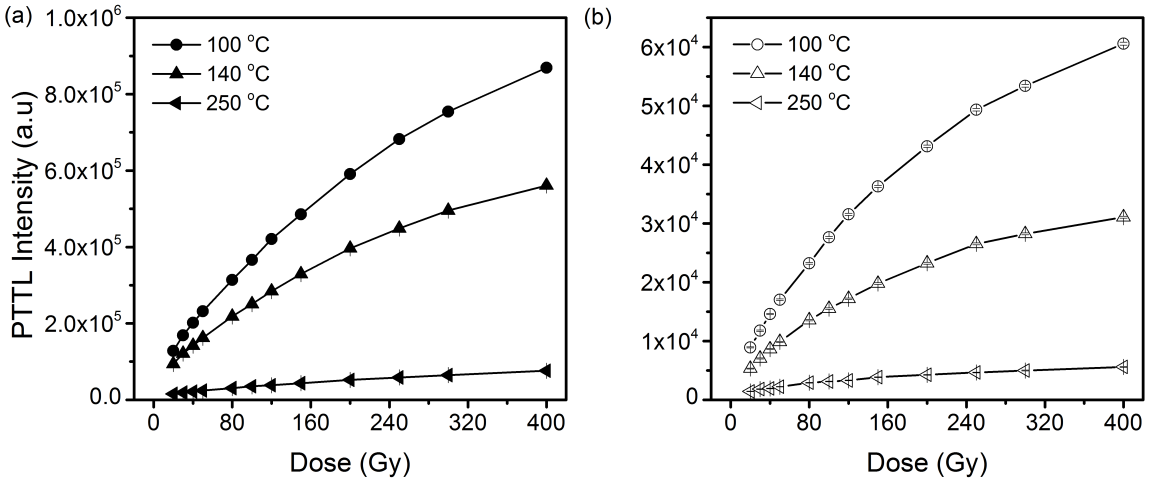

FIGURE 8.10: Dose dependence of PTTL intensity for peak P1 for the sample annealed for (a) 10 minutes (b) 1 hour.

8.1.5 Mathematical models of PTTL

PTTL is a multi-step process involving irradiation to fill electron traps, preheating to empty the shallow traps, illumination to transfer charge from deep traps to the

empty shallow ones, and heating to monitor any PTTL peaks. The number of electron traps acting as acceptors or donors changes with preheating temperature. To analyse the illumination time-dependent profiles of PTTL, we adopt the method of Chithambo *et al.* (2017a) where PTTL is described for any combination of donors and an acceptor using families of linear differential equations with analytical solutions. This is in contrast to the discussion of say, Alexander and McKeever (1998) where PTTL was discussed for an exemplar of an acceptor and donor using non-linear differential equations without analytical solutions. In the latter, computational modelling is required to produce a numerical solution that closely matches experimental data. In contrast, the analytical solutions in the method of Chithambo *et al.* (2017a) can be applied directly to experimental data.

Figure 8.11 shows the energy band model used to explain PTTL in this study.

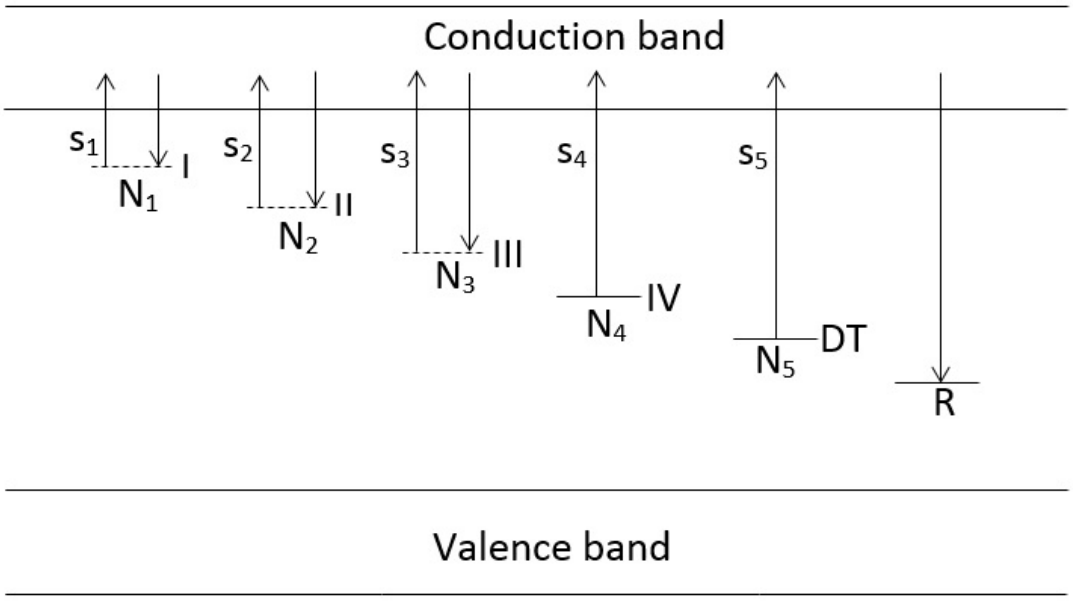

FIGURE 8.11: An energy band model used to discuss PTTL. The symbols I, II, III refers to the acceptor traps whereas IV and DT represent the donor traps. The recombination centre R producing luminescence is included for completeness. The optical stimulation rates are labelled as s_i and the concentration at each electron trap as N_i (where $i = 1, \cdots, 5$).

Electron traps corresponding to peaks P1, P2, P3, and IV are labelled as I, II, III, and IV. A deep trap, the supposed source trap corresponding to any PTTL observed after preheating to 500 °C is shown as DT. Since the number of deep traps is unknown, we limit this to one, DT. We describe the transport of charge of PTTL from the donor(s) to an acceptor trap only at the illumination stage using

linear differential equations. We assume that during illumination, electrons are stimulated from the deep or donor traps at a stimulation rate $s = \Phi\sigma$ (where Φ is the intensity of the stimulation light and σ the photoionisation cross-section). Some of the electrons are captured at the acceptor trap. We set up coupled first-order linear differential equations and apply their analytical solutions directly to our experimental data. From the model, we determine the photoionisation cross-sections of the acceptor traps corresponding to each preheating temperature. The dependence of PTTL intensity on duration of illumination is discussed in four categories based on the preheating temperature used.

8.1.5.1 PTTL following preheating to 100 °C to remove peak I

When the quartz sample is preheated to 100 °C, peak I is removed and then reproduced under phototransfer. Electron traps corresponding to peaks II, III and IV as well as DT serve as donors whereas the trap corresponding to peak P1 acts as an acceptor. The system therefore comprises of one acceptor and four donors. The coupled differential equations for the system can be expressed as

$$\frac{dN_2}{dt} = -s_2 N_2 \tag{8.1}$$

$$\frac{dN_3}{dt} = -s_3 N_3 \tag{8.2}$$

$$\frac{dN_4}{dt} = -s_4 N_4 \tag{8.3}$$

$$\frac{dN_5}{dt} = -s_5 N_5 \tag{8.4}$$

$$\frac{dN_1}{dt} = -s_1 N_1 + a_2 s_2 N_2 + a_3 s_3 N_3 + a_4 s_4 N_4 + a_5 s_5 N_5 \tag{8.5}$$

Equations (8.1) - (8.4) represent the optical stimulation of electrons from the donor traps at the designated levels. Equation (8.5) describes charge transport at the acceptor. The last four terms in equation (8.5) state that a portion of electrons released from each donor trap is retrapped at the acceptor. The first term reflects the possibility of optical loss of trapped charge at a rate s_1. The solution of the coupled linear differential equations (8.1) - (8.5) is thus

$$N_1 = A(e^{-s_2 t} - e^{-s_1 t}) + B(e^{-s_3 t} - e^{-s_1 t}) + C(e^{-s_4 t} - e^{-s_1 t}) + D(e^{-s_5 t} - e^{-s_1 t}) \tag{8.6}$$

where $A = \frac{a_2 s_2 N_{2i}}{s_1 - s_2}$, $B = \frac{a_3 s_3 N_{3i}}{s_1 - s_3}$, $C = \frac{a_4 s_4 N_{4i}}{s_1 - s_4}$, $D = \frac{a_5 s_5 N_{5i}}{s_1 - s_5}$. N_{2i}, N_{3i}, N_{4i}, and N_{5i} are each the initial concentration of electrons at the electron traps II, III, IV and the deep trap respectively; the a_i's are constants of proportionality; s_1 represents the probability of electron stimulation from the acceptor trap; s_2, s_3, s_4, and s_5 represent the probability of stimulation from the donor traps.

Although this model is for a system of one acceptor and four donors, it is imperative to verify if the donors act as such (or are competitors) before concluding on the model that fits the data. To do this, we examine the change of intensity of the peaks corresponding to the donor traps with illumination time. For a pure donor, it is expected that the intensity decreases consistently with illumination. Figure 8.12(a)-(c) shows the variation of intensity with duration of illumination for peaks II - IV for the sample annealed for 10 minutes and for 1 hour. Peak II is not properly defined for the sample annealed for 10 minutes, so instead of recording the value at peak maximum, we record the intensity at a fixed temperature of 130 °C, which we assume to be the temperature of the peak maximum. This data is shown in Figure 8.12(a)(solid symbol). The intensity of peaks II and III (solid symbols) decreases consistently with illumination time as expected of a pure donor. However for peak IV in Figure 8.12(c), the intensity was vacillating. Similar results for peaks II - IV (open symbols) are recorded for the sample annealed for 1 hour. Since the change of intensity of peak IV with time has no definite pattern, its contribution to phototransfer is considered to be negligible. This consideration is in line with the pulse annealing experiment (Figure 8.3) which revealed that the change of intensity of peak IV with preheating is negligible. Thus, the electron trap corresponding to peak IV is redundant as a donor.
The time-dependence of the electron concentrations corresponding to P1 now becomes

$$N_1 = A'(e^{-s_2 t} - e^{-s_1 t}) + B'(e^{-s_3 t} - e^{-s_1 t}) + C'(e^{-s_5 t} - e^{-s_1 t}) \tag{8.7}$$

where $A' = \frac{a'_2 s_2 N_{2i}}{s_1 - s_2}$, $B' = \frac{a'_3 s_3 N_{3i}}{s_1 - s_3}$, $C' = \frac{a'_5 s_5 N_{5i}}{s_1 - s_5}$ and a_i's are each a constant of proportionality.
Equation (8.7) describes a system of one acceptor and three donors.

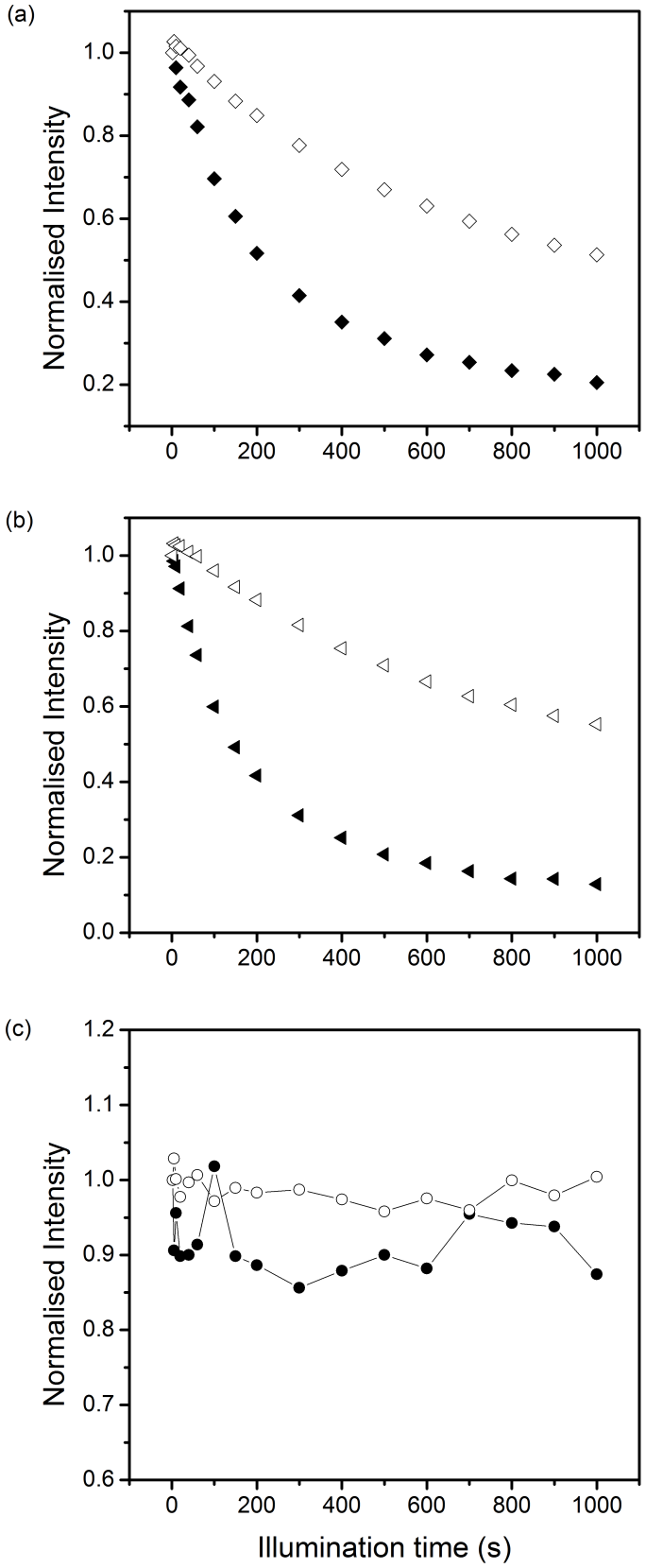

FIGURE 8.12: Change of intensity with illumination time following preheating to 100 °C for (a) peak II (b) peak III (c) peak IV. The solid and open symbols represent data corresponding to the samples annealed for 10 minutes and 1 hour respectively.

8.1.5.2 PTTL following preheating to 140 °C to remove peaks I and II

Preheating the sample to 140 °C removes peaks I and II with the expectation that both peaks should be reproduced by phototransfer. However, only peak I is reproduced for the sample annealed for 10 minutes whereas the removed peaks are reproduced as expected for the sample annealed for 1 hour. The electron traps for peak P1 (for both samples) and peak P2 (for the sample annealed for 1 hour) are acceptors whereas those for peaks III and IV as well as the deep trap act as donors. As a way of confirming the authenticity of the donors, we examine the change of intensity of peaks III and IV with illumination time. Figure 8.6 already shows that peak III for both samples can act as a donor, though competition effects on peak III for the sample annealed for 10 minutes is conspicuous.

Figure 8.13 shows the time-dependence of intensity for peak IV corresponding to preheating to 140 °C. The intensity of peak IV for the sample annealed for 10 minutes shown in Figure 8.13(a) decreases slowly for the first 200 s and consistently thereafter, confirming its role as a donor. This means that while peak IV acts as a donor, it also captures some of the charges released from the deep trap showing competition effects. However, its role as a donor is what is important at this point. For the sample annealed for 1 hour in Figure 8.13(b), the intensity of peak IV is independent of illumination time. Hence, we consider the concentration at its trap negligible and redundant as a donor.

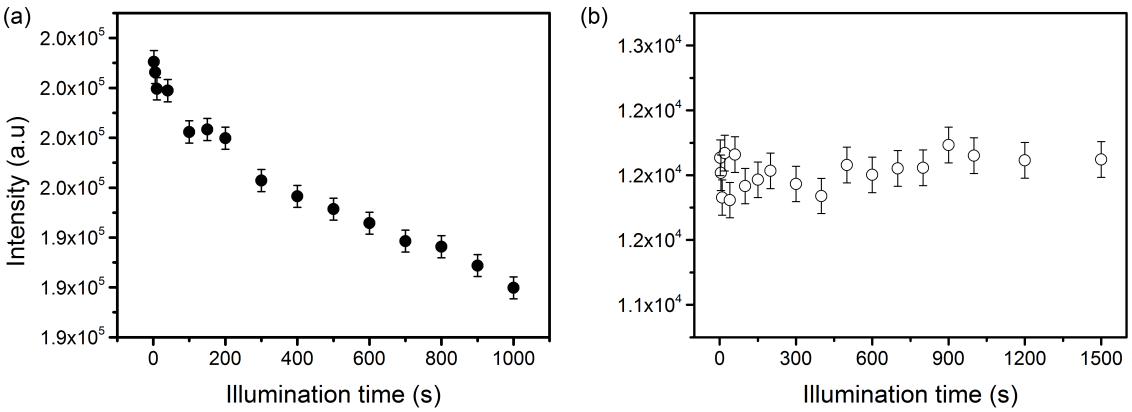

FIGURE 8.13: PTTL intensity of peak IV versus illumination time for the sample annealed for (a) 10 minutes (b) 1 hour after preheating to 140 °C.

Thus, the system for the sample annealed for 10 minutes comprises one acceptor and three donors whereas for the sample annealed for 1 hour, it is a system of one

acceptor and two donors.

The coupled differential equations for the system annealed for 10 minutes are

$$\frac{dN_3}{dt} = -s_3 N_3 \tag{8.8}$$

$$\frac{dN_4}{dt} = -s_4 N_4 \tag{8.9}$$

$$\frac{dN_5}{dt} = -s_5 N_5 \tag{8.10}$$

$$\frac{dN_1}{dt} = -s_1 N_1 + b_3 s_3 N_3 + b_4 s_4 N_4 + b_5 s_5 N_5 \tag{8.11}$$

It is to be noted that equations (8.8) - (8.10) though similar to equations (8.2) - (8.4) are not repetition. The similar looking equations which will occur most times in a set, are each part of a system and are important to solve for that particular system. The solution of the coupled differential equations (8.8) - (8.11) is

$$N_1 = A_1(e^{-s_3 t} - e^{-s_1 t}) + A_2(e^{-s_4 t} - e^{-s_1 t}) + A_3(e^{-s_5 t} - e^{-s_1 t}) \tag{8.12}$$

where $A_1 = \frac{a_3^* s_3 N_{3i}}{s_1 - s_3}$, $A_2 = \frac{a_4^* s_4 N_{4i}}{s_1 - s_4}$, $A_3 = \frac{a_5^* s_5 N_{5i}}{s_1 - s_5}$ and a_i^*'s are each a constant of proportionality and other parameters are as defined previously.

For the sample annealed for 1 hour, we solve for N_1 and N_2 taking into account that the concentration at level IV is negligible. Thus, we have

$$N_1 = A_1^*(e^{-s_3 t} - e^{-s_1 t}) + A_3^*(e^{-s_5 t} - e^{-s_1 t}) \tag{8.13}$$

$$N_2 = B_1(e^{-s_3 t} - e^{-s_2 t}) + B_2(e^{-s_5 t} - e^{-s_2 t}) \tag{8.14}$$

where $A_1^* = \frac{a_3^{**} s_3 N_{3i}}{s_1 - s_3}$, $A_3 = \frac{a_5^{**} s_5 N_{5i}}{s_1 - s_5}$, $B_1 = \frac{b_3 s_3 N_{3i}}{s_2 - s_3}$, $B_2 = \frac{b_5 s_5 N_{5i}}{s_2 - s_5}$; a_3^{**}, a_5^{**}, b_3, b_5 are constants of proportionality.

8.1.5.3 PTTL following preheating to 250 °C to remove peaks I - III

When the sample is preheated to 250 °C to remove peaks I, II and III, all the removed peaks are reproduced under phototransfer for both samples. The electron traps corresponding to peaks P1, P2 and P3 are acceptors whereas those for peak IV and DT are donors. Examining the change of intensity of peak IV with preheating temperatures above 250 °C (Figure 8.3) shows a decrease in intensity

with preheating confirming its role as a donor. We thus have three systems of one acceptor and two donors. The transport of electrons leading to the photoinduction of P3 is given by the family

$$\frac{dN_4}{dt} = -s_4 N_4 \tag{8.15}$$

$$\frac{dN_5}{dt} = -s_5 N_5 \tag{8.16}$$

$$\frac{dN_3}{dt} = -s_3 N_3 + c_4 s_4 N_4 + c_5 s_5 N_5 \tag{8.17}$$

We emphasize again that equations (8.15) and (8.16) are not repetition.
The solution of equations (8.15) - (8.17) is

$$N_3 = D(e^{-s_4 t} - e^{-s_3 t}) + E(e^{-s_5 t} - e^{-s_3 t}) \tag{8.18}$$

where $D = \frac{c_4 s_4 N_{4i}}{s_3 - s_4}$, $E = \frac{c_5 s_5 N_{5i}}{s_3 - s_5}$; c_4, c_5 are constants of proportionality.

Similarly for P2 and P1, the concentration of electrons with time at levels II and I are

$$N_2 = D^*(e^{-s_4 t} - e^{-s_2 t}) + E^*(e^{-s_5 t} - e^{-s_2 t}) \tag{8.19}$$

$$N_1 = D^{**}(e^{-s_4 t} - e^{-s_1 t}) + E^{**}(e^{-s_5 t} - e^{-s_1 t}) \tag{8.20}$$

where $D^* = \frac{c_4^* s_4 N_{4i}}{s_2 - s_4}$, $E^* = \frac{c_5^* s_5 N_{5i}}{s_2 - s_5}$, $D^{**} = \frac{c_4^{**} s_4 N_{4i}}{s_1 - s_4}$, $E^{**} = \frac{c_5^{**} s_5 N_{5i}}{s_1 - s_5}$; c_4^*, c_4^{**}, c_5^*, c_5^{**} are constants of proportionality.

8.1.5.4 PTTL following preheating to 500 °C

Preheating the irradiated sample to 500 °C to remove all the peaks in the glow curve and exposing it to blue LEDs reproduces peak I and peak III for the sample annealed for 10 minutes only. No peak was reproduced for the sample annealed for 1 hour. Electron traps corresponding to peaks P1 and P3 are thus regarded as acceptors. The electron trap for DT is the only donor. For each PTTL peak, we have a simple case of one acceptor and one donor. The coupled differential

equations for the traps corresponding to P3 and DT are

$$\frac{dN_5}{dt} = -s_5 N_5 \tag{8.21}$$

$$\frac{dN_3}{dt} = -s_3 N_3 + q_5 s_5 N_5 \tag{8.22}$$

The solution of the set (8.21) and (8.22) is

$$N_3 = Q(e^{-s_5 t} - e^{-s_3 t}) \tag{8.23}$$

Similarly, the time-dependence of the electron concentration corresponding to P1 is

$$N_1 = Q^*(e^{-s_5 t} - e^{-s_1 t}) \tag{8.24}$$

where $Q = \frac{q_5 s_5 N_{5i}}{s_3 - s_5}$, $Q^* = \frac{q_5^* s_5 N_{5i}}{s_1 - s_5}$; q_5 and q_5^* are constants of proportionality.

8.1.6 Application of models

We have shown in the preceding section the mathematical models derived for PTTL corresponding to different preheating temperatures. All developed models are based on experimental evidence and are fitted to experimental data. The intensity is assumed to be proportional to the concentration of trapped electrons N_i at an acceptor as before (Wintle and Murray, 1997; Chithambo *et al.*, 2017a, 2018). The results for peak P1 corresponding to preheating to 100 °C for a system of one acceptor and three donors are shown in Figure 8.14 for the sample annealed for 10 minutes and 1 hour. The line passing through the data points is the best fit of equation (8.7).

The photoionisation cross-section σ was determined from the stimulation probability $s = \Phi\sigma$ as 6.4×10^{-18} cm^2 for the sample annealed for 10 minutes. The photon flux Φ given by Φ = maximum power density/energy per photon equals $\Phi = 1.70 \times 10^{17}$ cm^{-2}s^{-1} given a maximum power density of 72 mWcm^{-2} at sample position and a stimulation wavelength of 470 nm. The photoionisation cross-section for peak P1 for the sample annealed for 1 hour (Figure 8.14(b)) was calculated as 6.1×10^{-18} cm^2.

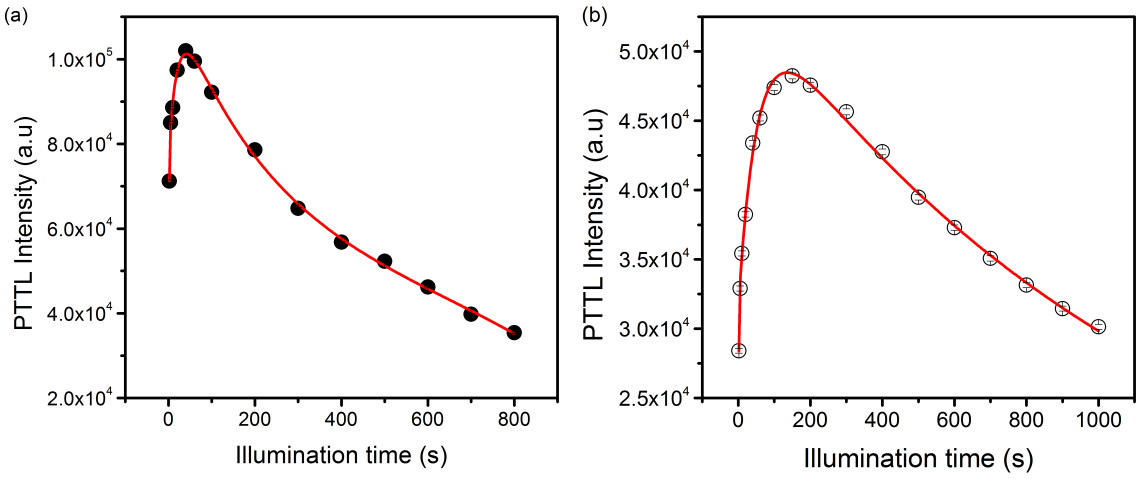

FIGURE 8.14: Plots of PTTL intensity versus illumination time for peak P1 after preheating to 100 °C for the sample annealed for (a) 10 minutes (b) 1 hour.

Figure 8.15 shows the results for peak P1 corresponding to preheating to 140 °C for the case of one acceptor and three donors for the sample annealed for 10 minutes. The data is fitted with equation (8.12). The photoionisation cross-section was calculated as 5.1×10^{-18} cm^2.

Figure 8.15(b) shows the fits for a system of one acceptor and two donors for peak P1 and in Figure 8.15(c) for peak P2 corresponding to preheating to 140 °C. These results are for the quartz annealed for 1 hour. The photoionisation cross-section was evaluated as $\sigma_1 = 2.1 \times 10^{-18}$ cm^2 and $\sigma_2 = 15.6 \times 10^{-18}$ cm^2.

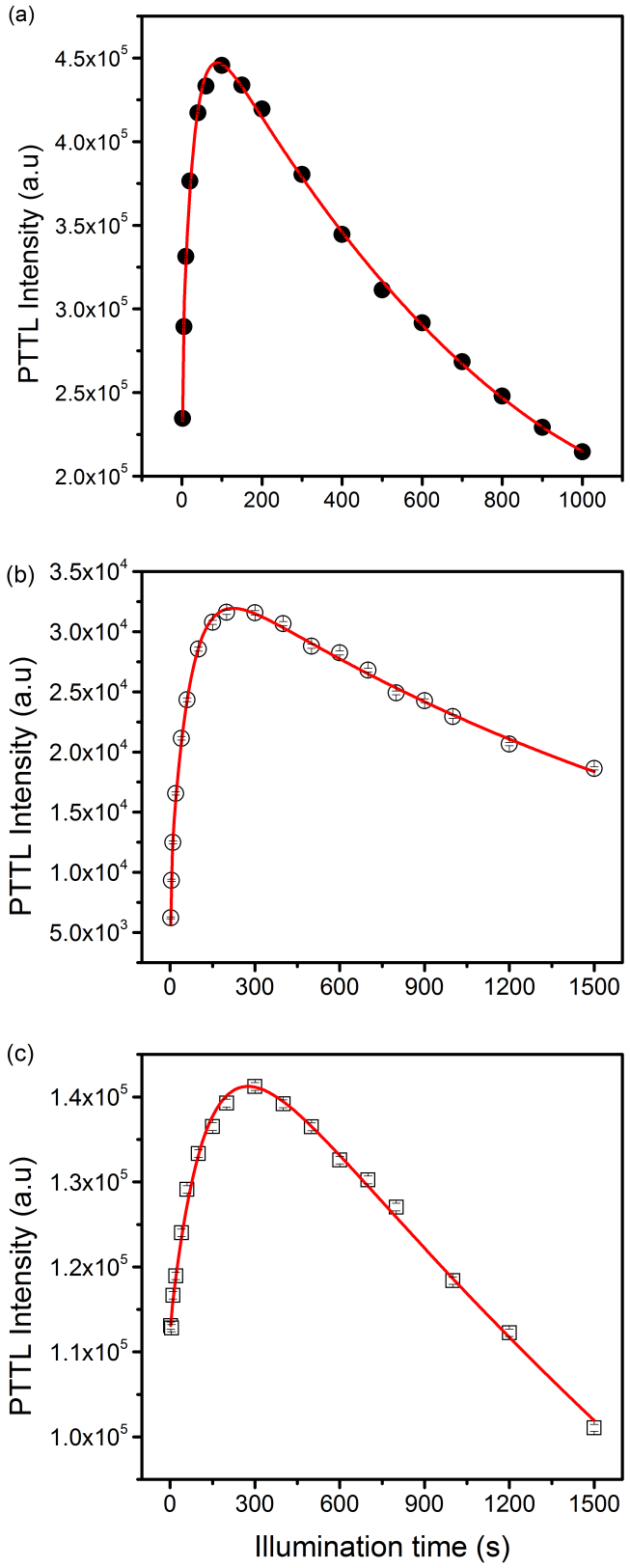

FIGURE 8.15: Plots of PTTL intensity against illumination time following pre-heating to 140 °C fitted with equations (8.12), (8.13), and (8.14). The plots are for peak (a) P1 for the sample annealed for 10 minutes (b) P1 for the sample annealed for 1 hour (c) P2 for the sample annealed for 1 hour.

Figure 8.16 shows the best fits for peaks P1, P2, and P3 for preheating to 250 °C for the samples annealed for 10 minutes and 1 hour. The best fit of equation (8.20) for peak P1 for a system of one acceptor and two donors for the sample annealed for 10 minutes is shown in Figure 8.16(a). From the fit, the stimulation probability s_1 from trap I greatly exceeds those from traps IV and DT. Thus, equation (8.20) reduces to a sum of two simple exponentials. The fit for peak P1 for the sample annealed for 1 hour is shown in Figure 8.16(b). The photoionisation cross-section was evaluated as 1.5×10^{-18} cm^2. Figures 8.16(c) and (d) show the best fits of equation (8.19) for peak P2 for the samples annealed for 10 minutes and 1 hour. The photoionisation cross-sections were calculated as $\sigma_{10\ \mathrm{min}} = 2.9 \times 10^{-18}$ cm^2 and $\sigma_{1\ \mathrm{hr}} = 1.6 \times 10^{-18}$ cm^2. For peak P3, the best fits of equation (8.18) for a case of one acceptor and two donors are shown in Figure 8.16(e) and (f) for both samples. The photoionisation cross-sections calculated from the fits are 2.8×10^{-18} and 1.9×10^{-18} cm^2 for the samples annealed for 10 minutes and 1 hour respectively.

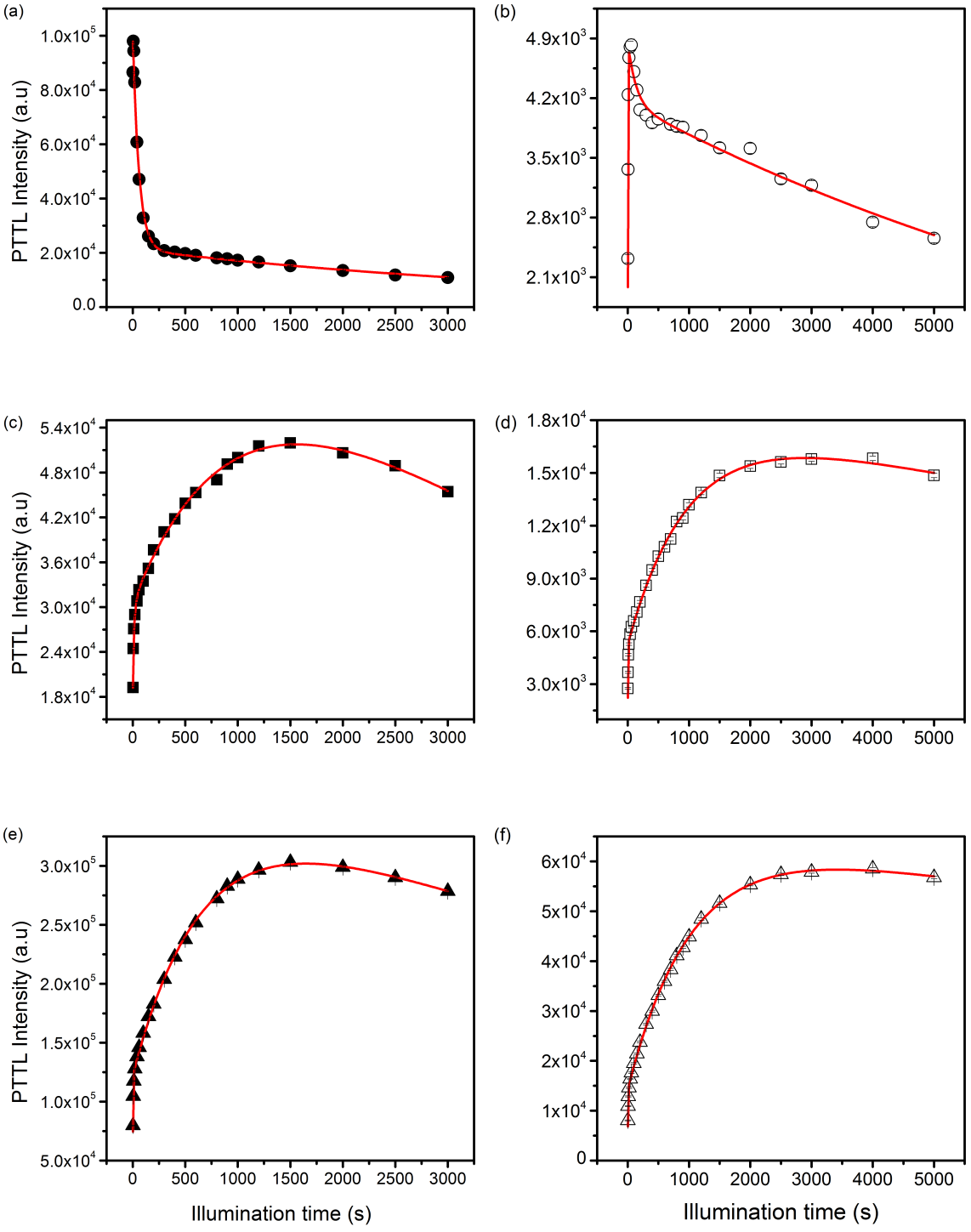

FIGURE 8.16: Plots of PTTL intensity against illumination time fitted with various equations as explained in the text for peak (a) P1 for the sample annealed for 10 minutes (b) P1 for the sample annealed for 1 hour (c) P2 for the sample annealed for 10 minutes (d) P2 for the sample annealed for 1 hour (e) P3 for the sample annealed for 10 minutes and (f) P3 for the sample annealed for 1 hour after preheating to 250 °C.

Finally, for results corresponding to preheating to 500 °C, the best fits of equation (8.24) for peak P1 and equation (8.23) for peak P3 are shown in Figure 8.17. This is for a system of one acceptor and one donor. The photoionisation cross-sections for these fits were determined as 1.1×10^{-18} cm^2 for peak P1 and 7.6×10^{-21} cm^2 for peak P3.

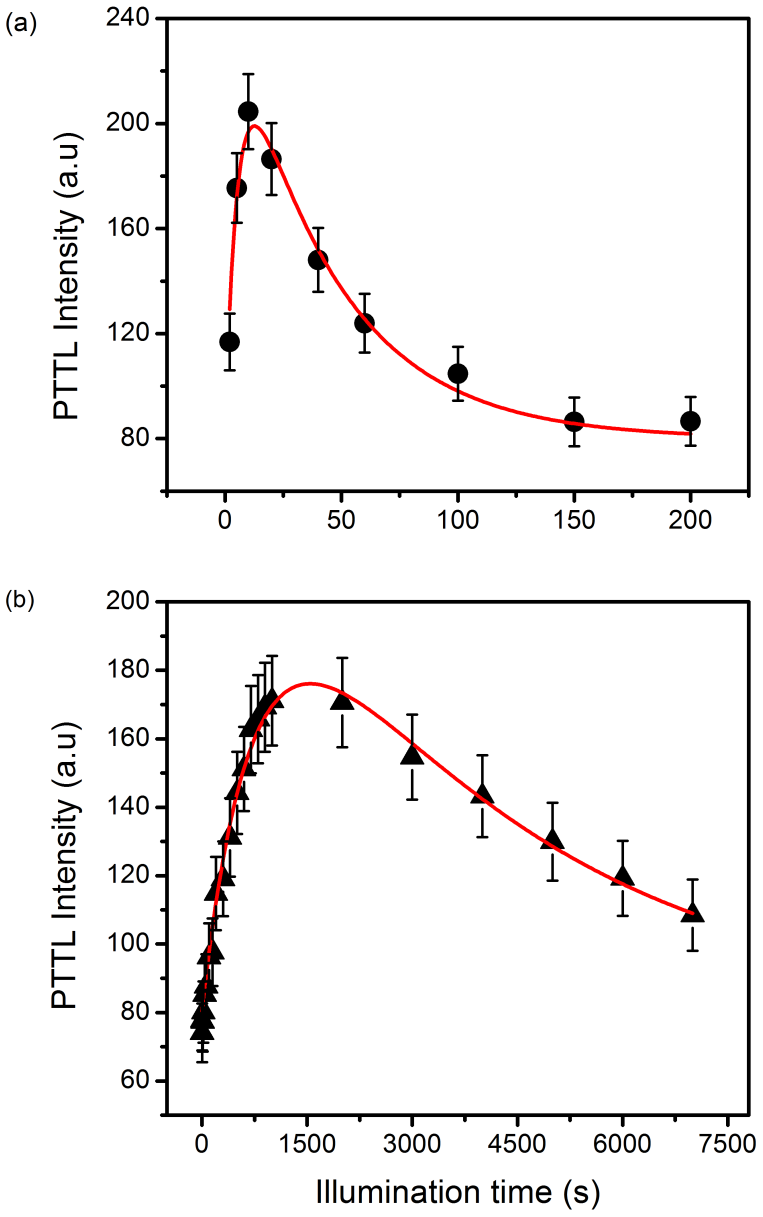

FIGURE 8.17: PTTL intensity versus illumination time for peak (a) P1 (b) P3 after preheating to 500 °C for the sample annealed for 10 minutes. The plots (a) and (b) are fitted with equations (8.23) and (8.24) respectively.

The results presented thus far show that the various models, formulated on the basis of experimental results, accurately describe the time-dependent profiles of PTTL intensity. The photoionisation cross-sections for the acceptor traps at each preheating temperature compare favourably and are of the order of 10^{-18} cm^2. The photoionisation cross-sections serve as a means to describe the extent to which an electron trap can be optically stimulated. The value obtained for each acceptor was noted to decrease with preheating temperatures. In general, the photoionisation cross-sections for the acceptor traps are of the order of 10^{-18} cm^2. The σ values reported in this work are in satisfactory agreement with values reported in the literature for different quartz samples e.g. $\sim 10^{-20}-\sim 10^{17}$ cm^2 (Larsen *et al.*, 2000), $\sim 10^{-21}-\sim 10^{17}$ cm^2 (Singarayer and Bailey, 2003), and $\sim 10^{-22}-\sim 10^{15}$ cm^2 (Kiyak *et al.*, 2007). Table 8.1 presents the photoionisation cross-sections obtained for each acceptor corresponding to the various preheating temperatures.

TABLE 8.1: The photoionisation cross-sections of the acceptor traps for the samples annealed for 10 minutes and 1 hour.

		1000 °C, 10 min	1000 °C, 1 hr
PTTL Peak	Preheat Temp (°C)	σ (cm^2)	σ (cm^2)
P1	100	6.4×10^{-18}	6.1×10^{-18}
	140	5.1×10^{-18}	2.1×10^{-18}
	250	-	1.5×10^{-18}
	500	1.1×10^{-18}	-
P2	140	-	15.6×10^{-18}
	250	2.9×10^{-18}	1.6×10^{-18}
P3	250	2.8×10^{-18}	1.9×10^{-18}
	500	7.6×10^{-21}	-

8.1.7 Competition effects in phototransferred thermoluminescence

We showed previously in Figure 8.6 for the sample annealed for 10 minutes, that the electron traps corresponding to peak III act as a donor and as an effective competitor for stimulated charge from the deep trap during preheating to 140 °C.

At other preheating temperatures, the traps at level III act as a pure donor. Hence, we describe its competition effects with respect to the duration of illumination at only preheating to 140 °C. We consider levels III, IV and V for the competition effects. Electron traps corresponding to peaks IV and V act as donors. We recall from Figure 8.13(a) that while peak IV acts as a donor, it showed evidence of competition effects by capturing some of the charges released from the deep traps in the first 200 s.

The transport of charge for traps corresponding to peak III, taking into account the competition effect from IV can be written as

$$\frac{dN_5}{dt} = -s_5 N_5 \tag{8.25}$$

$$\frac{dN_4}{dt} = -s_4 N_4 + \alpha_5 s_5 N_5 \tag{8.26}$$

$$\frac{dN_3}{dt} = -s_3 N_3 + \gamma_4 s_4 N_4 + \gamma_5 s_5 N_5 \tag{8.27}$$

Equation (8.25) describes the optical removal of electrons from the deep trap. Equation (8.26) describes the loss of charge at level IV during illumination and competitive capture of some electrons from the deep trap. The first term in equation (8.27) accounts for the loss of electrons from the acceptor (level III) during illumination. The second and third terms reflect the fact that a portion of electrons released from levels IV and V are captured at level III.
The solution of the coupled equations (8.25) - (8.27), giving the time dependence of the intensity of peak III owing to optical illumination is

$$N_3 = C_1(e^{-s_5 t} - e^{-s_3 t}) - C_2(e^{-s_4 t} - e^{-s_3 t}) + C_3(e^{-s_5 t} - e^{-s_3 t}) \tag{8.28}$$

where $C_1 = \frac{\gamma_4 s_4 \alpha_5 s_5 N_{5i}}{(s_3 - s_5)(s_4 - s_5)}$, $C_2 = \frac{\gamma_4 s_4 \alpha_5 s_5 N_{5i}}{(s_3 - s_4)(s_4 - s_5)}$, $C_3 = \frac{\gamma_5 s_5 N_{5i}}{s_3 - s_5}$.

Figure 8.18 shows the best fit of equation (8.28) for peak III corresponding to preheating to 140 °C showing competition effects. The fit shows that the model correctly describes the experimental data.

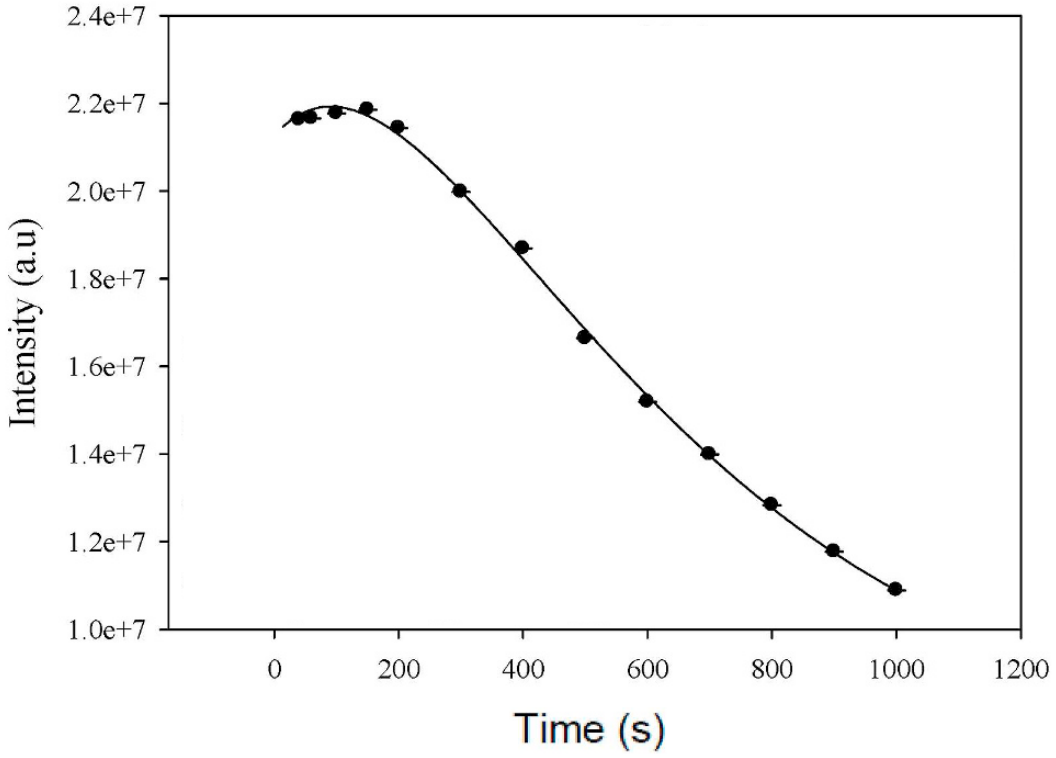

FIGURE 8.18: The time-dependence of PTTL intensity for peak III displaying competition effects when the quartz sample annealed at 1000 °C for 10 minutes is preheated to 140 °C.

8.2 PTTL of quartz annealed at 800 °C for 10 minutes

We report in this section a comparative phototransferred thermoluminescence (PTTL) in natural quartz annealed at 800 °C for 10 minutes illuminated by sets of 470 and 525 nm LEDs with an optical power density of 72 and 36 mWcm^{-2} at sample position. Measurements were done using a RISO TL/OSL Luminescence Reader with a Hoya U-340 detection filter (transmission band 250 - 390 nm). For completeness and to aid discussion, kinetic analysis of the conventional thermoluminescence (TL) main peak and PTTL peak is included.

8.2.1 Features of the TL glow curve

Figure 8.19 shows a glow curve measured at 1 °Cs^{-1} from a sample irradiated to 50 Gy. This is the same glow curve studied for kinetic analysis in Chapter 6. The

glow curve shows five peaks; an intense dominant peak at 73 °C (labelled I), and other peaks at 120 °C, 186 °C, 286 °C, and 334 °C labelled II, III, IV, and V respectively. In comparison, (Chithambo, 2014) reported three peaks at 90, 200 and 350 °C for the same sample measured at 5 °Cs^{-1} following irradiation to 10 Gy. It is known universally that peak positions in quartz do not always occur at fixed temperatures due to different heating rates, nature of the sample, and other experimental conditions. However, the most common peak positions have been cited at 110, 230, 270, 325, and 375 °C (Preusser *et al.*, 2009).

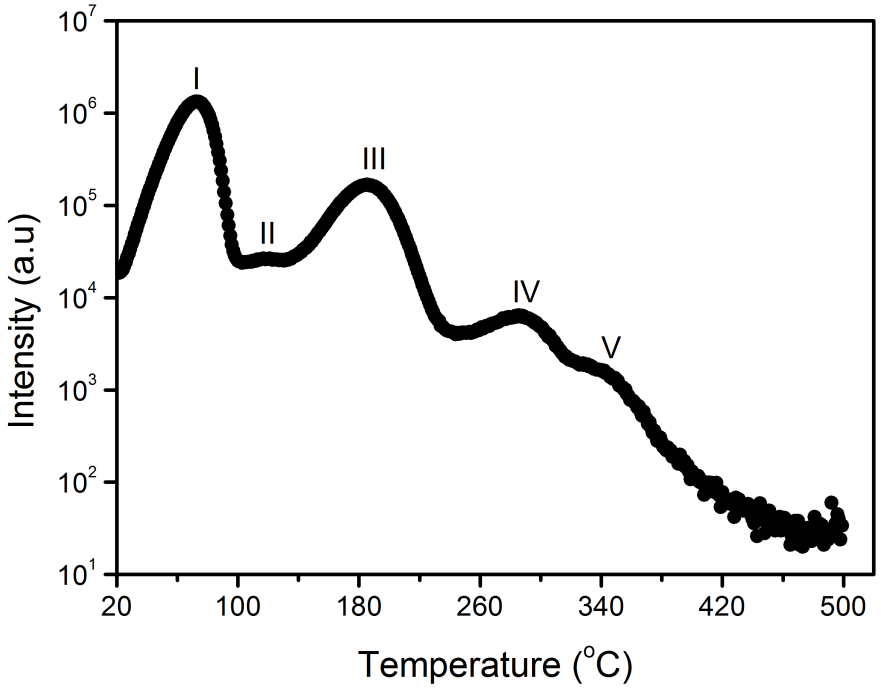

FIGURE 8.19: A TL glow curve measured from natural quartz annealed at 800 °C for 10 minutes, irradiated to 50 Gy and heated at 1 °C s^{-1}.

8.2.2 Identification of electron traps as donors and acceptors by pulse annealing

In the study of PTTL, it is expected that some electron traps get depleted while others get filled after every preheat. The depleted traps are otherwise called donors, whereas the filled traps are called acceptors. To qualitatively determine and identify which of the traps act as acceptors and which as donors, the pulse

annealing experiment (Bøtter-Jensen *et al.*, 2003) was carried out. The method relies on the influence of preheating temperature on PTTL intensity. For this study, the sample irradiated to 50 Gy was preheated to 100 °C beyond the position of peak I at 1 °Cs^{-1} and cooled. PTTL was recorded following illumination for 60 s using green and blue LEDs. The procedure was repeated on the same sample, irradiated each time to 50 Gy and preheated to temperatures between 100 and 380 °C at intervals of 10 °C. The peak intensities were noted as peak heights for both light sources.

Figure 8.20 shows the peak intensities against preheating temperatures for peaks I, III, and V after illumination by blue and green light. The intensity of peak I, an acceptor at 73 °C, decreased systematically with preheating between 100 and 380 °C when illuminated under 470 nm blue light. This decrease in intensity implies a reduction in the concentration of charge from its donors. Thus, electron traps corresponding to peaks II – V act as donors. However, in the case of illumination under 525 nm green light, the intensity of peak I was constant for preheating between 100 and 130 °C. The constant intensity for preheating between 100 and 130 °C implies that the concentration of charge at its donors is minimally affected by preheating. The intensity further increases slowly with preheating up to 260 °C before decreasing to 300 °C. That the intensity increases with preheating from 130 to 260 °C is unusual and could mean that the electron traps corresponding to peak II act as a competitor. Unfortunately, this peak is not visible between 130 and 220 °C and could not be investigated. The intensity of peak II though visible from 220 °C could not be reliably studied under blue and green lights. This is because the peak is embedded between the falling edge of peak I and the rising edge of peak III. The intensity of peak III, at 186 °C is constant between 100 and 150 °C but decreases significantly with further preheating up to 230 °C under blue and green illuminations. For the intensity to remain constant for preheating between 100 and 150 °C indicates that the donor electron traps are slightly affected by the preheating. The intensity then decreased sharply from 160 to 230 °C, indicating that peak III is a PTTL peak within these temperatures. Between 240 and 300 °C, the intensity decreased slowly, indicating a decrease in the concentration of charge at its donors. Peak IV was not visible at all for the pulse annealing experiment. For peak V, which occurred at 320 °C for pulse annealing, the intensity was constant between 100 and 300 °C under blue and green illuminations. The constant intensity of this peak indicates that its electron trap is not affected by preheating and acts as a donor to other electron traps whose peaks occur at lower

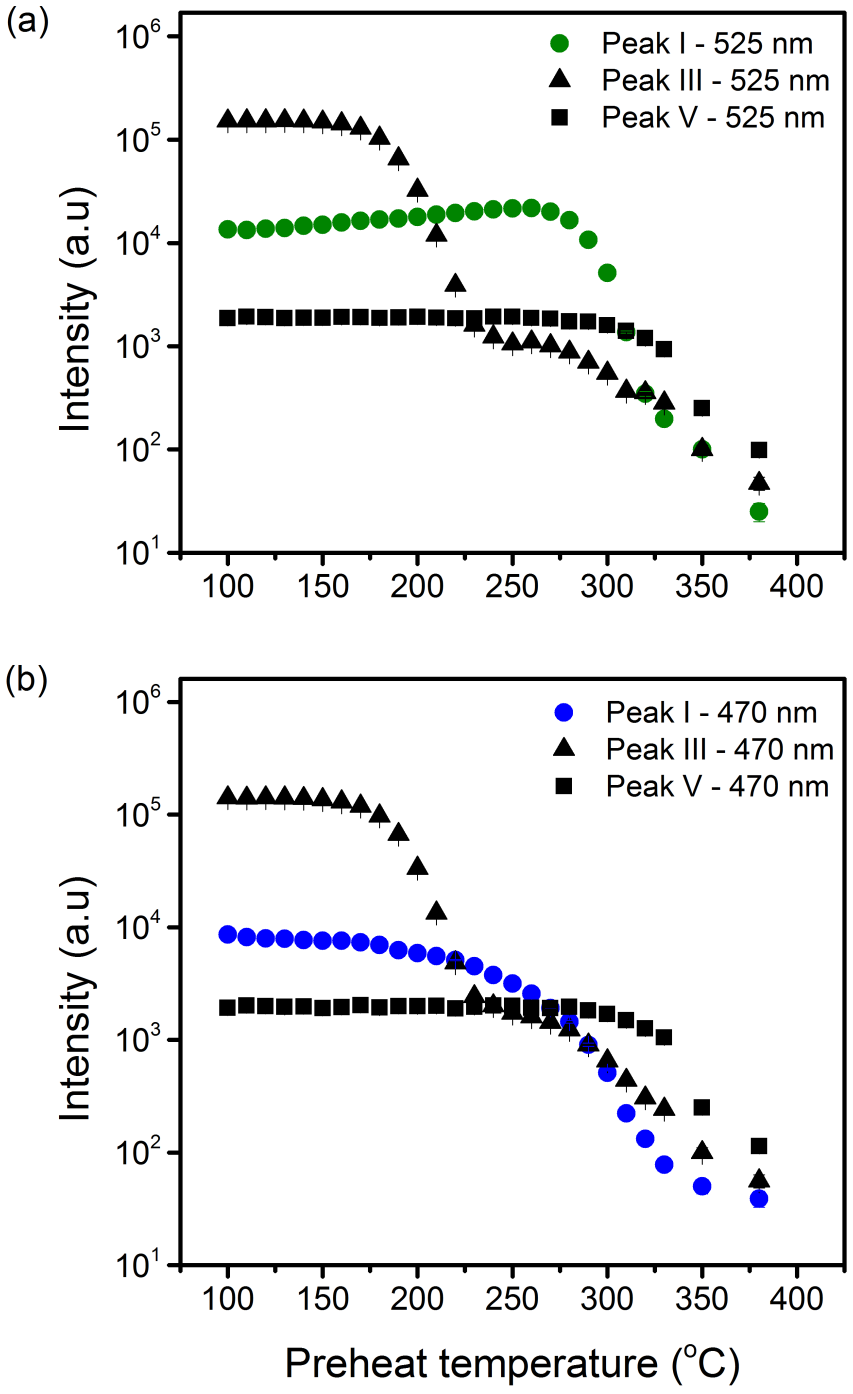

FIGURE 8.20: The influence of preheating temperature on peak intensity in a pulse annealing experiment after illumination by (a) green light and (b) blue light.

temperatures.

8.2.3 PTTL intensity as a function of illumination time

In order to study PTTL as a function of illumination time, the sample irradiated to 50 Gy was preheated to 100, 135, and 240 °C. PTTL was then monitored at different illumination times between 2 and 1000 s. For ease of reference, PTTL peaks reproduced after the removal of peaks I, II, and III are labelled and referred to as P1, P2, and P3, respectively. No PTTL was observed for peaks IV and V at all.

8.2.3.1 PTTL following preheating to 100 °C

Figure 8.21 shows an example of glow curves measured immediately after irradiation, preheating to 100 °C, and illumination under green and blue lights for 20 s. The glow curves show that peak I, originally removed by preheating, is reproduced under phototransfer at 73 °C and is labelled as P1. The dependence of

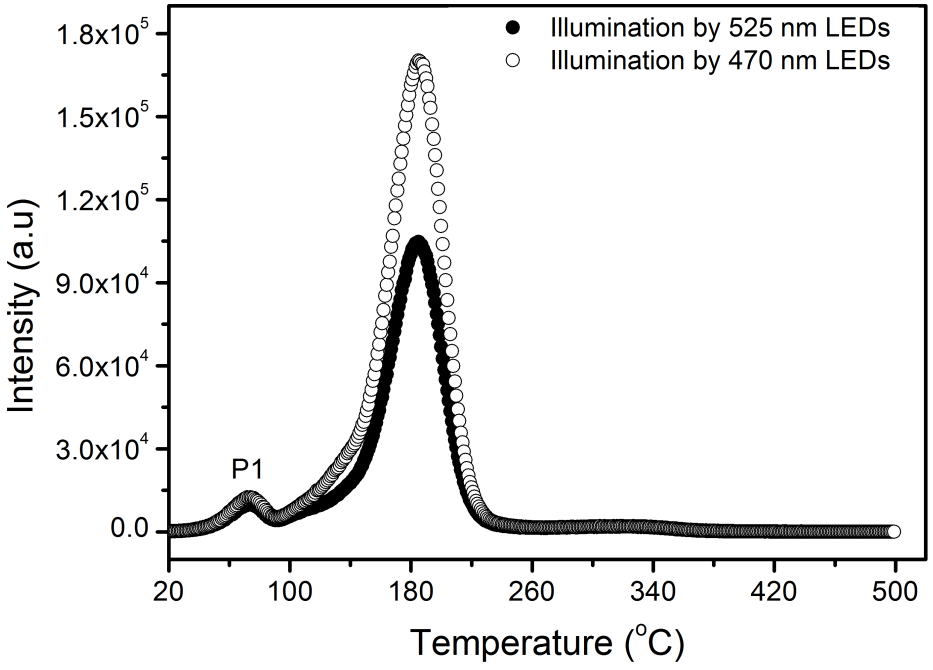

FIGURE 8.21: An example of PTTL glow curves measured at 1 °C s^{-1} following irradiation to 50 Gy, preheating to 100 °C and illumination for 20 s.

its PTTL intensity on illumination time was then studied between 2 and 1000 s under green and blue lights and shown in Figure 8.22. The PTTL intensity from

P1 increases up to a maximum of 40 s and decreases thereafter under green illumination. This is typical of PTTL signals from quartz but exposed to blue light e.g. (Milanovich-Reichhalter and Vana, 1991; Chithambo *et al.*, 2018), α-Al_2O_3:C e.g. (Bulur and Göksu, 1999; Chithambo *et al.*, 2017a). The increase of intensity at short illumination times implies that the trapping of electrons in the shallow trap exceeds any loss by optical stimulation (Chithambo *et al.*, 2017a). The decrease of the PTTL intensity at long illumination times suggests that loss of electrons from the shallow trap by optical stimulation exceeds any trapping. In comparison with optical stimulation by blue light in Figure 8.22(b), the intensity of P1 decreases significantly with illumination time without any initial increase in a manner similar to a donor. This significant decrease in intensity of P1 with time indicates a dominant loss of electrons during illumination and should not be ascribed the role of a donor.

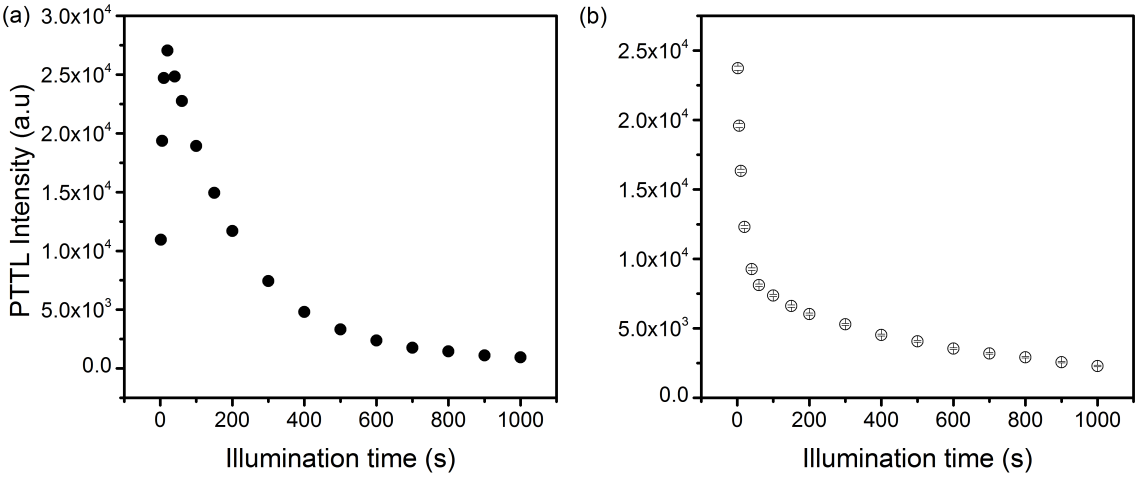

FIGURE 8.22: The dependence of PTTL intensity on the duration of illumination by (a) 525 nm green LEDs (b) 470 nm blue LEDs for P1 following preheating to 100 °C.

8.2.3.2 PTTL following preheating to 135 °C

The PTTL peak P1 at 73 °C, as seen in Figure 8.21 is also observed after preheating to 135 °C to remove peaks I and II and illumination for 20 s under 470 and 525 nm lights. Peak II did not show any PTTL. The time-dependence of the PTTL intensity from P1 is shown in Figure 8.23. The PTTL intensity of P1 also goes through a maximum of 20 s before decreasing when exposed to green light. Its

intensity decreases consistently with illumination time in similar behaviour as described when preheated to 100 °C under blue light.

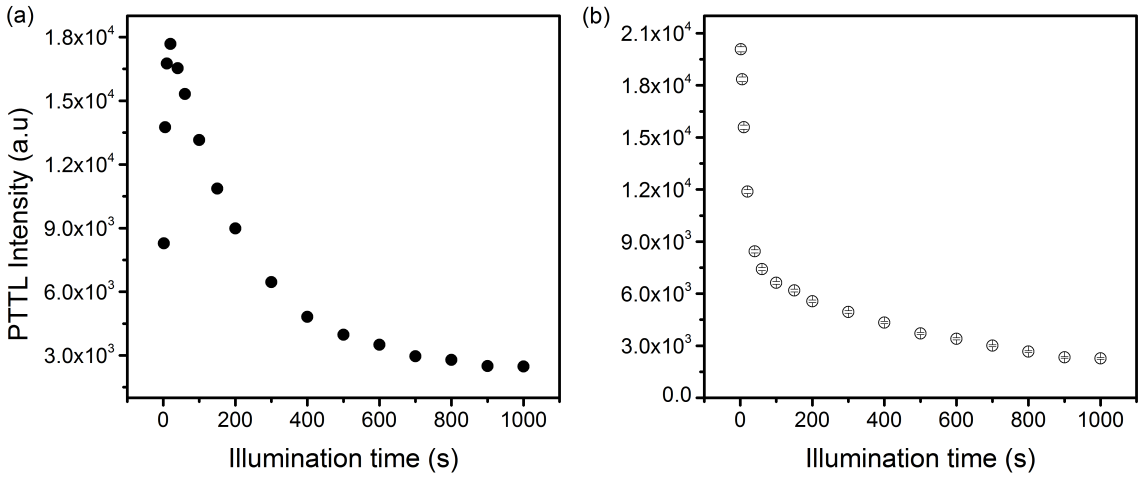

FIGURE 8.23: Variation of PTTL intensity with illumination time for P1 after preheating to 135 °C and exposure to (a) 525 nm green and (b) 470 nm blue lights.

8.2.3.3 PTTL following preheating to 240 °C

Figure 8.24 shows semi-logarithmic plots of glow curves measured after preheating to 240 °C and illumination for 20 s. Peaks I, II, and III are reproduced under phototransfer at 73, 130, and 188 °C respectively and shown as P1, P2, and P3. Of these peaks, peak P2 is poorly defined and of weak intensity. This is consistent with the previous plot (Figure 8.19), which reflects that peak II is embedded between peaks I and III.

Figure 8.25 shows the influence of illumination times on PTTL intensity for peaks P1 and P3. Figure 8.25(a) shows the behaviour for peak P1 where the intensity goes through a peak under green light and decreases without an initial rise when exposed to blue light (Figure 8.25(b)). The time-dependence of the PTTL from peak P3 is shown in Figure 8.25(c). The PTTL intensity of peak P3 increases significantly towards a steady state saturation under green light stimulation. A similar time response curve of peak P3 in this study has been reported in quartz e.g. (Alexander *et al.*, 1997) and α-Al_2O_3:C e.g. (Chithambo *et al.*, 2017a) exposed to blue light. Whereas for blue light stimulation (Figure 8.25(d)), peak P3 increases slowly in a projectile manner before decreasing. The time-dependence of PTTL intensity from peak II could not be monitored because of its weakness.

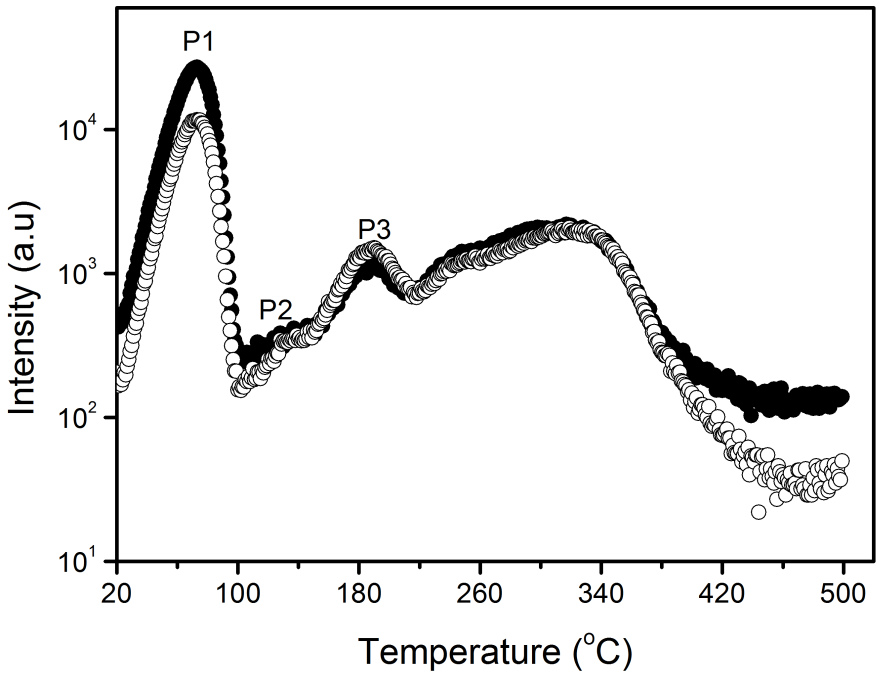

FIGURE 8.24: Examples of glow curves measured at 1 °Cs^{-1} after a dose of 50 Gy, preheating to 240 °C and illumination for 20 s. The solid and open symbols represent data for illumination under 525 and 470 nm LEDs.

8.2.3.4 PTTL following preheating to 450 or 500 °C

Preheating the irradiated sample to temperatures between 400 and 500 °C to remove all peaks in the glow curve produced no PTTL peak after illumination. However, when the sample was irradiated to 300 Gy, preheated to 450 °C and illuminated for 500 s under blue light, a weak PTTL peak P3 was observed. This PTTL peak is shown in Figure 8.26. The appearance of P3 at this preheating temperature indicates the presence of deep electron trap. The time-dependence of the PTTL intensity from P3 could not be studied since this peak is poorly defined, and the peak position difficult to be determined at longer illumination time.

8.2.4 Kinetic analysis of conventional TL and PTTL peak

The preceding section has shown that the position of peak I of the conventional TL remained unchanged when reproduced under phototransfer by blue and green illuminations following preheating to 100, 135, and 240 °C. It is thus expected that the kinetic parameters of PTTL peak P1 should be similar to those of the

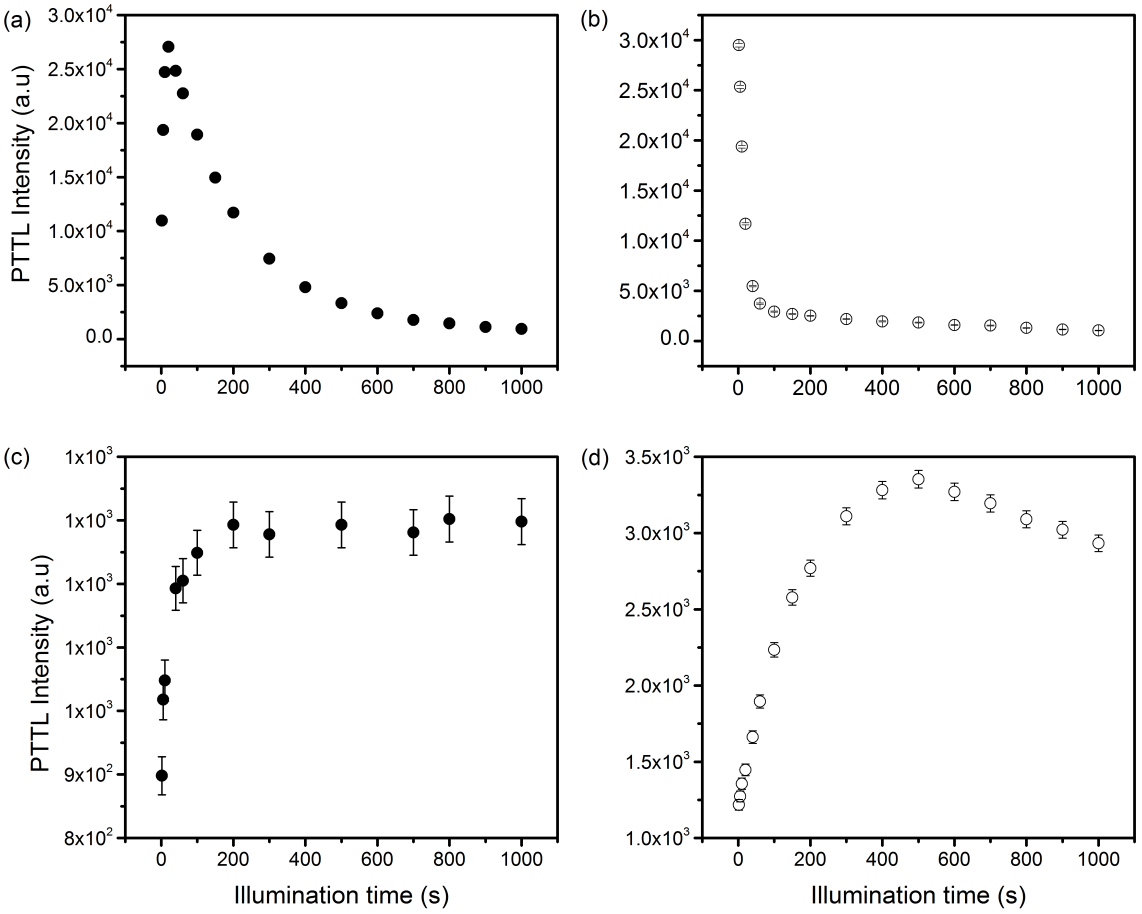

FIGURE 8.25: The dependence of PTTL intensity on the duration of illumination by (a) 525 nm green LEDs b) 470 nm blue LEDs for P1 following preheating to 240 °C.

conventional TL peak I. In order to verify the similarity of the kinetic parameters, we analyse these peaks (conventional peak I, P1 exposed to blue and green lights for 60 s after preheating to 100, 135, and 240 °C) using the initial rise, whole glow peak, curve fitting and peak shape methods (Pagonis *et al.*, 2006). Multiple methods are used to ascertain for consistency in results and not to determine which of the methods is best for analysis. In analysing the PTTL peaks using methods of kinetic analysis, the activation energy E, order of kinetics b, and frequency factor s were determined.

8.2.4.1 Initial rise method

Peaks I and P1 were first analysed using the initial rise method, applicable to the rising edge of a glow peak. The activation energy E determined from the slope

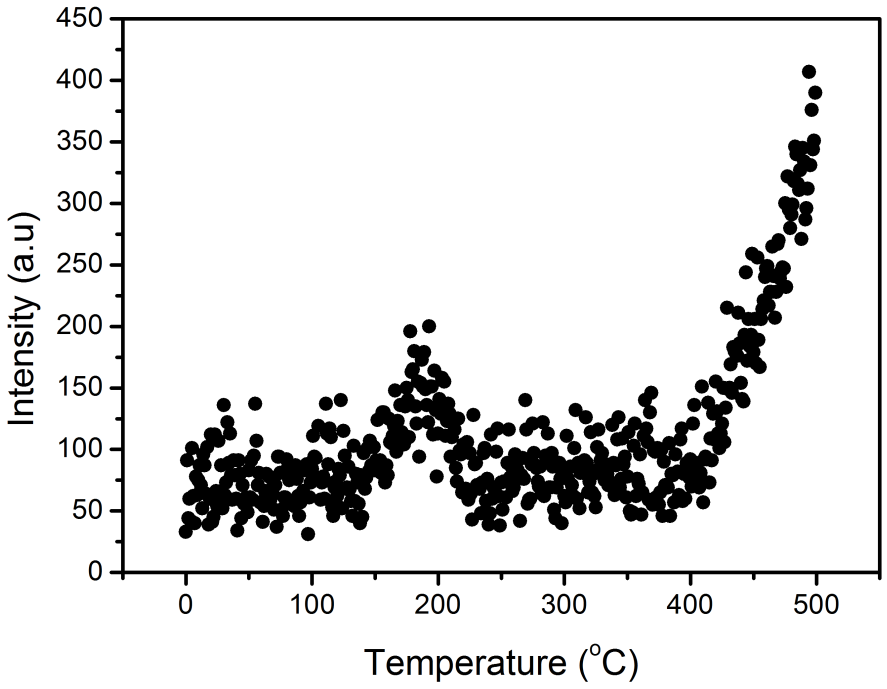

FIGURE 8.26: An example of a glow curve measured at 1 °Cs^{-1} after a dose of 300 Gy, preheating to 450 °C, and illumination for 500 s under blue light.

of a plot of $ln\, I$ versus $1/kT$ for peak I is 0.93 ± 0.01 eV. This is consistent with 0.94 ± 0.01 eV reported by Chithambo (2014) for the same sample irradiated to 10 Gy. For P1 exposed to green light, the value of E was determined as 0.92 ± 0.04, 0.90 ± 0.02, and 0.90 ± 0.01 eV for preheating to 100, 135, and 240 °C respectively. The values of E are consistent and independent of preheating temperature. These values are also consistent with 0.91 ± 0.01 eV reported by Folley and Chithambo (2018) for the same sample also annealed at 800 °C but for 1 hour. Similarly, for P1 exposed to blue light, activation energy was determined as 0.82 ± 0.03, 0.88 ± 0.02, and 0.91 ± 0.05 eV for preheating to 100, 135, and 240 °C respectively. These values are comparable within the margins of error. The E values determined for P1 under blue illumination for preheating to 135 and 240 °C are in satisfactory agreement with those from green illumination.

8.2.4.2 Whole glow peak method

Figure 8.27 shows the plots of $ln(I/n^b)$ against $1/kT$ for the whole glow peak method. The order of kinetics of peak I and P1 were determined to be first order (i.e. $b = 1.0$). The activation energy and effective frequency factor for peak I were

found as 0.90 ± 0.01 eV and $9.45 \times 10^{11} s^{-1}$ respectively. The value of E for peak I is in good agreement with 0.91 ± 0.04, 0.93 ± 0.02, and 0.94 ± 0.01 eV for preheating to 100, 135, and 240 °C respectively for P1 exposed to green light. The frequency factors were determined as $s_{100°C} = 1.65 \times 10^{12} s^{-1}$, $s_{135°C} = 2.90 \times 10^{12} s^{-1}$, and $s_{240°C} = 3.81 \times 10^{12} s^{-1}$. For P1 exposed to blue light, activation energy was evaluated as 0.85 ± 0.01, 0.88 ± 0.01, and 0.92 ± 0.01 eV for preheating to 100, 135, and 240 °C respectively. The frequency factors were also evaluated as $s_{100°C} = 4.98 \times 10^{11} s^{-1}$, $s_{135°C} = 5.00 \times 10^{11} s^{-1}$, and $s_{240°C} = 2.45 \times 10^{12} s^{-1}$. The E values for peak I and P1 in this method are also consistent with those from the initial rise method.

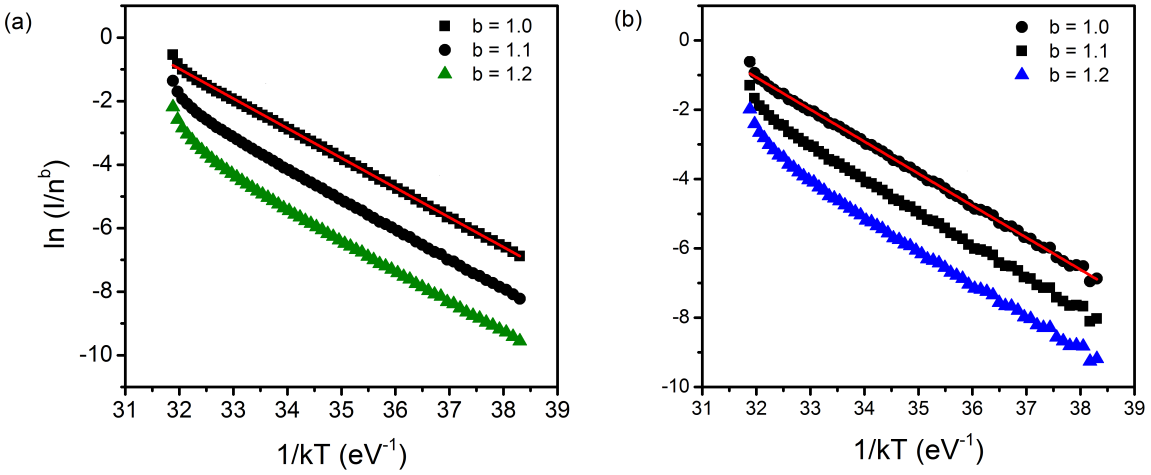

FIGURE 8.27: The whole glow peak method applied to P1 after preheating to 240 °C and exposure to (a) 525 nm green and (b) 470 nm blue lights.

8.2.4.3 Curve fitting method

Peaks I and P1 were also analysed by curve fitting using Kitis (2001)' general order equation (2.26).

Figure 8.28 shows the fits for peak I (square) and P1 (circles) from which $E = 0.95 \pm 0.01$ eV, $b = 1.038 \pm 0.003$ and $s = 6.34 \times 10^{12}$ s^{-1} for peak I. For P1 (solid circles) exposed to green light, the activation energy was found as 1.01 ± 0.01, 0.98 ± 0.01, and 0.95 ± 0.01 eV for preheating to 100, 135, and 240 °C respectively. The frequency factors were determined as 5.05×10^{13}, 1.27×10^{13}, and 6.34×10^{12} s^{-1} corresponding to 100, 135, and 240 °C respectively. The activation energy for P1 (open circles) exposed to blue light following preheating to 100, 135, and 240 °C were found as 0.97 ± 0.02, 0.98 ± 0.01, and 0.94 ± 0.01 eV respectively. These

values of E compare favourably with the values from peak I and P1 illuminated by blue LEDs. The frequency factors were evaluated as 1.15×10^{13}, 1.79×10^{13}, and $4.49 \times 10^{1}2$ s^{-1} for preheating to 100, 135, and 240 °C respectively.

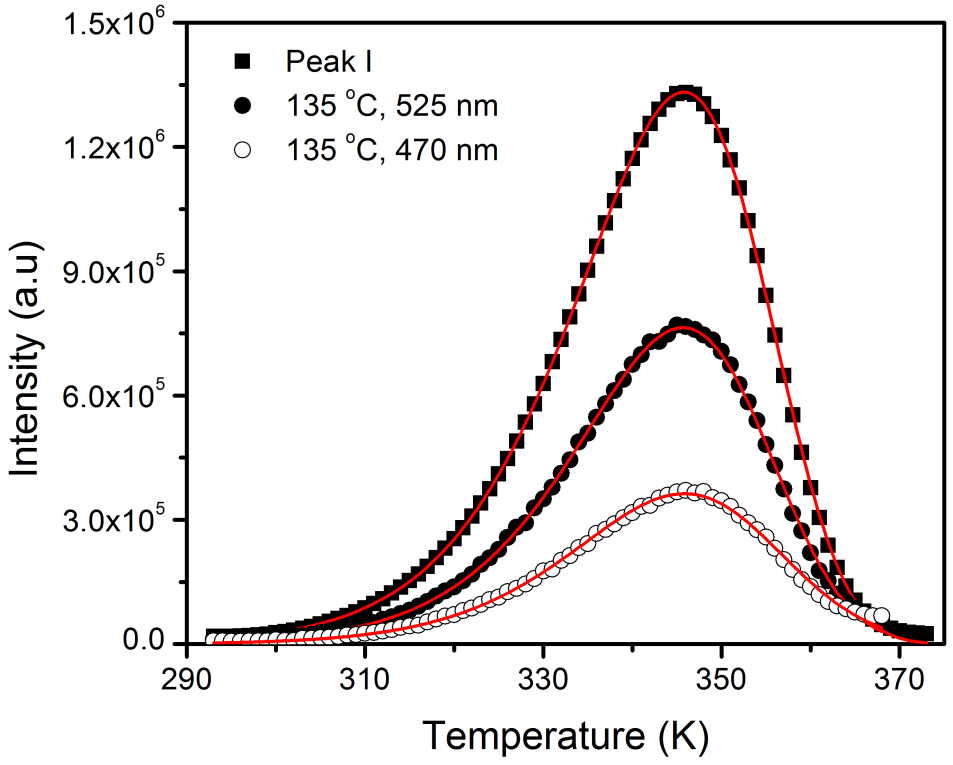

FIGURE 8.28: Results of curve fitting for conventional TL peak I (squares), P1 exposed to 525 nm light (solid circles) and P1 exposed to 470 nm (open circles) after preheating to 135 °C. The intensities of P1 have been scaled by x50 to aid visibility. The solid lines passing through the data points are the best fits of Eq. (2.26).

8.2.4.4 Peak shape method

The order of kinetics of the peaks was determined to be first order in the peak shape method. The values of the activation energy for peak I were calculated as $E_\tau = 0.94 \pm 0.05$ eV, $E_\delta = 0.92 \pm 0.04$ eV, $E_\omega = 0.94 \pm 0.05$ eV. Activation energy for P1 exposed to blue and green lights were also calculated for preheating to 100, 135, and 240 °C. The values of E corresponding to 100 °C for both light stimulations were calculated as $E_\tau = 1.02 \pm 0.04$ eV, $E_\delta = 1.01 \pm 0.04$ eV, and $E_\omega = 1.02 \pm 0.04$ eV. For preheating to 135 °C under green light, the E values were

calculated as $E_\tau = 0.94 \pm 0.05$ eV, $E_\delta = 0.92 \pm 0.04$ eV, and $E_\omega = 0.9 \pm 0.05$ eV. These values are equivalent to the values of E calculated for preheating to 240 °C under green and blue lights. In comparison with the calculated E corresponding to 135 °C under blue light, $E_\tau = 0.90 \pm 0.04$ eV, $E_\delta = 0.90 \pm 0.04$ eV, $E_\omega = 0.91 \pm 0.04$ eV. In general, for this method, it is shown that the activation energies for peak I is equivalent to those from P1 corresponding to 240 °C under green and blue light stimulations. Table 8.2 shows a summary of results for the kinetic analysis conducted for peak I and P1 illuminated by green and blue LEDs. The results of the activation energy from the conventional TL are consistent with the values of E for P1 for both illuminations when preheated to 135 and 240 °C.

TABLE 8.2: Kinetic parameters of conventional TL peak I and PTTL peak P1 induced by 525 and 470 nm lights corresponding to 100, 135, and 240 °C preheats. The acronyms IR, WGP, CF, and PS refers to the initial rise, whole glow peak, curve fitting, and peak shape methods respectively. The indices a, b, and c corresponding to the peak shape method represent E_τ, E_δ, and E_ω respectively.

Method	Preheat (°C)	P1 – 525 nm green light		P1 – 470 nm blue light		Peak I - Conventional TL		Ref
		E (eV)	s (s^{-1})	E (eV)	s (s^{-1})	E (eV)	s (s^{-1})	
IR	100	0.92 ± 0.04	-	0.82 ± 0.03	-	0.93 ± 0.01	-	Sect. 6.1
	135	0.90 ± 0.02	-	0.88 ± 0.02	-			
	240	0.90 ± 0.01	-	0.91 ± 0.05	-			
WGP	100	0.91 ± 0.01	1.7×10^{12}	0.85 ± 0.01	5.0×10^{11}	0.90 ± 0.01	9.5×10^{11}	Sect. 6.2
	135	0.93 ± 0.01	2.9×10^{12}	0.88 ± 0.01	5.0×10^{11}			
	240	0.94 ± 0.01	3.8×10^{12}	0.92 ± 0.01	2.5×10^{12}			
CF	100	1.01 ± 0.01	5.1×10^{13}	0.97 ± 0.02	1.2×10^{13}			Sect. 6.3
	135	0.98 ± 0.01	1.3×10^{13}	0.98 ± 0.01	1.8×10^{13}			
	240	0.95 ± 0.01	6.3×10^{12}	0.94 ± 0.01	4.5×10^{12}	0.95 ± 0.01	6.3 ± 10^{12}	
PS	100	1.02 ± 0.04^a	-	1.02 ± 0.04^a	-			
		1.01 ± 0.04^b	-	1.01 ± 0.04^b	-			
		1.02 ± 0.04^c	-	1.02 ± 0.04^c	-			
	135	0.94 ± 0.05^a	-	0.90 ± 0.04^a	-			
		0.92 ± 0.04^b	-	0.90 ± 0.04^b	-			
		0.94 ± 0.05^c	-	0.91 ± 0.04^c	-			
	240	0.94 ± 0.05^a	-	0.94 ± 0.05^a	-	0.94 ± 0.05^a		
		0.92 ± 0.04^b	-	0.92 ± 0.04^b	-	0.92 ± 0.04^b		
		0.94 ± 0.05^c	-	0.94 ± 0.05^c	-	0.94 ± 0.05^c		

8.2.5 Summary

A comparative analysis of phototransferred thermoluminescence in natural quartz induced by 470 nm blue light and 525 nm green light has been investigated. The sample used for this study is annealed at 800 °C for 10 minutes. The glow curve of the sample irradiated to 50 Gy shows five peaks at 73, 120 °C, 186 °C, 286 °C, and 334 °C labelled I through V. PTTL was observed for peaks I – III (referred to as P1 – P3) corresponding to different preheating temperatures. No PTTL was observed for peaks IV and V at all. Electron traps corresponding to P1 act as acceptors at all preheating between 100 and 240 °C for both light stimulations. The PTTL – time response curve for P1 decays faster when illuminated under blue light whereas for the green light, P1 goes through a peak before the onset of a decrease in intensity. Kinetic analysis of peak P1 and TL peak I reveals that the peaks follow first-order kinetics and have consistent activation energy. The photoionisation cross-sections for P1 at 525 nm was observed to be equal in the order of 10^{-18} cm^2 for all preheating temperatures considered.

8.2.6 PTTL study of quartz annealed at 800 °C for 10 minutes using a BG-39 filter

The quartz sample described above was also studied for PTTL using a Schott BG-39 detection filter (transmission band 320 - 680 nm) under green light optical stimulation. Since BG-39 filter is a blue filter, it cannot be used in combination with blue LEDs for measurements. The aim of using a BG-39 filter is to monitor the behaviour of the phototransferred peaks with duration of illumination, and to examine if the results differ by a change of filter.

Figure 8.29 shows a glow curve measured at 1 $°Cs^{-1}$ through a schott BG-39 filter from a sample of natural quartz after a dose of 50 Gy. The glow curve shows five peaks at 78, 130, 212, 324, and 406 °C labelled I through V. The positions of these peaks were determined through thermal cleaning. The peak positions recorded from using a BG-39 filter differ from those recorded through a Hoya U-340 filter. (Preusser *et al.*, 2009) have shown that peak positions in quartz are not always consistent.

In order to measure PTTL, the sample irradiated to 50 Gy was at each turn preheated to 115, 160, and 280 °C to remove peaks I - III. Afterwards, the sample

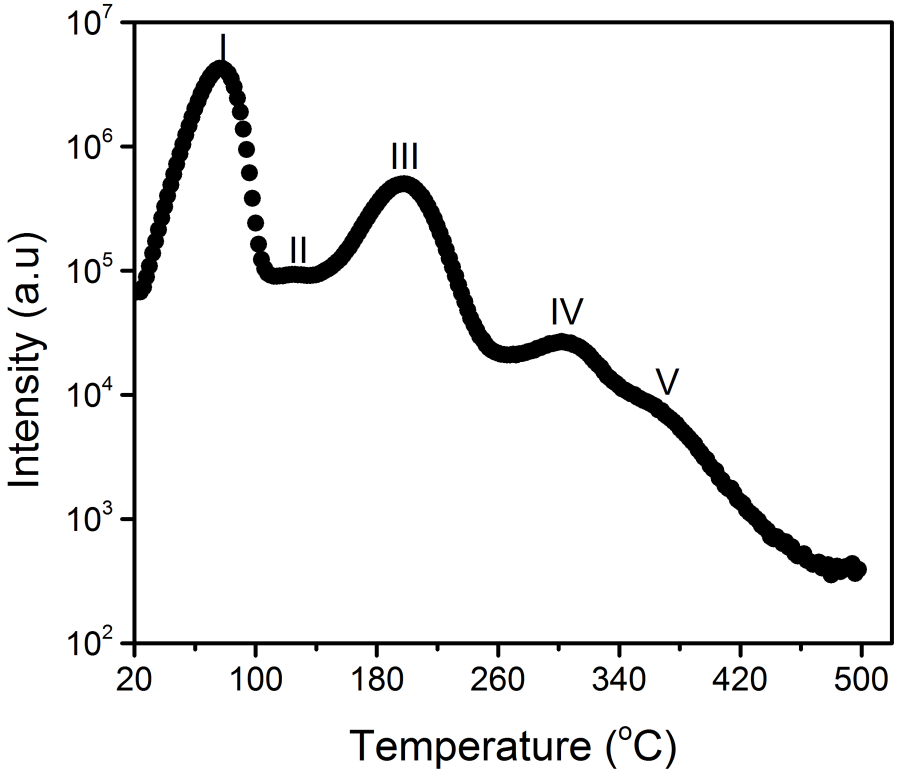

FIGURE 8.29: A TL glow curve measured at 1 °C s^{-1} after irradiation to 50 Gy. The luminescence is detected by a BG-39 filter.

was exposed to 525 nm light for a time t in order to cause the transfer of electrons from the unemptied electron traps to the emptied shallower traps. Finally, the sample was reheated to measure the complete glow curve in order to monitor any phototransferred peaks.

8.2.6.1 Assessment of electron traps as donors and acceptors

To assess which electron traps act as acceptor and which act as donor, the pulse annealing protocol was used. In the method, the sample irradiated to 50 Gy was preheated in turn to temperatures between 100 and 400 °C and illuminated for 60 s each time.

Figure 8.30 shows the dependence of peak intensity on preheating temperature for peaks I, III, and V. The error bars between data points are obtained using the square root rule for counting experiments. Peak I decreases slightly in intensity between 100 and 120 °C. The intensity of peak I was constant between 120 and 160 °C. This decrease in intensity implies that the effect of preheating on the donor

electron traps is negligible. The intensity of peak I further increases gradually when the preheating temperature is increased from 170 to 280 °C. This could mean that the electron trap corresponding to peak II acts as a competitor for stimulated charge. The intensity further decreases consistently all the way to 400 °C. Peak II is ill-defined and could not be monitored under phototransfer. For Peak III, the intensity decreases in three regions. In the first, the intensity of peak III decreases moderately with preheating from 100 to 200 °C. Between 200 and 260 °C, the intensity decreased sharply as a PTTL peak. The intensity then decreased progressively to 400 °C as a donor. Peak IV was not visible at all for the pulse annealing. The intensity of Peak V was independent of preheating between 100 and 330 °C and then decreased monotonically up to 400 °C. This implies that electron traps associated with peak IV act as a donor. The behaviour of these peaks is consistent with the pulse annealing experiment for the sample exposed to green light and measured using U-340 filter.

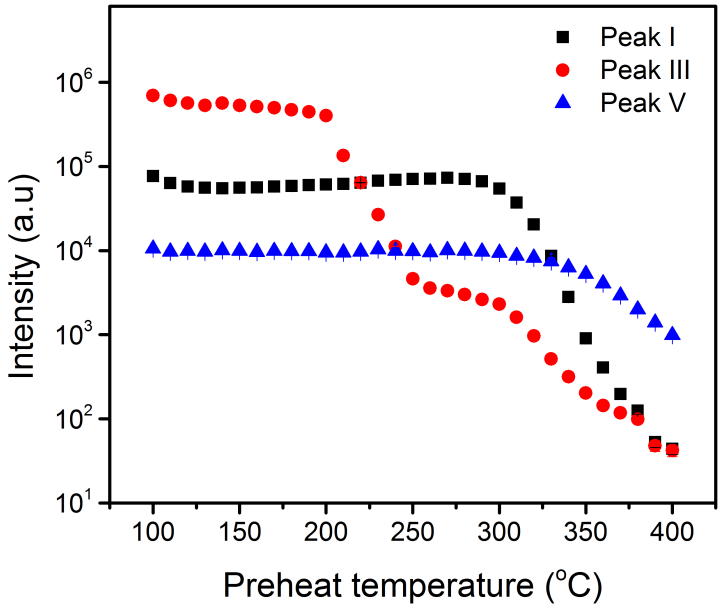

FIGURE 8.30: The dependence of PTTL intensity on preheating temperature for a pulse annealing experiment.

8.2.6.2 Influence of duration of illumination on PTTL intensity

The influence of duration of illumination on PTTL intensity was studied for the PTTL peaks P1 - P3 for preheating to 115, 160 and 280 °C. These are the same

temperatures used for thermal cleaning. For each preheating temperature, the intensity of a PTTL peak that is reproduced is monitored at different illumination times. Figure 8.31 shows the time-dependence plots for peaks P1 - P3 at the various preheating temperatures.

When the quartz sample irradiated to 50 Gy is preheated to 115 °C to remove

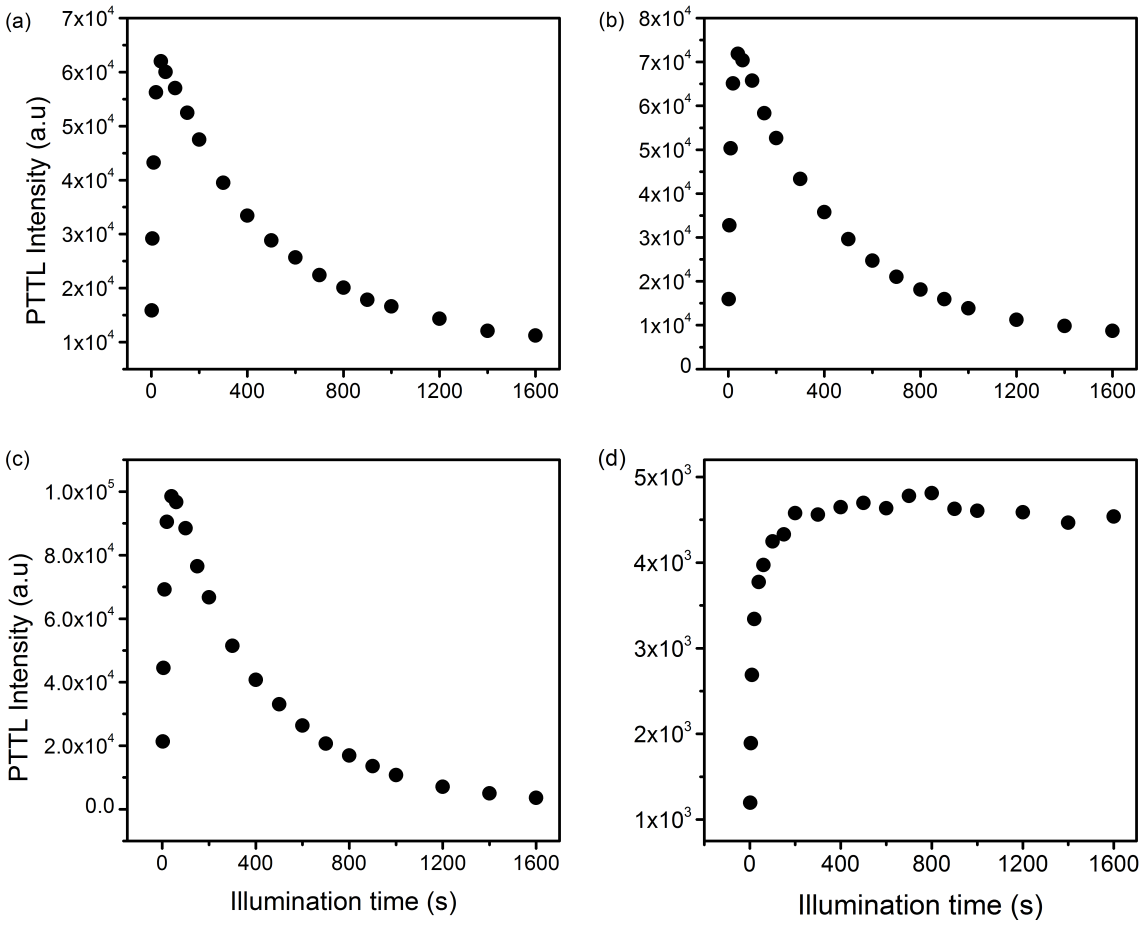

FIGURE 8.31: PTTL intensity as a function of the duration of illumination using a BG-39 filter for peak (a) P1 after preheating to 115 °C (b) P1 following preheating to 160 °C (c) P1 following preheating to 260 °C (d) P3 after preheating to 260 °C.

peak I and PTTL monitored following illumination, peak I is reproduced under phototransfer. This is the same peak that was reproduced when the Hoya U-340 filter was used. The intensity of peak P1 (Figure 8.31(a)) goes through a peak and decreases monotonically thereafter. This is similar to the behaviour of P1 for preheating to 100 °C using a Hoya U-340 filter and illumination by 525 nm light. Preheating the sample to 160 °C to remove peaks I and II reproduces only peak I after illumination. The intensity of P1 (Figure 8.31(b)) increases up to a maximum and decreases thereafter in a similar behaviour as for preheating

to 115 °C. The sample, irradiated to 50 Gy was further preheated to 280 °C to remove peaks I - III. As expected, the removed peaks were reproduced under phototansfer. The intensity of these peaks was monitored as a function of duration of illumination between 2 and 1600 s. The intensity of peak P1 (Figure 8.31(c)) goes through a maximum of 40 s before decreasing. However, peak P2 was ill-defined and its intensity could not be reliably monitored. The intensity of P3 (Figure 8.31(d)) increases progressively towards saturation. The results discussed here are consistent with those reported for measurements using a Hoya U-340 filter. Additionally, the results show that the intensity of the PTTL peaks is not influenced by the change of filter.

8.2.7 Kinetic analysis of the conventional TL peaks

The conventional TL peaks I and III reproduced as PTTL peaks P1 and P3 were analysed by methods of kinetic analysis. The intensities of the individual peaks were detected through a Schott BG-39 filter. Since the various methods of kinetic analysis have been described previously, only results of the analysis will be reported here.

Table 8.3 presents a summary of kinetic parameters for the conventional peaks I and III. The results show that peak I follows first order kinetics whereas peak III is of general order kinetics. The activation energy of peaks I and III are consistent at $\sim 0.80-\sim 0.90$ eV and ~ 1.0 eV respectively. Except for the whole glow peak method, the frequency factors are of the order of $10^{10} - 10^{13}$ s^{-1}.

TABLE 8.3: Kinetic parameters of conventional TL peaks I and III from measurements made through a BG-39 filter. The acronyms IR, WGP, PS, CF, VHR, and IDC refers to the initial rise-, whole glow peak-, peak shape-, curve fitting-, variable heating rate- and isothermal decay methods.

Peak	Method	E (eV)	b	s (s^{-1})
I	IR	0.866 ± 0.004		
	WGP	0.885 ± 0.002	1.1	4.3×10^{11}
	PS	$0.80 \pm 0.08^{\tau}$ $0.73 \pm 0.07^{\delta}$ $0.78 \pm 0.08^{\omega}$	$\mu_g = 0.39 \pm 0.05$	
	VHR	0.79 ± 0.02		1.5×10^{10}
	CF	0.90 ± 0.01	1.08 ± 0.01	8.5×10^{11}
	IDC, 1st order	0.892 ± 0.004		4.1×10^{11}
	IDC, Area	0.79 ± 0.01		
	IDC, CF	0.89 ± 0.01	1.07 ± 0.02	1.05×10^{12}
III	IR	0.95 ± 0.01		
	WGP	0.96 ± 0.01	1.2	7.0×10^{10}
	PS	$1.07 \pm 0.05^{\tau}$ $1.10 \pm 0.05^{\delta}$ $1.09 \pm 0.05^{\omega}$	$\mu_g = 0.48 \pm 0.03$	
	VHR	1.38 ± 0.03		4.1×10^{13}
	CF	1.08 ± 0.01	1.52 ± 0.01	8.9×10^{11}

8.3 PTTL of quartz annealed at 800 °C for 1 hour

We study phototransferred thermoluminescence for quartz annealed at 800 °C for 1 hour. The quartz was irradiated to 50 Gy. PTTL was monitored at preheating to 100, 150, and 240 temperatures °C in order to assess electron traps acting as donors, acceptors and competitors. The time-dependent profiles of the PTTL intensity were modelled using coupled first-order linear differential equations.

Figure 8.32 shows a TL glow curve from annealed quartz measured at 1 °C s^{-1} after an irradiation of 50 Gy. This is the same glow curve reported in Chapter 6. The glow curve shows six peaks at 72, 120, 180, 282, 334, and 364 °C. These

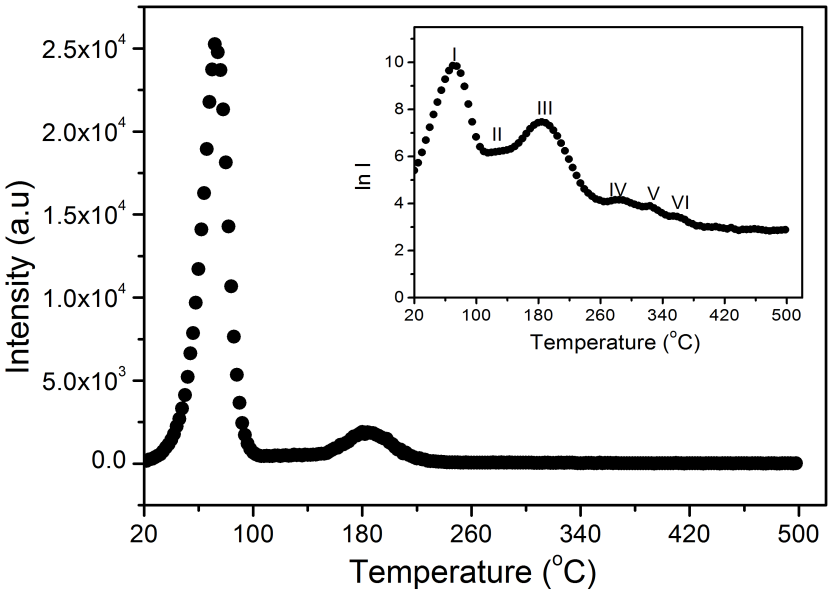

FIGURE 8.32: A thermoluminescence glow curve of the annealed quartz measured at 1 °Cs^{-1} after a dose of 50 Gy. The inset shows the presence of other peaks on a semilogarithmic scale.

are labelled I, II, III, IV, V, and VI as shown. PTTL is studied on the basis of preheating to 100, 150 and 240 °C.

8.3.1 A qualitative description of acceptor, donors, and competitors by pulse annealing

To investigate which electron traps act as acceptors and which act as donors in the PTTL study, the pulse annealing method (Bøtter-Jensen *et al.*, 2003) was used. In the method, a sample irradiated to 50 Gy was preheated to temperatures between 100 and 400 °C at intervals of 10 °C and illuminated for 60 s at every preheat. Figure 8.33 shows the dependence of PTTL intensity on preheating temperature for peaks I, III, and V. The intensity of peak I, an acceptor, increases moderately for preheating between 100 and 150 °C and remains constant with further preheating up to 240 °C. The increase in intensity of peak I suggests that peak II acts as

a competitor since its peak maximum (i.e. of peak II) is within the 100-150 °C range. The constant intensity of peak I between 150 and 240 °C is an indication

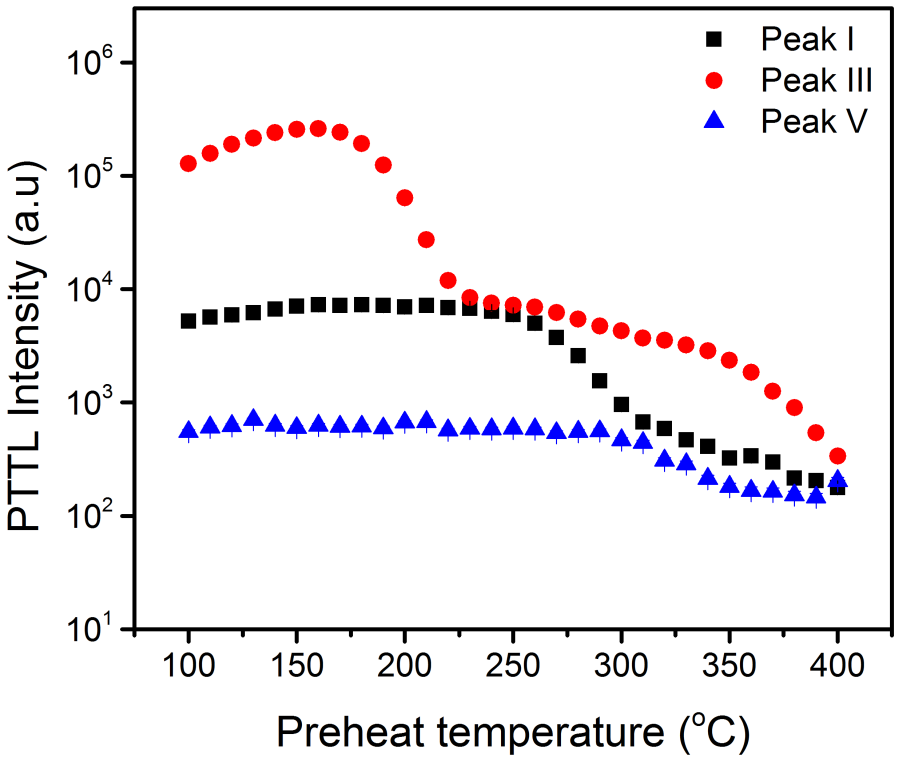

FIGURE 8.33: The dependence of peak intensity on preheating temperature in a pulse annealing experiment.

that the electron traps corresponding to peak I is minimally unaffected by the preheating. The increase of preheating temperature above the peak maximum of a peak is expected to deplete the trap, thereby causing it to act as an acceptor. Since the intensity of peak I remained unchanged with preheating above its peak maximum temperature, there is a likelihood that the electron traps corresponding to peaks II - V act as competitors for charge stimulated from the deep trap. Between 250 and 310 °C, the intensity of peak I decreases monotonically and further decreases gradually up to 400 °C. The decrease of intensity for preheating between 250 and 400 °C is an evidence that the traps corresponding to peak I act as an acceptor. Peak II is embedded between peaks I and III, thus, its intensity could not be reliably monitored. The intensity of peak III increases consistently with preheating between 100 and 150 °C. Since Peak III is not a PTTL peak within these temperatures, we expect that its intensity be unaffected by preheating. The increase in intensity of peak III suggests that the electron traps corresponding

to peak III act as a competitor for preheating between 100 and 150 °C. Between 160 and 240 °C, the intensity of peak III decreases monotonically suggesting its role as an acceptor. Indeed, peak III is a PTTL peak within these temperatures. When the preheating temperature was increased from 250 to 400 °C, the intensity of peak III decreased considerably confirming its role as a donor. Electron traps corresponding to peak III thus act as an acceptor, a competitor and a donor. Peaks IV and VI were not visible at all for the pulse annealing experiment. For peak V, the intensity was independent of preheating between 100 and 300 °C then decreased slowly up to 400 °C. The constant intensity of peak V is expected since the preheating is below its peak maximum temperature. The electron traps corresponding to peak V thus act as a donor to all electron traps occurring at lower temperature.

Pulse annealing is not the only tool used to determine which electron traps act as an acceptor or a donor in PTTL. Further experimental analysis e.g. time-dependence of PTTL intensity is also important.

8.3.2 Time-dependence of PTTL intensity relative to preheating temperatures

To further distinguish an acceptor from a donor, the dependence of PTTL intensity on the duration of illumination was studied for phototransferred peaks. In the measurements, an irradiated sample was preheated at each turn to 100, 150, and 240 °C. PTTL was then monitored on the basis of illumination between 2 and 1000 s. For reference purposes, any peak reproduced as a PTTL peak will be referred to as P1, P2, and P3. No PTTL was observed for peaks IV - VI.

8.3.2.1 PTTL after preheating to 100 °C

A PTTL peak P1 is produced when an irradiated sample is preheated to 100 °C to remove peak I and illuminated for 60 s. The dependence of its PTTL intensity (i.e. peak P1) on the duration of illumination is shown in Figure 8.34. The intensity increases minimally up to a maximum of 10 s as shown in the inset and decreases thereafter. We show in Figure 8.35 the influence of duration of illumination on the intensities of peaks II and III which are not PTTL peaks but act as donors to peak P1. Peak II was monitored at a fixed temperature of 130 °C. The intensities of

peaks II and III did not decrease consistently with illumination time as expected of a donor but increases up to a maximum before decreasing. This is an indication that peaks II and III are competitors for photostimulated charge from the deep trap.

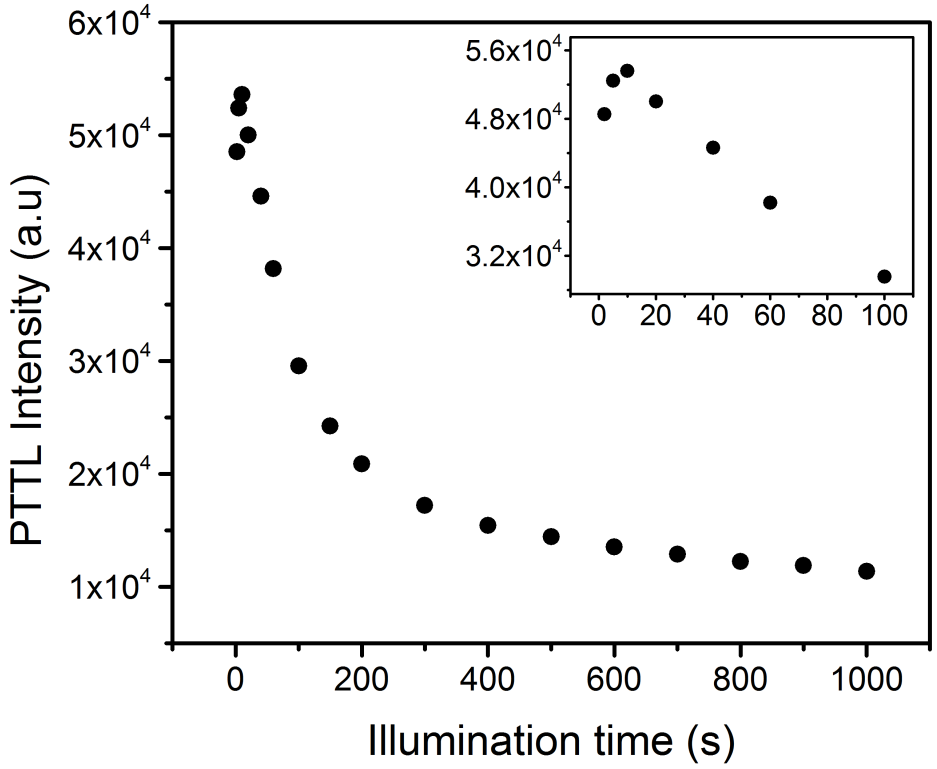

FIGURE 8.34: Dependence of PTTL intensity on duration of illumination for peak P1 after preheating to 100 °C. The inset shows the same plot for illumination between 2 and 100 s in order to show properly the increase in intensity of peak P1.

8.3.2.2 PTTL after preheating to 150 °C

Preheating the sample to 150 °C after irradiation to remove the first two peaks reproduces only peak I after illumination. Figure 8.36 shows the time-dependence of its PTTL intensity. The intensity of P1 increases up to a maximum and decreases afterwards in a similar behaviour as observed for preheating to 100 °C. Figure 8.37 shows the influence of duration on the intensity of peak III, a supposed donor. The intensity goes through a peak as in Figure 8.35(b) confirming its role as a competitor.

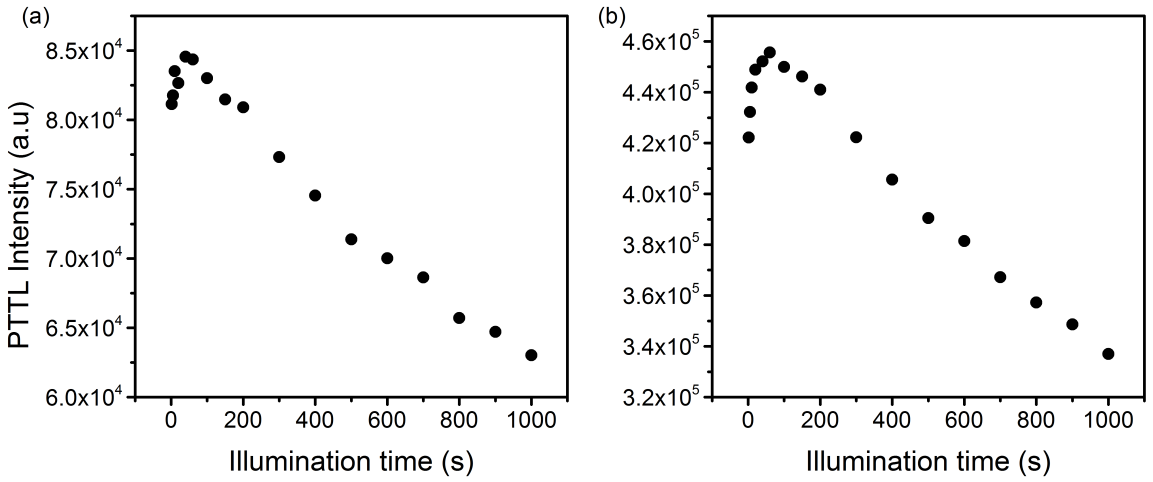

FIGURE 8.35: Change of PTTL intensity with illumination time for (a) peak II (b) peak III after preheating to 100 °C.

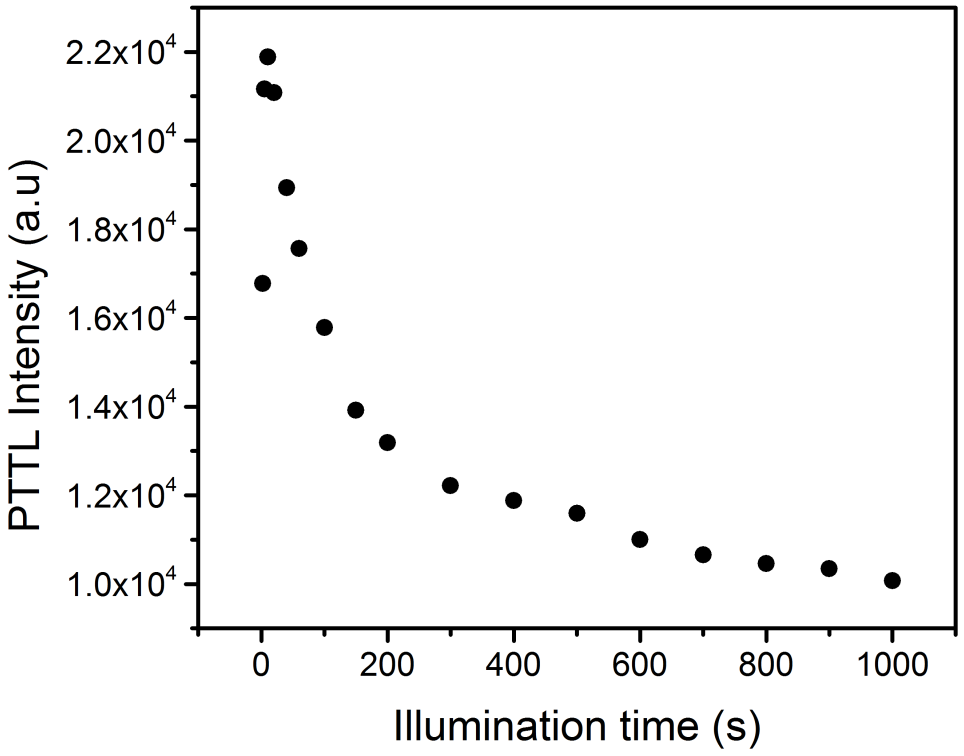

FIGURE 8.36: Time-dependence of PTTL intensity for peak P1 after preheating to 150 °C.

8.3.2.3 PTTL after preheating to 240 °C

When the sample is preheated to 240 °C to remove peaks I - III after irradiation, the peaks are reproduced under phototransfer as P1, P2, and P3. However, peak

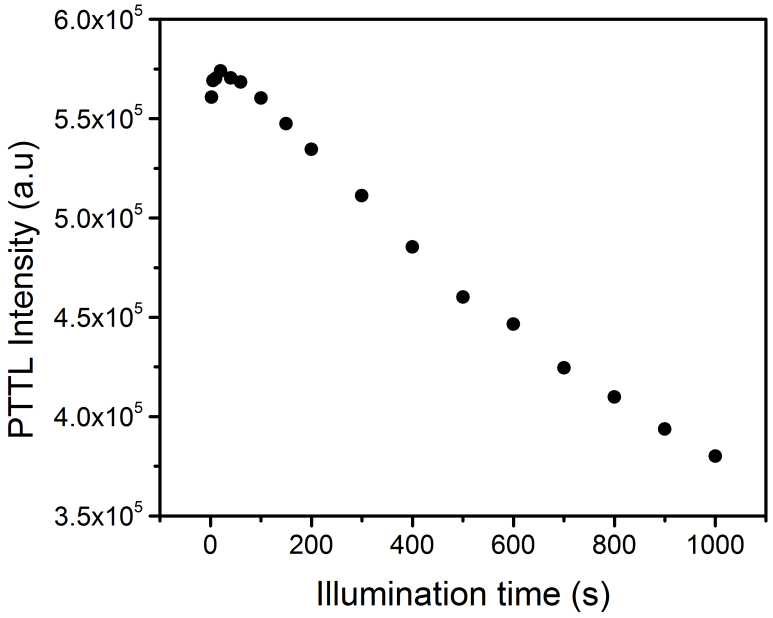

FIGURE 8.37: Influence of duration of illumination on intensity of peak III after preheating to 150 °C.

P2 is ill-defined and embedded between the falling edge of peak P1 and rising edge of P3. Hence, we monitor its PTTL intensity at 130 °C, the temperature of its conventional TL peak. Figure 8.38 shows the influence of duration of illumination on the PTTL intensity of peaks P1, P2, and P3. The intensity of peak P1 did not go through a peak as observed for preheating to 100 and 150 °C but decreases consistently with illumination time. This is an effect of competitive retrapping from electron traps corresponding to peaks II and III. This effect is noticeable in Figure 8.33 for peak I whose intensity was minimally affected by preheating at temperatures lower than 240 °C. For peaks P2 and P3, the intensities increase slowly for the first 100 s, then rapidly when the sample was illuminated for longer periods. The increase in intensity observed for these peaks is a result of their electron traps acting as competitors.

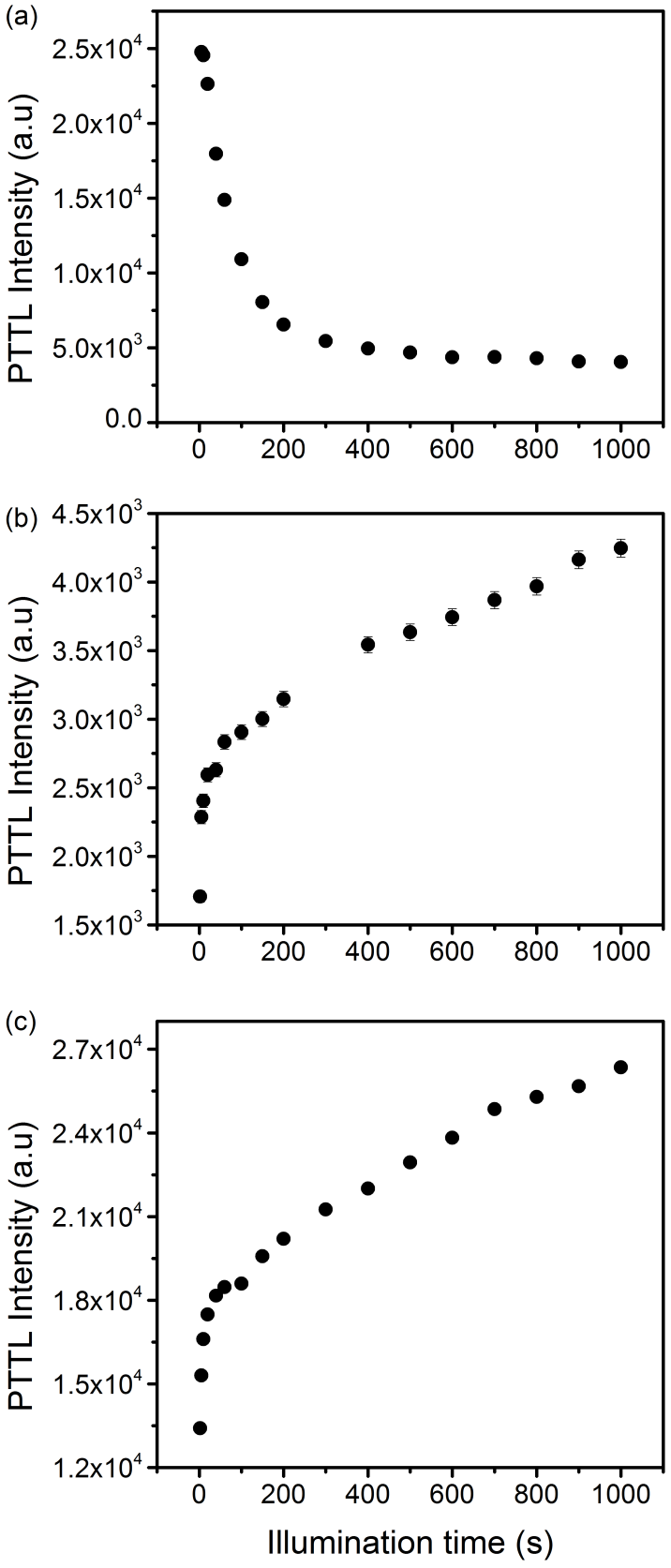

FIGURE 8.38: Change of PTTL intensity with illumination time following pre-heating to 240 °C for peak (a) P1 (b) P2 (c) P3.

8.3.2.4 PTTL after preheating to 450 °C

Preheating the sample to 450 °C to remove peaks I - VI reproduces an ill-defined peak III after illumination for 500 s. The dependence of its PTTL intensity with duration of illumination could not be monitored because of its weak intensity.
The time-dependence of the PTTL intensity presented in this section will be described using some mathematical models.

8.3.3 Mathematical model describing the time-dependence of PTTL

The dependence of PTTL intensity on the duration of illumination discussed in section 8.3.2 will be analysed using the method developed by (Chithambo *et al.*, 2017a). In their model, PTTL was described for any combination of donors and an acceptor using sets of coupled linear differential equations with analytical solutions. The PTTL process involves the stages of irradiation (filling of electron traps), preheating (emptying of the shallow traps), illumination (transfer of charge from deep trap to the empty shallower ones), and heating (monitoring of any PTTL peaks). Hence, the number of electron traps which can act as acceptors or donors change with preheating temperature in the PTTL process. We have shown that not all donors act as such.

In this work, we study a system of five electron traps, one of which is a deep trap. These are shown in Figure 8.39. Electron traps corresponding to peaks P1, P2, P3, and peak V are labelled as I, II, III, and V respectively. Since peaks IV and VI were not visible at all in the PTTL process, we exclude the electron traps corresponding to these peaks in our model. The deep trap corresponding to preheating above 450 °C is labelled as VII. We describe the transport of charge from the donor(s) to an acceptor trap at the illumination stage only using linear differential equations. During illumination, some of the electrons released from the donors are captured at an acceptor whereas others are lost from the electron traps. We assume that electrons are stimulated from the deep or donor traps at an optical stimulation rate $s = \sigma\Phi$, where Φ is the photon flux and σ the photoionisation cross-section which is wavelength dependent (Bøtter-Jensen *et al.*, 2003). The photon flux Φ (given by Φ = power density/energy per photon) equals 1.70×10^{17} photons.cm^{-2} s^{-1} for stimulation wavelength of 470 nm. For each preheating temperature, we set

up coupled first-order linear differential equations, apply their analytical solutions to our experimental data, and determine the photoionisation cross-sections of the acceptor traps. The model is discussed in four categories based on the preheating temperature used.

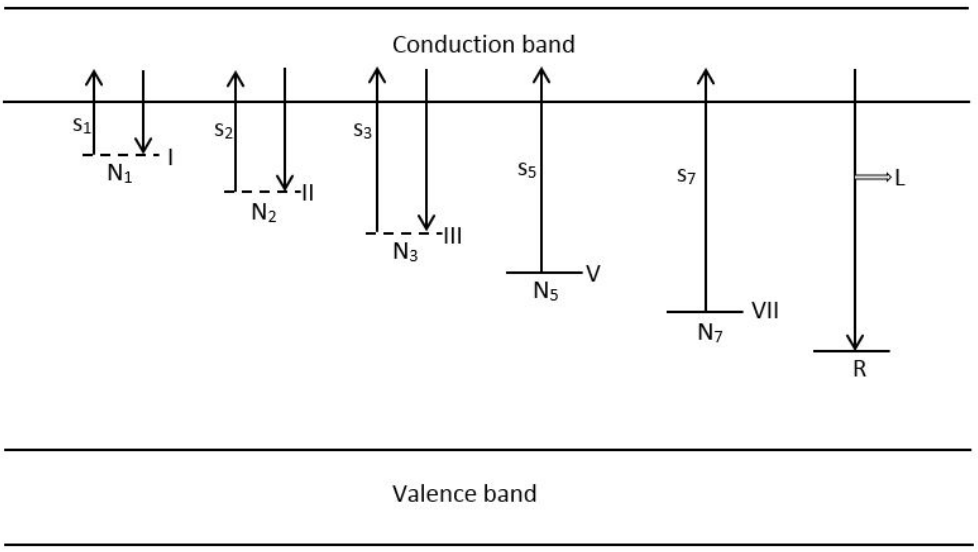

FIGURE 8.39: An energy band diagram used to discuss PTTL in natural quartz as reported. The symbols I, II, and III represent the acceptor traps. The donor traps are represented by the symbols V and VII. The optical stimulation rates are labelled as s_i, and the concentration at each electron trap as N_i (where $i = 1, \cdots, 3, 5, 7$). The recombination centre R producing luminescence L is included for completeness. The transitions at each level are described in the text.

8.3.3.1 PTTL after preheating to 100 °C

When the sample is preheated to 100 °C, peak I is removed but reproduced as P1. Level I acts as an acceptor whereas levels II, III, V and VII act as donors. It has been shown that levels II and III associated with peaks II and III respectively can act as donors. As a matter of interest, we show in Figure 8.40 the time-dependence of the intensity of peak V whose electron trap act as a donor in this study. The intensity of peak V neither increase nor decrease consistently for preheating to 100, 150 and 250 °C. Since the time-dependence of the intensity of peak V has no definite pattern, its contribution to phototransfer is considered to be negligible. Level V is thus regarded as a redundant donor. We therefore have a system of one acceptor and three donors. The transport of electrons from the donor traps to the

acceptor trap for this system can be expressed as

$$\frac{dN_2}{dt} = -s_2 N_2 \tag{8.29}$$

$$\frac{dN_3}{dt} = -s_3 N_3 \tag{8.30}$$

$$\frac{dN_7}{dt} = -s_7 N_7 \tag{8.31}$$

$$\frac{dN_1}{dt} = -s_1 N_1 + a_2 s_2 N_2 + a_3 s_3 N_3 + a_5 s_5 N_5 + a_7 s_7 N_7 \tag{8.32}$$

The rate equations (8.29)-(8.31) represent the optical stimulation of electrons

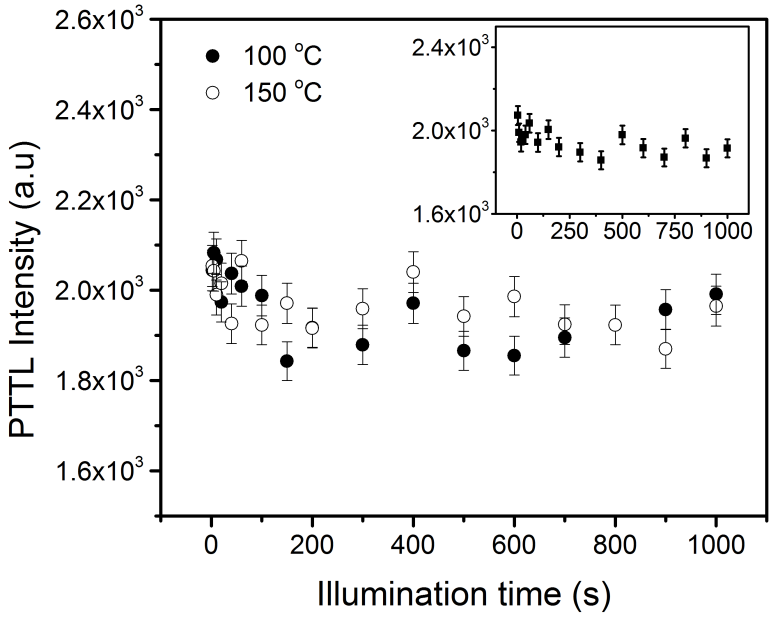

FIGURE 8.40: Time-dependence of intensity of peak V for preheating to 100 and 150 °C. The inset shows the plot for preheating to 240 °C. The error bars are determined by Poisson statistics for counting experiments.

from the corresponding donor traps. Equation (8.32) represents the transport of charge at the acceptor. It is important to note that not all electrons optically stimulated from the donor traps move to the acceptor trap. The first term in equation (8.32) describes a possibility of optical loss of trapped charge at a rate s_1. The other terms express that only a portion of electrons released from each donor trap is captured at the acceptor trap. Retrapping is ignored.

The solution of the set of coupled linear differential equations (8.29) - (8.32) is

$$N_1 = A_1(e^{-s_2 t} - e^{-s_1 t}) + A_2(e^{-s_3 t} - e^{-s_1 t}) + A_3(e^{-s_7 t} - e^{-s_1 t}) \tag{8.33}$$

where $A_1 = \frac{a_2 s_2 N_{2i}}{s_1 - s_2}$, $A_2 = \frac{a_3 s_3 N_{3i}}{s_1 - s_3}$, $A_3 = \frac{a_7 s_7 N_{7i}}{s_1 - s_7}$. N_{2i}, N_{3i}, and N_{7i} are each the initial concentration of electrons at the electron traps II, III, and VII respectively; the a_i's are constants of proportionality; s_1 represents the probability of electron stimulation from the acceptor trap; s_2, s_3, and s_7 represent the probability of stimulation from the donor traps.
We assume that the PTTL intensity is proportional to the concentration of electrons N at the acceptor trap as expressed in equation (8.33).

8.3.3.2 PTTL after preheating to 150 °C

Preheating the sample to 150 °C to remove peaks I and II reproduces only peak I. The electron trap for peak P1 (i.e. level I) is thus an acceptor. Levels III, V and VII are donors. However, level V is a redundant donor. The system under study comprises one acceptor and two donors. The coupled differential equations for this system are

$$\frac{dN_3}{dt} = -s_3 N_3 \tag{8.34}$$

$$\frac{dN_7}{dt} = -s_7 N_7 \tag{8.35}$$

$$\frac{dN_1}{dt} = -s_1 N_1 + b_3 s_3 N_3 + b_7 s_7 N_7 \tag{8.36}$$

The time-dependence of the electron concentration at the shallow trap I is given by

$$N_1 = B_1(e^{-s_3 t} - e^{-s_1 t}) + B_2(e^{-s_7 t} - e^{-s_1 t}) \tag{8.37}$$

where $B_1 = \frac{b_3 s_3 N_{3i}}{s_1 - s_3}$, $B_2 = \frac{b_7 s_7 N_{7i}}{s_1 - s_7}$ and b_i's are each a constant of proportionality and the other parameters are as defined previously.

8.3.3.3 PTTL after preheating to 240 °C

When the sample was preheated to 240 °C to remove peaks I, II, and III, all the removed peaks were reproduced under phototransfer. The acceptors are levels I, II, and III whereas the donors are levels V and VII. We showed previously in Figure 8.40(inset) that the contribution of electrons from peak V is negligible. We thus have three systems of one acceptor and one donor.
The transport of electrons from the donor trap VII to the acceptor trap III is given as

$$\frac{dN_7}{dt} = -s_7 N_7 \tag{8.38}$$

$$\frac{dN_3}{dt} = -s_3 N_3 + g_7 s_7 N_7 \tag{8.39}$$

The solution of the set (8.38) and (8.39) is

$$N_3 = G(e^{-s_7 t} - e^{-s_3 t}) \tag{8.40}$$

Similarly, the time-dependence of the electron concentration corresponding to levels II and I are

$$N_2 = G^*(e^{-s_7 t} - e^{-s_2 t}) \tag{8.41}$$

$$N_1 = G^{**}(e^{-s_7 t} - e^{-s_1 t}) \tag{8.42}$$

where $G = \frac{g_7 s_7 N_{7i}}{s_3 - s_7}$, $G^* = \frac{g_7^* s_7 N_{7i}}{s_2 - s_7}$, $G^{**} = \frac{g_7^{**} s_7 N_{7i}}{s_1 - s_7}$; g_7 and g_7^*, g_7^{**} are constants of proportionality.

8.3.3.4 PTTL after preheating to 450 °C

When all the peaks of the glow curve are removed by preheating to 450 °C, only peak III is reproduced under phototransfer. Electron traps corresponding to this peak (i.e. level III) act as an acceptor. Level VII corresponding to the deep trap is the only donor. We thus have a case of one acceptor and one donor. Since there was no time response curve to show or obtained for this preheating temperature,

only analytical solutions will be shown. The solution for the system is

$$N_3 = H(e^{-s_7 t} - e^{-s_3 t}) \tag{8.43}$$

where $H = \frac{h_7 s_7 N_{7i}}{s_3 - s_7}$ and h_7 is a constant of proportionality.

8.3.4 Application of models

Figure 8.41 shows the fits of the models to experimental data for peak P1. Figure 8.41(a) shows the fit for a system of one acceptor and three donors for peak P1 after preheating to 100 °C. Figure 8.41(b) shows the fit for a system of one acceptor and two donors following preheating to 150 °C. Figure 8.41(c) is a fit for peak P1 for a system of one acceptor and one donor after preheating to 240 °C. The various models properly describe the intensity-time profiles of the experimental data.

We have described qualitatively in the pulse annealing experiment and time-dependence of PTTL measurements that not all donor electron traps act completely as such. Some donor traps can act as effective competitors for photostimulated charge. This is new and of interest in PTTL research.

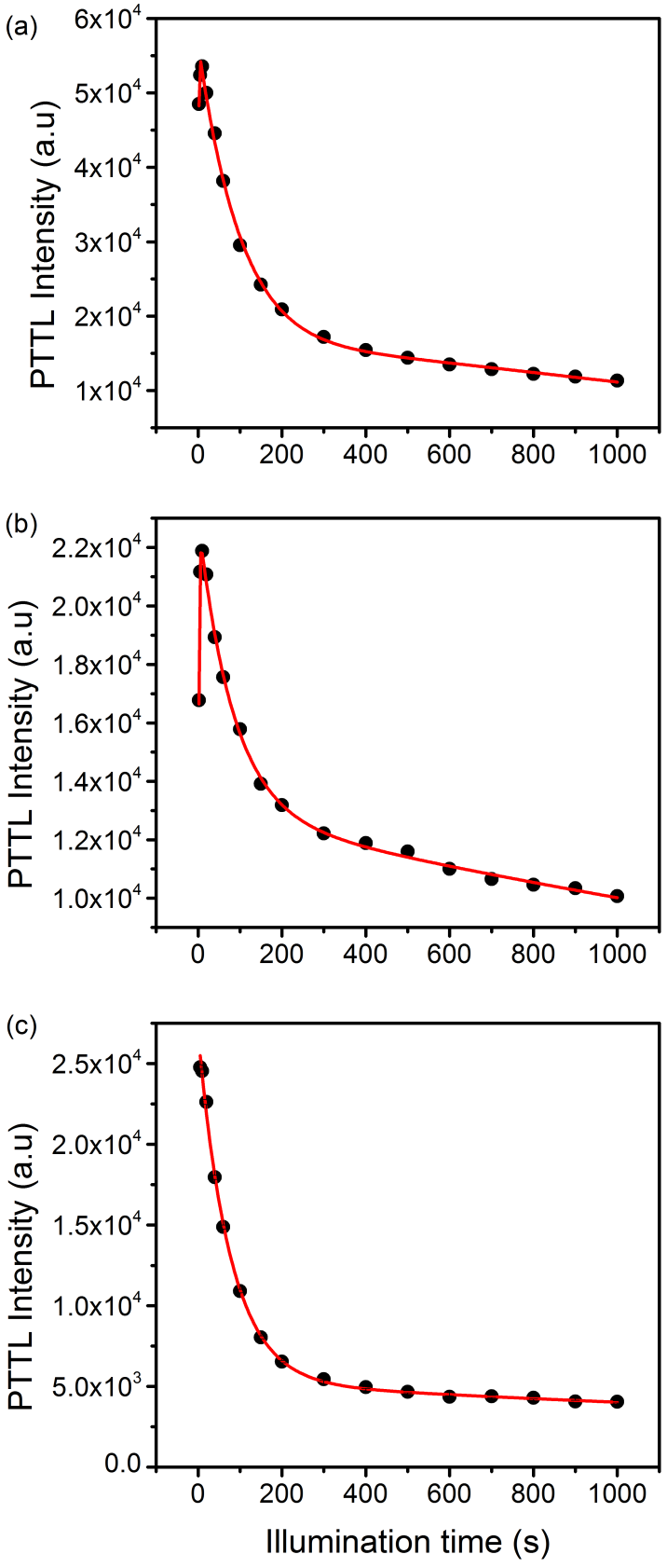

FIGURE 8.41: Plots of PTTL intensity against illumination time for peak P1 after preheating to (a)100 (b)150 (c) 240 °C.

Chapter 9

Conclusion

We have investigated the dynamics of stimulated luminescence in natural quartz by studying its thermoluminescence and phototransferred thermoluminescence properties. The study was conducted on samples of unannealed and annealed natural quartz. One of the aims of this thesis is to carry out kinetic analysis on the prominent peaks (peaks I and III) for each of the samples studied. The positions of the main peak (peak I) for all the samples studied were between 68 and 73 °C. The positions of the peaks were noted to be independent of repetitive measurement for all samples. Dosimetric features investigated for peak I for all the samples revealed that the main peak was sublinear with dose and fades exponentially with time. Results of kinetic analysis showed that the main peak is of first-order kinetics and that peak III is of general order kinetics. The values of the activation energy evaluated using various methods of kinetic analysis were consistent for each sample. The activation energy obtained using the various methods is ~ 1 eV for both peaks and agrees with published values in the literature. An important finding from our study is the presence of inverse thermal quenching on peak I for the sample annealed at 800 °C for 1 hour. The TL intensity of this peak increased with heating rate implying that the sample is not affected by thermal quenching. However, when the same sample was irradiated to a low dose of 3 Gy, the TL intensity decreases with heating rate showing presence of thermal quenching. We demonstrated the inverse-thermal quenching behaviour to be a dose-dependent feature. Inverse thermal quenching was not observed for other samples annealed at 800 °C for 10 minutes, 1000 °C for 10 minutes and 1 hour as well as the unannealed sample. We also demonstrated that as regards analysis for thermal quenching, the method based on the area under an isothermal decay curve (Chithambo, 2014) is

not influenced by the dose the sample is irradiated to unlike the conventional one based on change of TL intensity with heating rate.

The influence of annealing on thermoluminescence was also investigated for the samples annealed at 1000 °C. The values of the trap depth recorded for the sample annealed at 1000 °C for 10 minutes are higher compared with the sample annealed for 1 hour. In addition, annealing was noted to affect the thermal quenching of the peaks for each sample. The activation energy of thermal quenching for the sample annealed for 10 minutes is higher than for that recorded for 1 hour. This implies that the duration of annealing at 1000 °C has an effect on the trap parameters of the quartz sample.

Phototransferred thermoluminescence involving multiple acceptors and multiple donors was investigated in this study for the annealed samples only. The study revealed that peaks I, II, and III are phototransferred peaks. The dependence of the PTTL intensity of these peaks on the duration of illumination revealed that peaks II and III also act as competitors for photostimulated charge. The competition effects of these peaks were investigated by studying the processes that enhance the capture of charge during illumination. We adopted the phenomenological model by Chithambo *et al.* (2017a) on the time-dependent profiles of PTTL intensity. The models were formulated based on experimental evidence from the intensity-time plots corresponding to different preheating temperatures. The models formulated were applied to experimental data and properly describe the time-dependent profiles of the PTTL peaks.

9.1 Future works

Kinetic analysis of unannealed and annealed quartz have been studied extensively in this work. Information on defects and luminescence centres was missing in this study due to equipment limitations. Further studies are required to investigate the defects mechanism in quartz through spectral measurements. The influence of annealing on thermoluminescence of natural quartz using a high frequency electron paramagnetic resonance is also essential. This study would reveal the defects and recombination centres in these samples.

The thermal quenching effects from deep electron traps through thermally assisted-optically stimulated luminescence which was not conducted in this study is worthy

of investigation.

The studies carried out on the PTTL aspects are quite interesting. It will be worthwhile to study this phenomenon in future to understand the kinetic process with different wavelength light stimulations.

Appendix A Publications

Some of the results presented in this thesis have been published in Journal of Luminescence and Radiation measurements. The published papers are attached below.

Journal of Luminescence 216 (2019) 116730

Contents lists available at ScienceDirect

Journal of Luminescence

journal homepage: www.elsevier.com/locate/jlumin

Phototransferred thermoluminescence from natural quartz annealed at 1000 °C: Analysis of time-dependent evolution of intensity and competition effects

M.L. Chithambo[a,*], D.E. Folley[a], S. Chikwembani[b]

[a] Department of Physics and Electronics, Rhodes University, P.O. Box 94, Grahamstown, 6140, South Africa
[b] Department of Chemical & Physical Sciences, Walter Sisulu University, Mthatha, 5117, South Africa

ARTICLE INFO

Keywords:
Phototransferred thermoluminescence
Natural quartz
Acceptors
Donors
Models
Competition effects

ABSTRACT

Phototransferred thermoluminescence (PTTL) related to multiple acceptors and donors in natural quartz is reported. A glow curve measured at 1 °C s^{-1} after beta irradiation to 300 Gy has four peaks labelled I, II, III, and IV at 70, 124, 170, and 298 °C respectively. Preparatory to measurement of PTTL, these peaks were removed in turn by preheating to 100, 140, 250 and 500 °C. PTTL is observed for peak I after any of these preheating temperatures. This means that peak I is reproduced, under phototransfer, when any of peak I, II, III or IV has been removed. Peak II is only reproduced after preheating to 250 °C to remove peaks I, II and III. Peak II does not reappear after any preheating beyond 250 °C. Peak III re-appears under phototransfer following preheating to either 250 or 500 °C. No PTTL was observed for peak IV at all. The behaviour of peaks II and IV are suggestive of competition effects that merit investigation. This is addressed in this report. The dependence of PTTL intensity on the duration of illumination is studied for all PTTL peaks corresponding to various preheating temperatures. Peak I shows an initial increase in intensity followed by a decrease with illumination for preheating to 100, 140 and 500 °C. However when the sample is preheated to 250 °C, the intensity decreases monotonically. The PTTL intensity for peaks II and III go through a slow and extended growth up to 1500 s before the onset of any decrease. The change of intensity with illumination time is modelled using coupled first-order linear differential equations on the basis of systems of acceptors and donors whose number depends on the preheating temperature.

1. Introduction

If a previously irradiated material, typically an insulator, is heated at a controlled rate, the presence of any electron-trapping point defects within it is revealed as peaks in the temperature resolved plot of luminescence. The electron traps involved in such thermoluminescence (TL) are populated as a result of ionization during the irradiation the material is subjected to prior to measurement. If on the other hand, the material is purposely partially heated to empty only some of the electron traps, and then exposed to light of certain wavelengths to transfer charge from deeper lying (donor) traps to the empty shallower ones, the resulting phototransferred thermoluminescence (PTTL) can be instructive. Apart from providing a means to quantify kinetics of acceptor or donor levels, questions about the dynamics of charge transfer and competition effects, many of which are outstanding and are our primary interest, can be explored.

The literature on conventional thermoluminescence of quartz, the material of this work, is encyclopedic. In comparison, the body of work on PTTL from quartz is rather meagre. Indeed, there has been much and enduring interest on conventional TL of quartz covering such areas as analytical methods, mechanisms and applications as attested to by many reviews and texts [1–5]. In contrast except for a few examples that looked at wavelength response [6,7] or considered emission efficiency e.g. Ref. [8] or indeed dosimetry [7,9,10], the publication of work devoted to PTTL of quartz has been sporadic and many of them have tended to be rather qualitative.

The possibility of using PTTL for retrospective dosimetry was discussed by Bailiff et al. [9] on the premise that the amount of charge residual at a donor reflects the archaeological age. The unstated assumption here is that the signal monitored emanates from a single donor. Indeed although Bailiff et al. [9] monitored PTTL at the '110 °C' peak, they assumed that of the possible alternatives at 210, 325 and

* Corresponding author.
E-mail address: m.chithambo@ru.ac.za (M.L. Chithambo).

https://doi.org/10.1016/j.jlumin.2019.116730
Received 28 March 2019; Received in revised form 8 August 2019; Accepted 3 September 2019
Available online 09 September 2019

375 °C, the active donor was the 325 °C one. The possible role of the 325 °C level as a source trap had been mooted long before [11], examined [12–15] and in some cases assumed as fact [16]. On the question of PTTL dosimetry, Benny and Bhatt [10] studied quartz with peaks at 110, 220 and 370 °C and yet of these three, the one at 220 °C was not reproduced under phototransfer. This result, although not discussed in their report, obliquely hints at competition effects and is an example of puzzles within PTTL that require further investigation.

A number of studies on natural quartz annealed up to 1000 °C [8,16,17] or synthetic quartz annealed up to 900 °C [18] supposed the 325 °C peak as the donor for PTTL corresponding to various selected peaks. By preheating samples up to 700 °C and yet still observing PTTL, Bertucci et al. [18] deduced the presence of deep electron donor traps in quartz, a conclusion also drawn by Morris and McKeever [19] and Bailiff et al. [9]. In these examples, the time-dependent change of PTTL intensity on duration of illumination used to induce phototransfer was qualitatively ascribed to donor-to-acceptor charge transfer.

An attempt to model PTTL time-response behaviour for quartz was made by Wintle and Murray [15] for an idealized system of one acceptor (the '110 °C' peak) and one donor (the 325 °C level). This set-up implicitly excluded any role for the deep or any other electron donor trap. A detailed discussion of PTTL intensity as a function of illumination time was later reported by Alexander and Mckeever [20]. This work, based on numerical simulation, sought to predict expected time-dependent evolution profiles of PTTL intensity also for a system of one donor and one acceptor. However this study extended relevant earlier ones [6,15] by including in the model a non-radiative recombination centre as a way to assess the effect of competitive charge retrapping. Here the transfer of charge from the donor to the acceptor or competitor levels during illumination or heating to produce PTTL is formulated as coupled non-linear differential equations. Such equations do not have analytical solutions. By varying some parameters, for example charge concentrations, Alexander and McKeever [20] numerically predicted various types of time-response curves. Similar profiles were shown to arise for the same system for various combinations of rates of optical stimulation from electron traps [21]. Thus results obtained by simulation with one set of parameters could equally be found when the permutation involved a completely different set of parameters. It must be then that either both or one set is valid or that the exercise is academic.

The notion that analysis built on assumption may not relate to experimental results equally applies to analytical solutions. If one supposes, for a two-trap system, that there is loss of charge from the acceptor during illumination, the solution of the pair of linear differential equations describing the process is an intensity profile that goes through a peak with illumination time. If the assumption is dropped, the intensity increase is akin to a saturating exponential. In principle Alexander and Mckeever [20] cautioned that analytical solutions used to account for time-dependence of PTTL may or may not be valid for particular systems under experimental study.

An empirical model for PTTL was reported by Chithambo et al. [22]. The approach differs from that of Alexander and Mckeever [20] in several important respects. The method of Chithambo et al. [22] applies to any system with any number of acceptors and donors. The transport of charge from donors to an acceptor is described by sets of coupled linear first order differential equations. These families have analytical solutions that can be applied directly to experimental data. The method does not make *a priori* assumptions about any variable. The number of active donors and acceptors, and to what extent they are, is informed by experiment.

The aim of this work is to study PTTL from quartz annealed at 1000 °C. When quartz is heated, it undergoes phase inversion from α-quartz to β-quartz at 573 °C and from β-quartz to tridymite at 867 °C [23]. The heating also affects its luminescence sensitivity [24], lifetimes [25–27], and emission bands [28]. Properties of PTTL in annealed natural quartz have never been systematically studied and are therefore a justifiable concern. In this report, the dependence of PTTL intensity on duration of stimulation is described using coupled linear first order differential equations. Systems of an acceptor and multiple donors the number of which is determined experimentally are analysed. The role of any putative donor is not presumed but determined by experiment. It is seen that supposed acceptors or donors do not always act as such and the causative competition effects have been investigated and modelled. The objective of this work is to contribute to the understanding of phototransferred thermoluminescence in quartz.

2. Experimental details

Measurements were made on commercially available coarse grain natural quartz (BDH Ltd., UK). The quartz was annealed at 1000 °C for 10 min before use to improve its sensitivity to thermal stimulation and to remove any residual luminescence. The same annealed quartz has been used before [29]. Implications of annealing quartz to elevated temperatures were pointed out in the Introduction. Experiments were performed on a RISØ TL/OSL DA-20 Luminescence Reader. The luminescence was detected by an EMI 9235QB photomultiplier tube through a 7 mm Hoya U-340 filter (transmission band 250–390 nm). Samples were irradiated at room temperature using a $^{90}Sr/^{90}Y$ β source at a dose rate of 0.10 Gy s^{-1}. All measurements were carried out at 1 °C s^{-1} unless otherwise stated. To measure phototransferred thermoluminescence, an irradiated sample was first preheated to a specific temperature to remove a given glow peak. The sample was thereafter exposed to 470 nm blue light to induce transfer of charge from deeper to shallower electron traps. A complete glow curve was then measured after illumination and any PTTL monitored at this stage.

3. Glow curve characteristics

Fig. 1 shows a glow curve measured after an atypically high dose of 300 Gy. The high dose was intended to induce a good PTTL signal. The need for high energy to achieve phototransfer means that experimentally the trade-off is between combinations of either short optical wavelength and low dose or long wavelength and high dose. There are four peaks in Fig. 1; an intense one at 70 °C (labelled I), a poorly defined peak at 124 °C (labelled II) and other peaks at 170 and 298 °C labelled III and IV. The position of each of these peaks was verified by the thermal cleaning procedure described elsewhere [3]. PTTL was measured after preheating to the same temperatures as for thermal cleaning and illumination for a specific time. As an example, Fig. 2 shows a glow curve measured at 1 °C s^{-1} following irradiation to 300 Gy, preheating to 140 °C and illumination for 60 s. This shows a PTTL peak here

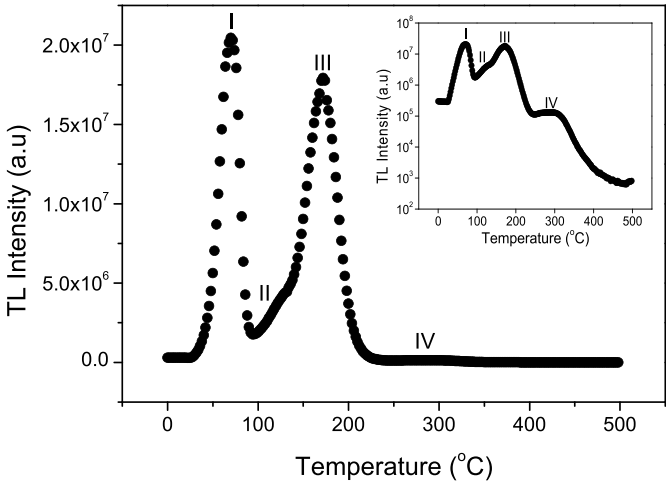

Fig. 1. A TL glow curve measured at 1 °C s^{-1} following irradiation to 300 Gy. The inset shows the same plot on a logarithmic scale to better show the presence of peak IV.

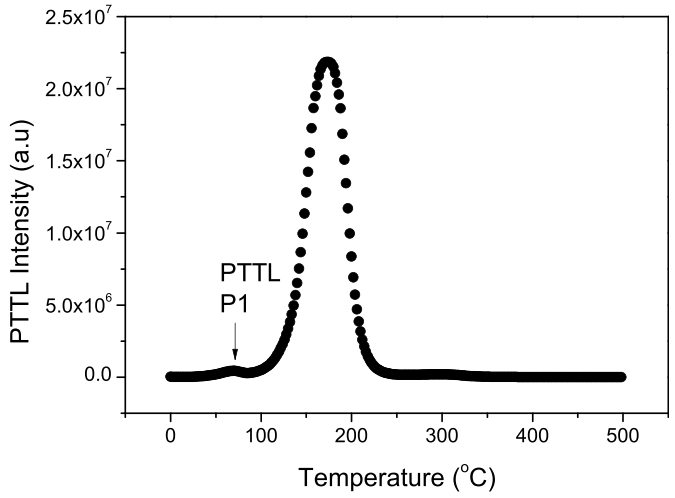

Fig. 2. A glow curve measured at 1 °C s^{-1} following a dose of 300 Gy, preheating to 140 °C and illumination for 60 s showing phototransfer at peak P1.

labelled P1. For ease of reference, PTTL peaks reproduced after removal of peaks I, II and III are referred to as P1, P2, and P3. No PTTL was observed for peak IV at all. Peak II appears under phototransfer only for some not all preheating temperatures.

4. Identification of electron traps as donors and acceptors by pulse annealing

To determine which electron traps contribute to the PTTL process as acceptors and which as donors, a protocol similar to the pulse annealing method [24] was used. As applied, the method monitored the PTTL intensity measured after preheating and illumination. Measurements were made on a sample irradiated to 300 Gy, preheated in turn to temperatures between 80 and 380 °C in steps of 10 °C and illuminated for 60 s each time.

Fig. 3 shows the peak intensity against preheating temperature for peaks I, III and IV. Peak I decreases consistently in intensity when the preheating temperature is increased from 80 to 350 °C. Since this peak is reproduced under phototransfer throughout, the decrease in its intensity likely occurs because the preheating depletes the amount of charge remanent at the source traps which in this case are electron traps corresponding to peaks II–IV. Peak II, flanked between peaks I and III, is ill-defined hence could not be reliably monitored and is discussed to a limited extent. The intensity of peak III goes through four regions with preheating temperature. In two of these, between 80 - 140 °C and 220–250 °C, the intensity is independent of preheating but decreases otherwise. The position of peak III is above 140 °C and any preheating to a temperature below this is irrelevant in the subsequent measurement because its intensity would be unaffected. The intensity of peak III decreases monotonically when the sample is preheated between 140 and 220 °C. Since these temperatures are within the expanse of peak III (see Fig. 1), preheating decreases the intensity of the apparent peak (peak III) because a portion of it is removed by the preheating prior to measurement of the glow curve where the intensity of this peak (peak III) is monitored. Indeed, the decrease caused by partial heating causes more of an effect on the peak than any additive effect due to inward phototransfer.

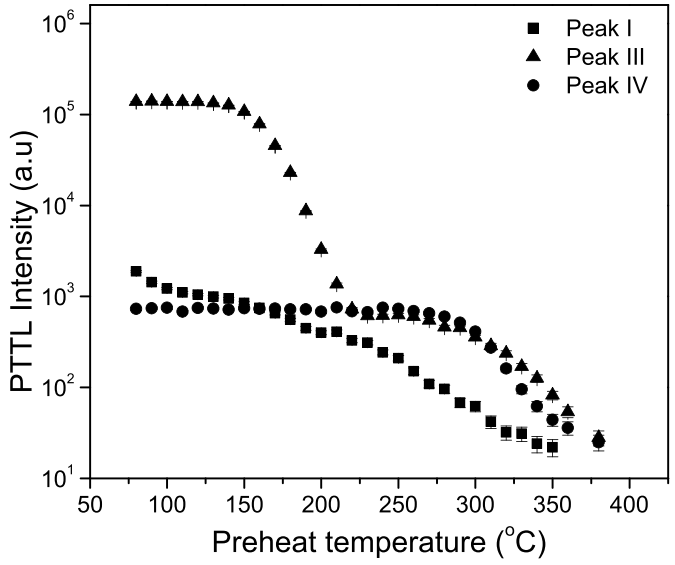

Fig. 3. The influence of preheating temperature on peak intensity in a pulse annealing experiment. The error bars in each data point are determined using the square root rule for counting experiments.

Between 220 and 250 °C, the intensity again becomes independent of preheating temperature. Here the peak monitored is a phototransferred one. The intensity remains unchanged because the effect of preheating or illumination on its donors is negligible. This is reflected in the plot for peak IV, a supposed donor, where the intensity is constant despite preheating between 220 and 250 °C.

The effect of depleting a donor can be further abstracted from the response to preheating from 240 to 380 °C for peak IV, a donor, and peak III, an acceptor. When the concentration of electrons in level IV is continually decreased by preheating, so is the amount remaining for phototransfer. The expected drop in intensity of peak IV becomes concomitant with that of peak III in the range 240–380 °C.

Although useful as a tool for explanation, PTTL in quartz cannot be accounted for in terms of only two electrons traps, one acting as the donor and the other as an acceptor. There is no such system in quartz. In hindsight, previous work that did this e.g. Ref. [15] can be seen as having treated an idealized system. The number of acceptors or donors in PTTL depends on a number of factors principal of which is the preheating temperature. That said, not all putative donors or acceptors act as such for any preheating temperature as exemplified by peak II. Thus where possible, PTTL must be examined based on experimental evidence with minimal assumptions.

5. A qualitative account of acceptors, donors and competition effects

The intensity of PTTL was studied as a function of duration of illumination. Preparatory to mathematical analysis later in the text, we provide a qualitative explanation of the illumination time profiles. In the measurements, the quartz was irradiated to 300 Gy and PTTL monitored after preheating to 100, 140, 250 and 500 °C. These are the same temperatures used for thermal cleaning except for the additional 500 °C included in the step to sense deep traps.

5.1. PTTL following preheating to 100 °C

When an irradiated sample is preheated to 100 °C, peak I is removed but is reproduced under phototransfer. Fig. 4 shows the dependence of its PTTL intensity (i.e of peak P1) on the duration of illumination. The change corresponding to preheating to 100 °C is shown in Fig. 4(a). The intensity increases to a maximum and decreases thereafter. This profile is archetypal and has been observed in various materials including quartz e.g. Refs. [17,30], α-Al_2O_3:C e.g. Refs. [22,31] and α-Al_2O_3:C, Mg [32]. The increase of intensity at short illumination times, as qualitatively explained elsewhere [22], implies that the trapping of electrons in the shallow trap exceeds any removal by optical stimulation. The decrease of intensity thereafter occurs when loss of electrons gradually exceeds retention.

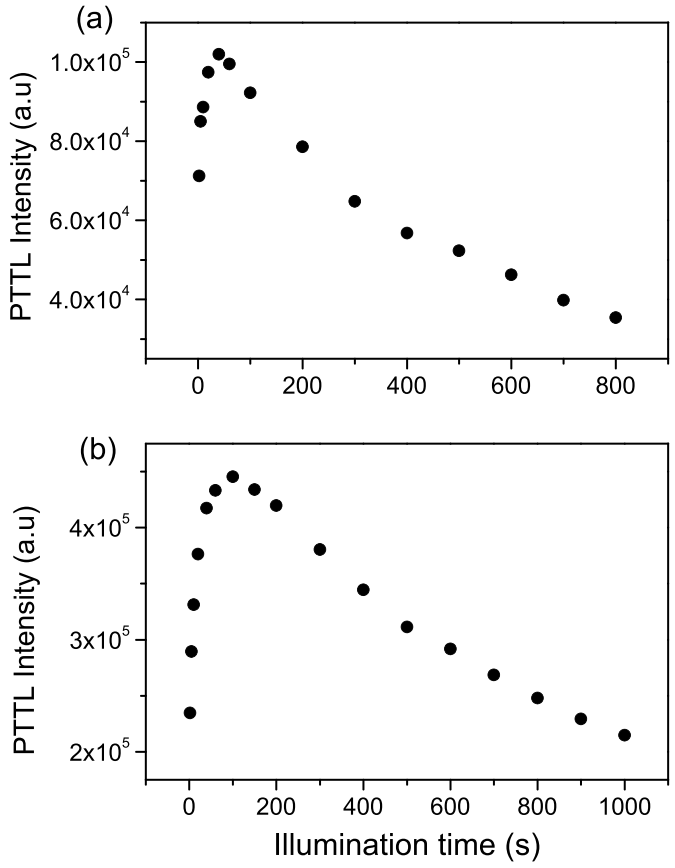

Fig. 4. Dependence of PTTL intensity on duration of illumination for peak P1 after preheating to (a) 100 °C (b) 140 °C.

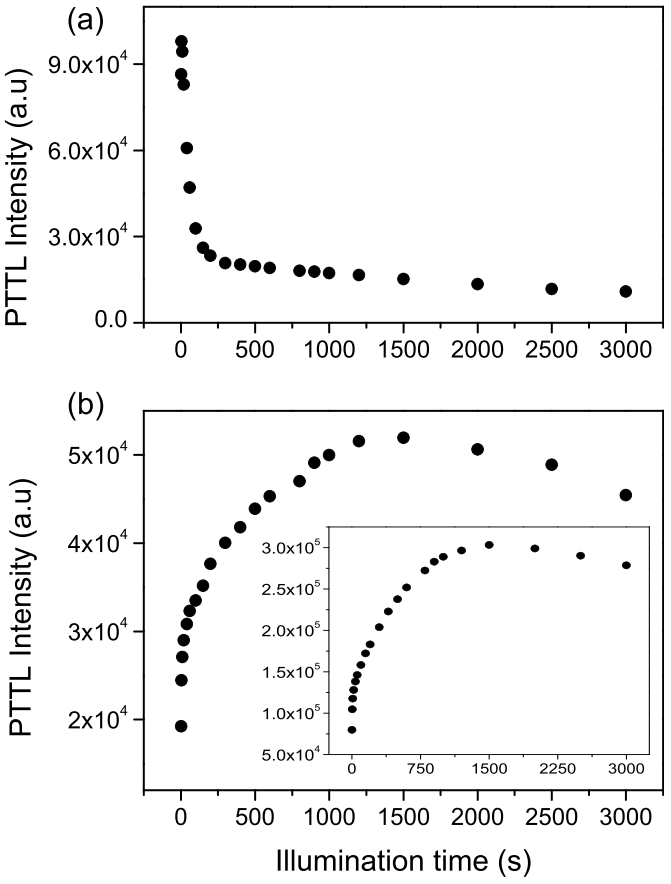

Fig. 5. Change of PTTL intensity with illumination time for peak P1 (a) peak P2 (b) and peak P3 (inset). This is for preheating to 250 °C.

5.2. PTTL following preheating to 140 °C

When the sample is preheated to 140 °C after irradiation to remove peaks I and II, only peak I is reproduced under phototransfer. Fig. 4(b) shows the time-dependence of its PTTL intensity. The intensity also goes through a peak with illumination time. Although the pattern of change resembles that in Fig. 4(a), the intensity is much greater. We attribute this to a portion of charge which would have produced peak II by phototransfer but now becomes available to other electron traps. The effect of this additional charge on other peaks will be described later in the text.

5.3. PTTL following preheating to 250 °C

When the sample is preheated to 250 °C, the removed first three peaks are reproduced under phototransfer. Fig. 5 shows the dependence of the PTTL intensity on duration of illumination for PTTL peaks P1, P2 and P3. Fig. 5(a) shows the change for P1. The intensity no longer goes through a peak as in Fig. 4 but decreases monotonically with illumination time. This is an effect of competitive retrapping at electron traps for peaks II and III. If owing to competitive retrapping elsewhere, fewer electrons are captured at the electron trap for peak I with each increase in duration of illumination, its intensity cannot other than only decrease. This behaviour is particularly manifest when the sample is illuminated for lengthy periods after irradiation and preheating. This is because during ionization, the number of electrons moved to the deep electron trap, the presumed primary donor, is finite. When the sample is illuminated, only a portion of the electrons sampled out of the deep trap can produce peak I. Some of this component may even be stimulated out prior to measurement of the PTTL. The remainder of the output from the deep trap produces peaks II and III and also transits to the recombination centre. Thus when the exposure time is extensive so are the losses. This is reflected in the continual decrease of intensity at long illumination times. The discussion above excludes peak IV as a donor since its intensity changes only minimally with re-measurement (Fig. 3). Further evidence will show that its role as a donor can indeed be neglected in this case.

The time-dependence of the PTTL intensity for P2 is shown in Fig. 5(b). The result for P3 is shown in the inset. The PTTL intensities in these two examples increase with time for an extended period of about 1500 s before the onset of a decrease. This is a result of their electron traps being effective charge competitors.

5.4. PTTL following preheating to 500 °C

When the sample is preheated to 500 °C, only peaks I and III are reproduced under phototransfer. Fig. 6 shows the time-dependence of the PTTL intensity for P1 and in the inset, for P3. The intensity is much lower than before since there is now only a single donor but both cases go through a maximum. The time-evolution of the PTTL intensity in Fig. 6 and others presented in this section will be described using mathematical models next.

6. Mathematical models of PTTL

PTTL is a multistep process involving irradiation to fill electron traps, preheating to empty some of them, illumination to transfer charge from deep traps to empty shallower ones, and heating to monitor any PTTL peaks. The number of electron traps acting as acceptors or donors changes with preheating temperature. An often overlooked fact is that not all putative acceptors or donors act as such. To analyze the illumination time profiles, we adopt the method of

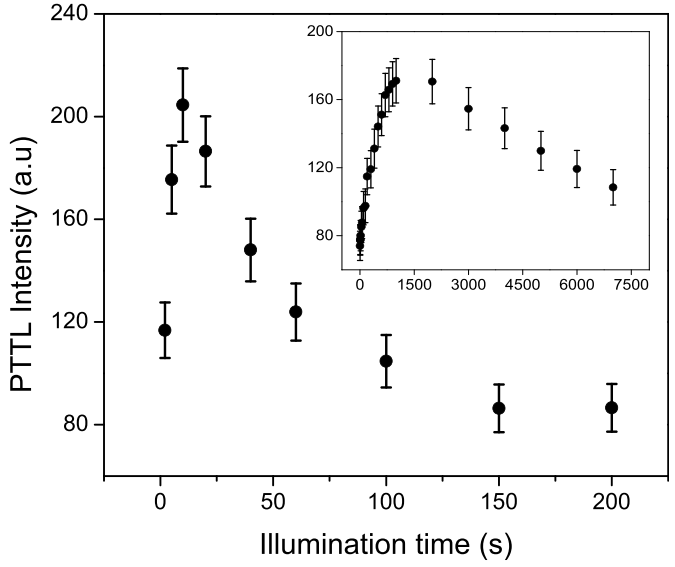

Fig. 6. PTTL intensity versus illumination time for peak P1 and peak P3 (inset) after preheating to 500 °C.

Chithambo et al. [22] where PTTL is described for any combination of donors and an acceptor using families of linear differential equations. The equations are formulated on the basis that only a certain portion of electrons optically stimulated from a donor are captured at an electron trap with the transitions proceeding via the conduction band. The equations have analytical solutions. This is in contrast to say, Alexander and McKeever [20] who discussed PTTL for an exemplar of one acceptor and one donor using non-linear differential equations. The latter do not have analytical solutions and recourse is made to numerical solutions. In comparison, the analytical solutions in the method of Chithambo et al. [22] can be applied directly to experimental data.

Fig. 7 shows the energy band model used to explain PTTL in this study. Electron traps corresponding to peaks P1, P2, P3 and IV are labelled I, II, III, and IV. A deep trap, responsible for PTTL observed after preheating to 500 °C, is shown as V. Since the number of deep traps is unknown, we limit this to one, V. The transport of charge from donor(s) to an acceptor is described only at the illumination stage using coupled linear first order differential equations. We assume that during illumination, electrons are stimulated from a donor trap at a stimulation rate $f = \Phi\sigma$ (where Φ is the incident photon flux and σ the photoionization cross-section). Only a certain fraction of these electrons is captured at the acceptor trap. Retrapping is neglected. In particular, peak P1 and P3 were determined to be subject to first order kinetics (see supplementary information) for which retrapping does not apply. The coupled first order linear differential equations that we set up account for the transport of electrons from donors to an acceptor. Their analytical solutions are applied directly to experimental data. From the model, one can also determine the photoionization cross-section of the acceptor traps. This is not a primary concern this time. The dependence of PTTL intensity on duration of illumination is discussed in four categories depending on the preheating temperature. The method used here and elsewhere [22,30] should not be confused with a kinetic approach where rate equations relate the concentration of holes at a recombination centre with the concentration of electrons at electron traps and in the conduction band.

6.1. PTTL following preheating to 100 °C to remove peak I

When the quartz is preheated to 100 °C, peak I is removed but reproduced under phototransfer. Levels II through V can be considered donors and level I, the acceptor. This is a system of one acceptor and four donors. The coupled differential equations describing movement of charge from donors to the acceptor for this system are

$$\frac{dN_2}{dt} = -f_2 N_2. \tag{1}$$

$$\frac{dN_3}{dt} = -f_3 N_3. \tag{2}$$

$$\frac{dN_4}{dt} = -f_4 N_4. \tag{3}$$

$$\frac{dN_5}{dt} = -f_5 N_5. \tag{4}$$

$$\frac{dN_1}{dt} = -f_1 N_1 + a_2 f_2 N_2 + a_3 f_3 N_3 + a_4 f_4 N_4 + a_5 f_5 N_5. \tag{5}$$

Eq (1)–(4) represent the optical stimulation of electrons from the

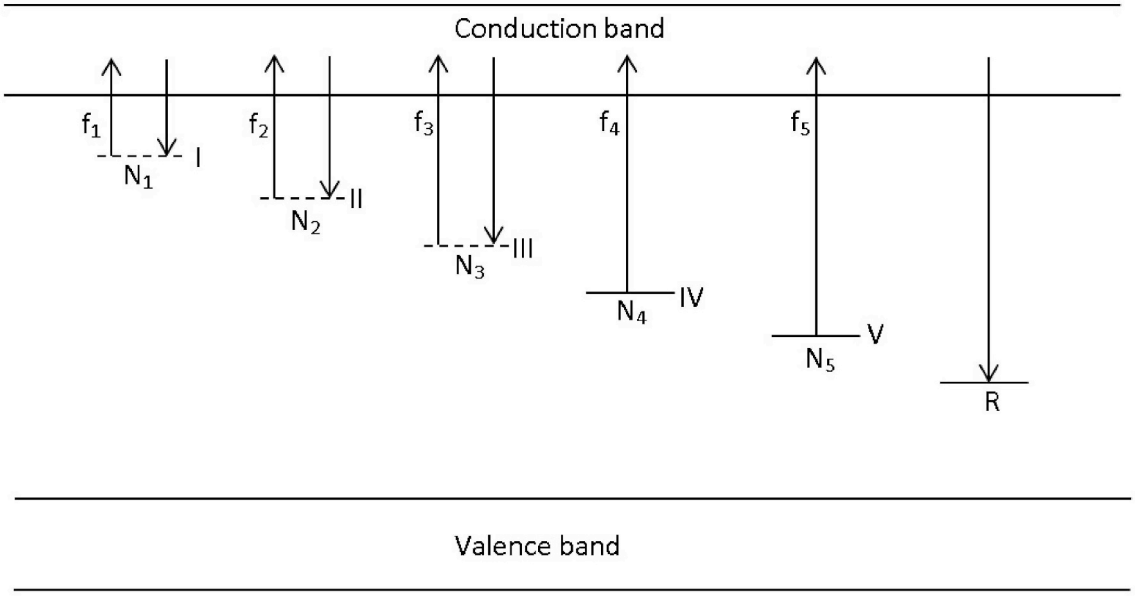

Fig. 7. An energy band model used to discuss PTTL. The electron traps are shown as I–V. The recombination centre R producing luminescence is included for completeness. The optical stimulation rates are labelled as f_i and the concentration at each electron trap as N_i (i = 1...5).

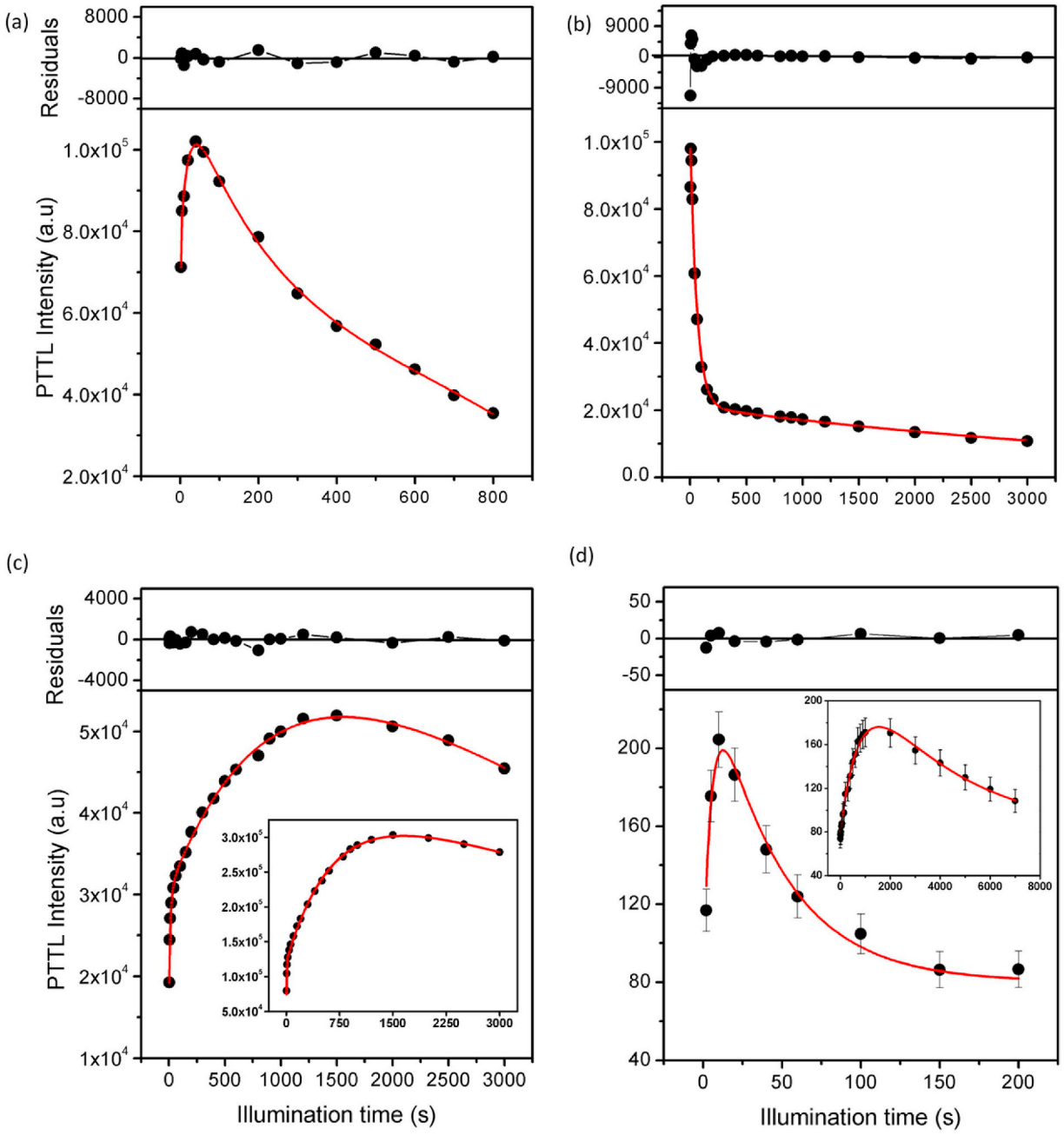

Fig. 8. Plots of PTTL intensity against illumination fitted with various equations as explained in the text. The graphs are for peak P1 after preheating to 100 °C (a), peak P1 corresponding to 250 °C (b) peak P2 (c) and P3 (inset) following preheating to 250 °C and in (d) for peaks P1 and P3 (inset) after preheating to 500 °C. The residuals in all fits are consistent with zero as evidence of proper fit.

donors. Eq (5) describes charge transport at the acceptor. The last four terms in Eq. (5) state that a portion of electrons released from each donor is retrapped at the acceptor. The first term reflects the possibility of optical loss of trapped charge at a rate f_1. The solution of the set (1)–(5) is

$$N_1 = A\left(e^{-f_2 t} - e^{-f_1 t}\right) + B\left(e^{-f_3 t} - e^{-f_1 t}\right) + C\left(e^{-f_4 t} - e^{-f_1 t}\right) + D\left(e^{-f_5 t} - e^{-f_1 t}\right) \quad (6)$$

where $A = \frac{a_2 f_2 N_{2i}}{f_1 - f_2}$, $B = \frac{a_3 f_3 N_{3i}}{f_1 - f_3}$, $C = \frac{a_4 f_4 N_{4i}}{f_1 - f_4}$, $D = \frac{a_5 f_5 N_{5i}}{f_1 - f_5}$. N_{2i}, N_{3i}, N_{4i} and N_{5i} are each the initial concentration of electrons at the electron traps II, III, IV and V respectively; the a_i terms are constants of proportionality; $f_i's$ are as defined earlier. However, experiments show that the change of intensity of peak IV with preheating is negligible (Fig. 3). Further evidence will also show that for preheating to 100 °C, the change of its intensity with illumination is likewise negligible. Level IV is thus redundant as a donor hence instead

$$N_1 = A'\left(e^{-f_2 t} - e^{-f_1 t}\right) + B'\left(e^{-f_3 t} - e^{-f_1 t}\right) + C'\left(e^{-f_5 t} - e^{-f_1 t}\right) \quad (7)$$

where $A' = \frac{a_2' f_2 N_{2i}}{f_1 - f_2}$, $B' = \frac{a_2' f_3 N_{3i}}{f_1 - f_3}$, $C' = \frac{a_2' f_5 N_{5i}}{f_1 - f_5}$ and a_i' are each a constant of proportionality.

6.2. PTTL following preheating to 250 °C to remove peaks I, II, and III

When the sample is preheated to 250 °C to remove peaks I, II and III, they are all reproduced under phototransfer. The acceptors are levels I, II and III and the source traps are IV and V. We thus have three systems of one acceptor and two donors. The transport of electrons leading to the photoinduction of P3 is given by the family

$$\frac{dN_4}{dt} = -f_4 N_4 \tag{8}$$

$$\frac{dN_5}{dt} = -f_5 N_5. \tag{9}$$

$$\frac{dN_3}{dt} = -f_3 N_3 + q_4 f_4 N_4 + q_5 f_5 N_5. \tag{10}$$

The solution of Eqs. (8)–(10) is

$$N_3 = D\left(e^{-f_4 t} - e^{-f_3 t}\right) + E\left(e^{-f_5 t} - e^{-f_3 t}\right) \tag{11}$$

where $A^* = \frac{q_4 f_4 N_{4i}}{f_3 - f_4}$, $B^* = \frac{q_5 f_5 N_{5i}}{f_3 - s_5}$; q_4 and q_5 are constants of proportionality. Similarly the change with time of the electron concentration at levels II and I are

$$N_2 = A'(e^{-f_4 t} - e^{-f_2 t}) + B'(e^{-f_5 t} - e^{-f_2 t}) \tag{12}$$

$$N_1 = A^{**}\left(e^{-f_4 t} - e^{-f_1 t}\right) + B^{**}\left(e^{-f_5 t} - e^{-f_1 t}\right) \tag{13}$$

where $A' = \frac{k_4 f_4 N_{4i}}{f_2 - s_4}$, $B' = \frac{k_5 f_5 N_{5i}}{f_2 - s_5}$, $A^{**} = \frac{k_4^* f_4 N_{4i}}{f_1 - s_4}$, $B^{**} = \frac{k_5^* f_5 N_{5i}}{f_1 - f_5}$; k_4, k_5, k_4^* and k_5^* are constants of proportionality. The reason for writing Eqs. (8)–(10) in full is to emphasize the point that sometimes similar looking equations such as (3) and (8) or (4) and (9) occur in different coupled equations. This is not repetition. The equations are each part of a set and are required to solve that particular family.

6.3. Phototransfer from deep traps following preheating to 500 °C

The phototransferred TL following preheating to 500 °C consists only of peaks I and III. The acceptors are levels I and III and the donor, V. These are two simple systems of one acceptor and one donor. The time-dependence of electron concentration at levels I and III are

$$N_3 = D^*\left(e^{-f_5 t} - e^{-f_3 t}\right) \tag{14}$$

$$N_1 = D^{**}\left(e^{-f_5 t} - e^{-f_1 t}\right) \tag{15}$$

where $D^{**} = \frac{q_5^* f_5 N_{5i}}{f_3 - f_5}$, $D^* = \frac{q_5^{**} f_5 N_{5i}}{f_3 - f_5}$; and q_5^{**} are constants of proportionality.

7. Application

Fig. 8 shows fits of various models to experimental data. The models are built on experimental evidence. Fig. 8(a) shows results for peak P1 corresponding to preheating to 100 °C. The line through data (solid circles) is a fit of Eq. (7). Equation (7) rather than (6) is used since experiments show that level IV is redundant as a donor. Fig. 8(b) shows the case for peak P1 when the sample is preheated to 250 °C. This type of response is unusual and is the first time it is being reported for quartz or any other material. The data is shown fitted by Eq. (13). The stimulation probability f_1 abstracted from the fit for level I greatly exceeds those of traps IV and V. The equation thus effectively reduces to a sum of two simple exponentials. In the qualitative discussion for Fig. 4(a), we mentioned that a growth in signal is possible if trapping exceeds stimulation. Therefore for Fig. 8(b) we can also approximate the process as

$$\frac{dN_5}{dt} = -f_5 N_5. \tag{16}$$

$$\frac{dN_1}{dt} = -a_5^* f_5 N_5. \tag{17}$$

giving $N_1 = C_1^* e^{-f_5 t}$ or $N_1 = C_4^* e^{-f_4 t} + C_5^* e^{-f_5 t}$ if both levels IV and V are theoretically included as donors. The approximations are consistent with experimental behaviour.

Fig. 8(c) shows fits for a system of one acceptor and two donors following preheating to 250 °C for peaks P2 (main graph) and P3 (inset). The lines through data are fits of Eq. (13) and inset, of Eq. (11). Finally, the lines through data in Fig. 8(d), corresponding to preheating to 500 °C are best fits of Eq. (15) for peak P1 (main graph) and Eq. (14) for peak P3 (inset). The various models formulated on the basis of experimental results properly describe the time-dependent profiles of PTTL intensity. The analysis as outlined is one means to determine the photoionization cross section. The photoionization cross-section describes the ease with which an electron trap can be optically stimulated. The smaller this value is, the less stable the electron trap is. For example, for peak P1 for the case of one acceptor and four donors one of which makes a negligible contribution (Eq. (8)), this was evaluated as 6.40×10^{-18} cm^2 whereas for the same peak but for a system of one acceptor and one donor, the value was determined as 1.10×10^{-18} cm^2. In general, all values are of the order of 10^{-18} cm^2 and are comparable with ones for natural quartz in the literature e.g Ref. [24].

8. Competition effects in phototransferred thermoluminescence

The conventional discussion of PTTL assumes that as electrons are released from source traps during illumination, they can follow any of three routes, namely, transit to recombination centres, get re-trapped or move to acceptors. While this idealized assumption facilitates mathematical description, phototransfer is far more complex and is subject to competition effects. By this we mean processes that enhance or depress the capture of charge at electron traps during illumination and how this affects the output from acceptors or contribution of donors. Competition affects were briefly discussed for PTTL in α-$A1_2O_3$:C [22] but have never been systematically investigated for PTTL in quartz.

In this work, competition effects are manifest when the sample is preheated to 500 °C but better so for preheating to 140 °C. For instance, when the sample is preheated to 140 or 500 °C, peak II is not reproduced at all. We will however discuss competition effects with respect to peak III. When the quartz is preheated to 140 °C, level III should be a donor for levels I and II. Fig. 9(a) (solid circles) shows the time-dependence of the intensity of peak III. The signal measured corresponds to its conventional TL at this stage. The intensity does not decrease consistently with illumination as might be expected of a donor but surprisingly increases for the first 150 s before the expected decrease sets in. Level III thus doubles up as a competitor for photostimulated charge from deeper electron traps and as a donor for shallower electron traps. Interestingly if the same measurement of peak III is made but corresponding to preheating to 100 °C when the electron trap for peak II is intact, the initial increase is not observed (Fig. 9, inset (i)). Thus we deduce that the initial said increase can be attributed to a portion of the additional charge that would have otherwise been responsible for peak II by phototransfer but is now available to other electron traps. The influence of removing peak II on the intensity of peaks other than this one can be understood by examining the time evolution of the intensity of peak II when the sample is preheated to 100 °C. Peak II is not properly defined so instead of reading off the value at peak maximum as customary, we instead use the intensity noted at a specific temperature of the peak as a proxy. The result is plotted as inset (ii) to Fig. 9(a). The intensity decreases consistently with illumination time showing that peak II also acts as a donor. Thus a portion of electrons released optically from deeper electron traps that would have ended up at this electron trap are instead trapped at peak I when the sample is preheated to 140 °C.

Since the additional electrons causing the change for peak III must be from levels IV and V, it is instructive to examine the change of intensity of peaks IV and V with illumination time. This is practical only for peak IV and is shown in Fig. 9(b) for measurements corresponding to preheating to 250, 140 and 100 °C. The margins of error on data points are determined by Poisson statistics for random counts. Without any light exposure, the intensity of peak IV would remain unchanged with re-measurement. However, if the only relevant effect is optical stimulation of electrons from level IV, the intensity should decrease, if not approximately exponentially then consistently. Fig. 9(b) (solid

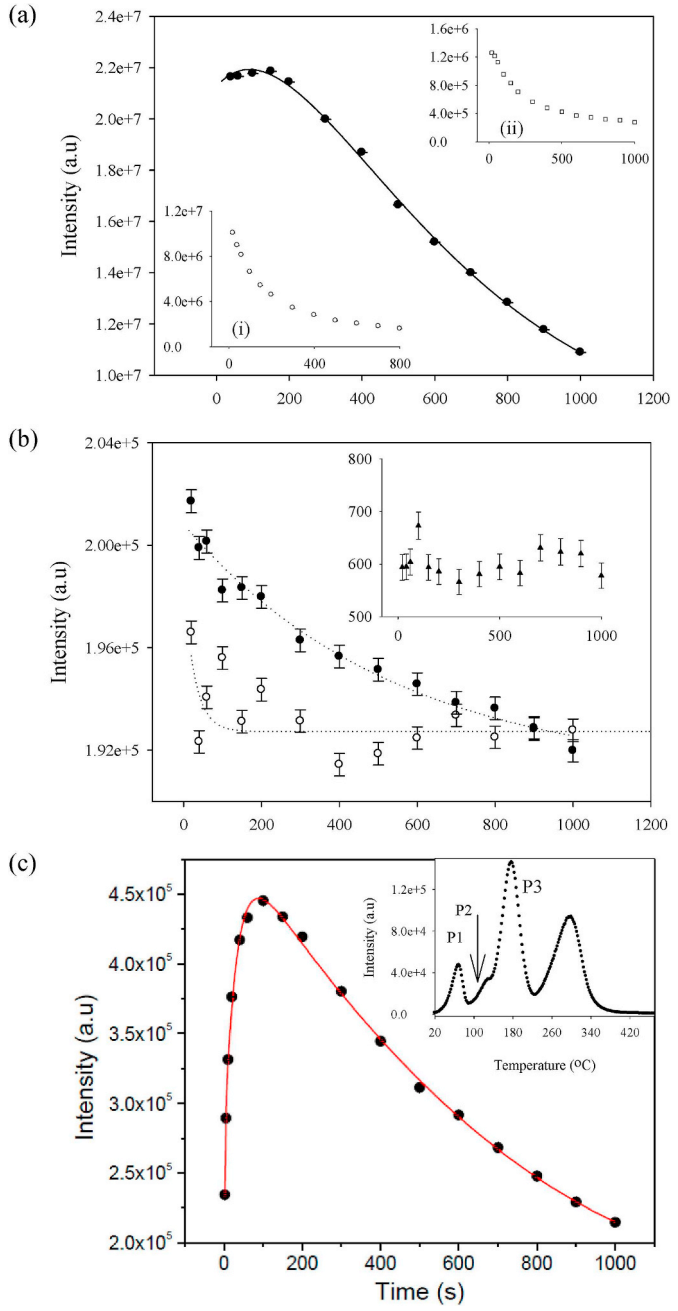

Fig. 9. The time dependence of PTTL intensity for peak III displaying competition effects when the sample is preheated to 140 °C (a) The insets are for donors level I (i) and level II (ii). The change with time of the intensity of peak IV (b) after preheating to 250 °C (open circles), 140 °C (solid symbols) and in the inset, to 100 °C. The line through data is the best fit of Eq. (21). The time dependence of PTTL for peak P1 after preheating to 140 °C shown fitted with Eq. (23) (c). The inset shows a glow curve measured after preheating to 250 °C and illumination for 60 s.

circles) shows the time dependence of intensity for peak IV corresponding to preheating to 140 °C. The intensity decreases but slower than expected. This implies that while level IV acts as a donor, it also captures some of the charge released from level IV. Therefore, the transport of charge causing the observed behaviour for peak III (solid), taking into account the competition effect can be written as

$$\frac{dN_5}{dt} = -f_5 N_5. \tag{18}$$

$$\frac{dN_4}{dt} = -f_4 N_4 + \gamma_5 f_5 N_5. \tag{19}$$

$$\frac{dN_3}{dt} = -f_3 N_3 + \delta_4 f_4 N_4 + \delta_5 f_5 N_5. \tag{20}$$

Eq (18) describes the optical removal of electrons from the deep trap. Eq (19) describes the loss of charge at level IV during illumination and competitive capture of some electrons from the deep trap. The first term in Eq. (20) accounts for the loss of electrons from the acceptor (level III) during illumination. The second and third terms reflect the fact that a portion of electrons released from levels IV and V are captured at level III. The solution of the coupled set (18)–(20), giving the time dependence of the intensity of peak III owing to optical illumination is

$$N_3 = E\left(e^{-f_5 t} - e^{-f_3 t}\right) - F\left(e^{-f_4 t} - e^{-f_3 t}\right) + G\left(e^{-f_5 t} - e^{-f_3 t}\right) \tag{21}$$

where $E = \delta_4 f_4 \gamma_5 N_{5i}/(f_4 - f_5)$, $F = \delta_4 f_4 \gamma_5 N_{5i}/(f_3 - f_4)$, and $G = \delta_5 f_5 N_{5i}/(f_3 - f_5)$. The solid line through data for peak III in Fig. 9(a) is the best fit of Eq. (21) showing that the model correctly describes the experimental results.

It is now instructive to consider the case of peak P1, the only one reproduced under phototransfer when the sample is preheated to 140 °C although both peaks I and II are removed by this preheating. Level I is the acceptor whereas levels IV and V act as donors. In this case, the system comprises one acceptor and three donors. In describing the phototransfer for peak I, the question of whether competition effects at the donors are relevant arises. If the competition effects are included in the model, the time-dependence of the electron concentration at level I is

$$N_1 = e^{-f_1 t} \int \sum_{j=3}^{5} (\Gamma_j s_j N_j) e^{f_1 t} dt + c\, e^{-f_1 t} \tag{22}$$

where for each option Γ_j is the constant of proportionality, f_j is the probability of stimulation, N_j the occupancy at the jth electron trap and c is the integration constant. The particular solution here is extensive and elaborate. Thus we advance the *ansatz* that competition effects are important only for peak III. Treating levels III and IV as ordinary donors we obtain for peak I

$$N_1 = A^{*'}\left(e^{-f_3 t} - e^{-f_1 t}\right) + B^{*'}\left(e^{-f_4 t} - e^{-f_1 t}\right) + C^{*'}\left(e^{-f_5 t} - e^{-f_1 t}\right) \tag{23}$$

where $A^{*'} = \frac{\gamma_3^* f_3 N_{3i}}{f_1 - f_3}$, $B^{*'} = \frac{\gamma_4^* f_4 N_{4i}}{f_1 - f_4}$, $C' = \frac{\gamma_5 f_5 N_{5i}}{f_1 - f_5}$; γ_3^* and γ_4^* are constants of proportionality. The best fit of Eq. (23) for a system of three donors one acceptor (level I) is shown in Fig. 9(c). The expression satisfactorily describes the time evolution profile of the intensity in this case.

Fig. 9(c) inset) shows a glow curve measured after preheating to 250 °C and illumination for 60 s. Peaks I, II and III are reproduced under phototransfer and are shown as P1, P2 and P3. Of these, the third not the first peak, is the most intense in contrast to Fig. 1 where the reverse is true. This is consistent with Fig. 9(a) which showed that the electron trap for peak III is an effective competitor for photostimulated electrons.

9. A kinetic description of PTTL preparatory to simulation

The discussion thus far has presented PTTL in terms of transfer of a portion of electrons from a donor to an acceptor. As an alternative method, charge transport leading to PTTL can also be described by sets of rate equations where the change of the concentration of electrons at the acceptor and donor electron traps takes into account the rate of electron flow through the conduction band. As an example, the transport of electrons for a system of, say, one acceptor and three donors can be written as

$$\frac{dn_{d1}}{dt} = -f_{d1} n_{d1} + n_c (N_{d1} - n_{d1}) A_{d1} \tag{24}$$

$$\frac{dn_{d2}}{dt} = -f_{d2}n_{d2} + n_c(N_{d2} - n_{d2})A_{d2} \quad (25)$$

$$\frac{dn_{d3}}{dt} = -f_{d3}n_{d3} + n_c(N_{d3} - n_{d3})A_{d3} \quad (26)$$

$$\frac{dn_c}{dt} = \sum f_{di}n_{di} - \sum n_{di}(N_{di} - n_{di})A_{di} - A_m m n_c \quad (27)$$

$$I_{PTTL} = \frac{dm}{dt} = -A_m m n_c \quad (28)$$

where N_{di} is the concentration of the ith electron trap, n_{di} the electron concentration at the ith electron traps, A_j the corresponding recombination probability and A_m the recombination probability at the recombination centre. Eq (24)–(26) describe the optical induced loss and, retrapping of electrons at donor levels. Eq. (27) is concerned with the electron flow through the conduction band whereas Eq. (28) describes the PTTL intensity. This is a set of non-linear coupled differential equations. The sets can also be written at the irradiation or heating stages. Such equations do not have analytical solutions and require computational simulation to approximate a solution whose form, under certain assumptions, produces the closest match between model and experimental data. This report is not concerned with this method.

10. Form of solutions

The PTTL in this work is modelled on the basis of coupled first order differential equations. It is important to address the question of whether the formulations may be described in terms of a general solution. Our method depends on experimental results because for each acceptor, the equations are formulated as informed by experiment. While some equations reflect competition effects, this is irrelevant in other cases. The time-dependence of the concentration N_k of electrons at the k^{th} acceptor can be written compactly as

$$N_k = e^{-\int R_j dt} \int (\sum \Phi_i(t)) e^{\int R_j dt} dt + c e^{-\int R_j dt} \quad (29)$$

where c is a constant of integration, R_j is the coefficient of N_k in its rate equation. The function $\Phi_i(t)$ for the charge movement at each donor is determined by experiment and must be solved for that donor and is a pre-requisite for the integration in Eq. (29). The functions $\Phi_i(t)$ are not identical because the role and contribution of donors are never so. In physical terms, electron traps acting as donors are point defects and cannot be expected to respond in an identical manner during the PTTL process for each and every material. The constant c can always be found because the initial values for each set are known. Therefore Eq. (29) cannot be applied to experimental data as is. Since Eq. (29) expresses an initial value problem, its solution is a particular not a general solution. In summary, the time-dependent evolution of PTTL cannot be represented by one general solution that describes any type of experimental behaviour for any material.

11. Summary

Phototransferred thermoluminescence (PTTL) involving multiple acceptors and donors in natural quartz has been reported. A glow curve measured at 1 °C s^{-1} following irradiation to 300 Gy has four peaks denoted I–IV. The peaks are reproduced under phototransfer only for certain preheating temperatures. Indeed peak II does not re-appear after any preheating beyond 250 °C and peak IV is not reproduced at all. The behaviour exemplifies often ignored competition effects in phototransfer. A clear instance of this is when the intensity of peak III, when as a donor, goes through a peak rather than decrease consistently as would be expected. The time evolution profiles and competition effects have been described using coupled first-order linear differential equations on the basis of systems of acceptors and donors whose number depends on the preheating temperature.

Acknowledgements

We acknowledge with gratitude financial support from Rhodes University and the National Research Foundation of South Africa.

Appendix A. Supplementary data

Supplementary data to this article can be found online at https://doi.org/10.1016/j.jlumin.2019.116730.

References

[1] F. Preusser, M.L. Chithambo, T. Götte, M. Martini, K. Ramseyer, E.J. Sendezera, G.J. Susino, A.G. Wintle, Earth Sci. Rev. 97 (2009) 196–226.
[2] A.J.J. Bos, High sensitivity thermoluminescence dosimetry, Nucl. Instrum. Meth. B. 184 (2001) 3–28.
[3] S.W.S. McKeever, Thermoluminescence of Solids, Cambridge University Press. Cambridge University Press, 1985.
[4] R. Chen, S.W.S. McKeever, Theory of Thermoluminescence and Related Phenomena, World Scientific, 1997.
[5] V. Pagonis, G. Kitis, C. Furetta, Numerical and Practical Exercises in Thermoluminescence, Springer, 2006.
[6] C.S. Alexander, M.F. Morris, S.W.S. McKeever, Radiat. Meas. 27 (1997) 153–159.
[7] L.E. Colyott, M.S. Akselrod, S.W.S. McKeever, Radiat. Prot. Dosim. 65 (1996) 263–266.
[8] I. Milanovich-Reichhalter, N. Vana, Radiat. Prot. Dosim. 33 (1990) 211–213.
[9] I.K. Bailiff, S.G.E. Bowman, S.F. Mobbs, M.J. Aitken, J. Electron. 3 (1977) 269–280.
[10] P. G. Benny, B. C. Bhatt, 56 (2002) 891 – 894.
[11] M. Schlesinger, J. Phys. Chem. Solids 26 (1965) 1761.
[12] M.J. Aitken, An Introduction to Optical Dating, OUP, Oxford, 1998.
[13] N.A. Spooner, Radiat. Meas. 23 (1994) 593–600.
[14] B.W. Smith, M.J. Aitken, E.J. Rhodes, P.D. Robinson, D.M. Geldard, Radiat. Prot. Dosim. 17 (1986) 229–233.
[15] A.G. Wintle, A.S. Murray, Radiat. Meas. 27 (1998) 611–624.
[16] A.J.J. Santos, J.F. de Lima, M.E.G. Valerio, Radiat. Meas. 33 (2001) 427–430.
[17] I. Milanovich-Reichhalter, N. Vana, Nucl. Tracks Radiat. Meas. 18 (1991) 67–69.
[18] M. Bertucci, I. Veronese, M.C. Cantone, Radiat. Meas. 46 (2011) 588–590.
[19] M.F. Morris, S.W.S. McKeever, Radiat. Meas. 23 (1994) 323–327.
[20] C.S. Alexander, S.W.S. McKeever, J. Phys. Appl. Phys. 31 (1998) 2908.
[21] M. Moscovitch, AIP Conference Proceedings, vol. 1345, 2011, pp. 323–334.
[22] M.L. Chithambo, C. Seneza, J.M. Kalita, Radiat. Meas. 105 (2017) 7–16.
[23] C.D. Gribble, Rutley's Elements of Mineralogy, Unwin Hyman Ltd., London, UK, 1988.
[24] L. Bøtter-Jensen, S.W.S. McKeever, A.G. Wintle, Optically Stimulated Luminescence Dosimetry, Elsevier, Amsterdam, 2003.
[25] R.B. Galloway, Radiat. Meas. 35 (2002) 67–77.
[26] M.L. Chithambo, F.O. Ogundare, Radiat. Meas. 44 (2009) 453–457.
[27] M.L. Chithambo, An Introduction to Time-Resolved Optically Stimulated Luminescence, Morgan & Claypool Publishers, Bristol, 2018.
[28] V. Pagonis, M.L. Chithambo, R. Chen, A. Chruścińska, M. Fasoli, S.H. Li, M. Martini, K. Ramseyer, J. Lumin. 145 (2014) 38–48.
[29] M.L. Chithambo, J. Phys. Appl. Phys. 40 (2007) 1880–1889.
[30] M.L. Chithambo, P. Niyonzima, J.M. Kalita, J. Lumin. 198 (2018) 146–154.
[31] E. Bulur, H.Y. Göksu, Radiat. Meas. 30 (1999) 203–206.
[32] J.M. Kalita, M.L. Chithambo, J. Lumin. 188 (2017) 371–377.

Radiation Measurements 120 (2018) 53–58

Contents lists available at ScienceDirect

Radiation Measurements

journal homepage: www.elsevier.com/locate/radmeas

Influence of annealing on thermoluminescence of natural quartz: Kinetic analysis and experimental study of apparent inverse thermal quenching

D.E. Folley, M.L. Chithambo*

Department of Physics and Electronics, Rhodes University, P.O. Box 94, Grahamstown 6140, South Africa

ARTICLE INFO

Keywords:
Thermoluminescence
Natural quartz
Annealing
Thermal quenching

ABSTRACT

The influence of annealing on the main thermoluminescence glow-peak of natural quartz is reported. For comparison, results from un-annealed quartz are included. The glow-curve measured at 1 °Cs^{-1} after beta irradiation to 50 Gy revealed six peaks each for quartz annealed at 800 °C for 1 h and the un-annealed sample. The main peak in both quartzes was observed at 72 °C. This report focusses on kinetic analysis of the main peak. The analysis was carried out using various methods consisting of the initial rise, whole glow-peak, peak shape, variable heating rate and phosphorescence-based methods. The activation energy obtained using the various methods ranges between 0.91 ± 0.01 eV and 1.19 ± 0.03 eV for the annealed sample and between 0.93 ± 0.01 eV and 1.26 ± 0.12 eV for the un-annealed sample. The result suggests that annealing has little effect on the activation energy. The luminescence intensity decreased with heating rate in the un-annealed sample in a manner suggestive of thermal quenching. In contrast, the dependence of intensity on heating rate in the annealed sample is influenced by the dose the sample is irradiated to. Whereas thermal quenching was noted for a dose of 50 Gy in the un-annealed sample, the annealed sample showed evidence of thermal quenching at a low dose of 3 Gy with the opposite effect when irradiated to 50 Gy. The activation energies of thermal quenching were found as 0.89 ± 0.06 eV and 0.99 ± 0.02 eV for the un-annealed and annealed samples respectively. We ascribe the apparent dependence of thermal quenching on dose in the annealed sample to competition between radiative and non-radiative transitions at the recombination centre.

1. Introduction

The use of natural quartz in dosimetry-related research using electron spin resonance (ESR), optically stimulated luminescence (OSL) and thermoluminescence (TL) is well documented (Preusser et al., 2009). One objective of thermoluminescence is to analyse data extracted from experimental glow-curves in order to obtain values for various parameters associated with charge transfer in the material under study. These parameters include the trap depth or activation energy, frequency factor, capture cross sections and the densities of various traps and recombination centres involved in the TL emission (McKeever, 1985). However, there are for quartz widely different values of trap parameters reported in the literature with the differences attributed to origin of quartz, impurity content and the methods used to derive the parameters (Mebhah et al., 2006).

The luminescence sensitivity of natural quartz is significantly enhanced if heated beyond its first and second crystal phase transitions prior to irradiation (Schilles et al., 2001). In his work, Chithambo (2003) explained that there is no evidence that annealing affects the physical processes of luminescence even though it enhances the sensitivity. The influence of annealing on thermoluminescence kinetics is therefore the motivation for this study of natural quartz.

The aim of this work is to carry out comparative kinetic analysis of thermoluminescence in annealed and un-annealed natural quartz as part of a study on mechanisms of luminescence. The study also includes a study of non-radiative transitions in both materials and addresses the question of apparent inverse quenching. The analysis was carried out on the most prominent peak only.

2. Experimental details

Samples used consisted of commercially available natural quartz (BDH Ltd., UK) some of which was annealed at 800 °C for 1 h and another portion left un-annealed. The same quartz has been used previously (Chithambo, 2003; Galloway, 2002). The quartz was annealed prior to use to improve its sensitivity and to remove any residual luminescence. Experiments were performed using a RISØ TL/OSL DA-20 Luminescence Reader. The luminescence was detected by an EMI

* Corresponding author.
E-mail address: m.chithambo@ru.ac.za (M.L. Chithambo).

https://doi.org/10.1016/j.radmeas.2018.04.010
Received 23 November 2017; Received in revised form 7 April 2018; Accepted 16 April 2018
Available online 17 April 2018

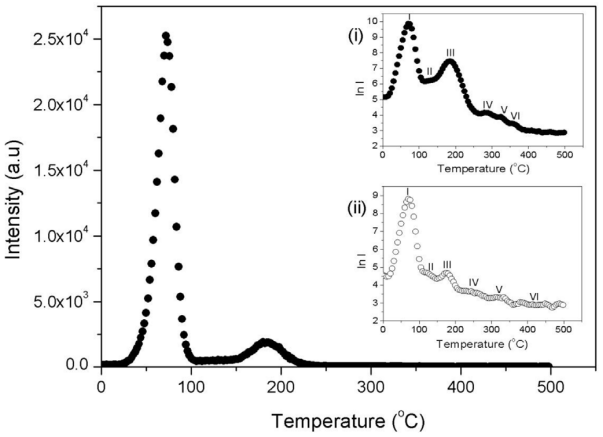

Fig. 1. A glow-curve of the annealed natural quartz measured at 1°Cs^{-1} following a dose of 50 Gy. The insets show the glow-curves of the (i) annealed, and (ii) un-annealed sample in a semi-logarithmic scale.

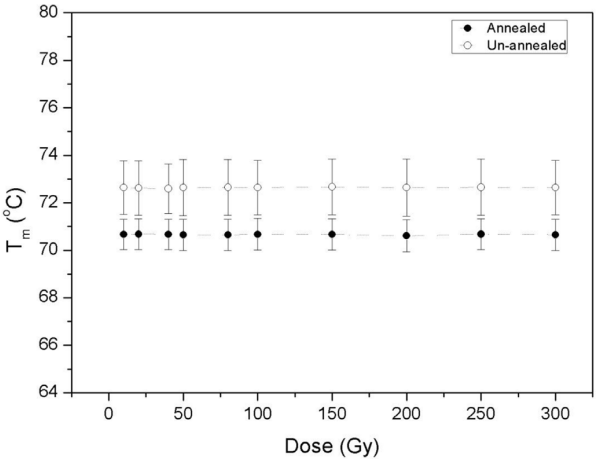

Fig. 2. Plots of T_m against dose. Each data point is an average of three measurements and the margin of error in T_m is the standard deviation of the set. The dotted line through the data points is only a visual guide.

9235QB photomultiplier tube through a 7 mm Hoya U-340 filter. Samples were irradiated at room temperature using a ^{90}Sr/^{90}Y β source at a rate of 0.10 Gys^{-1}. All measurements were carried out at a heating rate of 1°Cs^{-1} unless otherwise described.

3. General characteristics of glow-curves

Fig. 1 shows a glow-curve of the annealed quartz after irradiation to 50 Gy. The inset (i) shows the same glow-curve on a semi-logarithmic scale to better show presence of other peaks. For comparison, the glow-curve for the un-annealed sample is shown in inset (ii). The glow-curve of the annealed and un-annealed samples each consists of six peaks. The main peak (labelled I) in both cases is at 72 °C. The secondary peaks of the annealed quartz are at 120 °C, 182 °C, 282 °C, 334 °C and 364 °C whereas in the un-annealed sample, these are at 126 °C, 174 °C, 254 °C, 330 °C and 418 °C. The peaks are labelled II, III, IV, V and VI respectively as shown.

3.1. Assessing the order of kinetics for peak I

3.1.1. T_m-T_{stop} method

Using the T_m - T_{stop} method (McKeever, 1985), the position of the main peak (peak I) was determined to be independent of T_{stop} at 72.0 ± 0.1 °C for the annealed sample and at 72.5 ± 0.4 °C for the un-annealed one. Measurements were made for samples irradiated to 50 Gy. The results show that peak I is single and follows first-order kinetics.

3.1.2. Dose dependence of peak position

The order of kinetics of the main peak was further assessed using the dependence of peak position T_m on dose. Fig. 2 shows a plot of T_m against dose for doses between 10 and 300 Gy. T_m is independent of dose in both cases confirming that peak I is of first order kinetics.

3.2. Kinetic analysis

Kinetic analysis was carried out on the main peak using the initial rise, whole glow-peak, peak shape, variable heating rate, curve fitting, and phosphorescence-based methods. Multiple methods were used in evaluating the kinetic parameters in order to ascertain consistency in results.

3.2.1. Initial rise method

The initial rise method is applicable to the rising edge of a glow-peak whose intensity I and measurement temperature T are related as

$$I\,(T) = C' \exp\left(-\frac{E}{kT}\right) \tag{1}$$

where E is the activation energy, k is Boltzmann's constant, and C' is a constant. The method was applied on peak I giving $E = 0.91 \pm 0.01$ eV and $E = 0.93 \pm 0.03$ eV for the annealed and un-annealed samples respectively. The values are consistent suggesting that annealing has little effect on the activation energy. The value of E for the annealed quartz is in satisfactory agreement with 0.94 ± 0.02 eV reported by Chithambo (2014) for the same quartz but annealed at 800 °C for 10 min.

3.2.2. Whole glow-peak method

The second method used was the whole glow-peak method where the area under the whole glow-peak is related to the order of kinetics by

$$ln\left(\frac{I}{n^b}\right) = ln\left(\frac{s'}{\beta}\right) - \frac{E}{kT} \tag{2}$$

where s' (cm$^{3(b-1)}$ s^{-1}) is the effective frequency factor for general order kinetics, n is the area under the glow peak, b represents the order of kinetics, β is the heating rate and other parameters are as previously defined (Pagonis et al., 2006). A plot of $\ln(I/n^b)$ against $1/kT$ for a specific value of b should be linear, from which E can be evaluated from the slope and s' from the 'y' intercept. Fig. 3 shows the semi-logarithmic plot of (I/n^b) against $1/kT$ for different values of b. The best choice is for $b = 1.2$ ($R^2 = 0.999$) for the annealed sample. For the un-annealed sample (graph omitted), $b = 1.1$. The activation energy and frequency factor were evaluated as $E = 1.10 \pm 0.01$ eV and $s' = 8.5 \times 10^{13}$ s^{-1} respectively for the annealed sample. In comparison, values for the un-annealed sample were obtained as $E = 0.980 \pm 0.005$ eV and $s' = 8.9 \times 10^{12}$ s^{-1}.

3.2.3. Peak shape method

In order to further ascertain the kinetic parameters E, s and b of the glow-peak, the peak shape method introduced by Chen (1969) was used. Here

$$E_\alpha = c_\alpha\left(\frac{kT_M^2}{\alpha}\right) - b_\alpha(2kT_M) \tag{3}$$

where α represents any of τ (the half-width at the low temperature side of the peak) or δ (the half-width at the fall off side of the glow peak) or ω (total half-width). The values of c_α and b_α are listed elsewhere

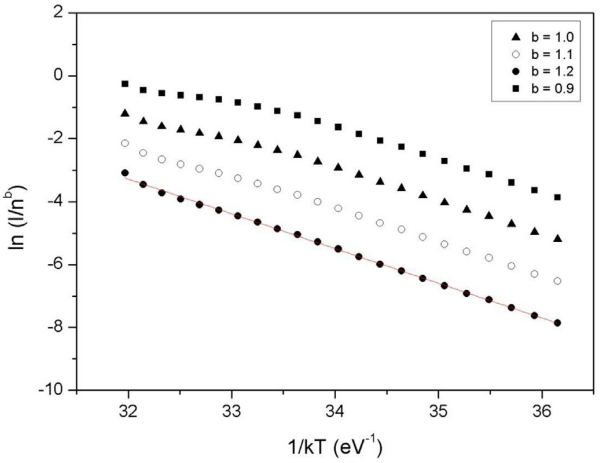

Fig. 3. A plot of $\ln(I/n^b)$ against $1/kT$ for different values of b.

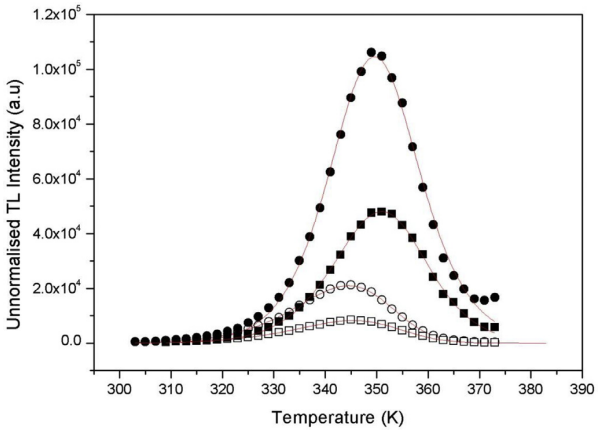

Fig. 4. Result of curve fitting for the main peak for the un-annealed sample (squares) and the annealed quartz (circles). The solid symbols represent same data corrected for thermal quenching. The solid lines are the best fits of Eq. (4).

(McKeever, 1985). The order of kinetics of the glow-peak depends on the geometrical factor μ which is equal to δ/ω. A peak is of first-order kinetics if μ = 0.42 and of second order if μ = 0.52. In this work, μ was calculated to be 0.42 ± 0.07 and 0.45 ± 0.07 for the annealed and un-annealed samples respectively. These μ-values suggest that the peak is of first-order kinetics and agree with the conclusions from the T_m-T_{stop} and whole glow-peak methods. The values of the activation energy were calculated as $E_\tau = 1.14 \pm 0.13$ eV, $E_\delta = 1.09 \pm 0.12$ eV, $E_\omega = 1.13 \pm 0.12$ eV for the annealed sample and $E_\tau = 1.26 \pm 0.13$ eV, $E_\delta = 1.23 \pm 0.13$ eV, $E_\omega = 1.26 \pm 0.12$ eV for the un-annealed sample. Although these values are necessarily dependent on τ, δ, ω, they are consistent for each sample. The E values of the annealed sample obtained using this method compare well with 1.10 ± 0.01 eV from the whole glow-peak method.

3.2.4. Curve fitting method

Kinetic analysis was also done by curve fitting using Kitis' general order equation (Kitis, 2001)

$$I(T) = I_m b^{\frac{b}{b-1}} exp(u)\left[(b-1)(1-\Delta)\frac{T^2}{T_m^2}exp(u) + Z_m\right]^{-\frac{b}{b-1}} \quad (4)$$

where I_m is the maximum peak intensity, $u = E(T - T_m)/kTT_m$, $\Delta = 2kT/E$, $\Delta_m = 2kT_m/E$, $Z_m = 1 + (b-1)\Delta_m$, and other parameters are as previously defined. The goodness of fit was tested by the Figure of Merit (FOM) proposed by Balian and Eddy (1977) which is defined as

$$\text{FOM}\ (\%) = \frac{\sum_p |y_{exp} - y_{fit}|}{A} \times 100\% \quad (5)$$

where y_{exp} and y_{fit} are the data for the experimental and the fitted glow-peaks respectively and A is the area of the fitted glow-peak. A fit is acceptable if $FOM \leq 3.5\%$ (Gartia and Singh, 2011).

Fig. 4 shows fits for the annealed quartz (open circles) from which $E = 1.17 \pm 0.02$ eV, $b = 1.20 \pm 0.03$, $s = 1.5 \times 10^{16}$ s^{-1}. For the un-annealed quartz (open squares) the values were $E = 1.08 \pm 0.01$ eV, $b = 1.17 \pm 0.02$, and $s = 6.1 \times 10^{14}$ s^{-1}. In both cases FOM ≤ 0.42%.

3.2.5. Variable heating rate method

In the variable heating rate method, the peak position T_m and heating rate β are related as

$$ln\left(\frac{T_m^2}{\beta}\right) = \left(\frac{E}{k}\right)\frac{1}{T_m} + ln\left(\frac{E}{sk}\right) \quad (6)$$

The kinetic parameters E and s can therefore be estimated from the gradient and intercept of the plot of Eq. (6) respectively. In this work, three different measurements were made on the quartz samples irradiated to 50 Gy using heating rates from 0.2 to 5.0 °Cs^{-1}. The analysis was done on peak I. The average values of the activation energy and frequency factor were found to be 0.81 ± 0.01 eV and 6.3×10^{10} s^{-1} respectively for the annealed quartz and 0.762 ± 0.007 eV and $7.7 \times 10^9 s^{-1}$ respectively for the un-annealed quartz. The VHR method seems to underestimate the value of E for the un-annealed sample. Pagonis et al. (2013) have also shown that the VHR method can systematically underestimate the value of the activation energy.

4. Kinetic analysis using phosphorescence

Further analysis used phosphorescence, the decay of thermoluminescence as a function of time at a constant temperature. Two methods were used, one based on change of intensity with time (McKeever, 1985) and the second one based on change of the area under an isothermal decay curve with measurement temperature (Chithambo, 2014).

4.1. Analysis of phosphorescence based on first order kinetics

For first order kinetics, the intensity I is given by $I(t) = I_0 \exp(-pt)$ where t is time, I_0 is the initial intensity and p is the probability of thermal simulation given by

$$p = s\ exp(-E/kT) \quad (7)$$

Measurements were made at different temperatures between 40 and 62 °C. Eq. (7) was used to obtain the activation energy and frequency factor by using the relation $\ln p = -\left(\frac{E}{kT_i}\right) + \ln s$. Fig. 5 shows a plot of $ln\ p$ against $1/kT_i$ for measurements made at various temperatures T_i for a sample irradiated to 50 Gy. The activation energy for the annealed quartz was found to be 1.03 ± 0.01 eV and the frequency factor as 1.1×10^{14} s^{-1}. In comparison, for the un-annealed quartz $E = 1.04 \pm 0.03$ eV and $s = 2.0 \times 10^{14}$ s^{-1}. It is thus still evident that annealing has little effect on E and s values of peak I.

4.2. Analysis of phosphorescence based on general order kinetics

The general order kinetics of phosphorescence based on the expression

$$I^{(1-b)/b} = 1 + n_0^{b-1}(b-1)s'exp(-E/kT)t \quad (8)$$

(McKeever, 1985) was used to examine the order of kinetics and activation energy by plotting $I^{(1-b)/b}$ against t. Plots of $\ln[(b-1)n_0^{b-1}s']$

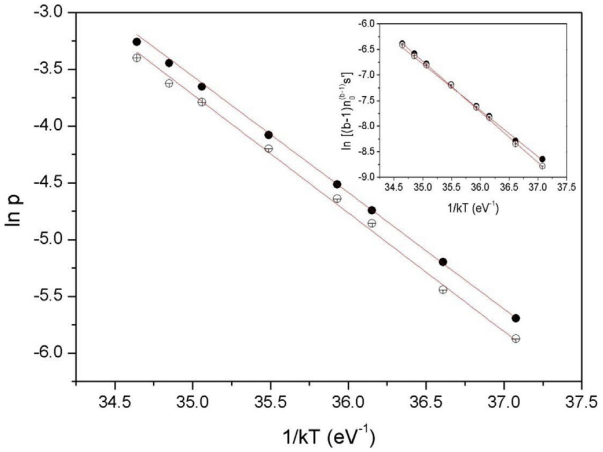

Fig. 5. A graph of $ln\ p$ against $1/kT$ to evaluate the activation energy for phosphorescence based on first order kinetics. The inset shows the plots for general order kinetics of phosphorescence.

against $1/kT_i$ are shown in the inset to Fig. 5 where $b = 1.1$ for both quartzes. The activation energy and frequency factor were evaluated as 0.91 ± 0.03 eV and 7.0×10^{10} s^{-1} respectively for the annealed quartz. For the un-annealed quartz, the values were 0.99 ± 0.02 eV and 1.3×10^{12} s^{-1} respectively. The E values from this method compare well with those from the initial rise and whole glow-peak methods.

4.3. Analysis of phosphorescence using the area under its isothermal decay curve

The area-based phosphorescence method developed by Chithambo (2014) was applied on isothermal decay curves. The method, which relies on the temperature-dependence of the area under the isothermal decay curve, is most suitable for first-order kinetics. The area requires only a small portion of the decay curve and is governed by

$$\Phi = B \exp(-E/kT) \quad (9)$$

where B is a constant and Φ is the area underneath a brief segment of an isothermal decay curve and all other parameters are as defined before.

Phosphorescence was measured for 5 s at temperatures between 30 and 58 °C after irradiation to 50 Gy. The area Φ was determined at each temperature. Fig. 6 shows a plot of $ln\ \Phi$ against $1/kT$ for the annealed

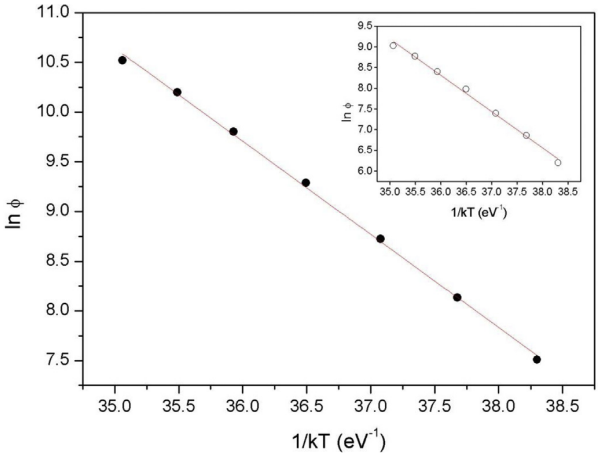

Fig. 6. A plot of $ln\ \Phi$ against $1/kT$ for the annealed quartz the inset shows the plot for the un-annealed sample.

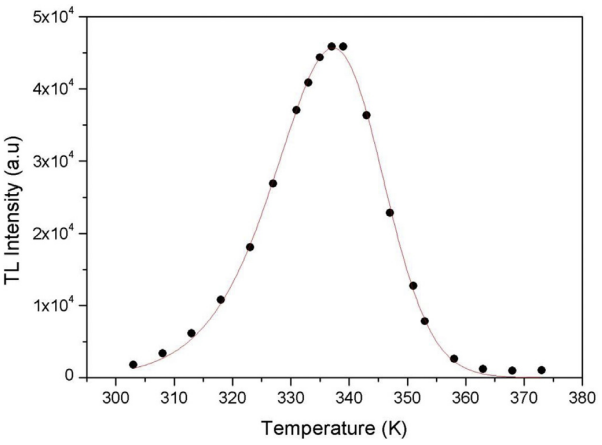

Fig. 7. The temperature dependence of the area under the isothermal decay curve in the annealed sample for 5 s. The solid line is the best fit of Eq. (4).

sample. The activation energy obtained from this plot is 0.91 ± 0.02 eV. This value is consistent with the values obtained from the initial rise and general-order phosphorescence methods. The inset shows the corresponding plot for the un-annealed quartz. The activation energy in this case was evaluated as 0.88 ± 0.03 eV in satisfactory agreement with the result of the annealed sample.

4.4. Analysis of the temperature-dependent areas by curve fitting

When Φ (termed intensity in this section) is plotted against temperature, it produces a TL-like glow-peak. This curve can then be analysed using Eq. (4). The basis of this method is given by Chithambo (2014). Fig. 7 shows the curve fitting from which E, b, s, and FOM for the annealed sample were found to be 1.19 ± 0.03 eV, 1.30 ± 0.05, 6.4×10^{16} s^{-1}, and 0.25% respectively. The E value here agrees with 1.17 ± 0.02 eV recorded earlier from the curve fitting method. For the un-annealed sample, the values were $E = 0.98 \pm 0.02$ eV, $b = 1.10 \pm 0.03$, $s = 3.3 \times 10^{13}$ s^{-1}, and $FOM = 0.17\%$. The E values for both samples suggest that annealing has little effect on the trap depth.

5. Thermal quenching

It has been shown in previous studies based on luminescence lifetimes that thermal quenching in quartz annealed at some temperatures e.g. 1000 °C is manifested in an unusual manner e.g. (Chithambo, 2015) whereas in quartz annealed up to 500 °C, the distribution of lifetimes with measurement temperature follows the usual Mott-Seitz behaviour. The aim of the study reported here was to explore the analysis of thermal quenching in quartz annealed at 800 °C using different TL-related methods. Thermal quenching was studied using the dependence of TL intensity on heating rate (Pagonis et al., 2006) and by the influence of measurement temperature on the area under an isothermal decay curve (Chithambo, 2014).

Fig. 8 shows the dependence of TL intensity (in counts/°C) on heating rate for the annealed sample irradiated to 50 Gy. The TL intensity increases monotonically with heating rate. This would indicate that the sample is not affected by thermal quenching. Repeated measurements on fresh aliquots gave a similar result. In comparison, the TL intensity decreased with heating rate in an un-annealed quartz irradiated to 50 Gy.

In order to examine any thermal quenching, the principle that luminescence emission is subject to competing radiative and non-radiative routes as applied on a secondary peak in α-Al_2O_3:C (Chithambo and Costin, 2017) was considered. In this case, the description of

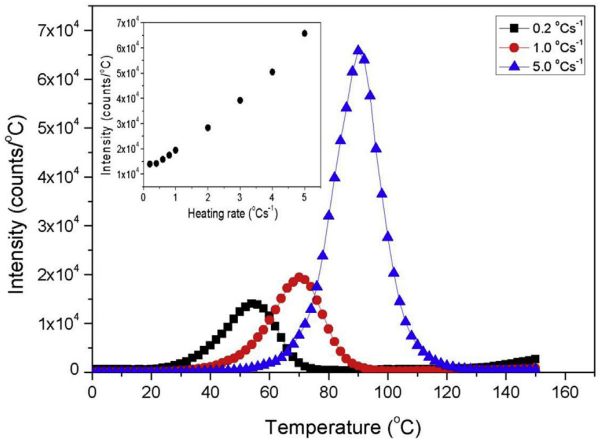

Fig. 8. Examples of TL glow-curves measured at different heating rates. The inset shows the dependence of intensity on heating rate.

luminescence is expressed as

$$\frac{1}{\tau} = \frac{1}{\tau_{rad}} + \frac{1}{\tau_{th}} exp\left(-\frac{\Delta E}{kT}\right) \tag{10}$$

where $1/\tau_{rad}$ is the probability of radiative emission which is independent of temperature whereas $1/\tau_{th}$ is the probability of thermal excitation and ΔE is the activation energy of thermal quenching (Agulló-López et al., 1988). As Chithambo and Costin (2017) point out, if the number of electrons undergoing transitions at the recombination centre is very low, the radiative transitions cannot be high enough to ameliorate against the non-radiative route. This fact can be used as an independent test for presence of any thermal quenching. This test was applied on the annealed quartz by considerably reducing the dose used from 50 to 3 Gy.

Fig. 9 shows the new effect of heating rate on TL intensity from the sample irradiated to 3 Gy. The TL intensity (in counts/°C) as well as the peak integral now decreases significantly with heating rate in a behaviour consistent with thermal quenching. Thus, the increase of TL intensity with heating rate cannot on its own be proof that a sample is not affected by thermal quenching.

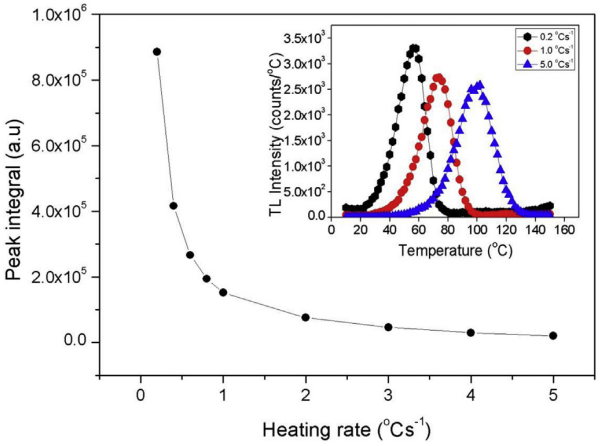

Fig. 9. A plot of peak integral against heating rate for the annealed sample irradiated to 3 Gy.

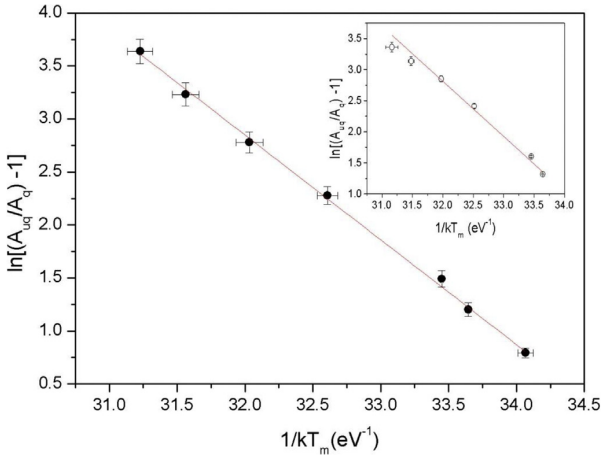

Fig. 10. A graph of $ln\,[(A_{uq}/A_q) - 1]$ against $1/kT_m$ for the annealed sample irradiated to 3 Gy. The inset shows the graph for the un-annealed sample irradiated to 50 Gy.

5.1. Analysis of thermal quenching using change of TL intensity with heating rate

The decrease of peak integral with heating rate can be expressed as

$$\frac{A_q}{A_{uq}} = \frac{1}{1 + C\ exp(-\Delta E/kT_m)} \tag{11}$$

where A_q and A_{uq} represent the most quenched and lesser quenched areas of the glow-peak measured at the highest and other heating rates respectively, C is a constant equal to the product of the frequency factor for non-radiative transitions and the radiative recombination lifetime (Chithambo, 2007). To determine ΔE, a graph of $ln[(A_{uq}/A_q) - 1]$ against $1/kT_m$ was plotted and is shown in Fig. 10. The activation energy, ΔE for the annealed sample for 3 Gy was evaluated as 0.99 ± 0.02 eV with $C = 9.3 \times 10^{14}$. For the un-annealed quartz (inset), ΔE was evaluated as 0.89 ± 0.06 eV with $C = 3.6 \times 10^{13}$. The ΔE values are in agreement with published values in the literature e.g. 0.79 ± 0.15 eV (Galloway, 2002).

5.2. Analysis of thermal quenching using the area under an isothermal decay-curve

As stated by Chithambo (2014), if a TL peak is affected by thermal quenching, then the area Φ_q under the isothermal decay-curve at a corresponding temperature T will be related to the unquenched ones Φ_u by definition as

$$\Phi_q = \frac{\Phi_u}{1 + C\ exp(-\Delta E/kT')} \tag{12}$$

In Eq. (12), Φ_q is defined as the area corresponding to the highest measurement temperature T'_q and Φ_u as areas corresponding to all other measurement temperatures T'_u in the rising edge of the graph of Φ against measurement temperature. Fig. 11 shows a graph of $ln(\Phi_q/\Phi_u)$ against $1/kT'$ for measurements made for 5 s. The value of the activation energy for thermal quenching determined from the slope of the graph is 0.96 ± 0.01 eV. This value is consistent with 0.99 ± 0.02 eV determined in Fig. 10 for an annealed sample irradiated to 3 Gy. For the un-annealed quartz (inset), the activation energy for thermal quenching was determined as 0.91 ± 0.02 eV for 5 s. This value is also consistent with 0.89 ± 0.06 eV evaluated in Fig. 10. An important conclusion from this study is that increase of TL intensity with heating rate, sometimes referred to as inverse thermal quenching e.g (Pagonis et al., 2013), does not necessarily imply the absence of thermal quenching. We have also

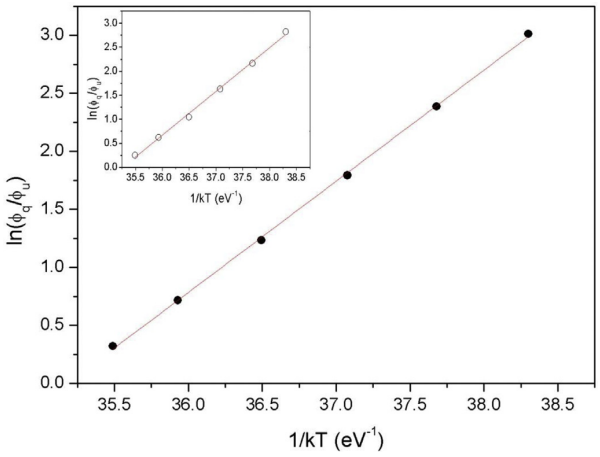

Fig. 11. A graph of $ln\ (\Phi_q/\Phi_u)$ against $1/kT$ in a study of thermal quenching using area under isothermal decay-curve in annealed quartz. The inset shows the plot for the un-annealed sample.

shown that with respect to thermal quenching, the method based on the area under an isothermal decay curve (Chithambo, 2014) is not influenced by the dose the sample is irradiated to unlike the conventional method based on change of TL intensity with heating rate.

Summary

The influence of annealing on thermoluminescence of natural quartz has been studied. The main TL glow-peak of the annealed and un-annealed natural quartz observed at 72 °C for both samples was studied using various methods of kinetic analysis. The peak in each case follows first order kinetics. The values of the trap depth of the annealed and un-annealed samples are consistent showing that annealing has little effect on the trap parameters of the glow-peak. However, the VHR method underestimates the value of the activation energy for both samples. The TL intensity (in counts/°C) of the annealed sample increased with heating rate for measurements corresponding to 50 Gy. This would imply that the sample is not affected by thermal quenching. However, when the same sample is irradiated to a significantly reduced dose of 3 Gy, the TL intensity decreases with heating rate showing presence of thermal quenching. We have demonstrated that as regards analysis for thermal quenching, the method based on the area under an isothermal decay curve (Chithambo, 2014) is not influenced by the dose unlike the conventional one based on change of TL intensity with heating rate.

Acknowledgements

The authors acknowledge with gratitude financial support from Rhodes University and the National Research Foundation, South Africa.

Appendix A. Supplementary data

Supplementary data related to this article can be found at http://dx.doi.org/10.1016/j.radmeas.2018.04.010.

References

Agulló-López, F., Catlow, C.R.A., Townsend, P.D., 1988. Point defects in Materials. Academic Press.
Balian, H.G., Eddy, N.W., 1977. Figure-of-merit (FOM), an improved criterion over the normalized chi-squared test for assessing goodness-of-fit of gamma-ray spectral peaks. Nucl. Instrum. Meth. 145, 389–395.
Chen, R., 1969. On the calculation of activation energies and frequency factors from glow curves. J. Appl. Phys. 40 (2), 570–585.
Chithambo, M.L., 2003. The influence of annealing and partial bleaching on luminescence lifetimes in quartz. Radiat. Meas. 37, 467–472.
Chithambo, M.L., 2007. The analysis of time-resolved optically stimulated luminescence: II. Computer simulations and experimental results. J. Phys. D Appl. Phys. 40, 1880–1889.
Chithambo, M.L., 2014. A method for kinetic analysis and study of thermal quenching in thermoluminescence based on use of the area under an isothermal decay-curve. J. Lumin. 151, 235–243.
Chithambo, M.L., 2015. Luminescence lifetimes in natural quartz annealed beyond its second phase inversion temperature. Radiat. Meas. 81, 198–204.
Chithambo, M.L., Costin, G., 2017. Temperature-dependence of time-resolved optically stimulated luminescence and composition heterogeneity of synthetic α-Al 2 O 3: C. J. Lumin. 182, 252–262.
Galloway, R.B., 2002. Luminescence lifetimes in quartz: dependence on annealing temperature prior to beta irradiation. Radiat. Meas. 35, 67–77.
Gartia, R.K., Singh, L.L., 2011. Evaluation of trapping parameter of quartz by deconvolution of the glow curves. Radiat. Meas. 46, 664–668.
Kitis, G., 2001. TL glow-curve deconvolution functions for various kinetics orders and continuous trap distribution: acceptance criteria for E and s values. J. Radioanal. Nucl. Chem. 3, 697–703.
McKeever, S.W.S., 1985. Thermoluminescence of Solids. Cambridge University Press.
Mebhah, D., Imatoukene, D., Abdelazziz, F.Z., Lounis-Mokrani, Z., 2006. Evaluation of trap parameters associated with thermoluminescence peaks in fired quartz. Radiat. Meas. 41, 813–818.
Pagonis, V., Blohm, L., Brengle, M., Mayonado, G., Woglam, P., 2013. Anomalous heating rate effect in Thermoluminescence intensity using a simplified semi-localized transition (SLT) model. Radiat. Meas. 51, 40–47.
Pagonis, V., Kitis, G., Furetta, C., 2006. Numerical and Practical Exercises in Thermoluminescence. Springer Science & Business Media.
Preusser, F., Chithambo, M.L., Götte, T., Martini, M., Ramseyer, K., Sendezera, E., Susino, G.J., Wintle, A.G., 2009. Quartz as a natural dosimeter. Earth Sci. Rev. 97, 184–214.
Schilles, T., Poolton, N., Bulur, E., Bøtter-Jensen, L., Murray, A., Smith, G., Riedi, P., Wagner, G., 2001. A multi-spectroscopic study of luminescence sensitivity changes in natural quartz induced by high-temperature annealing. J. Phys. D Appl. Phys. 34, 722.

Bibliography

F Agulló-López, CR Arthur Catlow, and PD Townsend. *Point defects in materials*. Academic press, 1988.

CS Alexander and SWS McKeever. Phototransferred thermoluminescence. *Journal of Physics D: Applied Physics*, 31(20):2908, 1998.

CS Alexander, MF Morris, and SWS McKeever. The time and wavelength response of phototransferred thermoluminescence in natural and synthetic quartz. *Radiation measurements*, 27(2):153–159, 1997.

IK Bailiff, SGE Bowman, SF Mobbs, and MJ Aitken. The phototransfer technique and its use in thermoluminescence dating. *Journal of Electrostatics*, 3(1-3):269–280, 1977.

HG Balian and NW Eddy. Figure-of-merit (fom), an improved criterion over the normalized chi-squared test for assessing goodness-of-fit of gamma-ray spectral peaks. *Nuclear Instruments and Methods*, 145(2):389–395, 1977.

M Bertucci, I Veronese, and MC Cantone. Photo-transferred thermoluminescence from deep traps in quartz. *Radiation measurements*, 46(6-7):588–590, 2011.

L Bøtter-Jensen and GAT Duller. A new system for measuring optically stimulated luminescence from quartz samples. *International Journal of Radiation Applications and Instrumentation. Part D. Nuclear Tracks and Radiation Measurements*, 20(4):549–553, 1992.

L Bøtter-Jensen, N Agersnap Larsen, V Mejdahl, NRJ Poolton, MF Morris, and SWS McKeever. Luminescence sensitivity changes in quartz as a result of annealing. *Radiation Measurements*, 24(4):535–541, 1995.

L Bøtter-Jensen, SWS McKeever, and AG Wintle. *Optically stimulated luminescence dosimetry*. Elsevier, 2003.

E Bulur and HY Göksu. Phototransferred thermoluminescence from α-al2o3: C using blue light emitting diodes. *Radiation measurements*, 30(2):203–206, 1999.

R Chen. On the calculation of activation energies and frequency factors from glow curves. *Journal of Applied Physics*, 40(2):570–585, 1969.

R Chen and SWS Mckeever. *Theory of thermoluminescence and related phenomena*. World Scientific, 1997.

R Chen and V Pagonis. *Thermally and optically stimulated luminescence: a simulation approach*. John Wiley & Sons, 2011.

ML Chithambo. The analysis of time-resolved optically stimulated luminescence: I. theoretical considerations. *Journal of Physics D: Applied Physics*, 40(7):1874, 2007.

ML Chithambo. A method for kinetic analysis and study of thermal quenching in thermoluminescence based on use of the area under an isothermal decay-curve. *Journal of Luminescence*, 151:235–243, 2014.

ML Chithambo. Luminescence lifetimes in natural quartz annealed beyond its second phase inversion temperature. *Radiation Measurements*, 81:198–204, 2015.

ML Chithambo. *An Introduction to Time-resolved Optically Stimulated Luminescence*. Morgan & Claypool Publishers, 2018.

ML Chithambo and G Costin. Temperature-dependence of time-resolved optically stimulated luminescence and composition heterogeneity of synthetic α-al2o3: C. *Journal of Luminescence*, 182:252–262, 2017.

ML Chithambo and RB Galloway. Temperature dependence of luminescence time-resolved spectra from quartz. *Radiation measurements*, 32(5-6):627–632, 2000.

ML Chithambo and FO Ogundare. Luminescence lifetime components in quartz: Influence of irradiation and annealing. *Radiation Measurements*, 44(5-6):453–457, 2009.

ML Chithambo, C Ankjærgaard, and V Pagonis. Time-resolved luminescence from quartz: An overview of contemporary developments and applications. *Physica B: Condensed Matter*, 481:8–18, 2016.

ML Chithambo, C Seneza, and JM Kalita. Phototransferred thermoluminescence of α-al2o3: C: Experimental results and empirical models. *Radiation Measurements*, 105:7–16, 2017a.

ML Chithambo, AH Wako, and AA Finch. Thermoluminescence of sral2o4: Eu2+, dy3+: Kinetic analysis of a composite-peak. *Radiation Measurements*, 97:1–13, 2017b.

ML Chithambo, P Niyonzima, and JM Kalita. Phototransferred thermoluminescence of synthetic quartz: Analysis of illumination-time response curves. *Journal of Luminescence*, 198:146–154, 2018.

ML Chithambo, DE Folley, and S Chikwembani. Phototransferred thermoluminescence from natural quartz annealed at 1000 ∘c: Analysis of time-dependent evolution of intensity and competition effects. *Journal of Luminescence*, 216: 116730, 2019.

DE Folley and ML Chithambo. Influence of annealing on thermoluminescence of natural quartz: Kinetic analysis and experimental study of apparent inverse thermal quenching. *Radiation Measurements*, 120:53–58, 2018.

H Fujita and T Hashimoto. Effects of annealing temperatures on some radiation-induced phenomena in natural quartz. *Radiation measurements*, 42(2):156–162, 2007.

C Furetta. *Handbook of thermoluminescence*. World Scientific, 2010.

RB Galloway. Luminescence lifetimes in quartz: dependence on annealing temperature prior to beta irradiation. *Radiation measurements*, 35(1):67–77, 2002.

GFJ Garlick and AF Gibson. The electron trap mechanism of luminescence in sulphide and silicate phosphors. *Proceedings of the physical society*, 60(6):574–589, 1948.

RK Gartia and LL Singh. Evaluation of trapping parameter of quartz by deconvolution of the glow curves. *Radiation Measurements*, 46(8):664–668, 2011.

SG Gorbics, AE Nash, and FH Attix. Thermal quenching of luminescence in six thermoluminescent dosimetry phosphors—i: Quenching of x-ray-excited radioluminescence. *The International Journal of Applied Radiation and Isotopes*, 20 (12):829–841, 1969.

T Hashimoto, S Sakaue, H Aoki, and M Ichino. Dependence of tl-property changes of natural quartzes on aluminium contents accompanied by thermal annealing treatment. *Radiation Measurements*, 23(2-3):293–299, 1994.

W Hoogenstraaten. Electron traps in zinc sulphide phosphors. *Philips Research Report*, 13:515–693, 1958.

N Itoh, D Stoneham, and AM Stoneham. Ionic and electronic processes in quartz: mechanisms of thermoluminescence and optically stimulated luminescence. *Journal of Applied Physics*, 92(9):5036–5044, 2002.

JM Kalita and ML Chithambo. Phototransferred thermoluminescence in α-al2o3: C, mg under 470 nm blue light stimulation. *Journal of Luminescence*, 188: 371–377, 2017.

G Kitis. Tl glow-curve deconvolution functions for various kinetic orders and continuous trap distribution: Acceptance criteria for e and s values. *Journal of Radioanalytical and Nuclear Chemistry*, 247(3):697–703, 2001.

G Kitis, JM Gomez-Ros, and JWN Tuyn. Thermoluminescence glow-curve deconvolution functions for first, second and general orders of kinetics. *Journal of Physics D: Applied Physics*, 31(19):2636, 1998.

NG Kiyak, George S Polymeris, and George Kitis. Component resolved osl dose response and sensitization of various sedimentary quartz samples. *Radiation Measurements*, 42(2):144–155, 2007.

N Agersnap Larsen, E Bulur, L Bøtter-Jensen, and SWS McKeever. Use of the lm-osl technique for the detection of partial bleaching in quartz. *Radiation Measurements*, 32(5-6):419–425, 2000.

A Mandowski. Semi-localized transitions model for thermoluminescence. *Journal of Physics D: Applied Physics*, 38(1):17, 2004.

M Martini, M Fasoli, I Villa, and P Guibert. Radioluminescence of synthetic and natural quartz. *Radiation Measurements*, 47(9):846–850, 2012.

CE May and JA Partridge. Thermoluminescent kinetics of alpha-irradiated alkali halides. *The Journal of Chemical Physics*, 40(5):1401–1409, 1964.

SWS McKeever. *Thermoluminescence of solids*, volume 3. Cambridge University Press, 1985.

SWS McKeever, CY Chen, and LE Halliburton. Point defects and the pre-dose effect in natural quartz. *Nuclear Tracks and Radiation Measurements (1982)*, 10(4-6):489–495, 1985.

SWS McKeever, L Bøtter-Jensen, N Agersnap Larsen, and GAT Duller. Temperature dependence of osl decay curves: experimental and theoretical aspects. *Radiation Measurements*, 27(2):161–170, 1997.

D Mebhah, D Imatoukene, FZ Abdelazziz, and Z Lounis-Mokrani. Evaluation of trap parameters associated with thermoluminescence peaks in fired quartz. *Radiation measurements*, 41(7-8):813–818, 2006.

D Mebhah, D Imatoukene, Z Lounis-Mokrani, and M Kechouane. Comparative study on the effect of annealing treatments on rtl mechanism in natural quartz from different origins. *Journal of Luminescence*, 129(12):1615–1618, 2009.

I Milanovich-Reichhalter and N Vana. Phototransferred thermoluminescence in quartz. *Radiation Protection Dosimetry*, 33(1-4):211–213, 1990.

I Milanovich-Reichhalter and N Vana. Phototransferred thermoluminescence in quartz annealed at 1000 c. *International Journal of Radiation Applications and Instrumentation. Part D. Nuclear Tracks and Radiation Measurements*, 18(1-2): 67–69, 1991.

KVR Murthy and HS Virk. Luminescence phenomena: An introduction. In *Defect and Diffusion Forum*, volume 347, pages 1–34. Trans Tech Publ, 2014.

R Nanjundaswamy, K Lepper, and S WS McKeever. Thermal quenching of thermoluminescence in natural quartz. *Radiation protection dosimetry*, 100(1-4): 305–308, 2002.

DTU Nutech. Guide to "the risø tl/osl reader", 2015.

DTU Nutech. The risø tl/osl reader model tl/osl-da-20. *Product catalogue 1803a*, 2018.

FO Ogundare and ML Chithambo. Thermoluminescence kinetic analysis of quartz with a glow peak that shifts in an unusual manner with irradiation dose. *Journal of Physics D: Applied Physics*, 40(1):247, 2006.

V Pagonis, G Kitis, and C Furetta. *Numerical and practical exercises in thermoluminescence*. Springer Science & Business Media, 2006.

V Pagonis, L Blohm, M Brengle, G Mayonado, and P Woglam. Anomalous heating rate effect in thermoluminescence intensity using a simplified semi-localized transition (slt) model. *Radiation Measurements*, 51:40–47, 2013.

V Pagonis, ML Chithambo, R Chen, A Chruścińska, M Fasoli, SH Li, M Martini, and K Ramseyer. Thermal dependence of luminescence lifetimes and radioluminescence in quartz. *Journal of luminescence*, 145:38–48, 2014.

NRJ Poolton, GM Smith, PC Riedi, E Bulur, L Bøtter-Jensen, AS Murray, and M Adrian. Luminescence sensitivity changes in natural quartz induced by high temperature annealing: a high frequency epr and osl study. *Journal of Physics D: Applied Physics*, 33(8):1007, 2000.

NRJ Poolton, E Bulur, J Wallinga, L Bøtter-Jensen, AS Murray, and F Willumsen. An automated system for the analysis of variable temperature radioluminescence. *Nuclear Instruments and Methods in Physics Research Section B: Beam Interactions with Materials and Atoms*, 179(4):575–584, 2001.

F Preusser, ML Chithambo, T Götte, M Martini, K Ramseyer, EJ Sendezera, GJ Susino, and AG Wintle. Quartz as a natural luminescence dosimeter. *Earth-Science Reviews*, 97(1-4):184–214, 2009.

JT Randall and MHF Wilkins. Phosphorescence and electron traps-i. the study of trap distributions. *Proceedings of the Royal Society of London. Series A. Mathematical and Physical Sciences*, 184(999):365–389, 1945.

HM Rendell, PD Townsend, RA Wood, and BJ Luff. Thermal treatments and emission spectra of tl from quartz. *Radiation Measurements*, 23(2-3):441–449, 1994.

F Rutley. *Rutley's elements of mineralogy*. Springer Science & Business Media, 2012.

AJJ Santos, JF de Lima, and MEG Valerio. Phototransferred thermoluminescence of quartz. *Radiation measurements*, 33(4):427–430, 2001.

T Schilles, NRJ Poolton, E Bulur, L Bøtter-Jensen, AS Murray, GM Smith, PC Riedi, and GA Wagner. A multi-spectroscopic study of luminescence sensitivity changes in natural quartz induced by high-temperature annealing. *Journal of Physics D: Applied Physics*, 34(5):722, 2001.

N Shimizu, N Mitamura, A Takeuchi, and T Hashimoto. Dependence of radioluminescence on tl-properties in natural quartz. *Radiation measurements*, 41 (7-8):831–835, 2006.

JS Singarayer and RM Bailey. Further investigations of the quartz optically stimulated luminescence components using linear modulation. *Radiation Measurements*, 37(4-5):451–458, 2003.

B Subedi, E Oniya, GS Polymeris, D Afouxenidis, NC Tsirliganis, and G Kitis. Thermal quenching of thermoluminescence in quartz samples of various origin. *Nuclear Instruments and Methods in Physics Research Section B: Beam Interactions with Materials and Atoms*, 269(6):572–581, 2011.

CM Sunta. *Unraveling thermoluminescence*, volume 1. Springer, 2015.

S Thomas and ML Chithambo. A study of the kinetics of a high temperature thermoluminescence peak in annealed natural quartz. *Journal of Luminescence*, 204:603–608, 2018.

S Toyoda and M Ikeya. Thermal stabilities of paramagnetic defect and impurity centers in quartz: Basis for esr dating of thermal history. *Geochemical Journal*, 25(6):437–445, 1991.

R Walther and D Zilles. Esr studies on bleached sedimentary quartz. *Quaternary Science Reviews*, 13(5-7):611–614, 1994.

OM Williams and NA Spooner. Defect pair mechanism for quartz intermediate temperature thermoluminescence bands. *Radiation Measurements*, 108:41–44, 2018.

OM Williams and NA Spooner. Quartz optically stimulated luminescence configurational coordinate model. *Radiation Measurements*, page 106259, 2020.

AG Wintle. Thermal quenching of thermoluminescence in quartz. *Geophysical Journal International*, 41(1):107–113, 1975.

AG Wintle and AS Murray. The relationship between quartz thermoluminescence, photo-transferred thermoluminescence, and optically stimulated luminescence. *Radiation Measurements*, 27(4):611–624, 1997.

AG Wintle and AS Murray. A review of quartz optically stimulated luminescence characteristics and their relevance in single-aliquot regeneration dating protocols. *Radiation measurements*, 41(4):369–391, 2006.

XH Yang and SWS McKeever. The pre-dose effect in crystalline quartz. *Journal of Physics D: Applied Physics*, 23(2):237, 1990.

AN Yazici and M Topaksu. The analysis of thermoluminescence glow peaks of unannealed synthetic quartz. *Journal of Physics D: Applied Physics*, 36(6):620, 2003.

M Yüksel, T Dogan, E Unsal, ZG Portakal, S Akca, Z Yegingil, and M Topaksu. Thermoluminescence properties of annealed natural quartz after beta irradiation. *Luminescence*, 31(8):1513–1518, 2016.

R Zhou, MJ Wei, B Song, Y Zhang, QY Zhao, BL Pan, and TF Li. Evaluation of trapping parameters of annealed natural quartz. *Nuclear Instruments and Methods in Physics Research Section B: Beam Interactions with Materials and Atoms*, 375:32–39, 2016.